

**Titre:** Sealing performance of gasketed bolted flanged joints : effect of  
Title: flange surface characteristics and application of fuzzy logic

**Auteur:** Jafar Arghavani  
Author:

**Date:** 2001

**Type:** Mémoire ou thèse / Dissertation or Thesis

**Référence:** Arghavani, J. (2001). Sealing performance of gasketed bolted flanged joints :  
Citation: effect of flange surface characteristics and application of fuzzy logic [Ph.D. thesis,  
École Polytechnique de Montréal]. PolyPublie.  
<https://publications.polymtl.ca/7050/>

 **Document en libre accès dans PolyPublie**  
Open Access document in PolyPublie

**URL de PolyPublie:** <https://publications.polymtl.ca/7050/>  
PolyPublie URL:

**Directeurs de  
recherche:** Michel Derenne, & Luc Marchand  
Advisors:

**Programme:** Unspecified  
Program:

## INFORMATION TO USERS

This manuscript has been reproduced from the microfilm master. UMI films the text directly from the original or copy submitted. Thus, some thesis and dissertation copies are in typewriter face, while others may be from any type of computer printer.

**The quality of this reproduction is dependent upon the quality of the copy submitted.** Broken or indistinct print, colored or poor quality illustrations and photographs, print bleedthrough, substandard margins, and improper alignment can adversely affect reproduction.

In the unlikely event that the author did not send UMI a complete manuscript and there are missing pages, these will be noted. Also, if unauthorized copyright material had to be removed, a note will indicate the deletion.

Oversize materials (e.g., maps, drawings, charts) are reproduced by sectioning the original, beginning at the upper left-hand corner and continuing from left to right in equal sections with small overlaps.

ProQuest Information and Learning  
300 North Zeeb Road, Ann Arbor, MI 48106-1346 USA  
800-521-0600

UMI<sup>®</sup>



UNIVERSITÉ DE MONTRÉAL

SEALING PERFORMANCE OF GASKETED BOLTED FLANGED JOINTS:  
Effect of Flange Surface Characteristics and Application of Fuzzy Logic

JAFAR ARGHAVANI  
DÉPARTEMENT DE GÉNIE MÉCANIQUE  
ÉCOLE POLYTECHNIQUE DE MONTRÉAL

THÈSE PRÉSENTÉE EN VUE DE L'OBTENTION  
DU DIPLÔME DE PHILOSOPHIE DOCTOR  
(GÉNIE MÉCANIQUE)  
AOÛT 2001





**National Library  
of Canada**

**Acquisitions and  
Bibliographic Services**

**395 Wellington Street  
Ottawa ON K1A 0N4  
Canada**

**Bibliothèque nationale  
du Canada**

**Acquisitions et  
services bibliographiques**

**395, rue Wellington  
Ottawa ON K1A 0N4  
Canada**

*Your file Votre référence*

*Our file Notre référence*

**The author has granted a non-exclusive licence allowing the National Library of Canada to reproduce, loan, distribute or sell copies of this thesis in microform, paper or electronic formats.**

**The author retains ownership of the copyright in this thesis. Neither the thesis nor substantial extracts from it may be printed or otherwise reproduced without the author's permission.**

**L'auteur a accordé une licence non exclusive permettant à la Bibliothèque nationale du Canada de reproduire, prêter, distribuer ou vendre des copies de cette thèse sous la forme de microfiche/film, de reproduction sur papier ou sur format électronique.**

**L'auteur conserve la propriété du droit d'auteur qui protège cette thèse. Ni la thèse ni des extraits substantiels de celle-ci ne doivent être imprimés ou autrement reproduits sans son autorisation.**

**0-612-71306-7**

**Canada**

UNIVERSITÉ DE MONTRÉAL

ÉCOLE POLYTECHNIQUE DE MONTRÉAL

Cette thèse intitulée:

**SEALING PERFORMANCE OF GASKETED BOLTED FLANGED JOINTS:  
Effect of Flange Surface Characteristics and Application of Fuzzy Logic**

présentée par: ARGHAVANI Jafar

en vue de l'obtention du diplôme de: Philosophiae Doctor

a été dûment acceptée par le jury d'examen constitué de:

M. ROUSSELET Jean, Ph.D., président

M. DERENNE Michel, M.Sc.A., membre et directeur de recherche

M. MARCHAND Luc, Ph.D., membre et codirecteur de recherche

M. BALAZINSKI Marek, Ph.D., membre

M. ASTAKHOV Viktor P., Ph.D., membre

**To my wife Sophie for her patience and support and  
to my Parents and Family**

## ACKNOWLEDGMENTS

I would like to express my sincere thanks to my research directors, Prof. Michel Derenne, and Prof. Luc Marchand for their guidance.

I would also like to thank the committee members for their valuable comments. Special thanks to Prof. Marek Balazinski for having made accessible the Fuzzy-Flou Decision Support System software. I would like to express my gratitude to Prof. Viktor P. Astakhov for his valuable comments and his encouragements.

This research was realized at the Mechanical Engineering Department, Section of Applied Mechanics, of Ecole Polytechnique of Montreal, and using the test equipments and facilities at the Tightness Testing and Research Laboratory Inc. (TTRL Inc.). I appreciated the assistance of the laboratory personnel.

Finally, I wish to thank my wife Sophie for her patience, support and constant encouragement.

## RÉSUMÉ

L'objectif premier de cette thèse est d'étudier l'effet du fini de surface des brides sur le comportement des assemblages à brides boulonnées munis de joints d'étanchéité. La réalisation de cet objectif a commencé par la mise en œuvre d'une étude expérimentale, en réalisant des tests de caractérisation des joints à l'étanchéité appelés ROTT (ROm Temperature Tightness) tests sur une machine d'essais dédiée à cet effet. Plusieurs types de joints d'étanchéité ont été testés en faisant varier le type de fini de surface des plateaux métalliques en contact avec ces joints permettant de comprimer ceux-ci. Trois types de joints ont été testés; deux joints en feuille à base de PTFE (Polytétrafluoroéthylène) et de graphite expansé et un joint composite avec spirale en acier inoxydable et remplissage de graphite.

Le problème de l'écoulement d'un fluide à travers les milieux poreux que sont les joints, et à l'interface joint-bride, est un phénomène des plus complexe. Ce phénomène dépend non seulement des paramètres définissant les finis de surface des brides (rugosité et forme) mais aussi d'autres paramètres comme le type de fluide pressurisé et sa pression et la porosité du joint variant avec la compression et la dégradation de celui-ci au cours du temps et de la température de fonctionnement.

Afin de faciliter la compréhension et l'analyse du phénomène de l'étanchéité des brides boulonnées munis de joints, et de fournir un outil permettant une meilleure prise de décisions sur les paramètres clés des systèmes requis, un outil de travail basé sur le concept de logique floue a été développé. Cet outil devrait permettre aux concepteurs d'assemblages à joints de faire un choix éclairé des paramètres les plus requis du couple joint d'étanchéité-fini de surface des brides pour obtenir un assemblage répondant aux critères de conception imposés. En conséquence, ce travail présente la mise en place d'un tel système de décision assistée par la logique floue appelé FDSS (Fuzzy Decision

Support System) dont les règles décisionnelles ont été développées à partir des résultats expérimentaux obtenus et de la connaissance acquise (Expert Knowledge).

Des algorithmes pour le FDSS ont été mis en place en considérant dans un premier temps que la pression du fluide, l'écrasement des joints et la force de compression appliquée sont les éléments clefs qui définissent l'étanchéité d'un assemblage prise comme critère de conception de celui-ci. Différents types de joint et de rugosité des surfaces de brides sont ainsi évalués.

Il a aussi été montré que le FDSS permettait de prédire le comportement à l'étanchéité à température ambiante d'un joint au cours d'un essai de caractérisation de type ROTT sans avoir à faire l'essai proprement dit.

Ainsi, il apparaît que les résultats obtenus avec le FDSS permettent d'interpréter correctement la nature complexe de l'étanchéité des assemblages pressurisés. Un tel outil permet de prédire correctement le comportement de tels assemblages. Ce travail démontre donc le potentiel de cet outil de prédiction capable de traiter des informations souvent complexes, imprécises ou manquantes qui sont caractéristiques du domaine des technologies de l'étanchéité.

## ABSTRACT

The objective of this thesis is to investigate the effect of surface characteristics on the leakage rate and on the leakage behavior of gasketed bolted flanged joints. This research considers the experimental study of the effect of surface characteristics on compressive stress, leakage rate and flow regimes. The sealing surfaces of the test platens of raised face types are produced with grinding, turning and milling procedures having different average arithmetic roughness values and are the subject of the experiments. Different types of gasket materials commonly used in industrial applications are considered, namely PTFE, flexible graphite G2 and spiral wound. The experiments are performed based on modified Room Temperature Tightness Test (ROTT) procedure, as opposed to the conventional ROTT test procedure, in order to reduce the experimental test points. The experimental results showing the surface characteristics, gasket stress and deflection, leakage rates and flow regimes are presented in tables and graphical form.

The analysis of sealing surface characteristics is complex and is influenced by many parameters that cannot be measured in a precise manner. The assessment of contact properties, macro and microstructure of the surfaces, with the gasket material adds to the complexity of the joint sealing phenomena, leakage rate and flow regime. The leakage rate and the state of flow regime depend on the geometry of the interfacial leak paths and on the gasket porosity, which are influenced by flange surface characteristics, gasket properties, gasket compressive stress and gas pressure. The combined effect of such parameters adds to the complexity of the joint system and is assessed in this thesis based on the relative measurement analysis.

To facilitate the understanding and the analysis of the gasketed bolted flanged joints sealing phenomena and to provide a tool for better decision making on the required system's parameters, the fuzzy logic is applied. Fuzzy logic algorithms are developed for the selection of gaskets and sealing surfaces to obtain optimal tightness of the joints,

based on the leakage rate. The fuzzy algorithms are a multivariate input and output system that considers parameters such as gas pressure, gasket deflection and leakage rate, gasket type, gasket stress and flange surface roughness. The system's fuzzy rules are developed based on the experimental results.

Other fuzzy logic algorithms are also developed based on limited test points from modified ROTT tests to predict the leakage rate, and to determine the new PVRC gasket constants,  $G_b$ ,  $a$ , and  $G_s$ , which are then used to determine the gasket minimum seating stress. The results obtained from the fuzzy logic algorithms are very close to the results of the experiments.

Finally, the models developed with fuzzy logic adequately address the complex nature of gaskets and sealing surfaces, and predict the experimental results from real situations, since they are capable of dealing with complex, vague information and missing/incomplete data. Based on the evidence presented in this thesis, it is shown conclusively that leakage rate through gasketed joint is predictable. The fuzzy decision support system approach, if more developed and refined, could effect a radical change in the method of selecting gaskets and estimating leakage rate in the field of gasketed bolted flanged joints.



## CONDENSÉ EN FRANÇAIS

Les fuites se produisant dans les assemblages pressurisés munis de joints d'étanchéité sont un problème auquel de nombreuses industries font face depuis de nombreuses années. Plusieurs études ont été conduites par des fabricants et utilisateurs de joints d'étanchéité pour essayer de remédier à ce problème. De plus, durant ces trois dernières décennies, d'importants programmes de recherche ont été entrepris aux États Unis dans ce domaine par le Pressure Vessel Research Committee (PVRC) à la demande d'organismes comme l'API (American Petroleum Institute) et l'ASME (American Society for Mechanical Engineers).

Bien que d'importants progrès aient été faits dans la mise au point de nouveaux produits d'étanchéité, il est apparu que la fuite des assemblages à brides boulonnées sous pression est un phénomène inévitable qui met en jeu de nombreux facteurs. Un joint d'étanchéité, en général de forme circulaire, est composé d'un élément scellant, plus ou moins mou, contenu ou pas dans une armature métallique. La fuite qui se produit est due à la porosité de cet élément scellant face à la pression du fluide (liquide ou gaz) contenu dans l'assemblage. Cette porosité est, quant à elle, fonction des conditions de fonctionnement de l'assemblage c'est à dire de la force de serrage appliquée pour déformer l'élément scellant, du fini de surface des brides en contact avec le joint, de la température de service et du temps d'utilisation, ces deux derniers facteurs agissant sur le vieillissement de l'élément scellant.

D'une façon générale, les fuites observées dans les installations se produisent de deux façons différentes. Il y a les grosses fuites souvent appelées "Blow-out" et celles qui passent souvent inaperçues car très petites qu'on appelle "émissions". Les fuites de type "émissions" sont les plus courantes et doivent être surveillées car étant petites, leur effet économique et environnemental, ne se fait sentir que sur le long terme. Elles peuvent aussi évoluer en intensité car elles dépendent essentiellement de la résistance du joint au

vieillissement (temps et température) et de la rigidité de l'assemblage (bride-boulons-joint). Elles peuvent finalement se transformer en grosses fuites qui se produisent quand la force de compression appliquée sur le joint n'est plus capable d'équilibrer la force de réaction exercée par la pression de fluide sur les brides. Cette situation survient quand l'élément scellant et son armature, s'il y en a une, se sont détériorés au point de n'être plus capable de réagir suffisamment à la force exercée par les boulons de la bride. Dans ce cas il peut y avoir rupture de l'équilibre et perte brutale de la pression du fluide contenu. Cette situation est à éviter car très dangereuse et très coûteuse.

Le but principal des études entreprises jusqu'à ce jour a été de développer des essais et des outils de caractérisation utilisables par fabricants et utilisateurs de joint d'étanchéité pour essayer d'obtenir l'étanchéité optimale de ces assemblages pressurisés dans tous les types d'applications, aussi bien existantes qu'à concevoir, et dans toutes sortes de conditions de fonctionnement (pression et température). Le joint performant est celui qui est capable au cours de ces essais de maintenir une étanchéité fixée sous des conditions d'essais qui simulent des conditions réelles de fonctionnement. Pour obtenir des outils de caractérisation efficaces, des recherches plus fondamentales ont été entreprises pour mieux comprendre l'écoulement d'un fluide au travers d'un milieu poreux et pour examiner la variation et le vieillissement de la porosité des divers types d'éléments scellants en fonction des conditions de fonctionnement susceptibles de la modifier. Parmi ces conditions, l'effet des caractéristiques de la surface de brides (forme et rugosité) n'a pas reçu à ce jour une attention soutenue. Ceci s'explique par le fait que les quelques études exploratoires entreprises dans ce domaine n'ont pas pu, dans les conditions des essais effectués, quantifier de façon concluante l'effet du fini de surface sur l'étanchéité de quelques éléments scellants utilisés pour fabriquer des joints.

Dans la présente recherche, les résultats des tests menés sur les joints de PTFE (Polytétrafluoroéthylène), de graphite expansé et de composite avec spirale en acier inoxydable et remplissage de graphite démontre que la rugosité de la surface,  $R_a$ , seule,

n'a pas d'effet significatif sur l'étanchéité du joint. Toutefois, la forme de la surface, quant à elle, a un effet prononcé, particulièrement lorsque la force de compression appliquée sur le joint est faible. Ces résultats démontrent que pour une évaluation plus précise de l'étanchéité des assemblages à brides boulonnées munis de joints, tous les paramètres clefs doivent être considérés conjointement avec les caractéristiques de la surface (rugosité et forme).

D'une façon générale, depuis plus de vingt ans, de grands progrès ont été faits dans la compréhension de l'étanchéité des assemblages pressurisés et dans la mise au point des essais et outils de caractérisation. Cependant beaucoup de travail reste à faire pour être capable de faire une sélection appropriée des paramètres qui vont contribuer à améliorer la fabrication des joints d'étanchéité et à choisir le meilleur joint susceptible de remplir correctement sa fonction dans une application donnée. Cette sélection constitue l'objectif ultime dans la planification, la production, le contrôle des procédés, la sécurité et les coûts. Une méthode unifiée adéquate pour faire une telle sélection n'a pas encore été développée, bien que beaucoup d'efforts soient faits pour trouver les paramètres optimaux permettant de réaliser des assemblages avec "zéro fuite". Les travaux théoriques et expérimentaux qui ont été faits semblent démontrer que la réalisation de cet objectif sera difficile à atteindre si on cherche à étudier systématiquement l'influence de tous les paramètres qui peuvent affecter l'étanchéité de ces assemblages qui sont soumis à d'innombrables conditions de fonctionnement. Comprendre les résultats expérimentaux, évaluer et comparer les performances afin de concevoir une application particulière la plus étanche possible ou de solutionner l'étanchéité d'une application existante est encore une opération exigeante, complexe et incertaine. L'expérience des concepteurs alliée aux connaissances accumulées de nos jours sont les éléments qui permettent de faire les meilleurs choix possibles. Cependant, cette approche ne sert pas de façon simple et efficace un utilisateur soucieux de la qualité des produits d'étanchéité qu'il utilise pour garantir la sécurité et le respect des normes environnementales de ses installations.

À partir de cette constatation, il nous a semblé intéressant d'introduire un nouvel outil décisionnel basé sur le concept de la logique floue et capable d'apporter des solutions à des systèmes complexes comportant des données imprécises ou manquantes. Le concept de logique floue a été utilisé durant ces trois dernières décennies dans le domaine industriel comme base pour développer des outils de prise de décision, de prédiction et de commande, particulièrement dans le domaine de l'ingénierie, des statistiques, de la médecine et de l'informatique. Ce concept est ici introduit pour effectuer la sélection des caractéristiques des joints d'étanchéité et des finis de surface des brides afin de minimiser ou de prédire les fuites d'un assemblage à brides boulonnées sous pression.

Cette thèse est présentée sous forme d'articles qui ont été publiés ou vont être publiés dans le "International Journal of Advanced Manufacturing Technology". Elle se divise en deux grandes parties. La première concerne l'analyse expérimentale de l'effet des finis de surface des brides sur l'étanchéité des assemblages à brides boulonnées. La seconde partie introduit le concept de logique floue pour la sélection des joints et la prédiction de leur étanchéité. La présentation du travail est divisée en six chapitres.

- Après une introduction générale, le chapitre 1 présente une revue de la littérature existante et pertinente concernant le sujet de recherche qui nous intéresse, et le chapitre 2 présente une synthèse.
- Le chapitre 3 présente l'approche expérimentale adoptée pour étudier l'effet des finis de surface des brides sur l'étanchéité des assemblages à brides boulonnées. Cette étude est présentée sous la forme d'un article intitulé " Effect of Surface Characteristics on Compressive Stress and Leakage Rate in Gasketed Flanged Joints". Des tests de caractérisation appelés ROTT (ROm Temperature Tightness) tests ont été réalisés à l'aide d'une machine d'essais dédiée à cet effet. Plusieurs types de joints d'étanchéité ont été testés en faisant varier le fini de surface (forme et rugosité) des plateaux métalliques en contact avec ces joints et permettant de

compresser ceux-ci. Le test ROTT consiste à faire varier la force (ou contrainte) de compression sur le joint testé, en l'augmentant ou la diminuant selon une procédure établie, et à chaque étape de mesurer les fuites qui se produisent pour deux niveaux de pression de d'Hélium (gaz utilisé pour pressuriser l'intérieur du joint). Le test ROTT utilisé ici a été simplifié au niveau de la procédure pour gagner du temps et ne considère que deux cycles de chargement-déchargement (nombre de points de mesure réduit) alors que la procédure proposée comme standard en comporte trois. Trois types de joints ont été testés; deux joints en feuille à base de PTFE (Polytétrafluoroéthylène) et de graphite expansé et un joint composite avec spirale en acier inoxydable et remplissage de graphite. Les finis de surface des plateaux utilisés sont le tournage, le fraisage et le meulage. Les résultats expérimentaux ont démontré que l'effet du fini de surface sur l'étanchéité des joints testés doit être considéré conjointement avec les autres paramètres clefs.

- Dans le chapitre 4, l'application du concept de logique floue à la détermination de l'étanchéité des assemblages à brides boulonnées est introduit sous forme d'un modèle simple de décision pour la détermination des finis de surface des brides permettant d'obtenir l'étanchéité maximale. Cette étude est présentée sous la forme d'un article intitulé " Sealing Performance of Gasketed Bolted Flanged Joints; A fuzzy Decision Support System Approach". Les résultats expérimentaux des tests ROTT effectués précédemment ont été utilisés pour établir les règles décisionnelles du modèle et valider ses résultats. Ce modèle se limite seulement aux finis de surface de type phonographique obtenus par tournage avec avance radiale continue avec trois profondeurs de passe donnant trois rugosités moyennes différentes.
- Le chapitre 5 présente la généralisation du concept de logique floue au domaine des assemblages à brides boulonnées. Cette présentation est faite sous forme d'un article intitulé " Fuzzy Logic Application in Gasket Selection and Sealing

Performance". Cet article traite de la détermination d'un ensemble optimal de paramètres de fonctionnement pour obtenir un assemblage le plus étanche possible. Le modèle mis en place considère que l'effet de certains de ces paramètres peut être mal connu ou même totalement inconnu. Ce modèle est limité à un seul fini de surface et une seule rugosité. Cependant il prend en compte les quatre possibilités de types de joints, plusieurs pressions de fluide et niveaux de chargement.

- Au chapitre 6, plusieurs modèles décisionnels basés sur le concept de logique floue sont développés pour prédire la performance d'un assemblage pressurisé. Cette étude est présentée sous la forme d'un article à publier intitulé "Fuzzy Logic Approach to Predict Gasket Leak Rate and to Obtain Gasket Minimum Seating Stress". Différents modèles sont développés et validés à partir des résultats expérimentaux obtenus avec des tests ROTT modifiés (nombre de points de mesure réduit). Les paramètres comme la pression de fluide, la contrainte sur le joint, les finis de surfaces des brides, le taux de fuite sont tous considérés dans ces modèles. Pour démontrer le caractère prédictif de ces modèles, ils ont été modifiés sur la base des connaissances acquises pour prédire le comportement d'un assemblage au cours d'un test ROTT de type standard avec plus de points de mesure. Les résultats expérimentaux et ceux obtenus des modèles basés sur la logique floue sont aussi utilisés pour déterminer les nouvelles constantes de joints  $G_b$ ,  $a$ , et  $G_s$ . Ces constantes sont ensuite utilisées afin d'obtenir la contrainte minimale à conserver sur le joint. La comparaison de cette prédiction avec de vrais tests ROTT existants au laboratoire TTRL est très bonne. Ceci indique que des modèles basés sur la logique floue, et construits avec certaines données incomplètes, sont capables de prédire le comportement à l'étanchéité d'un assemblage pressurisé.

- Finalement, les conclusions relatives à la contribution faite par ce travail au domaine de l'étanchéité des assemblages boulonnés sous pression sont présentées. De plus des remarques pour améliorer la recherche présentée et des recommandations pour conduire des recherches futures sont données.

## TABLE OF CONTENTS

<b>DEDICATION .....</b>	<b>iv</b>
<b>ACKNOWLEDGMENT .....</b>	<b>v</b>
<b>RÉSUMÉ .....</b>	<b>vi</b>
<b>ABSTRACT .....</b>	<b>viii</b>
<b>CONDENSÉ EN FRANÇAIS .....</b>	<b>x</b>
<b>TABLE OF CONTENTS .....</b>	<b>xvii</b>
<b>LIST OF TABLES .....</b>	<b>xxii</b>
<b>LIST OF FIGURES .....</b>	<b>xxv</b>
 <b>INTRODUCTION .....</b>	 <b>1</b>
 <b>CHAPTER 1:        LITERATURE REVIEW .....</b>	 <b>9</b>
1.1 Introduction .....	9
1.2 Contact area and compressive stress .....	9
1.3 Flange surface characteristics .....	11
1.4 Fuzzy logic application .....	19
 <b>CHAPTER 2:        SYNTHESIS .....</b>	 <b>21</b>
 <b>CHAPTER 3:        EFFECT OF SURFACE CHARACTERISTICS ON                               COMPRESSIVE STRESS AND LEAK RATE IN                               GASKETED FLANGED JOINTS .....</b>	   <b>27</b>
3.1 Presentation of the chapter.....	27
3.2 Abstract .....	28
3.3 Introduction .....	29
3.4 Theoretical analysis of surface form and roughness .....	34



3.4.1 Quantifying surface roughness .....	34
3.4.2 Pressure distribution and stress pattern .....	37
3.4.3 Microstructure of ground surface .....	37
3.4.4 Surface macrostructure .....	39
3.4.5 Gaps between rough surfaces in contact .....	44
3.5 Theoretical leak path and leak rate .....	49
3.5.1 Effect of surface pressure .....	49
3.5.2 Gas flow regimes .....	53
3.5.2.1 Determination of flow regimes .....	56
3.6 Experimental sealing investigation setup .....	61
3.6.1 Room-temperature hydraulic test rig: RTHR rig .....	61
3.6.2 Automatic test procedure .....	66
3.6.2.1 Estimated measurement error .....	68
3.6.3 ROTT test procedure .....	71
3.6.4 Modified ROTT test procedure .....	75
3.6.5 Differences between the ROTT test and modified ROTT test procedure .....	78
3.6.6 Platens surface configuration and surface characteristics....	78
3.6.7 Test gaskets .....	83
3.6.7.1 Specifications of PTFE sheet gasket Gylon 3504..	85
3.6.7.2 Specifications of flexible graphite sheet (G2) gasket, Grafoil GHR .....	86
3.6.7.3 Specifications of spiral wound graphite filled gasket (SW), Flexitallic .....	87
3.7 Experimental results .....	89
3.7.1 Tests conducted .....	89
3.7.2 Results of PTFE Gylon gasket tests .....	93
3.7.2.1 PTFE test results at gas pressure 200 psig .....	93
3.7.2.2 PTFE test results at gas pressure 800 psig .....	98

3.7.2.3 PTFE gasket deflections .....	101
3.7.2.4 Effect of surface roughness $Ra$ .....	103
3.7.2.5 Leak flow regimes on PTFE gasket .....	103
3.7.3 Results of UCAR flexible graphite sheet (G2) gasket tests .	104
3.7.3.1 G2 test results at gas pressure 200 psig .....	104
3.7.3.2 G2 test results at gas pressure 800 psig .....	106
3.7.3.3 G2 gasket deflections .....	109
3.7.3.4 Leak flow regimes on flexible graphite sheet (G2) gasket .....	110
3.7.3.5 G2 -Closing remarks .....	112
3.7.4 Results of spiral wound (SW) gasket tests .....	113
3.7.4.1 SW test results at gas pressure 200 psig .....	113
3.7.4.2 SW test results at gas pressure 800 psig .....	115
3.7.4.3 SW gasket deflections .....	117
3.7.4.4 Leak flow regimes on spiral wound gasket .....	117
3.8 Conclusion .....	118
3.9 References .....	120

#### **CHAPTER 4: SEALING PERFORMANCE OF GASKETED FLANGED JOINTS: A Fuzzy Decision Support**

<b>System Approach .....</b>	<b>158</b>
4.1 Presentation of the chapter .....	158
4.2 Abstract .....	159
4.3 Introduction .....	159
4.4 Literature review of gasketed bolted flanged joints .....	161
4.5 Literature review of fuzzy theory .....	162
4.6 Proposed approach .....	163
4.7 Basic theory of fuzzy logic .....	164
4.7.1 Compositional rule of inference .....	170

4.7.2 Fuzzification and defuzzification .....	172
4.7.3 Fuzzy rules .....	173
4.8 Case study .....	175
4.8.1 Flange surface selection .....	175
4.9 Experimental test procedures .....	176
4.9.1 Fuzzy model and validation .....	176
4.10 Conclusion .....	178
4.11 References .....	183

<b>CHAPTER 5: FUZZY LOGIC APPLICATION IN GASKET SELECTION AND SEALING PERFORMANCE .....</b>	<b>185</b>
5.1 Presentation of the chapter .....	185
5.2 Abstract .....	186
5.3 Introduction .....	186
5.4 Literature review of gasketed bolted flanged joints .....	187
5.5 Literature review of fuzzy set theory and fuzzy application .....	188
5.6 Present work .....	190
5.7 Fundamentals of fuzzy set theory .....	191
5.7.1 Practical aspects of fuzzy relations .....	194
5.7.2 Fuzzy set operations .....	196
5.7.3 Fuzzy algorithm .....	196
5.7.4 Fuzzification and defuzzification .....	197
5.8 Case study .....	199
5.8.1 Gasket selection .....	199
5.8.2 Experimental procedures .....	200
5.8.3 Fuzzy rules .....	204
5.8.4 Fuzzy model and obtained results .....	207
5.9 Conclusion .....	213
5.10 References .....	217

<b>CHAPTER 6:</b>	<b>FUZZY LOGIC APPROACH TO PREDICT GASKET LEAK RATE AND TO OBTAIN GASKET MINIMUM SEATING STRESS .....</b>	<b>220</b>
6.1	Presentation of the chapter .....	220
6.2	Abstract .....	221
6.3	Introduction .....	221
6.4	Gasket behaviour .....	223
6.4.1	PVRC gasket constants .....	226
6.4.2	Gasket minimum seating stress .....	227
6.5	The use of fuzzy logic .....	233
6.6	Present work .....	234
6.7	Experimental procedure and data .....	235
6.7.1	ROTT procedure .....	235
6.7.2	Modified ROTT procedure .....	236
6.7.3	Test gaskets .....	238
6.8	Fuzzy algorithms and rules .....	239
6.9	Fuzzy leakage prediction results .....	250
6.10	PVRC gasket constants and gasket minimum seating stress results .	262
6.11	Conclusion .....	269
6.12	References .....	270
<b>CONCLUSION .....</b>		<b>272</b>
<b>BIBLIOGRAPHY .....</b>		<b>275</b>

## LIST OF TABLES

Table 3.1.	Instrumentation capabilities and precision .....	70
Table 3.2.	Mass spectrometer ASM 180T specifications .....	70
Table 3.3	ROTT test procedure stress levels .....	73
Table 3.4.	Typical load-pressure sequence for "Standard" ROTT procedure ..	74
Table 3.5.	Stress levels on gasket for modified ROTT test .....	76
Table 3.6.	Machining parameters and procedures used to produce platens ....	81
Table 3.7.	PTFE gasket leak ratio Lrm (800 psig)/Lrm (200 psig) .....	124
Table 3.8.	G2 gasket leak ratio Lrm (800 psig)/Lrm (200 psig) .....	124
Table 3.9.	SW gasket leak ratio Lrm (800 psig)/Lrm (200 psig) .....	124
Table 3.10.	PTFE gasket leak ratio of all surface characteristics compared to ground surface III1 at 200 psig for different stress levels .....	125
Table 3.11.	G2 gasket leak ratio of all surface characteristics compared to ground surface III1 at 200 psig for different stress levels .....	125
Table 3.12.	SW gasket leak ratio of all surface characteristics compared to ground surface III1 at 200 psig for different stress levels .....	125
Table 3.13.	PTFE gasket leak ratio of all surface characteristics compared to ground surface III1 at 800 psig for different stress levels .....	126
Table 3.14.	G2 gasket leak ratio of all surface characteristics compared to ground surface III1 at 800 psig for different stress levels .....	126
Table 3.15.	SW gasket leak ratio of all surface characteristics compared to ground surface III1 at 800 psig for different stress levels .....	126
Table 3.16.	PTFE gasket leak and deflection ratio for all surface characteristics at different stress levels for 200 psig .....	127
Table 3.17.	G2 gasket leak and deflection ratio for all surface characteristics at different stress levels for 200 psig .....	127
Table 3.18.	SW gasket leak and deflection ratio for all surface characteristics at different stress levels for 200 psig .....	127

Table 3.19.	PTFE gasket leak and deflection ratio for all surface characteristics at different stress levels for 800 psig .....	128
Table 3.20.	G2 gasket leak and deflection ratio for all surface characteristics at different stress levels for 800 psig .....	128
Table 3.21	SW gasket leak and deflection ratio for all surface characteristics at different stress levels for 800 psig .....	128
Table 3.22.	PTFE gasket deflection ratio of all surface characteristics compared to ground surface III1 at 200 psig for different stress levels .....	129
Table 3.23.	G2 gasket deflection ratio of all surface characteristics compared to ground surface III1 at 200 psig for different stress levels .....	129
Table 3.24.	SW gasket deflection ratio of all surface characteristics compared to ground surface III1 at 200 psig for different stress levels .....	129
Table 3.25.	PTFE gasket deflection ratio of all surface characteristics compared to ground surface III1 at 800 psig for different stress levels .....	130
Table 3.26.	G2 gasket deflection ratio of all surface characteristics compared to ground surface III1 at 800 psig for different stress levels .....	130
Table 3.27.	SW gasket deflection ratio of all surface characteristics compared to ground surface III1 at 800 psig for different stress levels .....	130
Table 3.28	Slope of the lines based on log-log plot of leak versus pressure, representing the graphs of flow regimes on Figures 2.32 through 2.34 .....	131
Table 6.1.	Gasket tightness classes .....	225
Table 6.2.	Stress levels on gasket for the modified ROTT test procedure .....	237
Table 6.3.	PTFE tests results at 200 and 800 psig with platens I1 Ra 900 $\mu$ in. ....	242
Table 6.4.	PTFE tests results at 200 and 800 psig with platens III1 Ra 20 $\mu$ in. ....	243
Table 6.5.	G2 tests results at 200 and 800 psig, with platens I1 Ra 900 $\mu$ in. ...	244
Table 6.6.	G2 tests results at 200 and 800 psig, with platens III1 Ra 20 $\mu$ in. ...	245

Table 6.7.	SW tests results at 200 and 800 psig, with platens I1 Ra 900 $\mu$ in. ..	246
Table 6.8.	SW tests results at 200 and 800 psig, with platens III1 Ra 20 $\mu$ in. .	247
Table 6.9.	Fuzzy and experiment results of ROTT on PTFE Gylon 3504 .....	252
Table 6.10.	Fuzzy and experiment results of ROTT on UCAR flexible graphite G2 .....	253
Table 6.11.	Fuzzy and experiment results of ROTT on Flexitallic spiral wound gasket NPS 4-in class 600 lbs, flexible graphite filled .....	254
Table 6.12.	Gasket constants determination: $G_b$ , $a$ and $G_s$ , from experiments and fuzzy models, for PTFE, UCAR G2 and SW gaskets .....	265

## LIST OF FIGURES

Figure 3.1.	Pressure distribution and stress pattern for (a) A flat, (b) A groove with flat edges, (c) A cylinder and (d) A sphere .....	30
Figure 3.2.	Machined surfaces and their effect on gasket pore deformation and gas pressure distribution .....	32
Figure 3.3A.	Surface roughness average arithmetic height, $R_a$ , and root-mean-square (rms) roughness, $R_q$ .....	36
Figure 3.3.	Representing ground surfaces with sinusoidal form, and spherical micro-asperities .....	39
Figure 3.4.	Phenomena of leak cleansing by increase pressure .....	57
Figure 3.5.	Schematic of gasket test fixture cross-section, room-temperature hydraulic RTHR test rig .....	63
Figure 3.6.	ROTT test bench .....	64
Figure 3.7.	Room-temperature hydraulic test rig: RTHR rig .....	65
Figure 3.8.	Stress vs. deflection curve showing the generic ROTT test procedure sequence, typical results for a given gasket material .....	73
Figure 3.9.	Typical stress vs. deflection curve showing the modified ROTT test procedure sequence .....	76
Figure 3.10.	Typical bolted flanged joints assembly with raised face flange surface.....	77
Figure 3.11.	Different types of flange faces .....	79
Figure 3.11B	Typical cross section of expanded PTFE sheet, flexible graphite (G2) sheet and spiral wound gasket .....	88
Figure 3.12.	Topography of sealing surfaces .....	132
Figure 3.13.	Platens surface machining form .....	133
Figure 3.14.	PTFE, effect of surface finish; leak rate versus stress levels, for ground and turned concentric surfaces .....	134
Figure 3.15.	PTFE, effect of surface finish; leak rate versus stress levels, for	



	turned spiral and milled surfaces .....	135
Figure 3.16.	PTFE, effect of gas pressure; leak rate versus stress levels, for ground and turned concentric surfaces .....	136
Figure 3.17.	PTFE, effect of gas pressure; leak rate versus stress levels, for turned spiral and milled surfaces .....	137
Figure 3.18.	PTFE, leak rate and gasket deflection versus sealing surface characteristics, at stress S1, S3 and S5, at 200 psig .....	138
Figure 3.19.	PTFE, leak rate and gasket deflection versus sealing surface characteristics, at stress S1, S3 and S5, at 800 psig .....	139
Figure 3.20.	G2, effect of surface finish; leak rate versus stress levels, for ground and turned concentric surfaces .....	140
Figure 3.21.	G2, effect of surface finish; leak rate versus stress levels, for turned spiral and milled surfaces .....	141
Figure 3.22.	G2, effect of gas pressure; leak rate versus stress levels, for ground and turned concentric surfaces .....	142
Figure 3.23.	G2, effect of gas pressure; leak rate versus stress levels, for turned spiral and milled surfaces .....	143
Figure 3.24.	G2, leak rate and gasket deflection versus sealing surface characteristics, at stress S1, S3 and S5, at 200 psig .....	144
Figure 3.25.	G2, leak rate and gasket deflection versus sealing surface characteristics, at stress S1, S3 and S5, at 800 psig .....	145
Figure 3.26.	SW, effect of surface finish; leak rate versus stress levels, for ground and turned concentric surfaces .....	146
Figure 3.27.	SW, effect of surface finish; leak rate versus stress levels, for turned spiral and milled surfaces .....	147
Figure 3.28.	SW, effect of gas pressure; leak rate versus stress levels, for ground and turned concentric surfaces .....	148
Figure 3.29.	SW, effect of gas pressure; leak rate versus stress levels, for turned spiral and milled surfaces .....	149

Figure 3.30.	SW, leak rate and gasket deflection versus sealing surface characteristics, at stress S1, S3 and S5, at 200 psig .....	150
Figure 3.31.	SW, leak rate and gasket deflection versus sealing surface characteristics, at stress S1, S3 and S5, at 800 psig .....	151
Figure 3.32.	PTFE, log-log plots of leak rate versus gas pressure, for all surface characteristics.....	152
Figure 3.33.	G2, log-log plots of leak rate versus gas pressure, for all surface characteristics.....	154
Figure 3.34.	SW, log-log plots of leak rate versus gas pressure, for all surface characteristics .....	156
Figure 4.1.	Block diagram of fuzzy logic system, FLS .....	164
Figure 4.2.	Membership function of two linguistic values, e.g. defining the low and high gas pressure .....	167
Figure 4.3.	Membership function of three linguistic values, e.g. defining the low, medium and high gasket deflections .....	168
Figure 4.4.	Tightness parameter and leakage rate for three experiments based on surface roughness .....	179
Figure 4.5	Fuzzy decision support system. The inference rule of composition (CRI) used in SUM-PROD, and the fuzzification technique used is mean-of-maxima (MOM) .....	180
Figure 5.1.	True and false fuzzy sets. ....	192
Figure 5.2.	Large, very large, and extremely large fuzzy sets. ....	193
Figure 5.3.	Degree of belonging of elements in the sets. ....	193
Figure 5.4.	Architecture of fuzzy logic system. ....	198
Figure 5.5.	a) Leakage rate for G-LAM-GRT and UC-FLX-GRT gaskets vs. elapsed time with respect to gasket stress, b) Leakage rate for KLNLR and G-N-AS gaskets vs. elapsed time with respect to stress , c) Gasket deflection vs. gasket stress .....	203
Figure 5.6.	Multi-input multi-output classification task .....	205

Figure 5.7.	Network representation of possible fuzzy rules .....	206
Figure 5.8.	Fuzzy decision support system indicating input and output results. The computational rule of inference is SUM-PROD, and the defuzzification technique is COA .....	209
Figure 5.9.	Fuzzy decision support system indicating input and output results. The computational rule of inference is SUM-PROD, and COA is used as defuzzification technique .....	214
Figure 5.10.	Fuzzy decision support system indicating the effect of gas pressure on leakage rate in comparison with the input and output results presented in Fig. 5.9(a) .....	216
Figure 6.0.	Design relationship and the idealized Sg-Tp graph.....	232
Figure 6.1.	Modified generic ROTT test procedure sequence .....	237
Figure 6.2 A.	PTFE gasket, predicting the leakage rate at seating stress, for gas pressure 400-410 psig, surface characteristics Ra 240-260 $\mu$ in, and gasket stress 3900-4050 psi .....	248
Figure 6.2 B.	PTFE gasket, predicting the leakage rate at seating stress, for gas pressure 610-625 psig, surface characteristics Ra 500-515 $\mu$ in, and gasket stress 5950-6050 psi .....	249
Figure 6.3.	Fuzzy and experiment results for PTFE gasket, based on ROTT test	255
Figure 6.4.	Fuzzy and experiment results for G2 gasket, based on ROTT test ...	256
Figure 6.5.	Fuzzy and experiment results for SW gasket, based on ROTT test ..	257
Figure 6.6 A.	Fuzzy and experiment ROTT results, of leak versus stress, a) Part A at 400 psig, b) Part A at 800 psig, for PTFE, G2 and SW gaskets .....	258
Figure 6.6 B.	Fuzzy and experiment ROTT results, of leak versus stress; Part B at 800 psig, for PTFE, G2 and SW gaskets ....	259
Figure 6.7 A.	Fuzzy and experiment results of leak versus stress; Part A seating stress levels at 400 and 800 psig .....	260
Figure 6.7 B.	Fuzzy and experiment results of leak versus stress; Part B	

	operating stress levels at 800 psig .....	261
Figure 6.8.	Fuzzy and experiment results of gasket minimum seating stress versus gasket NPS size .....	266
Figure 6.9.	Fuzzy and experiment results of gasket minimum seating stress versus gasket NPS size .....	267
Figure 6.10.	Percent difference between fuzzy and experiment results of gasket minimum seating stress for different gasket NPS size .....	268

## INTRODUCTION

Leakage of gasketed bolted flanged joints, especially in pressurized systems, is a major concern that power companies as well as the petroleum, petrochemical and process industries are facing. Many researches have been conducted in order to understand and to predict the leakage through the gasketed joints. Furthermore, over the past three decades major research programs aimed at resolving problems associated with leakage have been undertaken by the Committee on Bolted Flanged Connections (CBFC) and its subcommittee on gasket testing of the Pressure Vessel Research Council (PVRC) in response to the needs of the American Petroleum Institute (API) and the American Society of Mechanical Engineers (ASME).

In spite of all efforts and progress made in the domain of sealing products, the leakage phenomena seem to be unavoidable and quite complex in the area of gasketed bolted flanged joints, due to numerous involved factors.

In general, a sealing gasket is of circular shape and is composed of a sealing element, more or less soft, that may be contained in a metallic frame. The leak that occurs is due to the porosity of the sealing element exposed to the pressure of the fluid (liquid or gas) contained in the assembly. This porosity depends on the bolt load and internal pressure, the surface characteristics of the flange in contact with the gasket, the operating temperature and the exposed operating time, the two last factors having an effect on the aging of the sealing element. These factors cause leakage, contribute to the reduction of the safety factor and increase the overall cost due to resulting damages and loss of media. Consequently, the works in this area have aimed at understanding the types of leaks, the determination of the factors involved for a given system and the optimisation of the critical factors for the reduction or the elimination of leakage.

In general, leaks are considered to be of two different natures, namely those that are considered large leaks, referred to as a “gross leak” or “blow-out”, and those falling in the small leakage category, called “emission” leaks. The gross leak is associated with the hydrostatic end load of the joint mechanisms. The hydrostatic end load is defined as the case of the equilibrium of liquid and the pressure exerted by liquid at rest. Gross leak may occur when the hydrostatic end force on a joint is closely equal to the total design bolt load.

Such situation may be seen when the bolt load has been reduced due to, for example, creep and relaxation (time-dependent and permanent deformation at elevated temperature and static mechanical stresses during the service) and when the gasket stress is closely equal to the internal pressure, forcing the joint apart. Gross leakage also can lead to the rupture of the joint and gasket, when the internal pressure is greater than the bolt load. Factors such as bolt stress, joint stiffness, joint elasticity, and bolt size play an important role in the gross leak. Likewise, joint aging and sudden temperature change or temperature disturbance are contributing factors. The physical phenomena, which greatly contribute to the bolt load loss and hence result in the gross leakage, are: elastic distribution, static and transient temperature differences, and joint relaxation. Elastic distortion is caused by the changes in the internal pressure and the elastic deformation of the materials involved in the flanged assembly.

On the other hand, small leaks, or fugitive emission leaks, are more frequent and are associated with gasket mechanical behaviour and characteristics, internal pressure and flange surface characteristics. Joint emission depends on the gasket type and flange face surface characteristics (roughness and form) as well as gasket aging and degradation. Joint emission increases with joint relaxation that causes gasket tightness reduction, and it is due to loss of gasket thickness, gasket creep, as well as flange and bolts creep. Emission leaks are unnoticeable if not monitored and may result, in long term, in serious damages to piping systems and plant. Emission leaks may also transform into blow-out.

The most important aspects of gasketed bolted flanged joints are their sealing performance and gasket tightness. The main concern of manufacturers and industries is to obtain the “optimal” sealing performance and tightness from the gaskets and the joint. The sealing performance depends on how well the gasket and the joint can maintain a low-leakage behaviour under certain operating conditions. The optimal result is achieved by minimising the leakage rate, thus reducing or preventing the loss of medium. A gasket is evaluated based on its sealability, and is said to be performing if it provides a low leakage rate under the applied load, during the service life.

To date, many researches have considered the effect of the gasket type, gasket geometry and gasket porosity on the leakage rate. Likewise, the effect of gas or liquid and the effect of internal pressure have been extensively analysed, in combination with different gasket properties, at room temperature. Other researches have also considered the gasketed joint's behaviour at elevated temperature. The effect of flange surface characteristics (surface form and roughness) in some degree has been analysed on the static sealing gasket performance in literatures, however to date no conclusive results have been reached due to the complexity involved in theoretical modelling, experiments and analysis of results. In the present research, the results of the experiments on the PTFE, flexible graphite, and spiral wound gaskets show that surface roughness,  $Ra$ , alone does not have a significant effect on the sealing performance, while the surface form has a pronounced effect, especially when the gasket is under low compressive stress. These results demonstrate that all the factors in combination with the surface characteristics (roughness and form) should be considered for a more accurate evaluation of sealing performance of gasketed bolted flanged joints.

Consequently, the proper selection of sealing parameters is very important in modern seal/gasket manufacturing and to end users in petroleum, petrochemical, pressure vessels, and power industries. It constitutes the ultimate goal in planning, production, process

control, safety and cost. An adequate unified method for such a selection has not yet been developed, although there have been many efforts and progress in finding the optimal parameters that can define the sealability of the joints and gasket performance under certain operating conditions, and ultimately achieve a leak free joint.

The previous researches have shown that a complete mathematical and theoretical analysis of the emission of gasketed bolted flanged joints is not yet feasible owing to the complexity of the leakage phenomena, and too many unknown and un-measurable parameters involved. Thus, experimental research and expert's knowledge acquired to date based on field experience are the most common ways of dealing with the leakage phenomena in sealing performance verification. Nonetheless, understanding the experimental results, evaluating and comparing gaskets and flange sealing characteristics to suit particular applications is very tedious, vague, time consuming and complex, and therefore it does not efficiently serve the manufacturers and the end users.

That is why, in addition to the experimental research and analysis performed in this work, we considered interesting to apply in this domain a tool, such as fuzzy logic, capable of dealing with complex systems with vague and imprecise data. Fuzzy logic has been applied, for the past three decades, in many industrial applications for decision-making, prediction and control, and more recently it has gained grounds in engineering, statistics, medicine, computer, and other technological fields.

Thus, as a contribution to the understanding of the leakage phenomena in gasketed bolted flanged joints, this research deals with the analysis of the effect of surface roughness and surface form for the determination of the leakage rate and leakage behaviour for the gasket sealing performance based on the application of fuzzy logic

The objective of this research is to provide an accurate analysis of the flange surfaces in order to obtain a low-leaking joint for given system requirements. The approach to such



complex phenomena considers a series of designed experiments and analysis of the results based on the existing methods. The experiments are designed to relatively reduce the number of run points, experimental time and cost based on the modified ROTT tests. In addition the fuzzy logic approach is introduced for the selection of gasket and sealing surface characteristics in order to achieve minimum leakage rate. This research shows that this simple yet powerful tool can deal with complex, vague and incomplete/missing data, and therefore is able to help simplifying the selection of gaskets and flange surface characteristics.

This thesis is presented by articles, and is broadly divided into two parts. The first part consists of the experimental analysis of flange surface characteristics while the second part introduces the fuzzy logic application for the selection of gaskets and the prediction of their sealing performance. The thesis is constituted of six chapters.

Following a general introduction, Chapter 1 presents a thorough literature review of the existing research in the domain of gasketed bolted flanged joints related to the present research. The synthesis of the thesis is given in Chapter 2.

Chapter 3 presents the experimental approach in the determination of the effect of surface characteristics on the leakage rate and leakage behaviour. This study is presented in the form of an article entitled "*Effect of Surface Characteristics on Compressive Stress and Leakage Rate in Gasketed Flanged Joints*". This article realises an experimental verification of the surface characteristics effect on the leakage rate of different gasket types, namely: PTFE (polytetrafluoroethylene) sheet Garlock Gylon 3504, UCAR flexible graphite sheet G2 and flexible graphite filled spiral wound Flexitallic NPS 4-in. class 600 lbs, using characterisation tests called ROTT (Room temperature tightness) tests.

The ROTT test consists in varying the applied load (stress) of compression on the tested gasket, by increasing or reducing such load according to an established procedure and by

measuring, at each stage the leaks that occur for two levels of helium pressure. The ROTT test used in this research used a simplified procedure, referred to as “modified ROTT test”, for the sake of saving time and used only two loading-unloading cycles as opposed to three cycles as per the standard procedure. The platens surfaces are limited to those machined by turning, milling and grinding procedures.

The analysis of the effect of sealing surface characteristics in combination with gasket properties, system pressure and gasket stress, on the leakage rate and the flow regimes is also presented in this chapter. Consequently, the effect of surface form and roughness on different types of gasket is discussed, and the resulting flow regimes based on different surface characteristics, stress levels and gas pressure are presented.

The experiments performed on different platens surface characteristics and on different gasketing materials reveal that the surface roughness value,  $Ra$ , should be evaluated by considering also the surface form and the machining procedure. The experiments also show that gasket properties, gas pressure, gasket stress, flanges surface macro and microstructure should be considered into the analysis of sealing performance. Nonetheless, the analysis of the leakage phenomena is very complex and the evaluation of all the contributing factors involved cannot be assessed in a precise manner. In addition the uncertainty and the vagueness in evaluating the combined effect of such factors add to the complexity of the analysis of the system.

Consequently, in view of the foregoing, and in order to determine means of reducing the experimental tests points, time and associated cost, a tool capable of dealing with such complex system called fuzzy logic is introduced.

In Chapter 4, simple fuzzy algorithms are developed for the determination of the surface roughness values which result in a minimal leakage rate for the given gasket type and system requirements. This study is presented in the form of an article entitled “*Sealing*

*Performance of Gasketed Bolted Flanged Joints: A Fuzzy Decision Support System Approach*". The experimental results of the room temperature tightness test (ROTT) were used to build and validate the models. The models are limited to platens surface form being machined only by turning procedure, with continuous feed rate. It considers platens surface roughness with three different average arithmetic roughness values.

Chapter 5 presents the concept and the implementation of a fuzzy logic approach in gasketed bolted flanged joints. This study is presented in the form of an article entitled "*Fuzzy Logic Application in Gasket Selection and Sealing Performance*", and considers the determination of optimal sets of parameters for better gasket selection based on the system requirements, taking into account the fact that many unknown parameters affect the leakage rate and the sealing performance. The model is limited to the study of the platens surface characteristics being machined only by turning procedure, with only one surface roughness value. It considers four different types of gaskets. Furthermore, the model considers the gasket performance and the leakage rate evaluation at different gas pressures and different stress levels.

In Chapter 6, fuzzy logic algorithms are developed to predict the leakage rate for a given pressurized system, based on the modified ROTT test procedure. This study is presented in the form of an article entitled "*Fuzzy Logic Approach to Predict Gasket Leak Rate and to Obtain Gasket Minimum Seating Stress*". Different fuzzy algorithms are developed and validated with experimental results based on the gasket types. The experimental results previously presented in Chapter 3 for the three types of gasket, PTFE sheet, UCAR flexible graphite sheet G2 and flexible graphite filled spiral wound are used. The fuzzy rules are defined based on the results obtained from the modified ROTT tests with limited test points. Parameters such as gas pressure, gasket stress, seating and operating stress levels (ROTT Part A and Part B stress levels), surface characteristics (roughness and form), and leakage rate are considered in the fuzzy models.

The fuzzy models are validated using experimental results of conventional ROTT tests. The experiment and fuzzy leak rates results are used to determine the new PVRC gasket constants,  $G_b$ ,  $a$ , and  $G_s$ . These constants are then used to obtain the joint gasket minimum seating stress for different gasket sizes (NPS 2in. to 24in.), ANSI/ASME B16.5, and for different internal gas pressures.

The results on gasket leakage rate and gasket minimum seating stress obtained from fuzzy models predict closely the experimental results. The application of fuzzy logic for the prediction of leakage rate and sealing performance reduces the number of experiments and test points, which consequently reduces experimental time and associated test costs. Therefore, fuzzy logic application has a good potential in the field of gasketed bolted flanged joints.

Finally, a general conclusion that includes recommendations for future research in the field of gasketed bolted flanged joints relating to sealing performance evaluation and leakage prediction is presented.

## **CHAPTER 1**

### **LITERATURE REVIEW**

#### **1.1 Introduction**

There have been numerous researches both theoretical and experimental on the subject of flange design, and gasketed bolted flanged joints for a better control leakage rate. Some of these research have considered the flange size and shape, bending moment effect, bolt load effect, bolt creep, bolting sequence and procedures, and gasket type, width, thickness and material properties, porosity, creep and material degradation. Some others have also investigated the effect of liquid or gas on the leakage rate, the media contained pressure, the gasket behaviour at ambient and elevated temperature, and the effect of temperature, stress and time on the leakage rate and gasket performance. In this chapter, the previous research in the area of gasketed bolted flanged connections which are closely related to the present research are discussed, i.e. the effect of surface contact and surface stress, platens surface roughness and surface form. Furthermore the existing theory of fuzzy logic and its approach to deal with complex, vague and missing data in gasketed bolted flanged joint is presented.

#### **1.2 Contact area and compressive stress**

The seal compression and seal constraint are two important factors dictating the required contact stress between the seal and the joint surfaces to maintain the joint tightness and to reduce the leakage rate. Jofriet et al. (1981) have studied the effect of surface contact stress and contact zone on the flange leakage performance. They considered the influence of the contact stress conditions for bolted flanged connections in the analysis of the

leakage behaviour. They have shown that the location, distribution and magnitude of the contact stress depend mainly on the ratio of the resultant contact stress over the assembly or bolted load.

In addition, the analysis of the location and intensity of the interface contact stress is an important criterion for a safe design of flanges to withstand fatigue failure and to ensure adequate sealing that can prevent or minimize leak. As shown by Jofriet et al. (1981), such analysis with numerical and theoretical approaches are complex and are not feasible without experimental approaches, due to the mixed nature of the boundary conditions on the interfacing surfaces, and because the contact regions are function of the flanges geometry, bolt load, internal pressure, etc.,

Based on the combination of experimental and numerical analysis, and on the consideration of mechanical properties of steel, using finite element models, Pindera and Sze (1973a,b) and Thompson et al. (1976) showed that the diameter of the contact zone depends mainly on the diameter of the flange (loading disk), and that it is independent of the bolthole size. However, it must be mentioned that this remark seems to be subjective. It is well known that the bolt force increases with the increase in the internal pressure of the flange in a non-linear manner that depends on the ratio of the bolts and flange stiffness. However, as stated by Pindera and Sze (1972), if the initial loading is sufficiently high, little increase will occur in typical flange connections, until the ratio of the resultant load to the assembly load exceeds the value of 0.3.

One must remark that the contact stress of the flange face and gasket required for the sealing performance highly depends on the flange mating surfaces. Thus, as far as the flange surface quality is concerned, Jofriet et al. (1981) indicated that as the roughness and waviness of the flange surface increases so does the contact stress level required to close all the free paths between the surface asperities. Therefore, in their studies on the ring-loaded flanges and bolted flanged connections, they indicated that in order to assess

the stress concentration at the critical regions, i.e. the fillet between the pipe end and the flange, the magnitude and distribution of the contact stress must first be determined or known a priori. Jofriet et al. (1981) stated that the results of the experimental and numerical analysis indicate that the location, magnitude and position of the normalized contact stress were independent of the internal pressure of the flange, due to the fact that identical results were obtained in cases with and without internal pressure. As they have mentioned, these results are subjective and similar results may not necessarily be obtained for other flange connections and other loading conditions.

### **1.3 Flange surface characteristics**

Many investigators have examined the performance of static seals with the view of reducing the leakage rate. There exist many publications dealing with gasketed bolted flanged joints, gasket test procedures, fluid effect, gasket characteristics and sealing performance, and contact stress. However, only a few deal with the surface roughness  $Ra$  effect on the gasket performance with the view of reducing the leakage rate. Most research show that the lower the surface roughness is, the better the gasket performance is and therefore the lower the leakage rate is, and this is mainly for metallic gaskets. It must be mentioned that the surface characteristic is interrelated with the contact stress aside from the stress applied by the bolt load exerted on the flanges.

One of the earliest investigations on the flange and sealing surface effect on the gasket may be traced back to the research of Thorn (1942) on the analysis of stress decay in rubber gaskets. Their test results show that if the bolting is not flexible enough, then the gasket joint will be subjected to stress decay, causing leakage. In another investigation on the effect of smooth and wavy flange surfaces, Thorn (1955) reported that the sealability of gasket materials is also affected by the flange surface quality. In his experimental test, three types of gasket materials were tested on two “smooth” and “wavy” types of flange

surfaces. They stated that the seating factors “ $m$ ” values were larger for rougher flange surfaces.

Mitchell and Rowe (1969) worked on the influence of asperity deformation on the gas leakage between the contacting surfaces. They examined the plastic deformation of wedge-shape model asperities, supported by rigid bases. They modelled a total leak rate through all channels between the two rigid mating surfaces by considering that the surfaces are separated by a uniform gap. They stated that the flow between the two surfaces in contact was affected by the way in which the surface asperities were deformed as a result of the contact load. Tückmantel (1990) presented experimental results on the effect of surface pressure on the leakage rate. Payne (1993, 1990) worked on the effect of surface roughness of stock finish turned surfaces, ANSI/ASME Standard B16.5 flanges, on the gasket constants. These are the room temperature gaskets constants  $G_b$ , “ $a$ ” and  $G_s$  for seating and operating conditions as related to a tightness parameter,  $T_p$ , representing the mass leakage rate and internal pressure. These gasket constants are determined from the ROTT test procedure that is being considered as an ASTM Standard. These constants are used to determine the design bolt load for gasketed bolted joints. It is to be noted that the gasket products can be of the forms of sheet or composite constructions. Matsuzaki and Kazamaki (1988) presented results on the effect of surface roughness on compressive stress, and on leakage rate in metal-to-metal seals and metal gasketed seals. It is to be noted that the metal-to-metal seal is the condition where the flange faces of the same or different material being mated together to provide sealant. Typical metal-to-metal seals include the flanges with tongue and groove, annular rise and flat, and two annular rise faces. The overall results presented by Matsuzaki and Kazamaki indicate that the evaluation of surface roughness effect is complex and depends on the surface form, the gasket type, and the applied stress. They also stated that the desirable compressive stress for sealing must be nearly 1.5 times the tensile strength of the gasket material, regardless of the extend of surface roughness ( $R_{max} \approx 7.87 \sim 8661.4 \mu\text{in}$  ( $0.2 \sim 220 \mu\text{m}$ )).



Greenwood and Williamson (1966), and Greenwood and Tripp (1970-71) presented works on the contact of nominally flat rough surfaces. Shimomura et al. (1991) studied the relationship between frictional characteristics and surface condition of mechanical seals. Derenne and Bouzid (1997) have performed a preliminary experimental study on the effect of flange surface finish at room temperature on gasket tightness and emissions. In most cases it has been found that the rougher the mating surfaces the larger is the leakage rate, and as the stress level increases the leakage rate decreases, due to the deformation or the penetration of surface asperities and higher contact area. Furthermore, the gasket type and the gas pressure also played an important role on the leakage rate results, from system to system.

Rathbun et al. (1963) determined that although gasket stress plays an important role on the leakage rate of gasketed joints, above a certain critical contact stress, the seal leakage can only be reduced by a further increase in the stress, whereas the increase of the path length does not reduce that leakage. Similar remarks were made in the investigation of Mitchell and Rowe (1969). Such remarks are based on the assumptions that the gas/fluid used in the test is an incompressible laminar flow through a uniform peripheral gap whose height is calculated to give an equivalent volume, and that there is a fixed/constant load available at all time.

As the contact area increases due to the increase of load/stress, the gaps between the mating surfaces become much smaller than characteristic dimensions of actual leakage paths. It is believed that this is due to the surface irregularities being filled up due to the increase of gasket stress level. Rathbun (1964b) has performed an experimental investigation of the leakage rate of helium through annular shaped sealing systems, taking into the consideration the leakage rate as a function of sealing stress for various combinations of material properties and sealing surface finish. Furthermore, he has analysed the leakage rate based on material deformation results due to loading stress.

Following his earlier work, Rathbun (1965) presented an experimental investigation on the effect of surface finish on leakage rate of metal-to-metal and metal-gasketed seals. Four surface finish were subject of the tests: diamond burnishing, fine circumferential machining, coarse circumferential machining and radial grind surface finish. Metallic gaskets such as: Indium, Lead, Aluminium, Copper, and Nickel were the subject of the tests. From these investigations he concluded that the "rough sealing surface causes sealing to be affected by elastic gasket deformation, and is quite unstable during removal of load"; "...the soft gasket materials which experience gross plastic deformation at low stress levels appear to have better potential in static fluid connector design than harder metal"; and also "if the sealing of a gasket system is caused by plastic flow of the materials mated, then the seal is very insensitive to removal of the deformation-causing stress". In view of this, the more plastic deformation required of the gasket materials to achieve a seal, the less sensitive the system is to stress removal.

Rathbun (1965) showed that the surface finish on the gaskets played a very small role in the overall sealing characteristics, as long as the materials of the flange face surface, to which the gaskets were mated possessed a yield strength significantly higher than the gasket yield strength, i.e. as low as 1.3 times under normal operating conditions, and at least 2.75 times the gasket's yield strength for a safe design. Further manipulation of the tests data resulted in the new observations. As a result, Rathbun (1965) remarked that the leakage, as a function of stress, is sensitive to surface finish but not to gasket materials (indicated earlier above), when gasket configuration was kept constant and the experimental data of the leakage rate were plotted versus the applied stress, on semi-log paper, and were grouped according to sealing surface finish. In addition as concerns the seal width he stated that it is not rationally possible to select a seal width by taking into consideration the effect of surface finish and the lack of uniformity of mating. He also indicated that different surface finishes result in different true area of contact, from system to system, under the same stress level condition. Nonetheless the area of contact itself is not an adequate prediction for sealing performance.

As concerns the state of the flow Rathbun (1965) showed that by plotting the log of leakage rate versus the log of internal gas pressure, the flow is in molecular regime when the slope of the line is equal to one, and if the slope is equal to two, laminar viscous flow is present.

The effect of gas pressure and gas properties in combination with surface characteristics have also been the subject of investigation on the sealing performance and on the nature of the flow regimes. Chivers et al. (1975) investigated the relationships between gas properties and surface roughness, and discussed the leakage flow regimes that resulted. They considered the sealing behaviour for a high gas pressure system combined with surface properties that defined the leakage flow regimes. Consequently, they stated that the flow regime is dictated by the path size, as a result of the residual surface roughness that is caused by machining process or by damages during assembly. They emphasised that, in the case of metallic gaskets, a radial scratch along the mating face would increase the leak rate greatly.

There are no general agreement on the specification of surface quality for sealing purposes, because of a lack of experimental data and investigation on the effect of surface quality and surface roughness on the gasket behaviour and leakage performance. However, some investigators have shown the importance of surface quality for the high integrity seals. An investigation by Peklenik (1968) has shown that a requirement for the high integrity seals is the fine turning surface machining with arithmetic average surface roughness about  $Ra = 55.11 \mu\text{in}$  ( $1.4 \mu\text{m}$ ). Chivers et al. (1974 & 1975) also investigated such surface roughness produced by fine turning surface finish, which was subjected to a series of compression. They analysed the residual peak to valley heights of the surface under test. Several gasket types were used, which included mostly the metal-to-metal seals so as to eliminate the permeation effect. They also used rubber and compressed asbestos fibre seals to consider the effect of permeation on the leakage rate. They found

that under atmospheric pressure of 30 to 40 psi (0.207 to 0.276 MPa), a laminar flow would dominate any flow losses, whereas, a molecular flow does not occur in this condition. But, some transition flow paths were observed. They indicated that in the case of scratches on the surface some larger leakage paths will exist that results to the creation of turbulent flow regime losses.

Leahy (1971) investigated the sealing performance with elastomeric materials and their applications on valve seal design for high pressure. He considered the deformation of a rough elastomer in contact with a smooth rigid body. He modelled the surface roughness as cylinders, and used elastic analysis to derive the stress required to eliminate the roughness on the seal causing leakage. He showed that the required sealing stress is a function of height of the surface asperity and the half base width of asperity. Thus he suggested that a parameter for assessing seal performance could be the surface slope, which is the ratio of the height to the half base width of asperity,  $a/w$ . It was shown that the lower the slope value (ratio value) the lower the required sealing stress.

Chivers and Hunt (1978a,b) investigated the effect of surface roughness and elastomeric sealing on the leakage performance of gasketed joints. Various factors affecting the leakage dominated by the permeation component were considered. They showed that the leakage integrity attainable is limited by the permeation due to sealing materials, and that the effective seal compression is related to surface finish, with respect to both factors of the surface arithmetic average roughness value  $R_a$  and the surface slope distribution.

As a result of sponsored research project of TTRL group by the Pressure Vessel Council committee of the Long Ranged Flanged Joint Improvement Program, Bazergui and Marchand (1984) presented work on the effect of surface finishes of flange face on the emission and gasket performance. The experimental results are published in the PVRC's Gasket test program II of the "Milestone" work. The surface roughness of the flange face ranging between 32  $\mu\text{in}$  (0.81  $\mu\text{m}$ ) to 1000  $\mu\text{in}$  (25.4  $\mu\text{m}$ ) Arithmetic Average Roughness

Height (AARH,  $Ra$ ) were investigated on the tightness of double jacketed, DJ, spiral wound, SW, and compressed asbestos, CA, gaskets in which the results of test data were obtained in terms of tightness, stress and deflection. It was concluded that for SW and DJ gaskets the platens surface finish has an effect on the tightness. However, for SW gasket all surface finishes tested provided the same order of magnitude of tightness factor  $L_p$ , which lumps pressure and leak rate into a single parameter. They concluded that surface finish has no pronounced effect on CA gaskets.

Payne (1990) discussed that the gasket type and the bolt preload have more influence on the leakage rate than does the surface finish. The experimental results of Payne (1992) show that flange face surface quality plays an important role in the emission, such that a serious radial scratch across the contact area of the jacketed gasket facing may increase the emission rate to 10 fold or more. Payne (1993) presented work on the effect of flange surface finish on the gasket constants for steel jacketed and other types of gaskets. In his work the data obtained by Bazergui and Marchand (1984) was used to evaluate the effect of flange facing surface finish in terms of deflection, stress and tightness. The surface finish effect was analysed on the defined gasket constants for Double jacketed (DJ) asbestos millboard filled gaskets, and spiral wound (SW) asbestos filled gaskets. It was concluded that the surface finish affects gasket performance, and it has a great influence on the leakage rate of DJ gasket, especially for small and low pressure joints where a coarse surface finish required a twice the design bolt load. Whereas the surface roughness effect was less pronounced on the performance of SW and CA gaskets. Furthermore, it was indicated that DJ gasket performs best with surface finishes 250  $\mu\text{in}$ .

Friction and surface topography are other elements that have an affect on the gasket performance. Friction may cause between the flange face and the gasket at the time of loading due to stress caused by bolting. Friction also is caused by the gasket movement on the flange surface due to the internal pressure exerted on the inner face radius of the gasket at the operating conditions. As a result Shimomura et al. (1991) argued that the

quality of the sealing surface is affected by the friction and asperities of the flange face. They studied the relationship between frictional characteristics and surface condition of mechanical face seals. Their experimental results were also analysed between topography of sealing surface of the mechanical face seal and sealing characteristics. They showed that the radius of curvature of the asperity in profiles of roughness curve of the mating ring has great influence on the friction and wear of the mechanical seals and, ultimately it has remarkable effects on the sealing characteristics of the seal.

Matsuzaki and Kazamaki (1988) showed that the surface roughness greatly effect the stress distribution on the mating surfaces caused by compressive load on static seals. Matsuzaki et al. (1992) have investigated the sealing performance based on the effect of contacting state of knife-edge seals by varying the apex semi-angle and apex width of the knife-edge. For the purpose of determining the required contact pressure for sealing, they classified the contacting state of the knife-edge seal into three types, according to the apex width of the knife-edge, as: penetration type with a narrow flat apex ( $b \leq 50 \mu\text{m}$ ), indentation type with a narrow flat apex ( $b \geq 500 \mu\text{m}$ ) which will be impressed onto the mating face, and intermediate type with a narrow flat apex ( $50 < b < 500 \mu\text{m}$ ). They determined that in the case of penetration type contact of knife-edge seal the value of compressive force per unit length, for the sealing purpose, was minimum due to the narrow apex width of the knife-edge. They also stated that these classifications can satisfactorily be applied to the case of high pressure or vacuum sealing devices, and that conversion from type to type (i.e. from penetration to indentation or intermediate case) does not occur, if the experimental conditions (applied compressive stress) are changed. The observation presented in the works presented by Matsuzaki and Kazamaki (1988) and Matsuzaki et al. (1992), indicate that the circumferential knife-edge apexes on surfaces can be improved for better sealing.

Much work has been done in the area of gasket characterization and sealing performance evaluation in gasketed bolted flanged joints. However, to date, the effect of surface characteristics (roughness and form) on the leak rate, in combination with gasketing material, gasket stress and gas pressure, have not been studied. These effects are addressed in this research.

#### **1.4 Fuzzy logic application**

In most real situations, because of the complex nature of systems, the determination of crisp values (an exact real number) is not feasible, unnecessary and most of the time not appropriate. Inversely, it might be best to present the system parameters with a range of data instead of crisp values. In addition, most real situations require data collection and data analysis to estimate properly the performance of the system. In data processing systems the objective is to understand the phenomena involved and to evaluate relevant parameters quantitatively. This requires the modelling of the system either analytically or by experimental design models. Analytical modelling uses mathematical and physical principles, whereas experimental modelling (empirical equation) is used when mathematical modelling is not possible. Thus, an intelligent soft computing system capable of dealing with the uncertainties of real situations involved in such models is required. Once the model of the system is made, the analysis of the system through, for example, sensitivity analysis, statistical regression, and analysis of variance, can be performed. As the complexity of the systems under investigation increases, the precision in the definition of statements becomes ambiguous. Furthermore, the larger the system is, the more parameters become involved and, as a result, the presentation and association of the ideas becomes vague, and statements about the systems tend to lose their meaning.

Zadeh's approach to deal with complex systems and imprecise information led him to present the fuzzy set theory, (Zadeh 1965). As a result, Zadeh's pioneering work in 1965,

and his seminal paper in 1973, (Zadeh 1973), persuaded other researchers to use the fuzzy rule-based approach for the analysis of complex systems and for decision making. Other works of Zadeh that provided support in this domain are the: probability measure of fuzzy events (Zadeh 1968), concept of linguistic variable and its application to approximate reasoning (Zadeh 1975), fuzzy set and basic theory of probability (Zadeh 1978), theory of approximate reasoning (Zadeh 1979), and fuzzy logic (Zadeh 1988).

Fuzzy set theory is a powerful tool capable of modelling any system with uncertainties, fuzziness and incomplete information obtained from real-world situations and experimental data. Tackling the problems involved in real-world situations, Mamdani (1977) was one of the pioneering researchers in the application of fuzzy set theory in the control system and decision making, which established the industrial application of this theory. Larsen (1980) has published his work related to the industrial application of fuzzy logic control. Theories and other researches pertaining to fuzzy logic and neural networks can be found in the publication of Tsoukalas and Uhring (1997). The work of Dubois and Prade (1980) presents valuable information on the theory and applications of fuzzy sets and systems. Balazinski et al. (1993) presented his work on the fuzzy logic application for decision-making and selection of cutting parameters in a machining process. Based on the fuzzy logic theory of Zadeh (Zadeh, 1965, 1973, and 1988), Balazinski et al. (1995) developed a fuzzy logic tool as a decision support system, called Fuzzy-Flou.

Industrial applications related to gasket selection and gasket sealing performance are considered to be highly complex with a high degree of uncertainty and cannot be accurately addressed by mathematical modelling. Up to now, there has been no research done on the application of fuzzy logic in the domain of gasketed bolted flanged joints. Therefore, this research addresses the uncertainties and complexities of the sealing performance of gasketed bolted flanged joints by applying fuzzy logic in gasket selection and leakage prediction.



## **CHAPTER 2**

### **SYNTHESIS**

With fugitive emissions becoming one of the most important environmental and safety issues, more emphasis is put on solutions to minimize such emissions through gasketed bolted flanged joints. In order to obtain a leak free joint, the process of properly selecting the key parameters is vital. Therefore one must take into consideration all external and internal parameters affecting the gasketed bolted flanged joint system.

The objective of this thesis is to study the effects of surface characteristics on the leakage rate and leakage behaviour of gasketed bolted flanged joints. The thesis also presents the application of fuzzy logic and fuzzy set theory on gasket selection and leakage rate prediction of the gasketed joints for their sealing performance.

The theoretical and experimental approaches on the effect of surface characteristics on the leakage rate and leakage behaviour are presented. Three types of gasket commonly used in industries are the subject of the research, namely: PTFE (polytetrafluoroethylene) sheet Garlock Gylon 3504, UCAR flexible graphite sheet G2 and flexible graphite filled spiral wound Flexitallic NPS 4-in. class 600 lbs. The room temperature tightness test (ROTT) procedure is used for gasket characterisation.

The ROTT test consists in varying the applied load (stress) of compression on the gasket, by incrementing and decrementing such load according to an established procedure and by measuring at each stage the leakage rates that occur for two levels of helium pressure. The ROTT test in this research has been modified for the sake of reducing the number of test points and saving experimental time. The modified ROTT test procedure uses only two loading-unloading cycles instead of three. The gas pressure throughout the test is kept

constant. The platens surfaces used are of raised face type and are machined by turning, milling and grinding procedures. Although the milled surfaces are not commonly used for flanges in industries, they are chosen in this research because of their great differences with the turned and the ground surfaces, which may reveal interesting results on the leakage rate and flow regime.

One of the objectives of the tests is to characterize gasket leakage behaviour, and to reduce emission accordingly. In this research the effect of surface characteristics on the leak rate is discussed. The sensitivity of the sealing phenomenon to the sealing surface characteristics, gas pressure and stress level, and to the cyclic load and unload effect is investigated. The resulting leakage rates and flow regimes are discussed based on the effect of surface form and roughness on different types of gasket under different applied stress levels and gas pressures.

The flange surface characteristics, micro and macrostructure, depend very much on the machining procedure used to produce the flange faces, which define the interconnecting interfacial leak paths in contact with the gasketing material. In general, surfaces produced with milling procedures, have radial grooves, as opposed to those produce by turning procedure that have circumferential grooves. The grinding procedure produces surfaces with literally no form other than deep tiny radial grooves that result from the abrasive grinding wheel.

The experimental results indicate that, except for the ground type surfaces, the flange roughness value  $Ra$  (average arithmetic height) does not have a pronounced effect on the sealing performance. Therefore, it should be considered in combination with the surface form and machining procedure. The results indicate that the surface form is a determining factor on the leakage rate and on the flow regime of the gasketed joints since it defines the geometry of the interfacial leak paths and the leak paths through the gasket material, that are function of gasket stress, gasket properties and internal gas pressure. The

experimental results indicate that the turned surface machining forms offer tighter sealing than other surfaces, for all gasket types, under the same operating conditions.

It is also shown that the sealing performance of the surfaces produced by different machining procedures is very much influenced by the gasket material, gasket stress and gas pressure. For an example, in the case of PTFE gasket, the rougher ground and milled sealing surfaces are more sensitive at low stress levels. However, at high stress levels most surface characteristics result in a similar sealing performance. As regards the flexible graphite G2 and the flexible graphite filled spiral wound gasket types, the surface characteristics are more sensitive to the combination of gasket stress and internal gas pressure.

The effect of sealing characteristics varies depending on the gasket properties, gas pressure, gasket stress and the flange surface characteristics. Up to now, the effect of surface characteristics on the sealing performance of gasketed joints has not been considered in the evaluation of the gasket leak rate. The results presented in this research demonstrate that the surface characteristics change substantially the joints leak rate and flow regimes, especially at low stresses. Consequently, when evaluating sealing performance of gasketed flanged joints, the effect of surface characteristic should be considered in combination with all other factors.

The parameters influencing the sealing phenomena such as gas pressure, gasket stress, sealing surfaces macro and microstructure (form and roughness), gasket properties, gasket porosity, leak path size and length as result of gas pressure and stress, thermal effect, etc. are not precisely measurable. In addition, their combined effects are not precisely quantifiable which adds to the vagueness and complexity of the sealing characterisation.

To date, gasket characterisation has been mostly done based on the analysis of a series of lengthy and costly tests. The analyzes and interpretation of the experimental results require experts' skills "know-how" and intuitive sense acquired through long-term experience in this domain. The vagueness of the sealing phenomena requires a tool capable of dealing with complex problems for which analytical and mathematical approaches do not exist, are not feasible, or are too complex and costly to develop. Consequently, the present work applies the concept of such a tool, called fuzzy logic, that is capable of dealing with such vagueness.

In this thesis, simple fuzzy algorithms are developed for the determination of the flange surface roughness that results in a reduced leakage rate for the given gasket type and system requirements. The experimental results of the room temperature tightness test (ROTT) are used to build and validate the fuzzy models. The models are limited to platens surface forms that are machined by the turning procedure with continuous feed rate. The models consider platens surface roughness with three different average arithmetic roughness values. The research also describes a fuzzy decision support system (FDSS) and its application in the selection of sets of optimal parameters to characterize the gasket sealing performance in gasketed bolted flanged joints. The fuzzy logic is applied considering the gas pressure, gasket deflection, and leakage rate based on the required gasket stress and flange surface roughness.

Other algorithms are developed for the selection of gaskets based on a given system requirements, taking into account the fact that many unknown parameters affect the leakage rate and the sealing performance. The models are limited to the study of the platens surface characteristics being machined by turning procedure, with only one surface roughness value. The models consider four different types of gasket and their leakage rate performance at different gas pressures and different stresses.

Finally, other fuzzy logic algorithms are developed to predict the gasket leakage rate for a given pressurized system. The algorithms are developed for different types of gasket properties that cover a wide range of gaskets commonly used in industrial applications, namely PTFE, flexible graphite G2 and spiral wound. To closely estimate the real operating conditions of the ROTT test, different parameters are incorporated in the fuzzy algorithms premises and consequents. Such parameters are: gas pressure, gasket stress, seating and operating stress levels (ROTT Part A and Part B stress levels), surface characteristics (roughness & form) and leakage rate. The fuzzy rules of these algorithms are defined based on the results obtained from the modified ROTT tests with limited test points. The fuzzy models are validated using the experimental results of conventional ROTT tests. The results indicate that the fuzzy models, developed based on limited data, are capable of predicting the gasket leakage rate compared with experimental results.

Furthermore, the leak rates obtained from the fuzzy algorithms are used to determine the PVRC gasket constants parameters ( $G_b$ ,  $a$ ,  $G_s$ ) for each gasketing material. The gasket constants from the ROTT tests and the fuzzy algorithms are used to determine the gasket minimum seating stress for different gasket NPS sizes at different helium gas pressures. The results obtained from the fuzzy algorithms closely correspond to those obtained from the experiments. The experimental observations based on the ROTT tests and the fuzzy algorithms are compared and presented in tables and graphs.

The primary validation test of the fuzzy models indicates that the fuzzy system can determine a set of system parameters for which a gasket can be characterized. The results in this research demonstrate that fuzzy logic can be used to deal with the complexity of the sealing phenomena and to increase the accessibility of design parameters for leakage control. Once the fuzzy decision support system is developed, the gasket leak rate prediction and system parameters selection can be made easily and accurately.

Up to now, no other research has been done on the application of fuzzy logic in the domain of gasketed bolted flanged joints. This research shows that the application of such a system would significantly reduce the number of experimental runs and tests points, facilitate the analysis of the results, save time and substantially reduce experimental costs.

Finally, a conclusion along with recommendations for future research in the field of gasketed bolted flanged joints, relating to sealing performance evaluation and leakage prediction is presented.

## **CHAPTER 3**

### **EFFECT OF SURFACE CHARACTERISTICS ON COMPRESSIVE STRESS AND LEAK RATE IN GASKETED FLANGED JOINTS**

J. Arghavani, M. Derenne and L. Marchand

Department of Mechanical Engineering, Applied Mechanics,

Ecole Polytechnique of Montreal

Montreal, Quebec, Canada

#### **3.1 Presentation of the chapter**

In the present chapter the effect of surface characteristics on the leak rate and gasket performance is experimentally analyzed. Platens surfaces are produced with turning, milling and grinding procedures. Each surface form is produced with different surface roughness values  $Ra$ . As a result, the effect of surface characteristics on the leak rate, and leak behavior is determined by testing three different gasket types, namely PTFE, flexible graphite and spiral wound. The experiments are designed considering the effect of gasket stress ( $S_g$ , psi.) and internal gas pressure ( $P$ , psig). The experimental results are analyzed and presented in graphical form.

### 3.2 Abstract

The effect of surface characteristics on compressive stress and leak rate in gasketed flanged joints is discussed qualitatively and quantitatively based on experimental verifications. The sensitivity of the sealing phenomenon to the sealing surface characteristics, gas pressure and stress level, load and unload is presented. Sealing surfaces produced with grinding, turning and milling procedures of different roughness values are the subject of the tests with three types of gasket namely: shived cut (virgin) polytetrafluoroethylene sheet (PTFE), flexible graphite sheet (G2), and spiral wound with flexible graphite filler (SW). The experimental results indicate that for sealing performance evaluation, the flange roughness value  $R_a$  (average arithmetic height) should be considered in combination with surface form and machining procedure. Surface roughness of approximately the same  $R_a$  value can be obtained from different surface forms produced by different machining procedures. For instance considering the ground type sealing surfaces, the rougher the surface (larger  $R_a$  value) the more pronounce its affect on sealing performance at different stress levels and gas pressures, and depending on the gasketing material. Consequently milled surfaces produced by different machining procedure have different surface characteristics, which behave differently depending on gasket material, gasket stress and gas pressure. In a general statement, the platens surface forms are found to be the determining factor on the leak rate and leak flow regimes for gasketed bolted flanged joints. It is shown that for PTFE gasket, the rougher ground and milled sealing surfaces are more sensitive at low stress levels and high internal gas pressure. However, at high stress levels (S3 to S5) most surface characteristics resulted in a similar sealing performance. The surface characteristics in combination with gasket stress level and internal gas pressure had also a significant effect on the sealing performance of graphite and spiral wound gasket types, at both low and high stress levels.

**Keywords:** Surface roughness and form, compressive stress, gas leak rate, flow regimes.



### 3.3 Introduction

Gaskets are used extensively in industrial applications to prevent gas leak through bolted flanged joints by filling in the flange surfaces imperfections and roughness. Many investigators have examined the performance of static seals with the view of reducing their leak rates. There are many publications dealing with gasketed bolted flanged joints, test procedures, fluid effect, gasket characteristics and sealing performance, however, only a few deal with the effect of surface roughness  $Ra$  and surface machining form on the gasket performance. In most papers it is shown that the lower the surface roughness is, the better the gasket performance is and the lower the leak rate is, and this being mainly valid for metallic gaskets. Bazergui and Marchand [1] presented a test procedure for the determination of gasket properties at room temperature. Bazergui and Marchand [2] further presented a work on the development of tightness test procedures for gaskets used in elevated temperature. Bazergui and Louis [3] presented experimental results on the effect of various gases in gasketed joint performance. Bazergui, Marchand and Payne [4] worked on the effect of fluid on the sealing behaviour of gaskets. Marchand and Derenne [5] presented experimental results on the fugitive emission characteristic of gaskets. Chivers, Hunt, Roger and Williams [6] presented work on the relationship between gas properties and surface roughness, and discussed flow regimes, on metallic gaskets; they argued that a radial scratch along the mating face would increase the leak rate greatly. Mitchell and Rowe [7] worked on the influence of asperity deformation on the gas leak between the contacting surfaces. Tückmantel [8] presented an experimental result on the effect of surface pressure on the leak rate, showing that leak follows an exponential law. Rathbun [9] presented a work on the sealing performance of the metal-to-metal and metal-gasketed seals. Bazergui, Marchand and Payne [10] presented their work on the effect of fluid on the sealing behaviour of gaskets. Payne [11—12] worked on the effect of surface roughness of stock finish turned surfaces on the gasket constants. Matsuzaki and Kazamaki [13] worked on the effect of surface roughness on compressive stress of static seals. Derenne and Bouzid [14] have performed preliminary experimental

studies on the effect of flange surface finish at room temperature of gasket tightness and emissions. Greenwood and Williamson [15] and Greenwood and Tripp [16] presented their works on the contact of nominally flat surfaces, and two nominally flat rough surfaces, respectively. Shimomura, Hirabayashi and Nakajima [17] studied the relationship between frictional characteristics and surface condition of mechanical seals. The concept of tribology and properties of materials being the fundamentals to analyse the contact mechanism in this domain can be found in many publications similar to those presented in the works of Halling [18] and Askeland [19], respectively. The concept of physics of flow through porous media is very well presented in the work of Scheidegger [20].

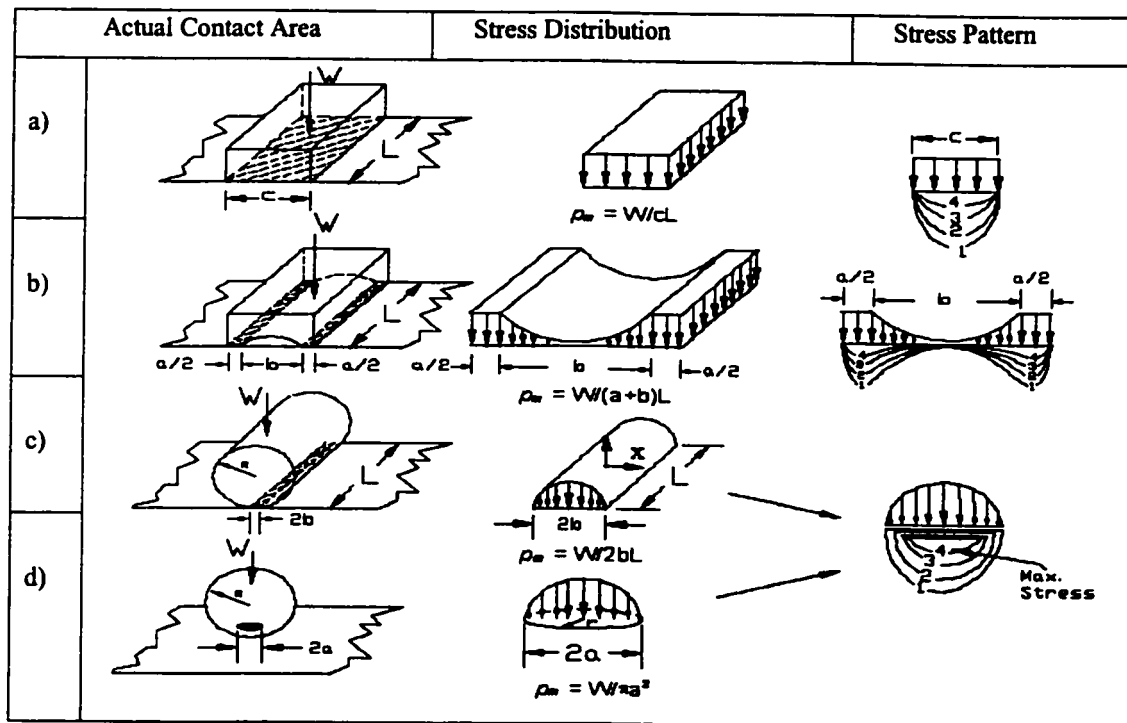


**Figure 3.1.** Pressure distribution and stress pattern for (a) A flat, (b) A groove with flat edges, (c) A cylinder and (d) A sphere, [18].

It is worth mentioning at this point that based on the theory of elasticity, the stress distribution and stress pattern for different contact areas can be defined as in Figure 3.1. Furthermore, Scheidegger [20] argued that porous medium may be presented by bundle of parallel capillaries of uniform diameter  $D$ , thus it is assumed that flow through gasket and flange interface is laminar then if there are  $n$  capillaries per unit area, the viscous laminar flow Hagen-Poiseuille equation for compressed ideal gases is:

$$L_{rm} = \frac{n\pi D^4}{128L} \frac{1}{\nu} \frac{1}{2P^*} (P_1^2 - P^{*2}).$$

Consequently, in gasketed flanged joints, depending on the flange surface characteristics, the leak paths on the mating surfaces and those due to the gasket porosity will be affected by the flange surface characteristics. Likewise it affects the pressure distribution through the leak paths from the high to low pressure side, Figure 3.2. Thus considering that the pressure in the larger section (gas chamber) is constant, then the pressure in the smaller section the capillary tube drops along gas flow direction. For uniform capillaries along leak path (i.e. width of the gasket) the pressure variation along the capillaries drops uniformly, this hypothetical assumption can be regarded as a gasket being in contact with smooth grind surfaces. However, if hypothetically it is assumed that the capillaries are deformed due to the platens surface form, in which multiple chambers are formed along the capillaries then the pressure variation along the gasket drops in exponential form. Such a hypothetical assumption can be associated to the gasket being pressed between platens with turned or milled surfaces, which generate multiple micro-chambers along the pore channel in the gasket. Based on the above hypothesis, gasket pore channels shape formation due to surface compression and platens surface form is shown Figure 3.2.

In general, the leak rate and the flow regime depend primarily on the leak path size, the equivalent diameter  $D$  and length  $L$ , and the mean free path length  $\lambda$  which is defined as the average distance a molecule of a specified type travels in the gas phase at the

prevailing pressure before colliding with another molecule of the same type. Mean free path increases with the increase in temperature and decreases with the increase of pressure and of the molecule size. Other factors also affect the sealing performance such as: fluid type, gasket material, gas pressure, temperature, gasket compressive stress and flange face roughness and form. The effect of surface form and roughness on the static sealing gasket performance have been analysed to some degree in literature.

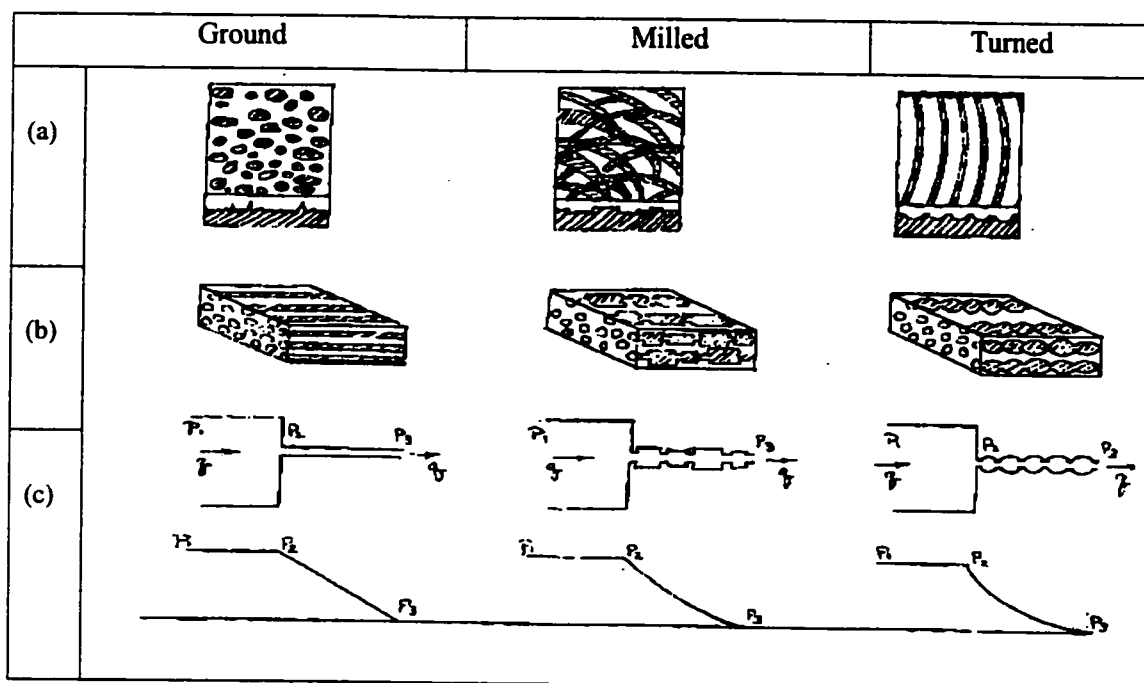


**Figure 3.2.** Machined surfaces and their effect on gasket pore deformation and gas pressure distribution:

- (a) Characteristic of ground, milled and turned surfaces.
- (b) Gasket pore and surface deformation with respect to the sealing surface form, [20].
- (c) Gas pressure distribution through the gasket and sealing surfaces, [18].

In this paper we examine the effect of surface characteristics on the leak rate and on static gasket sealing performance for a PTFE sheet (Garlock Gylon 3504), a flexible graphite sheet (UCAR GHR), and a flexible graphite filled spiral wound gasket. It is shown experimentally that for a given gasket, platens identical in material and surface roughness value  $Ra$  yield different leak rates depending on whether the surfaces are machined by turning, milling or grinding procedures. Experiments are carried out by applying different levels of gasket compressive stress and different gas pressures, as per modified ROTT test procedure described later in this chapter.

This chapter is divided into two broad sections of theoretical and experimental analysis. The theoretical section is divided into the followings. The theoretical analysis of the surface form and surface roughness describes the micro and macrostructure of the surface. The theoretical analysis of the leak paths and leak rates are presented based on the effect of surface form and contact stress, as well as the effect of helium gas pressure. The combined effect of surface form, contact stress and helium gas pressure on the leak rate and sealing performance is also presented theoretically.

In the experimental section the test apparatus is described in details, where figures and photos are presented for a better visualization. Then the platens surface characteristics and machining procedures used to produce them are presented proceeding the hypothesis to describe their effect on the gasket stress, sealing performance and the leak rate. Then the gaskets types, their material properties and their particular importance on the sealing performance analysis in gasketed bolted flanged joints are described in details. The experiments performed are described and are followed by the analysis of the experimental results on the sealing performance. The experimental analysis section is divided by gasket type, to better describe the effect of flange surface characteristics on the leak rate and on the sealing performance.

### 3.4 Theoretical analysis of surface form and roughness

#### 3.4.1 Quantifying surface roughness

It is most convenient to differentiate between the *roughness*, the small irregularities of surface, and the *form*. In the geometrical tolerancing and dimensioning, when using the term *form* we simply refer to the imperfection/irregularities generated by the machining procedure, that also can be considered as surface *waviness*, due to machining, or the deviation from nominal or the intended machining form tolerances. In the present paper, form is not related to the conventional *form error* which is the deviation from the shape of the surface form ideally intended (e.g. plane, spherical, etc.). The most commonly quoted measure of surface roughness is the average roughness, so called the arithmetic average, or the centre line average (c.l.a.), and shown by the symbol  $R_a$ , as it is defined as the arithmetic mean deviation of the surface height from the mean line through the profile, or the average arithmetic roughness height (AARH), ANSI/ASME B46.1, [21]. It is worth indicating that contact stylus instruments, of consecutive profile transformation, are commonly used for the measurement of surface roughness by profile method. Formally the average roughness  $R_a$ , Figure 3.3A, is defined by the horizontal line passing through the centre of area of the distribution curve,  $f(x)$ , given by equation (3.1).

$$R_a = \frac{1}{L} \int_0^L |f(x)| dx = \frac{\sum_{i=1}^n |f(x)|}{n} \quad (3.1)$$

where:  $y = f(x)$ , is the height of the surface above the mean line at a distance  $x$  from the origin, (ordinate of the curve of the profile),

$L$  is the overall length of the measured profile (evaluation length), and

$n$  is the number of sampling length in one individual evaluation length..

The r.m.s. roughness,  $R_q$ , Figure 3.3A, is defined as the root mean square deviation of the profile, within the sampling length, from the mean line. It is the standard deviation,  $\sigma$ , of the amplitude density function. In other words the r.m.s. roughness,  $\sigma$ , measures the spread of the surface heights about a mean plane for a normal distribution of heights. It is worth mentioning that the values of  $R_q$  in practice are determined within the evaluation length which includes several sampling lengths.

$$R_q = \sqrt{\frac{1}{L} \int_0^L f^2(x) dx} = \sqrt{\frac{\sum_{i=1}^n f^2(x)}{n}} \quad (3.2)$$

Although,  $R_q$  might be a better discriminating factor for the surface roughness than the  $R_a$ , for many surfaces, the value of  $R_q$  and  $R_a$  are similar; for a Gaussian distribution of surface height,  $R_q = 1.25 R_a$ . However, neither  $R_a$  or  $R_q$  give the required information on the shapes form or spacing of the surface irregularities, nor they indicate the probability of finding surface heights within certain limit. The characteristic of the amplitude density curve can be described by two parameters skewness and kurtosis. Skewness is the measure of asymmetry of the profile about the mean line; and it distinguishes between the asymmetrical profile of the same r.m.s.,  $R_q$ , of roughness,  $R_a$ . Whereas kurtosis is the measure of the sharpness of the peak of the distribution curve. Skewness,  $R_{sk}$ , is defined by [21]:

$$R_{sk} = \frac{1}{nR_q^3} \sum_{i=1}^n y_i^3 \quad (3.3)$$

where  $n$  is the number of data point in the profile. Kurtosis,  $R_{ku}$ , is defined by:

$$R_{ku} = \frac{1}{nR_q^4} \sum_{i=1}^n y_i^4 \quad (3.4)$$

The positive skewness corresponds to the surface profile with few long peaks, whereas in the contrary negative skewness is the indication of few deep valleys. A flange surface having positive skewness may result in damage to the gasketing material, due to indentation or penetration into the gasket causing the breakage of the bounding elements. Whereas negative skewness i.e. flange surface with few deep valleys, may require higher gasket compressive stress (depending on the gasketing material) in order to achieve an acceptable sealing performance. The disadvantage is that the application of higher gasket stresses may result in bolt and gasket creep over time. For the purpose of stress distribution between mating surfaces, especially in metal-to-metal surface contacts, when the surface profile distribution is skewed, the value of r.m.s roughness or the standard deviation,  $\sigma$ , of the amplitude density function should correspond to the upper portion of surface profile where the contact between two surfaces take place.

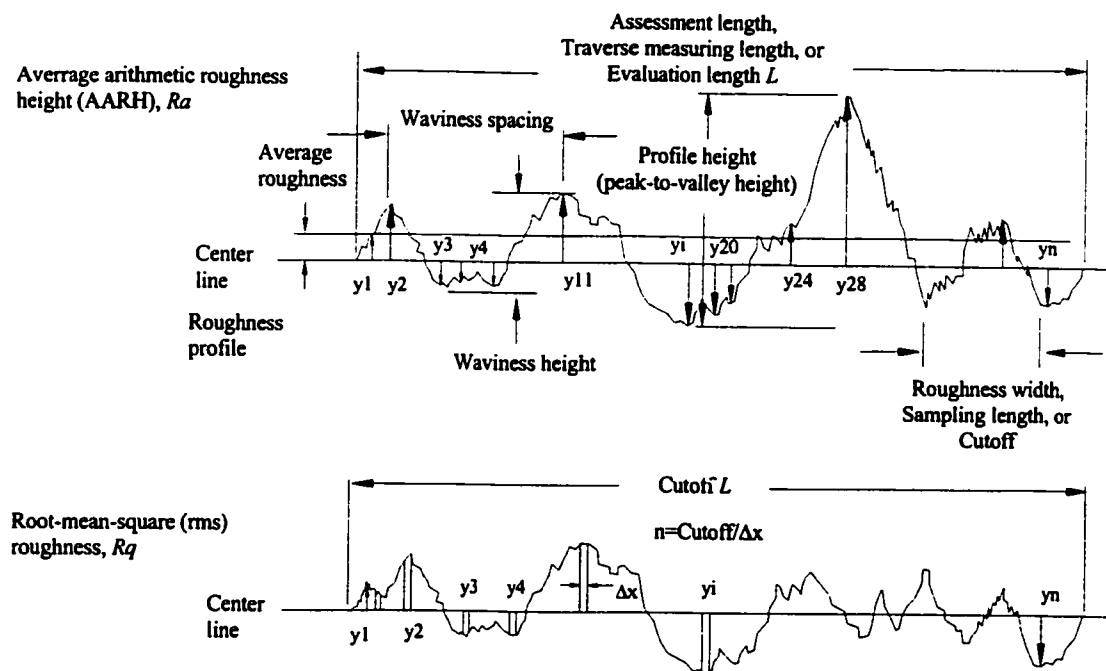


**Figure 3.3A.** Surface roughness average arithmetic height,  $Ra$ , and root-mean-square (rms) roughness,  $Rq$ .



### 3.4.2 Pressure distribution and stress pattern

The platens surface roughness and the asperities shape and size define the stress distribution and stress patterns on the gasket. Furthermore, those are the key elements for surface contact and mean free path. Based on the theory of elasticity, the mean pressure (compressive stress) over a rectangular surface is  $p_m = W/cL$  (Fig. 3.1 a), where  $W$  is the applied load, and  $c$  and  $L$  are the width and length of the exposed surface area. The mean pressure over a spherical body is  $p_m = W/\pi a^2$  (Fig. 3.1 d), where  $a$  is the radius of the circular spot in contact, [18]. When comparing a flat and a groove with flat edges (Fig. 3.1 b), it can be deduced that the groove provides higher stress pattern at each edge and lower stress level at its centre, for the same applied load. Thus, for such surface to provide a complete contact with the gasket, the knife-edge of the grooves must penetrate into the gasket surfaces. As the load increases, the actual size of contact zone also increases due to the increased indentation and penetration of the groove edges. Hence grooved patterned surfaces provide higher contact stress zone on the gasket compared to grind surface, for the same applied load. Milled surfaces also provide higher stress zone on the gasket compared to the ground surfaces since they possess non-uniform knife-edge grooves on their surface. Furthermore, some parts of the grooves generated by milling process are radial while those produced by turning are uniform and circumferential. Figure 3.1 shows the pressure distribution and stress pattern resulting from the contact of a flat, a sphere and a circular groove with flat edges on the gasket. Based on the theory of elasticity, the stress pattern lines with higher number carry the highest stress levels, [18].

### 3.4.3 Microstructure of ground surface

A ground surface may be considered as a surface having asperities height distributions which are nearly Gaussian. The surface asperities can be considered as spherical shape,

and the actual relationship for such contact is usually referred to as Hertzian contact, [18].

For a sphere on a plane, the circular radius of contact spot is  $a = \sqrt[3]{\frac{3WR(1-\nu^2)}{E}}$ . Thus the

pressure distribution on each spherical asperity on the plane is:  $p = \frac{3W}{2\pi a^2} \left(1 - \frac{R^2}{a^2}\right)^{1/2}$ ,

where:  $\nu$  is the Poisson ratio,  $E$  is the Young modulus,  $W$  is the applied load, and  $R$  is the radius of the sphere.

Considering the surface as an array of spherical asperities whose heights follow the Gaussian distribution's law, then the applied load  $W$  can be divided between all the asperities, according to their size and height with a value of  $W_i$ ,  $W = \sum_{i=1}^n W_i$ . Thus the total

real area of contact  $A$  is the sum of all areas  $A_i$ ,  $A = \sum_{i=1}^n A_i$ . If we assume that all asperities

are of the same height, we simply have  $W = nW_1$  and  $A = nA_1$ . As the load increases, the harder platens surfaces, or sealing surfaces, compress on the softer surface of the gasket. Then, the total real area of contact and the number of asperities in contact increase due to the penetration of asperities into the gasket. In the case of metallic gasket, if gasket material is harder than the flange material, the area of contact increases due to plastic deformation of the higher asperities with respect to the general surface asperity distribution. Thus, the area of contact is proportional to the applied load and to the stress level carried by each individual asperity. Since  $a_1 \propto W_1^{1/3}$  then  $A_1 = \pi a_1^2 \propto W_1^{2/3}$ , and by replacing for  $a$ , we have:

$$A = \pi \left( \frac{3WR(1-\nu^2)}{E} \right)^{2/3} = C \cdot W^{2/3}, \quad (3.5)$$

where the constant  $C = \pi \left( \frac{3R(1-\nu^2)}{E} \right)^{\frac{2}{3}}$ .

#### 3.4.4 Surface macrostructure

The microstructure asperities are a good representation of surface roughness when the length of contact is short. However, as the length of contact surface increases one must also take into account the surface macrostructure (form), since asperities alone cannot define the surface irregularities. Thus incorporating the surface asperities model into the surface macrostructure form, one can represent a ground surface with sinusoidal form having spherical micro-asperities on its layout, characterizing the surface roughness profile as shown in Figure 3.3.

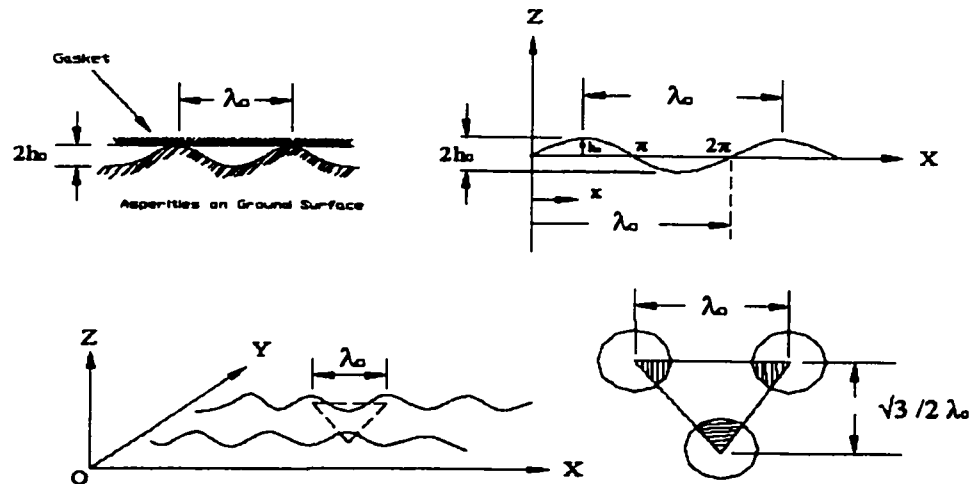


**Figure 3.3.** Representing ground surfaces with sinusoidal form, and spherical micro-asperities.

The sinusoidal curve, representing the flange surface profile, can be described by the radius of curvature of the asperity,  $\rho$ , the wavelength or distance between each peak of the asperity,  $\lambda_o$ , and the height between the peak and valley of the asperity  $2h_o$ . The sinusoidal curve in general is presented as:

$$f(x) = h_o \cdot \sin(\omega t + \phi_o) \quad (3.6)$$

where:  $\omega$  is the circular frequency,  $\phi_o$  is the phase shift,  $h_o$  is the curve amplitude, and  $t$  is the time.

If  $T$  is the period,  $2\pi/T = \omega$  (period of the profile  $T=2\pi/\omega$ ), then the wavelength,  $\lambda_o$ , corresponds to period,  $T$ , ( $\lambda_o \rightarrow T$ ), and distance,  $x$ , corresponds to time,  $t$ , ( $x \rightarrow t$ ). This can be seen from:

$$\omega t = \frac{2\pi}{T} t = 2\pi \cdot \frac{t}{T} \cdot \frac{u}{u} = 2\pi \cdot \frac{t \cdot u}{T \cdot u} = 2\pi \cdot \frac{x}{\lambda_o} \quad (3.7)$$

where,  $u$  is the velocity. The functional form of roughness profile  $f(x)$  of the flange can be written as:

$$f(x) = h_o \cdot \sin\left(2\pi \cdot \frac{x}{\lambda_o}\right) \quad (3.8)$$

If  $\rho$  is the radius of curvature at each peak, and  $f'(x)$  and  $f''(x)$  are the first and second derivatives of the roughness profile respectively, with respect to  $x$ , then the curvature  $K=1/\rho$  may be estimated as:

$$K = \frac{|f''(x)|}{\left([f'(x)]^2 + 1\right)^{3/2}} \quad (3.9)$$

If the rough surface profile described by a sinusoidal curve has asperities of the same height, the average depth or average amplitude is found at location  $x = \lambda_o / 4$ , Figure 3.3, the horizontal line passing through the centre of the profile, average arithmetic height,  $R_a$ . Also the amplitude  $h_o$  in terms of mean value of all maximum peak-to-valley heights, [17] is given by:

$$2h_o = R_{im}, \quad h_o = R_{im} / 2 \quad (3.10)$$

taking the first and second derivative of the surface profile function  $f(x)$ , with respect to  $x$ , the radius of curvature  $\rho$ , of the surface asperities may be determined from:

$$\rho = \frac{([f'(x)]^2 + 1)^{3/2}}{|f''(x)|} \quad (3.11)$$

at  $x = \lambda_o / 4$  the first derivative of profile is zero, thus the value of the numerator is equal to one, we have:

$$([f'(x)]^2 + 1)^{3/2} = 1 \quad (3.12)$$

The value of second derivative of the roughness profile, at  $x = \lambda_o / 4$ , is:

$$f''(x) = -\frac{4\pi^2 h_o}{\lambda_o^2} \cdot \sin(2\pi \cdot \frac{x}{\lambda_o}) = -\frac{4\pi^2 h_o}{\lambda_o^2} \quad (3.13)$$

Substituting for the first and second derivatives in the above equation the radius of curvature of asperity  $\rho$  can be estimated by using the roughness parameters of the surface, the minus sign is ignored due to the symmetry of the space:

$$\rho = \frac{\lambda_o^2}{4\pi^2 h_o} = \frac{\lambda_o^2}{2\pi^2 R_{im}} \quad (3.14)$$

As discussed above, if the asperities are considered to be of spherical form of equal size, and  $\lambda_o$  is the distance from centre of one to another, then for closely packed asperities it can be shown that the surface density (planar density),  $\eta$ , is determined by closeness of spheres. Thus for a closely packed spherical peaks, the surface density of asperity peaks,  $\eta$ , is the ratio of number of spheres per unit area whose centre lies on the plane. Thus for three spheres in a triangular plane [17, 19], we have:

$$\eta = \frac{\text{no. of spheres per face}}{\text{area of face}}, \text{ thus } \eta = (3 \times \frac{1}{6}) / \frac{1}{2} \times \left[ \frac{\sqrt{3}}{2} \lambda_o \times \lambda_o \right] = \frac{2}{\sqrt{3} \times \lambda_o^2} \quad (3.15)$$

For any surfaces having peaks and valleys, the occurrence of peak and valleys at various values of  $f(x)$ , can be represented by their distribution curve. Moreover slope of the profile is important, and it may be computed by an analogous way for all values of  $f(x)$ , and plot the distribution curve for slopes. Thus obtaining the distribution curve for slopes, peaks, valleys, and ordinate, etc., allow us to deal with them mathematically by representation of their shape. This allows us to specify the probability of their occurrence for a given value of  $f(x)$ , at a specific location on the assessment length of the profile.

In most cases, often it is found that these distributions are Gaussian, and their shapes are defined by the root mean square (r.m.s. = standard deviation,  $\sigma$ ) value of the profile. The expression for Gaussian distribution is given as:

$$f(x) = \frac{1}{\sigma \cdot \sqrt{2\pi}} \cdot e^{-\left(\frac{x^2}{2\sigma^2}\right)} \quad (3.16)$$

Hence, for a Gaussian distribution of surface asperities, the peak height distribution on the surface is also Gaussian with standard deviation,  $\sigma_1$ , then the distribution of sum of the heights is also Gaussian, [16], with standard deviation equal to:

$$\sigma = \sqrt{2} \cdot \sigma_1 \quad (3.17)$$

Thus, the relationship between the radius of curvature of asperities,  $\rho$ , the surface density of asperity peaks,  $\eta$ , and the standard deviation of peak heights distribution,  $\sigma$ , for metallic surfaces in contact is determined to be constant, [16, 17], and is given by:

$$\eta \rho \sigma = \sqrt{2} \cdot \eta \rho \sigma_1 = \alpha \quad (3.18)$$

Where  $\alpha$  (0.05), a statistical parameter which determines the asperity density of a rough surface, is used to determine the number of contacts, the surface pressure and the area of contact for contacting metals [16]. Shimomura et al. [17] determined that the  $\alpha$  value is 10 times less than that obtained by Greenwood and Tripp [16]. They indicated that the reason for this difference might be due to a combination of hard metal material with carbon graphite material which has the properties of low Young's modulus and low hardness; therefore they suggested further experimental evaluation of this subject is required.

### 3.4.5 Gaps between rough surfaces in contact

Assuming the surface asperities and surface roughness height follow a normal distribution, the penetration between two mating surfaces or the average existing gaps between mating surface under the applied load may be determined. Tsukizoe and Hisakado [22] indicated that the average clearance between two mating surfaces depends on the applied load, and apparent contact area, where means surface pressure is  $p_m = W/A_{app}$ , as described earlier, Figure 3.1. It has been found by that the theoretical average gap between two mating surfaces is the difference between the maximum asperities height,  $h_{max}$ , in contact from the mean profile line, and the depth of penetration,  $\Omega$ , of the asperities, [22]

$$\delta = h_{max} - \Omega \quad (3.19)$$

For a surface roughness following a normal distribution function such that the peak height distribution on the surface is Gaussian with peaks  $h_{1max}$ , and  $h_{2max}$ , the maximum peak height may be given by:  $h_{max} = \sqrt{h_{1max}^2 + h_{2max}^2}$ . If both surfaces have the same asperities height distributions,  $h_{1max} = h_{2max}$ , we get  $h_{max} = \sqrt{2}h_{1max}$ , and then

$$\delta = \sqrt{2}h_{max} - \Omega \quad (3.20)$$

The theoretical depth of penetration  $\Omega$  may be obtained from the difference between the distance from initial contact point,  $h_{max}$ , (maximum distance from the mean line of the profile) of the surface, and the deviation from the mean line of the surface profile curve,  $x$ , and it is given by:



$$\Omega = h_{\max} - x \quad (3.21)$$

Let  $h_{\max} = n\sigma$ , and replacing for  $x = m\sigma$ , the depth of penetration of the asperities become a function of standard deviation:

$$\Omega = n\sigma - m\sigma = (n - m)\sigma \quad (3.22)$$

We have assumed a Gaussian distribution for surface asperities, such that the peak height distribution on the surface is Gaussian with standard deviation  $\sigma_1$  and  $\sigma_2$ , therefore, the standard deviation of asperities of two surface is given by  $\sigma = \sqrt{\sigma_1^2 + \sigma_2^2}$ . The sum of the heights is also Gaussian with standard deviations  $\sigma$ . For the case where the roughness of both surfaces are equal we have  $\sigma_1 = \sigma_2$ , and

$$\sigma = \sqrt{2}\sigma_1 \quad (3.23)$$

thus, we obtain

$$\Omega = \sqrt{2}(n - m)\sigma \quad (3.24)$$

where:  $n$  and  $m$  are constant

$n\sigma$  is the distance between initial contact point and the average line of the surface roughness profile curve

$\Omega$  is the depth of penetration of asperities of mating surfaces

$\sigma$  as defined before, is the standard deviation (r.m.s.) of the asperities from the mean height.

It must be mentioned that this may be true only for two rigid surfaces mating at low stress levels. Where as for higher stress levels two dimensional model of surface asperity pattern provides a better understanding of the interaction between mating surfaces, and the possibilities of determining existing leak paths of gas flow in other directions than pure radial flow. Substituting for  $\Omega$  in the gap equation  $\delta$  we get

$$\delta = \sqrt{2}n\sigma - \sqrt{2}(n-m)\sigma \quad (3.25)$$

and thus the leak gap in terms of r.m.s., standard deviation of the roughness profile may be presented as

$$\delta = \sqrt{2}m\sigma \quad (3.26)$$

The variance of asperities' heights for  $N$  discrete values is:

$$\sigma^2 = \frac{1}{(N-1)} \sum_{i=1}^N [a_i^2 - \bar{a}^2] \quad (3.27)$$

and as a function of time in continuous form given as:

$$\sigma^2 = \lim_{T \rightarrow \infty} \frac{1}{T} \int_0^T (x - \bar{x})^2 dt \quad (3.28)$$

expanding the above equation it can be seen that

$$\sigma^2 = \overline{a^2} - (\bar{a})^2 \quad (3.29)$$

If the mean line of the profile is considered to be at zero level, then the standard deviation of the profile, given by the root mean square (r.m.s.), is found to be:  $\sigma = a/c$ ; then the maximum height of asperity is  $a_{max}=c\sigma$ , and the average leak gap existing between the two mating surfaces at low stress level may be found as a function of asperity heights.

On the other hand, the relationship between  $\sigma$  (r.m.s.) and  $R_a$  may be given by  $\sigma = K \cdot R_a$ . The constant  $K$  depends on the nature of the surface profile. Now it can be shown that if a surface asperities follow a regular sinusoidal waveform profile then the value of r.m.s. is  $\sigma = (\frac{1}{\sqrt{2}})A_a$ , and the mean of the profile is,  $R_a = (\frac{2}{\pi})A_a$ , where  $A_a$  is the sine amplitude. Therefore, the constant value of the ratio r.m.s. to mean value, for regular sinusoidal wave form, is  $K = \frac{\pi}{2\sqrt{2}}$ , and their relationship is given as:

$$\sigma = (\frac{\pi}{2\sqrt{2}})R_a \quad (3.30)$$

For a Gaussian random profile, similarly, we obtain,

$$\sigma = (\sqrt{\pi/2})R_a \quad (3.31)$$

Thus as it has been indicated earlier, for a Gaussian distribution surface height,  $K=1.25$ . From the above relationships and the leak gaps equation, it can be shown that the leak gap is proportional to the  $R_a$  value of surface roughness, given by equation

$$\delta = \sqrt{2}m\sigma = \sqrt{2}m.(\frac{\pi}{2\sqrt{2}})R_a = \frac{\pi}{2}mR_a \quad (3.32)$$

for a regular sinusoidal profile, and

$$\delta = \sqrt{2}m\sigma = \sqrt{2}m\left(\sqrt{\frac{\pi}{2}}\right)R_a = m\sqrt{\pi}R_a \quad (3.33)$$

for a Gaussian random profile.

These equations indicate the average clearance between two mating surfaces after penetration,  $\Omega = \sqrt{2}(n - m)\sigma$ , under the applied load. The main conclusion derived from the theory given above is that:

- 1) the clearance between two mating surfaces is directly proportional to the average arithmetic deviation from the mean line of the surface roughness profile; or similarly may be presented with respect to the root mean square of roughness.
- 2) the average clearance between two mating surfaces depends on the applied load, and apparent contact area, [22].
- 3) the real pressure in a local elastic and plastic indentation, for metal-to-metal contact, can be approximated by the mean surface pressure,  $p_m$ , or  $2p_m$ , respectively. This indicates that the leak clearance is dependent on the mean surface pressure (yield pressure) over the indentation  $W/A_r$ .

The theoretical average gap between two mating surfaces,  $\delta$ , presented above through equations (3.6) to (3.33) is based on the highest asperities on the surfaces, or the separation at which contact occurs; these are poor reference points. Assuming no roughness value for the gasketing material (specially for the non-metallic types) then the equation (3.26) reduces to  $\delta = m\sigma$ . Also considering that some initial stress is required for gasket seating, then the load-compliance based on the point of first contact may be expected to show scatter over the full range of surface. Thus the initial theoretical average gap must be less than that indicated above. Let  $p$  be the probability of a individual

asperity height that exceed the particular value  $z$ , and results in the initial contact of the gap, then the probability that in a sample, of length  $L$ , with  $n$  members all will lie below  $z$  is  $(1-p)^n$ . The present state of the knowledge does not allow for a rigorous application of such an assumption. Describing the probability distribution by its upper quartile range value, then  $3/4$  of the members of the population lie below them. Thus with  $m = 3/4$ , we have  $\delta = 0.75\sigma$ , and the initial theoretical leak gap between a flange faces and gasket can be approximated by the arithmetic surface roughness profile value  $R_a$ , of flange, assuming a Gaussian random profile and we have,

$$\delta = R_a \quad (3.34)$$

### 3.5 Theoretical leak path and leak rate

#### 3.5.1 Effect of surface pressure

The equivalent leak path size of both porous channels of the medium and paths existing due to surface irregularities depends on the surface pressure. It is a common sense that as the surface pressure  $p_s$  increases the highest asperity height  $h_o$  reduces due deformation (in case of metal to metal contact) or penetration (into soft gaskets), which results in increasing the number of surface asperities in contact. This can be presented by

$$N_{as} = C_1 \cdot e^{r_1 - h_o/p_s} \quad (3.35)$$

This results in reducing the leak path size or reducing the number of leak paths, which can be presented as

$$\xi_{P_{as}} = C_2 \cdot \sum_{i=1}^m \xi_i e^{\gamma_1 h_o / p_i} \quad (3.36)$$

Where,  $\xi_{P_{as}}$  is the total leak path on the surface due to asperities peak and valley,  $\xi_i$  is the  $i^{\text{th}}$  leak path size,  $C_1$  and  $C_2$  are constants,  $h_o = R_{tm}/2$ , and  $\gamma_1$  and  $\gamma_2$  are constants with unit of [Pa/m] or [psi/in]. It is worth noticing that the average clearance between the mating surface of the flange face and gasket depend on and is proportional to the maximum height of asperities  $h_o$ , as can be deduced from Figure 3.3. Furthermore, this average clearance is highly dependent on the apparent contact pressure, the ratio of load over the apparent contact area between two mating surfaces. The relationship  $N_{as}$  presented in the equation (3.35) agrees with the statement made by Chivers and Hunt [23], that as a result of surface compression the equivalent leak path dimension,  $h$ , decreases which results in the increase of the number of surface asperities in contact  $n$ . This is presented in the following relationship:

$$n = N_o \cdot e^{-\frac{h}{c}} \quad (3.37)$$

where  $N_o$  and  $c$  are constants.

In general the leak through the sealing surfaces maybe dominated by that past the lowest compression region (i.e. surface valleys). As the seal/gasket is compressed further, sealing surfaces asperities (of flange faces) penetrate into the gasket material while the gasket material flows into the sealing surfaces leak paths reducing the number of surface leak paths and the leak path sizes. Consequently the flow past the sealing surfaces (surfaces between gasket and flange face) reduces. Furthermore, the ratio of the leak path length to the leak path size increases, resulting in both the reduction of the flow past sealing surfaces and the change in the flow regimes, as presented later in the section of the analysis of experimental results.

Furthermore, for a gasket between two sealing surfaces, increasing the normal stress results in the increase of gasket surface pressure and gasket compaction/compression, in addition to the asperities penetration or plastic deformation of local asperities of higher peak with respect to the general surface asperities, reducing the pore channel size (diameter) of the gasket,

$$D_t = C_3 \cdot \sum_{i=0}^n D_i e^{k \frac{D_i}{p_s}} \quad (3.38)$$

$D_t$  is the total number of pore channels on the gasket thickness face exposed to the internal gas pressure, and  $D_i$  is the  $i^{\text{th}}$  pore size. If it is assumed that all capillaries are of the same size, then we have:

$$D_t = C_3 \cdot nD \cdot e^{k \frac{D_i}{p_s}} = C_4 \cdot e^{k \frac{D_i}{p_s}} \quad (3.39)$$

$C_3$ ,  $C_4$  and  $k$  [Pa/m] or [psi/in] are constants. As a result the ratio  $D/p_s$  [m/Pa] or [in/psi] decreases as the surface pressure  $p_s$  increases.

The leak rate varies depending on both  $\xi_{p_s}$  (total leak path) and  $D_t$ , which are functions of surface pressure. Thus leak rate reduces as the stress level (or surface pressure) increases. This stress must represent those due to the applied load minus the total hydrostatic end forced ( $H = P \times Ai$ ) caused by the gas pressure acting on the gasket internal area. A uniform stress on the gasket is considered during the operation. Thus, the total stress acting on the gasket is evaluated using applied load, gas pressure, gasket full contact surface and internal surface exposed to the gas pressure, [2, 4], according to:

$$p_s = Sg = \frac{W}{Ag} - P \frac{Ai}{Ag} \quad (3.40)$$

where:

$Sg$  gasket stress based on gasket full contact area, (psi, MPa)

$W$  normal bolt load, (psi, MPa)

$Ag$  gasket full contact area on basic gasket width,

$$Ag = 2\pi b.(G_o - 2b)$$

$G_o$  design gasket outside diameter, for a raised face or lap ring flange in. (mm)

$b$  effective gasket seating width, (in., mm)

$2b=N$  actual gasket contact (compressed) width,  $N = \frac{(OD_g - ID_g)}{2}$

$OD_g$  outside diameter of the gasket, for a raised face or lap ring flange, in. (mm)

$ID_g$  inside diameter of gasket, in. (mm)

$Ai$  internal pressurized gasket area en-circled by effective gasket diameter,  $G$

$$Ai = \frac{\pi}{4}(G_o - 2b)^2 = \frac{\pi}{4}G^2$$

$G$  effective pressurized gasket diameter, or mean gasket diameter  $G = \frac{(OD_g + ID_g)}{2}$ ,  
 $= G_o - 2b$  (in., mm)

$P$  internal design gas pressure controlled in the rig test, (psig, MPa)

The described problem leads to the fact that the leak rate has a unique relationship between the gasket material, the flange surface characteristic, and the contained fluid (gas), thus:

$$L_{rm} = f(A_i, A_g, \Delta P, f(x), Y, E, W, p_m) \quad (3.41)$$



where:

- $\Delta P$  the gas pressure difference across the gasket width,
- $f(x)$  a function representing the surface characteristics (form and roughness),
- $Y$  yield strength of the weaker material (usually gasket),
- $E$  modulus of elasticity of weaker material,
- $W$  initial applied load,
- $p_m$  represents the mean surface pressure.

It is worth noticing that based on theory of elasticity for the same load “ $W$ ” applied axially on the platens, different surface pressure “ $p_m$ ” on the gasket can result depending on the platens surface form and asperities. As a result, because of the randomness of the surface characteristic (surface form and roughness), the surface flow path may differ substantially allowing for both viscous laminar and molecular flow to exist in the given seal under different applied loads.

An analytical solution to the problem described above is not feasible due to number of factors involved, and the fact that the physical phenomenon is not measurable, and also because the effect of each factor cannot be determined precisely due to their unknown combined effects. Thus, experimental procedure is the ultimate tool to determine the effect of some factors, such as surface roughness and surface form, in sealing evaluation.

### 3.5.2 Gas flow regimes

Study of flow regimes allows determination of sealing performance of gasketed joints based on test parameters: gas pressure, sealing surfaces characteristics and gasket compressive stress. The flow regimes indicate the sealing sensitivities to gas pressure increase as a function of gasket stress and of sealing surface characteristics. The flow regimes of the gas leak past the static seals have been the interest of many researchers

over the past decades, [6, 9, 20, 23, 24]. The flow regime is a function of the leak path size, the equivalent diameter  $D$  and length  $L$ , and the mean free path length  $\lambda$ . Where the ratio of  $\lambda/D$  is small such that the size of mean free path length is small relatively compared to the equivalent path size diameter  $D$ , the gas flow falls within a continuum hydrodynamics state, and can become laminar viscous or turbulent flow, and can be presented by Hagen-Poiseuille equation. Inversely where this ratio is large such that  $\lambda$  is relatively much larger than  $D$ , then the flow is in molecular state, and can be described by Knudsen's law:

$$L_{rm} = \frac{B_1 D^3}{L \sqrt{M}} (P - P^*) \quad (3.42)$$

Where:

- $B_1$  a constant
- $M$  the molecular weight of gas
- $D$  the equivalent leak path size diameter,
- $L$  the path length, approximated by gasket width.
- $P$  internal design gas pressure (upstream pressure),
- $P^*$  atmospheric pressure, (downstream pressure),

According to the kinetic theory of gases, the mean free path length  $\lambda$  is given by:

$$\lambda = c_1 \frac{\mu}{\bar{p}} \sqrt{\frac{RT}{M}} \quad (3.43)$$

where:

- $\lambda$  is measured at the mean gas pressure  $\bar{p}$ ,
- $c_1$  a constant approximately equal to 2,

- $\mu$       cinematic viscosity,  
 $R$       gas constant, and  
 $T$       absolute temperature

Sealing performance of gaskets based on different properties of gases was experimentally evaluated by Bazergui and Louis [24]. Based on this study it was demonstrated that, in the case of inert gases (i.e. helium, argon), leak rate can be fairly predicted for gas flow through a gasketed flanged interface using the laminar viscous flow theory, based on the Hagen-Poiseuille equation for compressed ideal gases:

$$L_{rm} = \frac{\pi D^4}{128L} \frac{1}{\nu} \frac{1}{2P^*} (P^2 - P^{*2}) \quad (3.44)$$

Where  $D$ ,  $L$ ,  $P$  and  $P^*$  are as indicated above and  $\nu = \mu / \rho$  is kinematic viscosity of gas.

Bazergui and Louis, [24], stated that for high performing seals the gas flow past the seal is in molecular regime, which is particularly undetectable at very low leak rates, unless sophisticated instrument such as mass spectrometer is used. Rathbun, [9] indicated that leakage levels in the range of  $10^{-3}$  are viscous laminar while for leakage levels below  $10^{-6}$ , the molecular flow regime is achieved. Chivers and Hunt, [23] and, Chivers and Williams, [25], argued that for high pressure high integrity seals laminar flow is most likely flow regime, with turbulent flow occurring if defects exist. They further indicated that it is possible, particularly with elastomers, to reduce path sizes to such dimensions that molecular flow should be considered. It must be argued here that considering a particular type of gasket (i.e. PTFE) and changing the flange surface characteristics based on different machining procedures, under similar test conditions, a transition to molecular flow regime can be observed, at some particular stress levels, when changing from the flange surfaces being produced by milling, to grinding and to turning. This is discussed further in analysis sections, later in this chapter.

From the flow equations presented above, it can be noted that for both laws, leak flow rate is inversely proportional to the leak path length. For molecular flow, the flow rate is inversely proportional to the square root of the molecular weight and proportional to the difference between upstream and downstream pressures. In the case of viscous laminar flow, the flow rate is inversely proportional to gas viscosity and proportional to the difference of the squares of the pressure.

Taking the log value of the molecular flow equation (3.42) above, where  $P^* = 0$ , [9, 26], it can be seen that:

$$\log L_{rm} = \log K_1 + \log P \quad (3.45)$$

Similarly for the viscous laminar flow, from equation (3.44), we have

$$\log L_{rm} = \log K_2 + 2 \log P \quad (3.46)$$

### 3.5.2.1 Determination of flow regimes

Flow regimes maybe determined based on two different methods. The first method determines the slope of the lines based on the leak variation as a result of gas pressure change, where the remaining test conditions are kept the same, [9, 26]. From the equations above, when plotting the  $\log (L_{rm})$  versus the  $\log P$ , with  $\log P$  on the ordinate and  $\log (L_{rm})$  on the abscissa, the molecular flow regime is present if the slope of the line is equal to one, whereas, if the slope of the line is equal to two, the flow is in viscous laminar state, see Figure 3.4. Rathbun, [9], argued that in several cases the trace of leakage versus pressure on log-log paper exceeded the slope of two. It should however be mentioned that this is not physically possible for a system with constant gap profile.

However, the variation in surface pressure/gasket stress and internal gas pressure may cause leak cleansing, increasing the leak rate which may result in slope of the line greater than two. A leak cleansing phenomena was noted in the work of Rathbun, [9], while the system internal gas pressure was increased for which sudden increase in the leak rate took place where the flow transited from molecular to laminar flow regime, Figure 3.4. He described the leak suddenly increased as if the leak path size were instantaneously enlarged, then the normal molecular or viscous flow would commence. Rathbun observations are based on metal-to-metal gaskets.

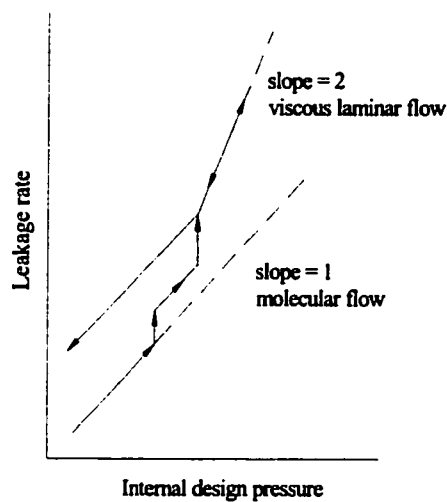


**Figure 3.4.** Phenomenon of leak cleansing by increase pressure, [9].

It should be indicated here that in the present experimental research slopes as low as 0.3 and as high as 4.9 have been noticed, for the test performed with (non metallic and semi-metallic gaskets) such as PTFE sheet, flexible graphite sheet and spiral wound gasket with flexible graphite filler. These results are discussed in the experimental analysis section of this work. Such a phenomenon may clearly be an indication of leak cleansing phenomena that has taken place for test points at high gas pressure (800 psig) and low

stress level (S1). Nevertheless, such phenomena is hypothetically discussed in this paper since the gas pressure during the tests is kept constant, so the graphical results of incremental gas pressure increase versus leak rate increase can not be presented graphically to show the leak cleansing phenomena as presented by Rathbun [9].

The second method is based on the determination of Knudsen and Reynolds numbers, as a function of pressure gradient, path length and size, and fluid properties. Unfortunately, any correlation is subject to limitations as the Reynolds number and Knudsen number depend significantly upon the definition of a pore/path size diameter, which can not be achieved properly. The recognized parameter to determine whether the flow should be treated as continuum or as non-continuum (molecular) is the Knudsen number. Knudsen's number,  $Kn = \lambda / D$ , is defined as the ratio of the mean free path length to the path size diameter. For a very large Knudsen number the flow is in molecular flow regime, with essentially no molecule in collision with another one, whereas when the Knudsen number is small the flow is considered to be in the continuum (laminar) flow regime. Between these two extremes, two other flow regimes namely slip flow and transition flow are often specified. The flow regimes are defined approximately by Knudsen's number,  $Kn = \lambda / D$ , so to distinguish between flow in molecular ( $D/\lambda \leq 0.1$ ), transition ( $0.1 < D/\lambda \leq 10$ ), slip ( $10 < D/\lambda \leq 100$ ), or in laminar regimes ( $Re \leq 2000$ , and  $D/\lambda \geq 100$ ). Whereas, Reynolds number  $Re = \rho V D / \mu$  of the viscous flows can be used to determine whether the flow is in turbulent or laminar regimes. Transition from laminar to turbulent flow regimes in unstable condition occurs for flow ranging between ( $2000 \leq Re \leq 2500$ ), and turbulent flow regimes exist if the Reynolds number exceeds 2500, ( $Re \geq 2500$ ), [6, 20]. It must be emphasized here that for the size of leaks of interest in vacuum and leak detection, turbulent flow shall not take place.

Certain assumptions have to be made in order to determine the state of the flow from the experimental results. By determining the equivalent path size diameter  $D_{tot}$  from the flow

equation and experimental leak results, the number of channels can be obtained  $n = D_{tot} / \delta$ , Consequently mass flow rate through one channel may be obtained from the ratio of total mass leak over the number of channels,  $Q_i = Q_{mass} / n$ . The Reynolds number  $Re = \rho V D / \mu$  is a function of mass flow rate  $Q_{mass}$  and the leakage path diameter  $D$ ,  $Re = f(Q_{mass}, D)$ . Where  $V = 4Q_{vol} / \pi D^2 = 4Q_{mass} / \rho \pi D^2$ . Substitute in  $Re$ , we have,  $Re = 4Q_{mass} / \mu \pi D$ . It is argued earlier that the leakage path diameter is a function of surface stress, and it is assumed to be equal to the surface roughness value,  $\delta = Ra$ .

Now in order to determine the Reynolds number from the experimental leakage rate result, at each stress level, the leak through one leak path size diameter must be determined first. Thus, we can tackle this issue from following perspectives. Considering that overall leak path size is affected by the surface pressure exerted on the interposed gasket between the flange faces, based on the assumption made through equations (3.35) to (38), then we can assume that the leakage path size diameter  $D$  changes at each subsequent stress level scaled with leakage rate. Thus determining the mass flow  $Q_i$  through one leak path size, the Reynolds  $Re = 4Q_i / \mu \pi D$  and Knudsen's  $Kn = \lambda / D$  numbers, can be determined, leading to the state of the flow regimes. Now if it can be assumed that leak flow path can be approximated with the average arithmetic surface roughness value  $Ra$  at the initial stress level, we have  $D_1 = \delta = R_a$ , then at the second stress level the value of  $D_2$  can be determine from the following relations:

$$Q_1 = \rho V A = \rho V \frac{D_1^2}{4}, \text{ and } Q_2 = \rho V A = \rho V \frac{D_2^2}{4}, \text{ then } D_2 = D_1 \sqrt{\frac{Q_2}{Q_1}} \quad (3.47)$$

Consequently the value of  $D$  at other stress levels can be determined similarly, for which, it can be used along with the mass flow rate value at the same stress level, such that the Reynolds number is established. Simultaneously the Knudsen's number is obtained based

on equivalent leak path size diameter and mean free path length at mean gas pressure, and then the flow regime is established, based on the approximations discussed above.

One must appreciate that both methods discussed here are based on approximations and only provide estimations to the state of the flow. The first method is a generalized method and especially since the path size may very well be function of gasket material properties and its behaviour at different operating stress, pressure and temperature, the slope of the line from the log-log plot of leak versus pressure may only provide an approximation to flow regime. Obtaining the flow regimes based on the considerations of the Reynolds and Knudsen numbers has its own challenges, in static seals of gasketed flanged joints. Such that the accuracy of the application of this method depends significantly upon the assumptions made in the determination of the leak path size on the sealing surfaces, and the definition of pore size of the gasket material. This involves its own complexities and so far there exists no theory to correctly and precisely cover these, due to many undeterminable parameters involving the gasketed flanged joints. Nonetheless, in the analysis of the experimental results, section 3.7, we present the flow regimes results based on the slope of the line from the log-log plot of leak versus pressure.



### **3.6 Experimental sealing investigation setup**

#### **3.6.1 Room-temperature hydraulic test rig: RTHR rig**

In order to isolate the sealing problem affected by surface characteristics and gasket properties from the substructure problem (geometry, flexibility) of the test system, an apparatus is used allowing the measurement of the leak rate as a function of gas pressure and applied gasket stress at room temperature. The leak rate is measured taking into consideration the importance of the load uniformity. The RTHR rig shown in Figure 3.5 is designed to achieve a uniform gasket-load distribution without the need of bolting, therefore eliminating the uneven bolt tightening and flange rotation effects. A solid aluminium assembly structure is designed to withhold the test chamber, and the hydraulic ram. The test chamber consists of two cylinders in which the two removable stainless steel test platens of 6.188 in (157.175 mm) diameter are located, with the test gasket being sandwiched in the middle. In real joints, Flanges come in different types such as “Tongue and Groove”, “Full Face/Flat face”, “Raised Face” and “Ring Joint”, etc., as presented later in this chapter. The only type of geometry of flanges (in this work: test platens) considered for this research is the “Raised Face” machined from 20  $\mu\text{in}$  (0.508  $\mu\text{m}$ ) up-to 1000  $\mu\text{in}$  (25.4  $\mu\text{m}$ ) arithmetic average roughness height (AARH) with different machining procedures. The characteristics of surfaces are explained later in this chapter.

Inside the lower section of the assembly structure, a hydraulically actuated 17.0 in (432.0 mm) diameter ram give raise to the lower test chamber cylinder compressing the test gasket between the two removable steel platens. Fluid pressure is applied through the lower test chamber cylinder and through the centre of lower test platen in a high-pressure-tight chamber created by the test platens and test gasket. A hermetic leak collection (low pressure tight) chamber is created and ensured by locating O-ring seals under the lower test platens as well as in between the upper and lower section of the test chambers. The low-pressure chamber is connected to the leak measurement system through a tapped

hole. The test fixture is rated 2000 psig (13.8 Mpa, 138 Bar) hydraulic pressure corresponding to a maximum load capacity of 400 Klb (200 ton). The test gaskets used are NPS 4-in (100 mm) nominal diameter, and the test fluid is helium at pressure up to 1500 psig. Adjustable L-shape blocks are mounted on the exterior walls of the upper and lower test chamber cylinders for the installation of two deflection transducers, DC LVDT, with a stroke range up to  $\pm 0.1$  in ( $\pm 2.5$  mm), having linearity of 0.3% a non-repeatability of less than  $5.9 \mu\text{in}$  ( $< 0.15 \mu\text{m}$ ) and temperature sensitivity less than 0.01% FS/ $^{\circ}\text{C}$ , at temperature ranging between  $-20$  to  $+ 80^{\circ}\text{C}$ . See Table 3.1. Three guide pins in the test chambers ensure the exact positioning of the two chamber sections. The gasket test fixture cross-section, of the room-temperature hydraulic test rig: RTHR rig, is presented in Figure 3.5. Figures 3.6 and 3.7 show a general photo of the test assembly and a detailed one respectively.

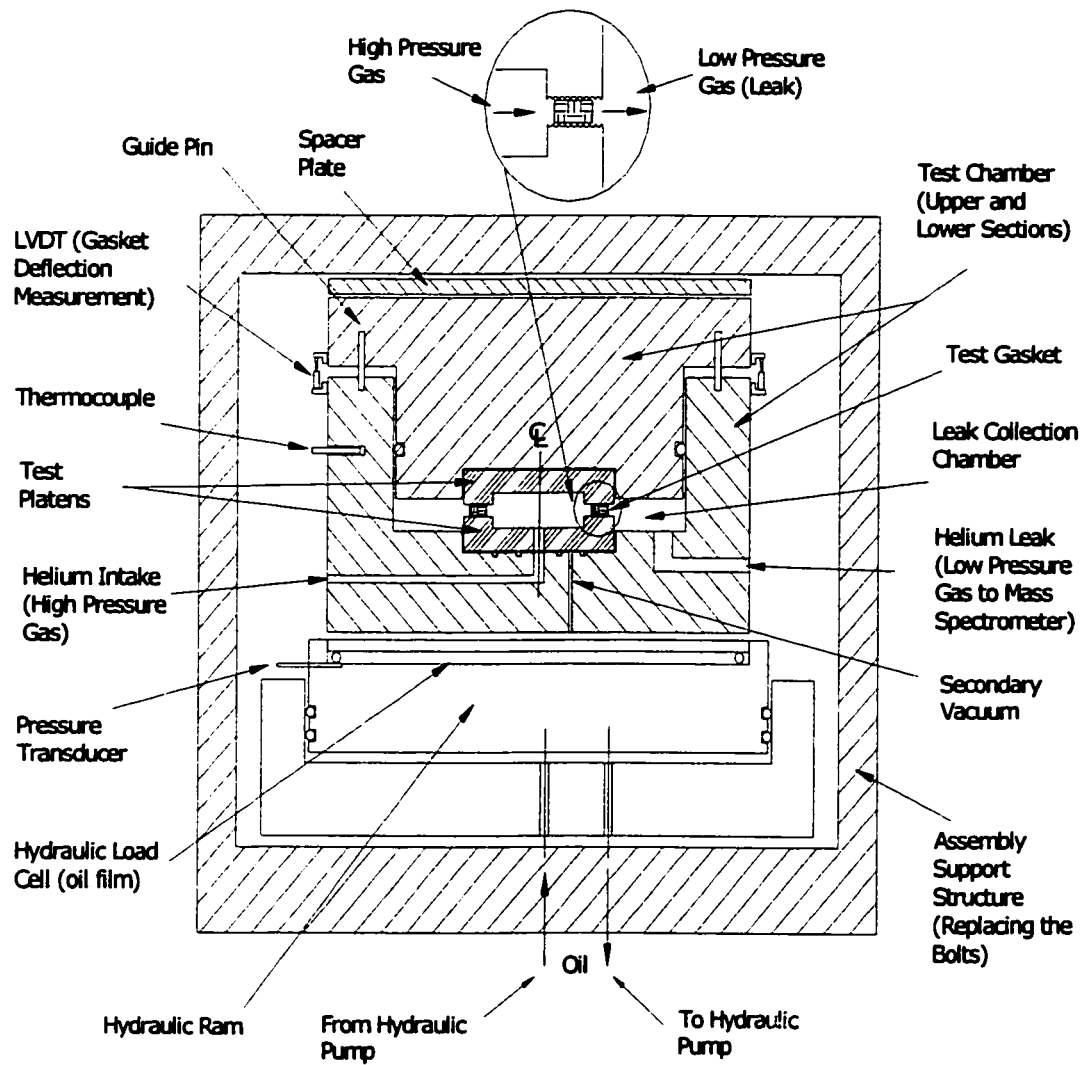


**Figure 3.5.** Schematic of gasket test fixture cross-section, room-temperature hydraulic RTHR test rig. (Not to scale)

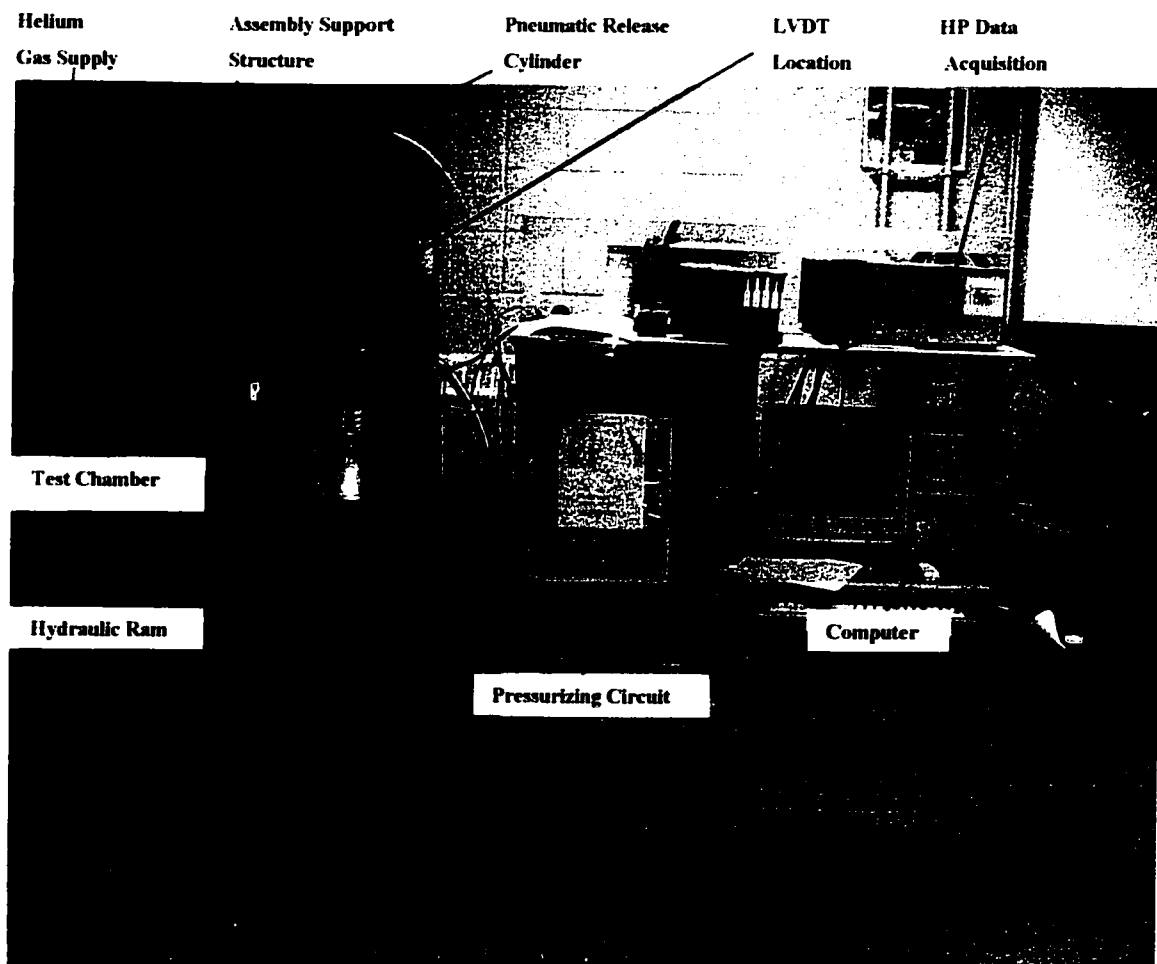


**Figure 3.6.** ROTT test bench.

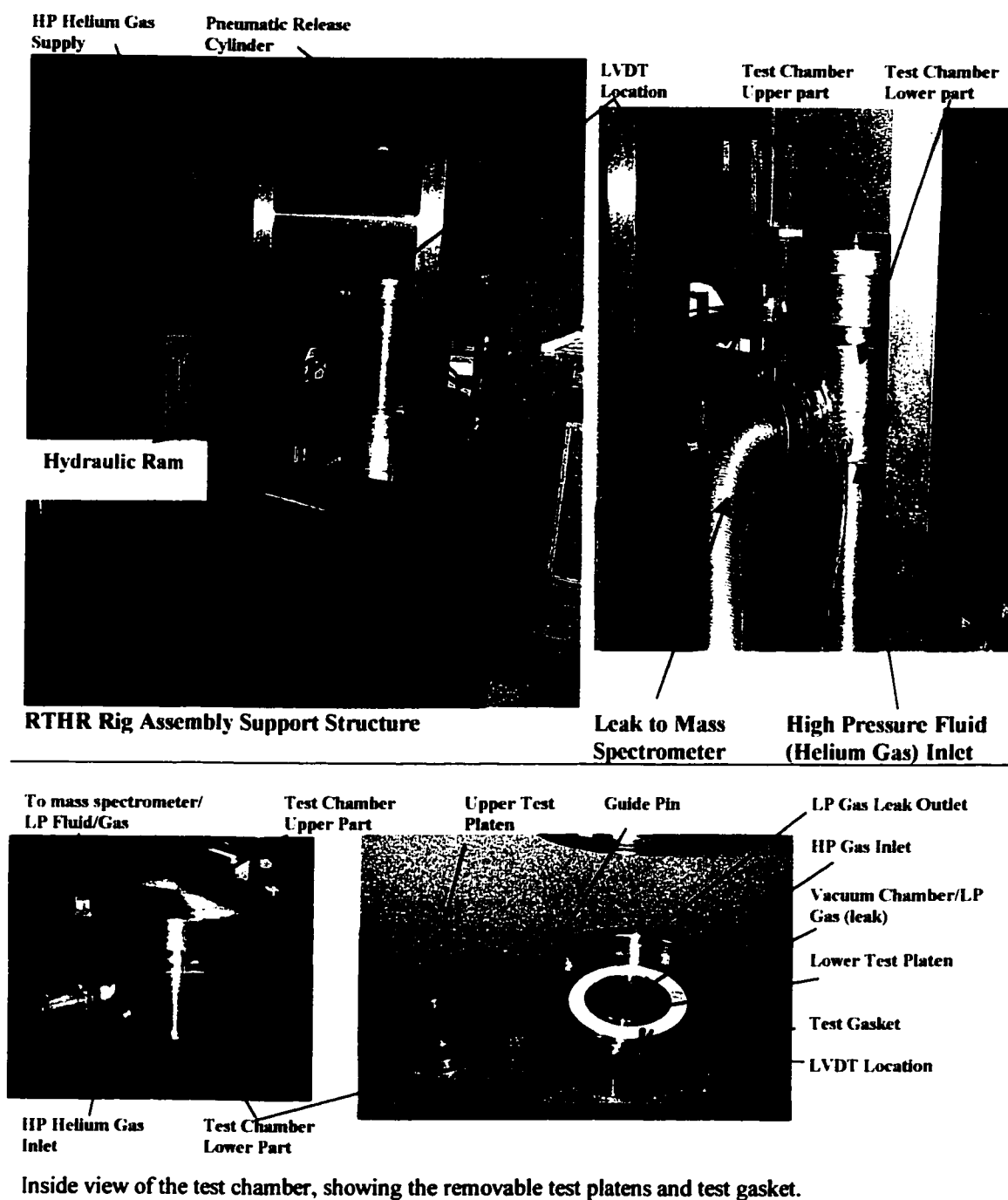


**Figure 3.7.** Room-temperature hydraulic test rig: RTHR rig.

### 3.6.2 Automatic test procedure

The test is performed automatically, after installation of the gasket, without the intervention of the user. The program controlling the test bench and its different components is written in LabView programming language. The test program starts based on the command file that carries all the test steps. Such program and its command files allow a great flexibility in controlling and modifying the test parameters such as: applied stress, gas pressure variation and control, duration of each test step, and so on. Furthermore, the program allows for graphical interface for the duration of the test, the evaluation of parameters and the measured results. It is also possible to interrupt the test and carry-on with manual instructions on certain operations. Essentially, the test gasket is installed between two platens with the desired surface finish, which are then placed in the centre of the apparatus (or test chamber). A uniform load is applied on the chamber by the hydraulic ram, which is then transferred onto the platens and on the gasket. The system is charged with an air driven hydraulic pump.

As mentioned before, the gasket compressive stress is regulated by a computer program control, that automatically adjusts the hydraulic ram pressure to compensate for the effect of internal gas pressure (end load effect). The total load applied by the ram is measured with a hydraulic load cell, placed on the ram, and fitted with an electronic pressure transducer. The air driven pump has a relatively large piston on its airside that drives a very small diameter cylinder to pump the oil. A small amount of oil (less than a drop) is driven into the hydraulic circuit at each pumping stroke. This amount of oil is approximately 0.03 cc/per stroke. When increasing the pressure, because of the limited elasticity of the components in the system (i.e. the hosepipe, the supporting frame deformation, the gasket, etc.) even such small amount of oil may generate a large load variation that limits load control precision. To overcome this limitation, a spring loaded accumulator is connected to the hydraulic circuit, reducing the pressure variations generated by each pump stroke. The accumulator also compensates for gasket creep and small leaks. On the

other hand, the pressure is released by a solenoid valve through a restrictor needle valve that opens to purge oil out of the circuit.

The internal gas pressure setting on the gasket is controlled and adjusted by a electronic pressure flow controller, MKS Model 1250A-0, It is purged through a valve that is controllable directly by the computer program. The maximum allowable internal pressure of the pressurization system is limited to 83 bar (1200 p.s.i.). See Table 3.1 for instrumentation descriptions.

The system is capable of measuring the gasket leak rate by three different means: a flow-meter, the pressure drop method and a helium mass spectrometer. A mass spectrometer is used where stringent leak detection is required. The helium mass spectrometer leak detector develops a vacuum which enables it to detect traces of helium gas. The helium mass spectrometer used in this experimental research is an Alcatel ASM 180T that has a leak detection resolution as small as  $1 \times 10^{-10}$  mg/s of He typical range (1 cc every 7 month). The helium mass spectrometer leak detection range varies from  $10^{-10}$  up to  $10^{-1}$  mbar.L/sec (mL/s at atm pressure) for fine leaks between  $10^{-8}$  and  $10^{-2}$  mbar.L/sec (mL/s at atm pressure), for gross leak. The gas leak through the sealing surfaces enters a vacuum leak collection chamber built around the gasketed joints (Figure 3.5.) which is connected to the helium mass spectrometer Alcatel ASM 180T. The singularity of the leak and of the leak path is assured by a secondary vacuum which precludes the leak from going from the lower test platen and lower test chamber to the leak detection apparatus by O-rings being placed between their mating surfaces, see Figure 3.5.

The flow-meter leak measurement starts if the leak rate is larger than 0.8 mg/s. The flow meter leak upper range is 5.3 mg/s (2L/min). If the flow rate ranges between 0.018 mg/s and 0.8 mg/s the flow rate measurement is performed by the pressure drop method, because any leak rate larger than 0.018 mg/s would not be safe for the mass spectrometer, since the flow would saturate it easily. The pressure drop method consist in recording the

decrease or drop of the internal volume pressure over time. Prior to the beginning of the measurement, the internal volume is sealed so that no new gas can be inputted to compensate for gasket leak. The leak rate is calculated using the perfect gas law. For leak rate smaller than 0.018 mg/s measurement is performed by helium mass spectrometer. It takes place with intervals of 15 minutes (consisting of a waiting period of 15 minutes and of a 15 sec measuring time), the whole measurement lasting for a minimum period of 2 hours. Then the statistical analysis on the last three measured points is performed to determine whether the leak rate has been stabilized or not. The leak rate is considered stable when the ratio of the standard deviation from the mean over the mean leakage value for the last three measurements is less than 2%,  $((\sigma_{L_m} / \bar{L_m}) \times 100 \leq 2\%)$ . Until such a result is obtained the measurement is continued, up to a maximum period of 5 hours. For the leaks measured with the flow meter or the pressure drop method, the measuring times vary between 1 min. to 5 min., since for leak rate above 0.018 mg/s, leak rate stabilization is not an issue.

On the periphery of the test chamber, two linear variable differential transformers (LVDT) are mounted at 180° apart, Figure 3.5. These LVDTs provide measurement on the gasket deflection (thickness change).

### **3.6.2.1 Estimated measurement error**

When the experiment is repeated under the same conditions the results obtained are never quite identical. Experimental error is the experimental variation or the fluctuation that occurs for one repeated test to another. The experimental variation or error is most often unavoidable. Many sources contribute to experimental errors, i.e. experimental runs, experimental set up, inconsistency in applying the test parameters, human errors, in addition to errors of measurement, analysis and sampling. Considering the fact that the experimental tests in the present research are designed carefully and handled with care,



and that tests are ran and measured with automatic computer controlled test machine, then the estimated error of measurements of the experimental results depends on the uncertainty in experiment calculated from root-sum-square of individual uncertainties of the measurement devices  $E_{rss} = \pm 2 \sqrt{\sum_{i=1}^n e_i^2} \%$ . The amount of error associated with a particular measurement may be considered from the point of view of precision or accuracy. The precision of a measurement expresses the error (deviation) of the measurement from the average of a large number of measurements of the same quantity, while the accuracy of a measured value expresses the deviation of the measurement from the true value of the quantity. Error estimation based on accuracy is performed when the true value of a quantity is known, however when the true value is unknown the error estimation must be performed based on precision instead of accuracy. It must be noted that it is impossible to obtain accuracy if precision cannot be obtained. On the other hand precision does not guarantee the accuracy of the system, and furthermore accuracy can be improved up to but not beyond the precision of an instrument by calibration. The precision (or vice versa the error) of a measurement depends on the limitations of the apparatus used to carry out the measurement procedure. The limitations of the apparatus used for the ROTT experiments defined by the manufacturer and are given in the Tables 3.1 and 3.2.

It must be noted that since experimental tests are performed with the same test rig under the same test procedure, and since the results are being used for comparison, therefore the important factor for elimination of the measurement error is the repeatability of the tests. Thus, as it is shown in the experimental analysis section, the tests performed in this research are repeatable. The repeatability of the test results can be observed form the most critical data point at initial stress S1 level at 200 psig that are overlapping, for the same gasket and the same sealing surfaces. Furthermore, form the data and graphs presented in that section it can be seen that test results follow the same trend, and that no abnormality can be seen in the measurement results.

**Table 3.1. Instrumentation capabilities and precision**

Measure quantity	Instrument type	Range	Precision	Resolution
Gas flow inlet	Mass Flow Transducer, Datametrics Model 831	0-2 s lpm	± 0.15% FS*	
Internal fluid pressure	Pressure Transducer, Heise Model 621	0-1500 psig	0.10% FS	0.1 psig
Hydraulic pressure	Pressure Transducer, OMEGA Model PX303- 5kG10V, 1-11 VDC	0-5000 psig	0.25% FS	0.5 psig
Gasket deflection	Schlumberger, DC LVDT, Model 100 DC-SE	± 0.100 in	0.25% FS	0.00004 in
Leak chamber temperature	Thermocouple Type K grounded	N/A	±1°C abs	0.1°C

\* Full Scale

**Table 3.2. Mass spectrometer ASM 180T specifications.**

Specifications	Range
Standard roughing system	20 m <sup>3</sup> /h (15cfm) oil sealed pump
High vacuum pump	130 l/s hybrid pump
Fine leak, Helium signal reading range	10 <sup>-10</sup> – 10 <sup>-1</sup> m bar.L/s (mL/s at P <sup>*</sup> )
Gross leak, Helium signal reading range	10 <sup>-8</sup> – 10 <sup>-2</sup> m bar.L/s (mL/s at P <sup>*</sup> )
Accuracy	Depends on the calibrated leak used for mass spectrometer calibration, and on the leak rate range
Maximum absolute error	<100% of measured value
Repeatability error	<1% of the measured value

\* Atmospheric pressure

### 3.6.3 ROTT test procedure

The ROTT test procedure is documented in the ASTM method Draft no. 9 of the *standard test method for gasket constants for bolted joint design*, [27], and references [28, 29], and it is briefly describe herein. The ROTT test is performed on a NPS 4-in gasket and platens surface finish of 250  $\mu$ -in (6.3  $\mu$ m) AARH, machined with turning procedure of spiral cut. The mass leak rate measurement is based on NPS 4 gasket ( $\approx$ 150mm gasket O.D.) and it is calibrated based on a reference mass leak rate  $L_{rm}^*$  defined as 1.0 mg/s for a reference diameter 150 mm gasket. The RTHR rig test is used with helium gas as the pressurised fluid. The gasket loading takes place by hydraulic machine for initial compressive stress levels starting at 1025 up to 15,160 psi, based on full-contact gasket area. The gasket loading consists of two different parts, A and B, as shown in Figure 3.8, which includes three seating or loading (Part A) and three unloading (Part B) cycles.

**Part A** represents initial gasket seating stress and joint tightening. Test includes five main stress levels S1 to S5, and intermediate stress levels S2.5, S3.5, and S4.5. The stress levels correspond to a low-to-high range of typical pipe-fitter-imposed bolting stress and their values depend on the type of tested gasket. The helium gas pressure is alternated at the main stress levels to 400 and 800 psig. For each main stress level, leak is measured at these two helium pressures, except at the stress level S1. The helium gas pressure at initial stress level S1 depend on the gasket leakage. Such a precaution is necessary to avoid an uncontrolled gasket blow out, or unnecessary mass spectrometer saturation. The test is performed at ambient temperature. Part A sequence simulates the seating performance of a gasket during initial tightening, and its data is also used to determine the required seating stress which is similar to the  $y$  factor of the ASME code, Appendix 2, [30].

**Part B** sequence of the ROTT test simulates the operating conditions, of bolted flanged joints, by performing unload-reload cycles, representing the gasket unloading, relaxation and retightening during operations. The leak rate is measured at each stress levels during Part B cycles while the helium gas pressure is maintained constant at 800 psig. Data obtained from Part B sequence is used to determine the operating gasket load, and is similar to the  $m$  factor of the ASME code, [30]. As precautions, it has to be emphasized that ROTT test cannot be used to determine the  $m$  factor. The part B data is used in conjunction with part A data to evaluate the minimum gasket seating stress that is required in order to maintain a certain sealability level. In other words, not to exceed a certain leak rate value under the joint operating conditions.

The main stress levels on the gasket depend on the gasket materials and they are categorised in three sets, namely *soft*, *standard* and *hard (solid metal)* test procedures, as described in Table 3.3. Soft stress values are considered for gaskets such as neoprene rubber and PTFE sheets and spiral wound gaskets of the class 150. Standard stress values are applied to most sheets and composite gaskets such as graphite sheets, metal jacketed and spiral wound types (except class 150, for which the soft procedure is applied). Where, hard (solid metal) stress values are applied to flat steel, nubbin facing against flat steel, corrugated steel, and steel ring-type-joint (RTJ) gaskets, [28]. The gasket testing using the ROTT test procedure takes up to 3 days depending on the gasket sealing characteristics. It has to be emphasized here that ROTT test is so far best gasket test procedure at room temperature, a proven testing method that simulates the gasket behavior in real operating conditions.

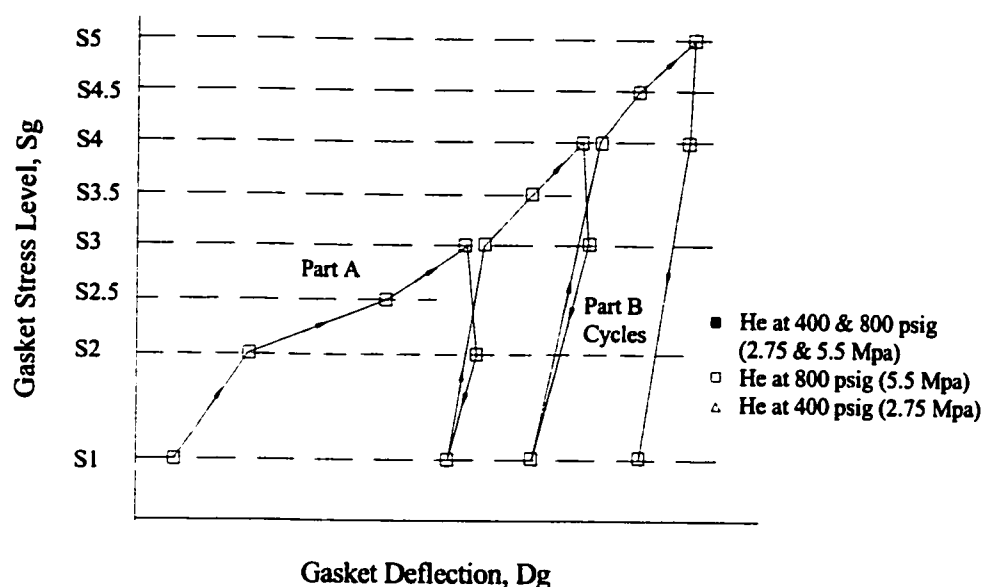


**Figure 3.8.** Stress vs. deflection curve showing the generic ROTT test procedure sequence, typical results for a given gasket material. [28].

**Table 3.3.** ROTT test procedure stress levels [28].

S level	Gasket stress, Sg					
	Standard		Solid Metal		Soft	
	Mpa	psi	Mpa	psi	Mpa	psi
S1	7.1	1,025	10.6	1,540	7.1	1,025
S2	31.4	4,560	47.1	6,840	20.9	3,040
S2.5	431.6	6,330	65.4	9,490	29.1	4,220
S3	55.8	8,090	83.7	14,140	37.2	5,390
S3.5	68.0	9,860	102.0	14,790	45.3	6,575
S4	80.2	11,630	120.3	17,450	53.5	7,750
S4.5	92.4	13,395	138.5	20,095	61.6	8,930
S5	104.2	15,160	156.8	22,740	69.7	10,110

**Table 3.4.** Typical load-pressure sequence for the “Standard” ROTT procedure [28].

Test step	Test step	S level	Gasket stress		Test gas pressure	
			Mpa	psi	Mpa	psig
1	A	S1	7.1	1,025	2.8	400
2	A	S2	31.4	4,560	2.8	400
3	A	S2	31.4	4,560	5.5	800
4	A	S2.5	43.6	6,330	5.5	800
5	A	S3	55.8	8,090	2.8	400
6	A	S3	55.8	8,090	5.5	800
6	B	S3	55.8	8,090	5.5	800
7	B	S2	31.4	4,560	5.5	800
8	B	S1	7.1	1,025	5.5	800
9	B	S3	55.8	8,090	5.5	800
10	A	S3.5	68	9,860	5.5	800
11	A	S4	80.2	11,630	2.8	400
12	A	S4	80.2	11,630	5.5	800
12	B	S4	80.2	11,630	5.5	800
13	B	S3	55.8	8,090	5.5	800
14	B	S1	7.1	1,025	5.5	800
15	B	S4	80.2	11,630	5.5	800
16	A	S4.5	90.4	13,400	5.5	800
17	A	S5	104.2	15,160	2.8	400
18	A	S5	104.2	15,160	5.5	800
18	B	S5	104.2	15,160	5.5	800
19	B	S4	80.2	11,630	5.5	800
20	B	S1	7.1	1,025	5.5	800

### **3.6.4 Modified ROTT test procedure**

In the present research, the common ROTT test procedure steps are modified, using the same RTHR rig test machine, for the purpose of evaluating the sealing surface characteristics on the sealing performance of gasketed flanged joints. The modified ROTT test procedure considers two part stress level cycles for both soft and standard procedures. In each cycle the stress is increased incrementally, and then decreased to the initial stress level, Table 3.1. This simulates both the end load effect and bolt load relaxation during the service, and perhaps the most important information gained is the sensitivity of the system under investigation to the loss of compressive stress. The stress level at each test point remains constant until a stabilized leak rate is measured, then it is incremented or decremented to the next stress level, while the helium gas pressure is kept constant during the entire experiment. Keeping the gas pressure constant ensures the elimination of transitory gas pressure effect on the gasket leak rate. Only the effect of stress level and platens surface characteristic is evaluated for the given test gasket.

The leak rate decreases while incrementing the gasket stress, and it is expected to increase at the decrementing loads, however for the same stress level, as in the first loading (Part A) the leak rate is somewhat less. This is due to the fact that while the gasket stress level is increased to its maximum level in a cycle, the gasket compaction increases, thus reducing the overall pore size of the gasket. Also there is the phenomenon of flow of softer material (gasket) into the hard rougher surface (flange face), and the adaptation of the gasket to the platens surface form, filling-in the irregularities of the flange face. These result in the reduction of the leak through the pore channels of the gasket, as well as leak between the mating faces. Thus, we should assume that different surface characteristics should have different effects on the leak rate and gasket sealability, for a give gasket. Therefore, the effect of gasket stress, gas pressure and flange surface characteristics can be evaluated from a series of test by changing only these test parameters.

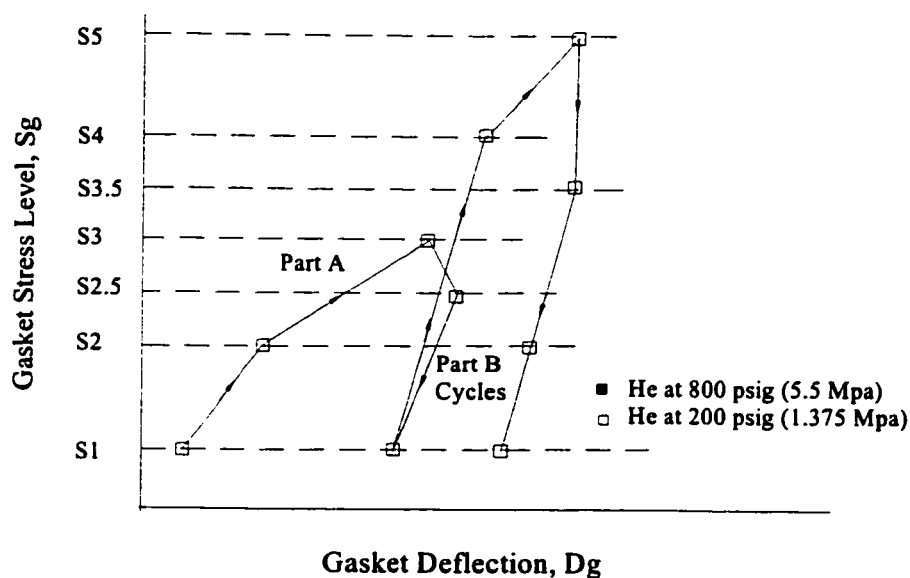


**Figure 3.9.** Typical stress vs. deflection curve showing the modified ROTT test procedure sequence.

**Table 3.5.** Stress levels on gasket for the modified ROTT test.

	Stress	Soft	Standard		Gas Pressure, psig				
	Levels	Stress values	Stress values		Test	Series 1	Test	Series 2	
		(PTFE)	(SW, graphite sheet)						
Cycle 1		psi	MPa	psi	MPa	psig	MPa	psig	MPa
Cycle 2	S1	1025	7.07	1025	7.07	200	1.38	800	5.52
	S2	3040	20.98	4560	31.46	200	1.38	800	5.52
	S3	5390	37.20	8090	55.82	200	1.38	800	5.52
	S2.5	4220	29.12	6325	43.64	200	1.38	800	5.52
	S1	1025	7.07	1025	7.07	200	1.38	800	5.52
	S1	1025	7.07	1025	7.07	200	1.38	800	5.52
	S4	7750	53.50	11630	80.25	200	1.38	800	5.52
	S5	10107	69.70	15160	104.60	200	1.38	800	5.52
	S3.5	6575	45.37	9860	68.03	200	1.38	800	5.52
	S2	3040	20.98	4560	31.46	200	1.38	800	5.52
	S1	1025	7.07	1025	7.07	200	1.38	800	5.52



If the same test procedure is repeated for a given gasket type (from the same batch) using platens with different surface characteristics, the comparison of two or more tests provides information on the effect of surface characteristic on gasket compaction (deflection), as well as on its leak rate.

The effect of gas pressure under different stress levels and different surface characteristics can be determined by repeating the same test procedure at different helium gas pressure, on the same gasket type. And once again keeping the gas pressure constant during each test will ensure the singularity of both the gas pressure effect and the characteristic of the leak flow regimes. Also, while increasing the stress level the amount of stress required to ensure sealing at different gas pressures can be determined.

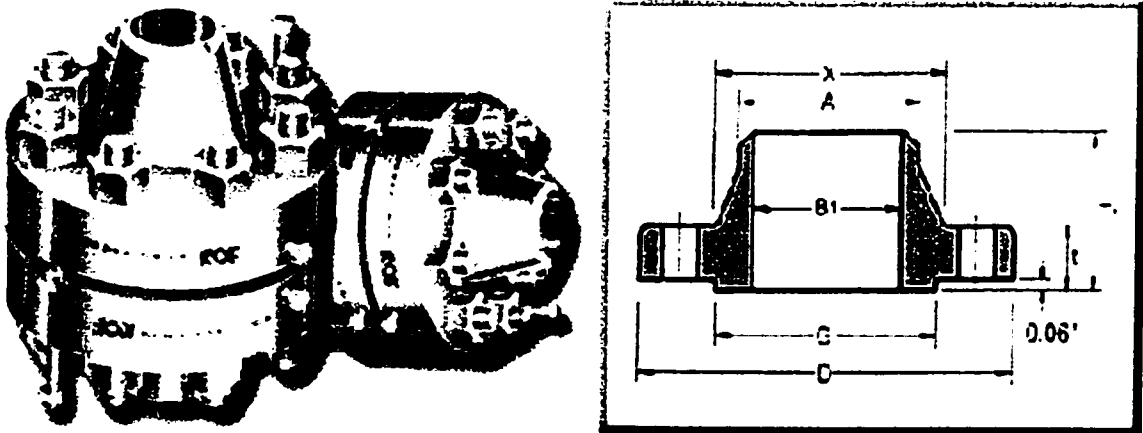


**Figure 3.10.** Typical bolted flanged joints assembly with raised face flange surface.

### **3.6.5 Differences between the ROTT test and the modified ROTT test procedure**

ROTT test is a well recognized gasket qualification test procedure at ambient temperature, as described earlier. While the modified ROTT test procedure applied in this experimental research simply uses the main stress levels S1-S5, it differs from the standard ROTT procedure by which its number of measurement points are reduces from 20 to 9, and the number of load cycles are also reduced from 3 to 2. (See Figures 3.8 and 3.9). Furthermore, unlike the generic ROTT test that, at the main stress levels, interchange the helium gas pressure level between 400 and 800 psig, the gas pressure is kept constant, for the duration of the test, in the modified ROTT test procedure. The modified ROTT test is performed at 200 and 800 psig helium gas pressures. While the pressure of 800 psig corresponds to one of the gas pressure applied in the generic ROTT test procedure, and as such, can be used as a reference, it is for some non-metallic gasket material (i.e. PTFE Gylon 3504) considered the maximum allowable gas pressure at which the test can be performed safely, in order to avoid gasket blow out at low stress levels. The low level helium gas pressure at 200 psig is selected to allow the determination of the leak flow regimes, in comparison with the test ran under similar conditions at 800 psig, as well as the development of fuzzy decision support system algorithms presented later in this research.

### **3.6.6 Platens surface configuration and surface characteristics**

While the flange sealing surface configurations are limited to a few numbers in the case of metal-to-metal seals (i.e. annular raise and flat, annular raises, tongue and groove), when an intermediate material is used between sealing surfaces, the number of configurations increases considerably. Flange geometries may be produced in different configurations such as Tongue and Groove, Full Face/Flat face, Raised Face and Ring Joint, etc. In all configurations the sealing is dictated by the portion of the flange surfaces

in contact with the intermediate gasket material providing the required sealing. It also depends on the sealing surface characteristics, the apparent area of contact and associated stress, which are extremely difficult to calculate depending whether the seal is metallic, non-metallic, combination of both, or if the materials are in the plastic or elastic range. The only type of test platens (flanges) geometry considered for this experimental research is the “Raised Face”, Figure 3.11, machined from 20- $\mu\text{in}$  (0.508  $\mu\text{m}$ ) up to 1000- $\mu\text{in}$  (25.4  $\mu\text{m}$ ) with different machining procedures, as described in Table 3.6.

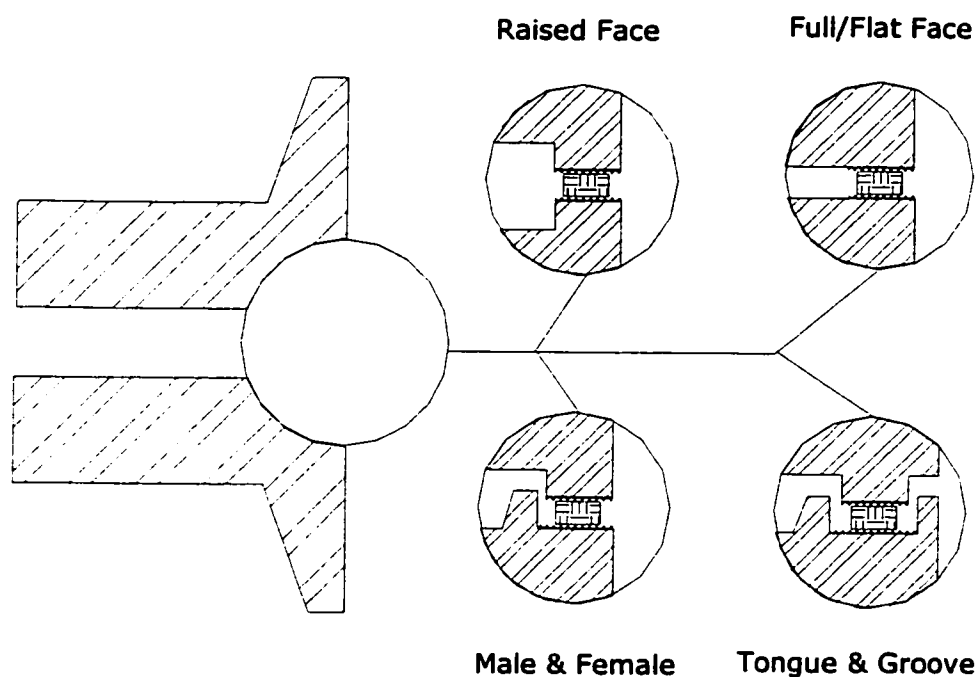


**Figure 3.11.** Different types of flange faces.

Sealing surface characteristics play an important role in the sealability of the system. In this work it is shown experimentally that different sealing systems, identical in material and sealing surfaces, yield different leaks under identical applied stresses, depending whether surfaces are produced by milling, turning or grinding procedures. Thus, the

experiments are designed to investigate and to measure the sensitivity of sealing to such parameters as surface characteristics, gasket material, sealing stress and contained fluid pressure. As a result, eight different surfaces are produced by grinding, turning and milling machining procedures.

While ground type surfaces have low peak-to-valleys asperities (with least radial channels) relative to the milled surface, they lack substantially the gripping force that milled surfaces will provide on the gasket. So, the use of ground type surfaces may result on gasket radial slippage and blow out, especially at low stress level with high internal fluid pressure, when soft gasket material is used. Being considered rough, milled surfaces may provide better gasket stability under similar conditions.

Milled type surface are not commonly used in the industry, but their inclusion in the present study may shed some light about the leaks and flow behaviour as well as the sensitivity of gasket material and of sealing surfaces at different gas pressures and stresses. Surfaces produced by milling generally have large radial leak paths encroaching from the pressure side to the atmospheric side. Milled surface can be produce with different machining procedures resulting in very different surface characteristics, as described later in this section. Ground surfaces of different surface roughness also provide valuable information above their sealability for which their surface asperities peak-to-valleys differ. Turned surface are commonly used in industries, and surface roughness of 150 to 500  $\mu\text{in}$  (3.15 to 12.6  $\mu\text{m}$ ) is recommended in the flange standards, such as ASME/ANSI B16.5, [31]. Turned surfaces of concentric and continuous spiral cut of different surface roughness are being subject of the tests. The later has spiral leak path from pressure side to the atmospheric side. Thus the comparison of leak and flow behaviours resulting from the two turned surfaces under different operating conditions should provide valuable information of the effect of the sealing surface to parameters such as the gasket material, pressure and stress. The surface characteristics of the test platens are described in the following.

The platens are made of stainless steel 304, a material commonly used for flanges in industrial applications. Two ground surfaces with roughness values of  $Ra$  17~25  $\mu\text{in}$  (0.43~0.635  $\mu\text{m}$ ) and 75~85  $\mu\text{in}$  (1.9~2.16  $\mu\text{m}$ ) are machined. Two milled surfaces with surface roughness values ranging from  $Ra$  135~315  $\mu\text{in}$  (3.43~8.0  $\mu\text{m}$ ) and 350~870  $\mu\text{in}$  (8.9~22.1  $\mu\text{m}$ ) are machined using two different tooling and milling procedures. The milled surfaces of roughness 135~315  $\mu\text{in}$  (3.43~8.0  $\mu\text{m}$ ) are machined with two linear pass cuts. The platens are fixed stationary, and a milling tool of 2.362 in. (60 mm) in diameter is used. The milled surfaces of roughness 350~870  $\mu\text{in}$  (8.9~22.1  $\mu\text{m}$ ) are machined with one pass cut, where the platen is set on the rotating platform, and a milling tool of 1.969 in. (50 mm) in diameter is used.

**Table 3.6.** Machining parameters and procedures used to produce platens.

Machining Procedure	Surface Form	Ra ( $\mu\text{in}$ )	Ra ( $\mu\text{m}$ )	Platens ID	Tool Tip Radius (in.)	Depth of Cut (in.)	Tool Feed Groove Spacing (in.)	Speed of Cut (RPM)	Feed
Turning	Spiral Stock Finish	650-720	16.5-18.3	I3	1/16	~ 0.020	~ 0.080	265	C <sup>*1</sup>
		860-900	21.8-22.8	II	1/32	~ 0.031	~ 0.075	265	C <sup>*1</sup>
	Concentric Stock Finish	630-710	16-18	J3	1/16	0.020	0.080	265	R <sup>*2</sup>
		840-900	21.3-22.8	J1	1/32	0.031	0.075	265	R <sup>*2</sup>
Milling	Milled Two Passes	135-315	3.43-8.0	II2	$\varnothing$ 2.362	----	N/A	----	C <sup>*1</sup>
	Milled One Pass	350-870	8.9-22.1	II3	$\varnothing$ 1.969	----	N/A	----	C <sup>*1</sup>
Grinding	Grind	17-25	0.43-0.64	III1	N/A	N/A	N/A	N/A	N/A
	Grind	75-85	1.9-2.16	III2	N/A	N/A	N/A	N/A	N/A

\*1 Continuous

\*2 Retracting Tool

Four types of turned surfaces are machined, two of which are of spiral cut stock finish and two others of concentric cut stock finish, with roughness values ranging between  $Ra$  630~720  $\mu\text{in}$  (16~18  $\mu\text{m}$ ), and 840~900  $\mu\text{in}$  (21.3~22.86  $\mu\text{m}$ ). The spiral cut stock finish surfaces of roughness 650~720  $\mu\text{in}$  (16.5~18  $\mu\text{m}$ ), are produced with continuous tool feed

rate of 0.044 in. per revolution (1.12 mm/rev), using a tool tip radius of 1/16 in. (1.6 mm). The spiral cut stock finish surfaces of roughness 860~900  $\mu\text{in}$  (21.85~22.86  $\mu\text{m}$ ), are produced using a 1/32 in. (0.8 mm) tool tip radius with continuous feed rate of 0.031 in. per revolution (0.787 mm/rev).

Concentric cut stock finish surfaces are produced by repositioning the tool after cutting each groove in a complete revolution. To produce a concentric stock finish surface form of roughness value  $Ra$  630~710  $\mu\text{in}$  (16~18  $\mu\text{m}$ ), a cutting tool with tip radius of 1/16 in. (1.6 mm) is used. The depth of the cut is 0.020 in. (0.508 mm) with a groove spacing of 0.080 in. (2.03 mm), and the speed of the cut is kept constant at 265 r.p.m. The concentric cut stock finish surfaces of 840~900  $\mu\text{in}$  roughness are machined using a tool of tip radius 1/32 in. (0.8 mm). The depth of the cut is 0.031 in. (0.787 mm) at 265 r.p.m., with a groove spacing of 0.075 in. (1.9 mm).

The surface characteristics of the test platens described above are summarized in Table 3.6, along with their identification ID, roughness values, surface form and the machining parameters used to produce them. The test platens surface topography results, presented in Figure 3.12, are measured in X direction for turned surfaces II, I3, J1, and J3, while the measurements for milled and ground type surfaces II2, II3, III1 and III2 are taken in the Z direction as indicated on Figure 3.13. Refer to the rectangular Cartesian coordinate system shown at the top-right corner of Figure 3.13. From these topographies it can be deduced that surface roughness and waviness of turned surfaces along the X direction, provide stress distribution that lays perpendicular to the direction of the fluid flow, from the pressurized side to the vacuum side of the platens. Opposite to these are the topographies of milled and ground surfaces where their peak-to-valleys surface asperities and waviness provide stress distribution somewhat parallel to the fluid flow direction.

It is worth mentioning that the test platens described in this section are originally produced by CETIM (Centre Technique des Industries Mecaniques/The Technical Center

for Mechanical Engineering Industries of France in Nantes). These platens were sent to TTRL for a series of experimental investigations based ROTT and Crush Tests with various gasket types, designated by CETIM and European gasket manufacturers. Consequently, the present experimental work took advantage of the availability of these platens to also investigate their effects on the sealing performance of expanded PTFE sheet, flexible graphite sheet, and spiral wound gaskets, as described in the following section. In addition to the ground, milled and turned spiral finished test platens of CETIM, other test platens of turned concentric finished are produced, at Machining Centre of Ecole Polytechnique of Montreal, to match those of turned spiral finished. It has to be indicated that the turned spiral cut surface of roughness value  $Ra = 250 \mu\text{in}$  is the standard finish for ROTT test, and it is used commonly in most industrial applications. The experimental data with this finish were already available for the test gaskets selected for the present research, thus experiments with turned finished surfaces of other roughness values described above would reveal interesting results on the effect of roughness for turned surface form.

### 3.6.7 Test gaskets

The three gasket types selected for the present research are,

- 1) PTFE GYLON 3504 sheet,
- 2) Flexible graphite (G2) sheet, **Grafoil GHR™**
- 3) Flexitallic spiral wound with flexible graphite filling.

These gaskets are selected because they are most commonly used in the industries. There have been many test performed on these types of gaskets for the evaluation of their sealability. The test performed on these gaskets can cover a broad range of gaskets since they have very different designs that distinguish one from another. When testing these gaskets with different surfaces, under different applied load they do not deteriorate the

test surfaces, this is mainly true for PTFE and graphite type gaskets. So the test platens/flanges could be reused for further tests without remachining.

The PTFE gasket provides a high degree of flexibility to fill-in the surface roughness and irregularities and the existing gaps generated by the machining process on the platens surfaces, under a moderate to high load. Usually PTFE gasket types have low strength and exhibit a permanent creep. The strength and creep of PTFE gasket can be improved with incorporating into the material fillers such as carbon fiber, glass microspheres (fibers), graphite and precipitated silica or other inorganic fillers, [34,35]. The leak flow may be mainly due to interfacial leaks past sealing surfaces, considering a low porosity for this type of gaskets. The leak behaviour of this type of gasket varies depending on the load and flange surface characteristics especially at low stress level. If the gasket has gone through plastic deformation at high stress levels, then it is going to be more sensitive to unloading depending on the flange surface characteristics. This will be demonstrated later in the analysis of the experimental results, section 3.7.2.

The flexible graphite sheet gasket is typically made of particulate graphite flakes and provides the necessary filling in the platens surfaces irregularities, due to its flexibility and should remain sticking to the flange surfaces provided that the load remains stable. However, the gasket type is fairly porous since it is made of particulate graphite flake. The flexible graphite tends to cling to the platens surfaces. It might be speculated that the leak flow through the gasket should be of the molecular type since gas molecules have to pass through pores of the particulate flakes. The flow may become laminar if as a result of load-unloading stress levels gasket degradation occurs such that the interfacial and pore channel leak paths sizes are increased under the increase of gas pressure, resulting in the larger leak flow rates.

The spiral wound gasket selected for this research is made of stainless steel metallic windings with flexible graphite filler, (this type of gasket is considered as semi-metallic).



The graphite material provides initial filling of the irregularities on the flange faces at the initial loadings. No porosity can be considered for this type of gasket because of the presence of the metallic winding, thus the leak through the gasket can be simply ignored, except for the leak through the pores of graphite material encroaching/intruding the platens surfaces. Although the leak rate through the gasket may be assumed very low, or simply be ignored, the interfacial leak on the mating surfaces may be large due to the improper mating of the sealing surfaces and the gasket's metal strip winding, especially in the case of milled type surfaces which have radial channels from the upstream to the downstream pressure sections.

In order to provide a consistency between the experimental data, all PTFE and flexible graphite sheet gaskets are cut from the same respective sheets. Gaskets of sheet materials are pre-cut to  $4.875 \pm 0.010$  in. ID ( $123.8 \pm 0.25$  mm) and  $5.875 \pm 0.010$  in. OD ( $149 \pm 0.25$  mm). The PTFE gaskets are cut from a sheet of 0.064 in, thickness, whereas the flexible graphite gaskets G2 are cut from a sheet of 0.62 in, thickness. All gaskets are inspected to be free of defect, clean and free of burs. Gaskets selected are considered to be consistent with the 150 mm reference diameter of the ROTT test, and have a nominal area of  $A_g = 8.45 \text{ in}^2$  ( $5450 \text{ mm}^2$ ). The Flexitallic spiral wound gaskets are made to the standard size 4" NPS Class 600, having dimensions of 4.75 in. ID  $\times$  5.875 in. OD  $\times$  0.175 in. thick ( $149 \times 121 \times 4.45 \text{ mm}^3$ ). It is consistent with the 4-inch NPS gasket size, with outside diameter suitable for the ROTT fixture, the RTHT rig. The gasket specifications are described in the following.

#### **3.6.7.1 Specifications for PTFE sheet gasket Gylon 3504**

The PTFE gasket is made by polymerisation of its monomer tetrafluoroethylene (TFE) and reinforced by glass microspheres, with strong bonding structure at temperature lower than  $400^\circ\text{C}$ . It may be considered to have a low degree of porosity, with permeability less

than 0.015 cc/min, (Gore-Tex Gylon manufacturer web site.) Blue PTFE gasket Gylon 3504 has a very compressibility, ranging between 25% to 45% of its initial thickness, due to its inorganic microspheres, and has a minimum recovery of 30%. This enables the gasket to mate better the flange face surface, thus provides tighter sealing under lower gasket loads. It has tensile strength of 2000 psi (14 N/mm<sup>2</sup>) with a creep relaxation of up to 30%. The operating temperature range as specified by the manufacturer is from -210°C to +260°C, where the maximum allowable operating pressure is 800 psig (55 bar). This gasket has a permeability of less than 0.015 cc/min, (ref.: Gore-Tex Gylon gasket manufacturer web site.)

### **3.6.7.2 Specifications of flexible graphite sheet (G2) gasket, Grafoil GHR™**

Flexible graphite sheet (G2) gasket, Grafoil GHR™ is metal reinforced laminate with flat 316/316L stainless steel foil insert (0.002 in./0.05 mm. thick) adhesively bonded to Standard Industrial Grade GTB flexible graphite sheet facing. In general flexible graphite has found applications in chemical gaskets, high temperature automotive gasket, heat shielding, and noise damping components. Flexible graphite has gained importance in industrial application due to banning of asbestos gasket material. It can be used as a replacement material for asbestos or other inferior substitutes because its non-fibrous structure withstands the harshest chemicals. Flexible graphite is fire resistant has high excellent tensile strength and is in some degree environmentally safe, typically containing 98% elemental carbon by weight. The standard density of GRAFOIL flexible graphite (G2) is 70 lbs/ft<sup>3</sup> (1.12 g/cc), (ref.: Flexible Graphite Grafoil® gasket manufacturer web site). Grafoil flexible graphite is flexible, compressible, resilient, chemically inert, fire safe, and stable under load and temperature. It is also anisotropic due to its crystalline structure and has excellent directional, electrical and thermal conduction properties.

However, flexible graphite can be considered as highly porous media since it is produced from particulate graphite flakes. The graphite flakes are processed through an intercalation process using strong mineral acids, and then heated to volatilise the acids and expand the flake to many times its original size. This expansion process produces a wormlike, dendritic-like structure that is then formed by moulding or calendering (glazed) into sheets. No binders are introduced in the manufacturing process.

### **3.6.7.3 Specifications of spiral wound graphite filled gasket (SW), Flexitallic**

The necessity to seal effective under high pressure and temperature variations, flange rotation and vibrations, demands a gasket with adequate stress retention, flexibility and recovery. Spiral-wound gaskets have been especially designed for this purpose. Spiral element with various fillers are used for tongue and groove flange faces, with metallic inner ring for use with "male and female" flanges, with metallic outer ring for use with flat face and raised face flanges, with metallic inner and outer ring for use with flat face and raised face flanges. Metallic inner ring protects sealing element from high temperatures, prevents turbulences in piping and protects flange from corrosion; prevents the inward buckling of the spiral element. Metallic outer ring ensures proper positioning and prevents over-compression, of the gasket metallic strip windings. Material for metal winding strip is stainless steel AISI 304, roughly 0.0067-0.007 in. thickness, where material is used for the supporting outer ring is carbon steel. Spiral wound comes with different filler materials, depending on the applications. The spiral wound gasket used in this research is the Flexitallic (Nominal Pipe Size) NPS 4-in class 600, type Flexicarb CG, that has flexible graphite filler and outer support ring. The maximum operating temperature for graphite filled is 550°C (1022°F), as specified by the manufacturer. It must be noted that the Standard ROTT test stress values are applied on this gasket, see detail in section "3.6.3 ROTT test procedure". The gaskets standards for metallic and non-metallic gasket types can be found in the references [32, 33], respectively.

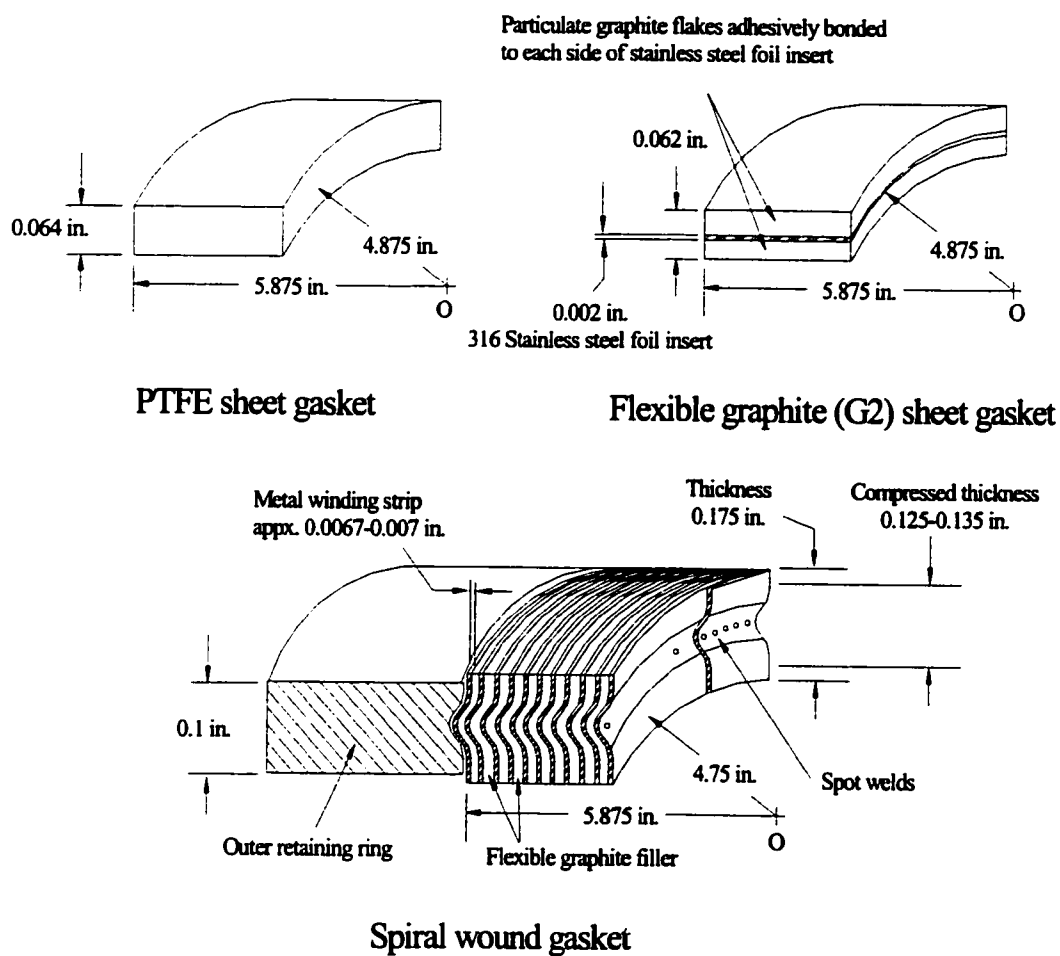


**Figure 3.11B.** Typical cross section of expanded PTFE sheet, flexible graphite (G2) sheet and spiral wound gasket.

### **3.7 Experimental results**

#### **3.7.1 Tests conducted**

A total of 48 tests are performed on eight surface characteristics and three types of gaskets at 200 and 800 psig helium gas pressure levels. The two cycles test procedure sequences (modified ROTT test) is used, see Figure 3.9 and Table 3.5. Platens of the same identification number representing the same surface finish are mated with gaskets always in pairs, no direct metal-to-metal seal is used. These surfaces are described in Table 3.6, and their topographies are presented in Figures 3.12 & 3.13. The gaskets are inspected before tests to ensure that they are uniformly thick and free of defect (surface defect, radial scratch, damage due to bent, pre-stressed surface, etc.) that could affect the leak results. The gaskets are never reused. Each gasket material is utilized with each of the eight different sealing surfaces, such that for a given gasket material, the effect of the different surface characteristics could be appraised.

For every test the gasket is initially compressed between a pair of platens, the surfaces of which have some asperity distribution, so that the higher asperities on the sealing surfaces (platens) would mate. When the gasket stress is increased to the first stress level S1 (see Table 3.5), and sufficient time is given for the gasket stabilization, the surface asperities penetrated into the gasket. As a result of, the area of contact slightly increased. Then the internal volume of the gasket is pressurized to a predetermined constant pressure, and some time is given for leakage stabilization before the leak measurement.

The test results for PTFE gasket are presented in the graphs of Figures 3.14 through 3.19. Whereas, the test results for flexible graphite G2 gasket are given in the graphs of Figures 3.20 through 3.25, and the test results for spiral wound gasket are shown in the graphs of Figures 3.26 through 3.31. Flow regimes indicate the behaviour of gasket and sealing surfaces under different gasket compressive stress and internal gas pressure. As a results, the leak flow regimes based on the slope of the line from log-log plot of leak rate versus

pressure are presented in Figures 3.32, 3.33 and 3.34 for all surface characteristics tested with PTFE, flexible graphite G2 and spiral wound gaskets, respectively.

For PTFE gasket, the effect of gasket compressive stress levels on the leak rate based on different surface characteristics are presented in Figures 3.14 and 3.15 for a specified internal helium pressure. Test results in Figures 3.14(a & c) and Figures 3.15(a & c) are at 200 psig, while the results in Figures 3.14 (b & d) and Figures 3.15(b & d) are at 800 psig. The effect of helium gas pressure on the leak rates under the applied gasket stress levels, for a specific platen surface characteristic is presented in Figures 3.16 and 3.17. Furthermore, Figures 3.18(a & b) and 3.19(a & b) present the leak rates results as a function of surface characteristics, for specified stress levels, and specified gas pressure. Whereas Figures 3.18(c & d) and 3.19(c & d) present the gasket deflection results as a function of surface characteristics, for all surfaces, for specified stress levels, and specified gas pressures. Test results in Figure 3.18 are at 200 psig, while the test results in Figure 3.19 are at 800 psig.

Test results for flexible graphite G2 gasket given in Figures 3.20 and 3.21 present the effect of gasket stress levels on the leak rate based on the effect of surface characteristics, for a specified internal helium pressure. Test results in Figures 3.20(a & c) and Figures 3.21(a & c) are at 200 psig, while the results in Figures 3.20(b & d) and Figures 3.21(b & d) are at 800 psig. Effect of helium gas pressure on the leak rate based on platens surface characteristic under the applied gasket compressive stress levels are given in Figures 3.22 and 3.23. Furthermore, Figures 3.24(a & b) and 3.25(a & b) present the leak rate results as a function of surface characteristics, for specified stress levels and gas pressures. The gasket deflection results as a function of surface characteristics, for specified stress levels and gas pressure are given in Figures 3.24(c & d) and 3.25(c & d). Test results in Figure 3.24 are at 200 psig, while the test results in Figure 3.25 are at 800 psig.

Test results for spiral wound gasket presenting the effect of gasket stress levels on the leak rate while comparing the effect of surface characteristics for a specified internal helium pressure are given in the graphs of Figures 3.26 and 3.27. Test results in Figures 3.26(a & c) and Figures 3.27(a & c) are at 200 psig, while the results in Figures 3.26(b & d) and Figures 3.27(b & d) are at 800 psig. The effect of helium gas pressure on the leak rate based on platens surface characteristic under the applied gasket compressive stress levels are given in Figures 3.28 and 3.29. The leak rate results as a function of surface characteristics for specified stress levels, and gas pressures are presented in Figures 3.30(a & b) and 3.30(a & b). The gasket deflection results as a function of surface characteristics based on specified gasket compressive stress levels, and gas pressure are given Figures 3.30(c & d) and 3.31(c & d). Test results in Figure 3.30 are at 200 psig, while the test results in Figure 3.31 are at 800 psig.

It is worth indicating that for most tests performed at 800 psig the gas pressure at the initial stress level S1 is set to 200 psig instead of 800 psig, (for definition of stress levels S1 to S5 refer to Figure 3.9 and Table 3.5). This is designed to avoid gasket blow out especially in the case of ground surfaces and also to avoid saturation of the mass spectrometer due to high leak rates in the case of Milled surfaces. Thus, in order to provide a clear indication of this change on the graphs, if the first stress S1 value of 800 psig test series is set to 200 psig or less, it is marked on the graph. For PTFE sheet gasket see Figures 3.14 to 3.17, for flexible graphite G2 sheet gasket see Figures 3.20 to 3.23, and spiral wound gasket see Figures 3.26 to 3.29.

For all tests, the leak rate at each stress level is plotted for the different flange surface finishes. The reduction in leak rate due to the increase of normally applied stress level on the gaskets can be observed comparing the consecutive plots in Figures 3.14 to 3.15 for PTFE gasket. Similar plot for graphite and spiral wound gaskets, are given in Figures 3.20 to 3.21 and Figures 3.26 to 3.27 respectively. The increase in leak rate due to the increase of helium gas pressure can be observed from the plotted results on each platen

surface finish, in Figure 3.16 and 3.17 for PTFE, Figure 3.22 and 3.23 for G2, and Figure 3.28 and 3.29 for SW gasket.

In order to better appreciate the effect of surface characteristics (roughness and form) on the leak rate, the leak behaviour and the gasket deflection at different stress levels and gas pressures, the ground type flange surface III1 of 20  $\mu$ in roughness is used as a reference (see Table 3.6 for definition of surface characteristics). This surface is selected as a reference since it does not present a pronounced surface machining form, and assuming that surface form error are negligible, it has the lowest roughness value among others that can be used as a reference surface finish. Consequently the leak rate and gasket deflection ratio of other surfaces to the reference surface are obtained. The results are provided in Tables 3.7 through 3.27.

Experimental test results indicating the effect of gas pressure on the leak rate at a given stress level for all surface characteristics are presented by the leak ratio at 800 psig to 200 psig. These results are given in Tables 3.7, 3.8 and 3.9 for tests on PTFE, flexible graphite G2 and spiral wound gaskets, respectively. In order to appreciate the effect of surface characteristics on the leak rate, for a given gasket stress level, the experimental test results are presented as the leak ratio of each surface to the reference ground surface III1. These results, for test performed at helium gas pressure 200 psig, are presented in Tables 3.10, 3.11 and 3.12 for PTFE, flexible graphite G2 and spiral wound gaskets, respectively. Similarly, for tests performed at helium gas pressure of 800 psig, results are presented in Tables 3.13, 3.14 and 3.15 for PTFE, flexible graphite G2 and spiral wound gaskets, respectively.

Furthermore, the effect of surface characteristics on the leak rate and gasket deflection may be better appreciated by presenting the results as the leak rate and gasket deflection ratio, based on the gasket load and unloading stress levels ratio, for given surface characteristics. Therefore, the test results for PTFE, flexible graphite G2 and spiral wound



gaskets, presenting the leak and deflection ratio of different stress levels at 200 psig, are given in Tables 3.16, 3.17 and 3.18, respectively. Similarly, test results for PTFE, flexible graphite G2 and spiral wound gaskets presenting the leak and deflection ratio of different stress levels at 800 psig are given in Tables 3.19, 3.20 and 3.21, respectively.

In addition, experimental results presenting the gasket deflection ratio of each surface to the reference ground surface III1, would reveal interesting results on the effect of surface characteristics on the gasket deflection and material flow, at different stress and internal gas pressure. These results, at helium gas pressure 200 psig, for tests with PTFE, flexible graphite G2 and spiral wound gaskets are presented in Tables 3.22, 3.23 and 3.24, respectively. Similarly, the test results at helium gas pressure 800 psig are given in Tables 3.25, 3.26 and 3.27.

The effect of surface characteristics on the flow regimes for a specific gasket type may be better appreciated when the results are presented in numeric values in a table format. Table 3.28 presents the slope of the lines from log-log plot of the leak versus gas pressure, for PTFE, flexible graphite G2 and spiral wound gaskets, obtained from their respective graphs in Figures 3.32, 3.33 and 3.34, indicating the flow regimes for each surface characteristics. The analysis of the experimental results given in the figures and tables indicated above are presented as follows.

### **3.7.2 Results of PTFE Gylon gasket tests**

#### **3.7.2.1 PTFE test results at gas pressure 200 psig**

From the data in Table 3.10 and Figures 3.14(a & c) & 3.15(a & c), we can observe that there are large variations in the leakage rates, at initial stress S1 and gas pressure of 200 psig, i.e. variation of nearly factor of 106 for milled surface II2, and as low as factor of 0.002 for turned surface J3 compared with smooth ground surface III1. Milled surfaces

II2 and II3 performed similarly at all stress levels, except at the initial stress level S1, where the leak rate of surface II2 (315  $\mu\text{in}$ ) compared to II3 is 193 times larger, see Table 3.10 and Figure 3.15(c).

By comparing the results obtained for the turned surfaces we observe that similar trend exist for both concentric and spiral turned surfaces. The leak rate is attributed to the existence of interconnecting radial channels on the platens surface as a result of peak-to-valley's asperities on the grooves apex edges. At the first stress levels S1, a large leak reduction of approximately a factor of 15 can be observed between the concentric cut, Figure 3.14(c), and the spiral cut surfaces, Figure 3.15(a). This is probably attributed to the circumferential concentric grooves which provide lesser inter connecting leak path compared to the spiral cut.

For the ground surface type, the leak results obtained for the initial stress S1, at 200 psig gas pressure, reveal that as the surface roughness increases from 20 to 80  $\mu\text{in}$ , the leak rate increases by a factor of 17.4 and is nearly 40 times more at stress S1 after unloading from S3, see Table 3.10, Figure 3.14(a). Therefore, we can say that for ground type surfaces, the rougher the surface the larger the leak rate, especially at low stress levels. However, there is no significant change in the leak rates due to roughness, for the other surfaces, at stress S1 after unloading from S3, Figures 3.14(c & d) and 3.15 (a through d).

It can be noticed that sealing behaviour upon loading can be improved by first exposing the gasket to higher stress level such as S5. This can be considered as pre-compressing the gasket and then operating at lower stress levels. Of course this is true only for turned surfaces (since the groove peaks remain indented in the gasket) and such condition does not improve the sealing performance of other surfaces such as milled and ground type, see Table 3.16 and Figure 3.18(a).

The data presented in Table 3.16 reveals that the leak ratio at “unload to stress S1 in cycle 2” to “unload to stress S1 in cycle1”,  $C2U2S1/C1U1S1$ , is about 0.55 to 0.78 for turned surfaces, and this ratio is from 3.5 to 9 for ground and milled surfaces. Thus, it appears that for the turned surfaces, pre-compression or higher initial compression (large gasket deflection under high compressive stress S5) of the gasket improves its sealing performance such that it remains tight at unload to stress S1 in cycle 2 ( $C2U2S1$ ). However, this has a reverse effect for ground and milled type surfaces. As an hypothesis this can be explained such that, at unload stress S1, the groove edges on the turned surfaces remain indented in the PTFE gasket media, and provide larger local stress on the gasket compared to the ground surfaces. On the other hand, the ground surfaces being smooth with some deep valleys, when unloading the gasket, the leak rate can increase through the channels of the surface depression where the stress level is less than the average gasket stress. For a similar reason, the milled surfaces, having some radial channels, provide larger leak rates than the ground surfaces upon unloading. For both ground and milled surfaces, as a result of lower local stress on the gasket, the gas pressure infiltrates into the gasket width. Consequently, the end load effect is larger than the computed one, and the real gasket stress is less than the computed one, thus explaining the increased leak rate.

At this point it is worth discussing the effective, or real gasket compressive, stress. The applied gasket compressive stress,  $S_g$ , is computed based on the initial gasket dimensions while the end load effect is computed with the area delimited by the initial gasket internal diameter subject to the gas pressure, see equation (3.40). It is likely that the computed and applied compressive stress on the gasket is not exact. This can be explained as follows: when the gas pressure is applied, if it infiltrates into the gasket width, the end-load on the gasket is larger than the computed one that is based on the initial gasket ID. As a result, the real gasket compressive stress is less than the computed one, equation (3.40). We can call this hypothesis “the end load & stress release (ELSR) effect”. Similarly, an overestimate of the gasket stress may occur if the gasket material is flowing radially,

increasing the gasket width. Therefore, the real gasket area will be larger than the computed one.

The total load on the gasket is divided between all the asperities based on their size and height. The largest and highest asperities come in contact first and carry larger contact stresses. The real area of contact is based on the sum of the surface areas in contact, for the applied gas pressure and the gasket compressive stress. Thus, the surfaces at depression areas are considered the leak paths. Therefore, considering the contact areas based on the platens surface characteristics, we can deduce that for the same applied load, the ground and the milled surfaces provide less local compressive stress on the gasket compared to the turned surfaces, see Figure 3.1.

In addition, because of the radial grooves on the milled surfaces, there are radial bands of low compressive stress on the gasket under the depression areas. Therefore, for the same applied load, there are larger leak paths on the milled surfaces. This results in larger leak rates, especially at unloading to low stress levels. At higher stress levels the distribution of the stress on the gasket becomes more uniform for all surfaces, since the PTFE gasket material flows into the grooves, resulting in leaks similar to ones measured with the other surfaces

From the data in Figure 3.18(a) it can be noticed that neither of milled nor ground surfaces provide tight sealing at final low stress S1 (C2U2S1), compared to turned surfaces. This stems from the fact that ground and milled surfaces have radial grooves encroaching from the pressure side to the non-pressure side of the surfaces, as shown in the topography in Figures 3.12 and 3.13. In addition, as discussed earlier, this effect is undoubtedly the result of larger leak paths generation between the gasket material and the flange surfaces, at surface areas with local depression, due to internal pressure when reducing the compressive gasket stress. Consequently, this results in higher leak rates past milled and ground sealing surfaces compared to turned surfaces. It is interesting to note

that the ground sealing surfaces provided somewhat larger leak rates compared to the milled surfaces, in spite of the fact that the latter has more radial leak paths on their surfaces. An hypothetical explanation for this finding could be that, for the same applied load, the grooves apex of the milled surfaces generate higher local stress on the gasket causing the penetration of the grooves apex into the gasket, and that the gasket material flows into the shallow grooves of the milled surfaces, resulting in the blockage of some of the leak paths.

From the data presented in Table 3.10, Figure 3.18(b), at stress levels higher than S3 up to S5, all surfaces provided approximately the same leak rate, resulting in a similar sealing performance. Perhaps, it is possible that at stress levels higher than S3, platens surface asperities and grooves apex penetrate the gasket material better than at lower stress levels, and that gasket material flows into the platens surface irregularities blocking the leak paths. The second mechanism could be enhanced by the gasket creep since when reaching the stress level S3, the load on the gasket have been maintained for more than 2 hours, which results in creep occurrence. As mentioned earlier, usually PTFE material have low strength and exhibit a permanent deformation, [34,35], but in the present case the tensile strength and creep properties of PTFE gasket tested have been improved by the incorporation of glass microspheres (fibers) into the PTFE material.

As shown in Table 3.10, for stress S5, there are slight variations in the leak rate of III2 and II2 with respect to III1. For instance, the rougher ground surface III2 results in 24% higher leak rate compared to III1. This might be due to the existence of deeper valleys in III2 surface. For milled II2 surface, the leak rate is about 15% higher than III1. These variations are not considered significant, taking into consideration that experimental errors or uncertainties on the applied stress, the gas pressure, the leak rate measurement, as well as the differences that exist between two gasket specimens cut from the same sheet, that are all possible factors contributing to the leak rate variation. Therefore, since

the variations indicated above are not significant we can conclude that at stress S5 all surfaces perform the same.

### **3.7.2.2 PTFE test results at gas pressure 800 psig**

As in the case of the results at 200 psig discussed above, the test results at gas pressure of 800 psig have the same trends or the similar pattern of leak rates versus stress levels (no abnormalities). However, at 800 psig, the effect of gas pressure is more pronounced on the leak rates at low stress levels S1 (initial, cycle 1 and cycle 2), especially for ground and milled surfaces where we see a large increase in the leak rates, see Table 3.7. At higher stress levels, a normal leak rate increase can be seen for turned, milled and ground surfaces.

From the data in Table 3.13 and Figures 3.14(b & d) & 3.15(b & d), we can observe that taking III1 surface as a reference, there is a large variation in the leakage rates, at unload to stress S1 in cycle 1 (C1U1S1). This variation is nearly factor of 0.11 for turned surfaces J1, J3, I1 and I3, a factor of 7.0 for milled surfaces II2 and II3, and a factor of 23 for rougher ground surface III2, compared with smooth ground surface III1. In other words, a leak reduction by 9 times for turned surfaces, 7 times larger leaks for milled surfaces and 23 times larger leak for rougher ground surface III2. The variation becomes even larger for the turned surfaces at unload to S1 in cycle 2 (C2U2S1), where it is nearly a factor of 0.002 to 0.009, compared to the ground surface III1, in other words, a leak reduction by 500 to 111 times for turned surfaces. However, both ground surfaces III2 and III1 perform the same, at unload to S1 in cycle 2. At this stress level, the performance of the milled surfaces remains at 7.0 compared to ground III1.

By comparing the results obtained for the turned surfaces we observe that similar trend exists for both concentric and spiral turned surfaces. Thus this type of surfaces provide tight sealing upon unloading.

As mentioned above, the leak ratios of turned surfaces to the reference ground surface III1 are much less at unload to S1 (cycle 2) compared to unload S1 (cycle 1). This is attributed to the fact that the ground surface III1 has larger leak rates at unload to S1 (cycle 2) compared to unload at S1 (cycle1), see Figure 3.14(b). This phenomenon is attributed to “the end load stress release effect” discussed earlier. The results discussed are relative comparisons. On the other hand, we can say, hypothetically, that the low leak rates of turned surfaces are attributed to the higher initial compression effect of the gasket and to the penetration of the apex into the gasket media blocking the leak paths on the platens surfaces. Therefore, since the gasket material is retained by the grooves, it is probable that at higher stress levels, the PTFE flows into the surface imperfections (grooves), and consequently blocks permanently most of the leak paths even when the load is reduced to stress S1.

For the milled surfaces at unload to S1, as a result of “the end load stress release effect”, the leak paths size open up at surfaces with local depressions resulting in higher leak rates.

Nonetheless, at stress S5 (see Table 3.14) all surfaces have between 7% and 27% lower leak rates compared to ground surface III1. It is probable that at such stress level the PTFE material fill most of the surface imperfections, blocking the interfacial leak paths. What is left are diffusion leaks through the gasket material, explaining the similarity of leak rates noticed in Table 3.14. Thus, we can conclude that at stress S5 all surfaces perform the same, under the given operating gas pressure.

Looking at the leak versus the stress graph of ground surface III2 on Figures 3.14(a & b), we notice that unload to S1 results in approximately the same large leak rates at both 200 and 800 psig gas pressure. We can speculate that the large leak rates at unload to stress S1 are attributed to the generation of larger leak paths between the gasket and the platens' surfaces at local depression. The generation of such larger leak paths is probably attributed to gasket higher initial compression (large gasket deflection under high compressive stress S5), and to the end load effect when the gasket compressive stress is reduced to S1.

For ground surface III1, the leak ratio of 800 to 200 psig at final stress S1 is 85 times (Table 3.7). The result indicates that for the smoother ground surface III1, the sealing is greatly affected when increasing the gas pressure. This is undoubtedly a result of hydrostatic end load, causing an opening of leak paths between the gasket and the platens surfaces due to the increase in gas pressure, especially when the load is reduced to a very low value. Thus, the leak probably occurs through local areas of the surface depression, which have lower contact stress than the average gasket stress. Such results are not observed in the case of flexible graphite gasket, with ground surfaces III1 and III2, Table 3.8, therefore it can be speculated that such an effect is most likely depending on the gasket material.

From the data in Table 3.7 and in Figure 3.19(a), it can be noticed that neither milled nor ground surfaces provide tight sealing at unload stress S1, compared to turned surfaces, at gas pressure 800 psig. This is attributed to the fact that ground and milled surfaces have radial grooves. As a result of the combined effect of the increase in gas pressure and of the reduction of compressive gasket stress, the leak paths size on the sealing surface increases at local areas of depression. Furthermore, when comparing the milled and ground surfaces, it can be observed that milled sealing surfaces have larger leak rates compared to ground surfaces, since the formers have more radial paths, which make the surfaces more sensitive to hydrostatic end load as a result of gas pressure increase, see



Table 3.7 and Figure 3.19(a). In other words, the surfaces are more prone to gas pressure infiltration between the gasket and the platens surfaces, thus increasing the pressurized area and consequently, the end load. Ultimately this translates into a much lower real compressive gasket stress. Consequently, larger leak rates take place at areas with lower local stress level than average gasket stress.

### **3.7.2.3 PTFE gasket deflections**

The data presented in Tables 3.16 and 3.19 highlight that the gasket deflection ratios at S5 to S3 for both test series at 200 and 800 psig gas pressure are approximately the same for their respective surfaces. This indicates that gas pressure might not have much effect on gasket deflection. However, some interesting observations can be made by comparing the deflections obtained with different surfaces.

It can be observed that the turned surfaces result in lower gasket deflection compared to milled surfaces, Figures 3.18(c & d), 3.19(c & d). This is probably due to the restriction of gasket material radial flow, which is confined by the circumferential grooves of turned surfaces, thus, not allowing the increase in the gasket width, therefore resulting in lower gasket deflection. Among all the turned surfaces, the turned surface I3 has higher gasket deflection compared to the others. This might be attributed to slightly wider grooves (0.080 in. vs. 0.075 in.) on I3 surfaces compared to the others.

The larger gasket deflection in milled surfaces might be attributed to the profile of the surfaces with radial grooves, which instead of restricting the material flow, directs it radially, resulting in larger gasket deflection and increased width for the same applied stress. The increase in gasket width increases the area of contact and the leak path length to size ratio.

In general, one would assume that the gasket deflection for ground type surfaces should be higher than the others, since there is less restriction to the gasket radial flow. However, the results show that it is not the case for the PTFE gasket, since the gasket deflection in the ground type surfaces is less than those of the milled surfaces, probably because there exist no radial grooves/edges on ground surfaces to facilitate lateral flow of gasket material.

For PTFE gasket, all surfaces leak are about the same at stress levels higher than S3 (Tables 3.10 and 3.13), but each for a different physical reason. The turned surfaces constrain the radial flow of gasket material within the grooves in which it penetrates, blocking the leak paths size and reducing the leak rates. In the case of milled and ground surfaces, the gasket material flows radially since there is less restriction, thus the gasket width increases. The gasket material flows into the surface asperities, increasing the leak paths length to size ratio, reducing the leak rate. Hypothetically, if all the surfaces leak rates are the same under high compressive stresses, while the gasket deflections are not, this indicates that the interfacial leaks are much lower than the diffusion leaks through the gasket. These results represent the hypothesis presented in the theoretical section in equations (3.35) to (3.40), and show that the number of asperities in contact increases by increased stress, reducing the number of interfacial leak paths.

From stress distribution patterns shown in Figure 3.1, it appears that the gasket stress at a point beneath the platens groove edges is higher than the average gasket compressive stress, whereas the gasket stress in surfaces with local depression is lower than the average gasket compressive stress. Therefore, as the joint internal pressure increases, the gasket real compressive stress reduces as a result of end load effect, leading to larger leak paths channels on the areas of surface depression of low initial stress, causing the interfacial gas to infiltrate through. This corresponds to the deflection results obtained for milled and ground surfaces at unloading, as shown in Figures 3.18(a), and 3.19(a).

### **3.7.2.4 Effect of surface roughness $Ra$**

The test results for PTFE gasket indicate that the surface roughness value  $Ra$  alone is not a critical factor for the leak rate, and it has to be evaluated in combination with surface finish type. For instance, in the case of ground type sealing surfaces, the roughness value plays an important role on the sealing performance at low compressive gasket stresses, Figure 3.14(a & b). However, the surface form, as a result of different machining procedures, plays more important role in the sealing phenomena, such that surfaces having grooves resulting from the machining are apparently not very sensitive to the  $Ra$  value of the surfaces. This is observed in the case of milled, turned spiral and turned concentric surfaces, Figures 3.14 and 3.15. Refer to Table 3.6 for  $Ra$  value of different surfaces.

### **3.7.2.5 Leak flow regimes on PTFE gasket**

The study of flow regimes allows the determination of sealing sensitivities to gas pressure increase as a function of gasket compressive stress and sealing surface characteristics. The flow regime data provide an insight of the probable geometry of the leak paths at the interface between the platens surfaces and the gasket. As such, it can be a powerful tool to understand the effect of surface form and roughness on the sealing performance. The different flow regimes obtained from the slope of the lines based on log-log plot of leak rate versus gas pressure are presented in Figure 3.4. The molecular flow regime is present if the slope of the line is equal to one, whereas, if the slope of the line is equal to two, the flow is in viscous laminar state, as earlier defined through equations (3.45) and (3.46).

From the log-log plot of leak versus pressure, at stress levels S2 through S5 (part A) the flows with PTFE gaskets are in molecular state, regardless of the surface finish, see Figure 3.32, and Table 3.28. At unload to stress S1 (cycle1), laminar flow regime is

obtained for turned and ground surfaces, while for milled surfaces the slope exceeds two. At unload to S1-cycle 2, turned surfaces I1 and J1, and ground III2 remain in molecular state, while the turned surfaces I3 and J3, are in laminar state. For milled surfaces II2 and II3 the slopes are nearly 5 and 4, respectively. The ground surface III1 also has a slope of 3, Figure 3.32, Table 3.28.

The large leak increase with pressure in milled surfaces is believed to be caused by the existence of the radial paths on the surfaces, that allow gas pressure infiltration between the gasket and platens surfaces through surface areas at local depressions, at unload to S1. Therefore, at higher gas pressure (800 psig) and low stress S1, as a result of the additional hydrostatic end load, the real gasket compressive stress is lower than the calculated one. This results in larger leak paths size and in a substantial increase of the interfacial leak rates. The same is true for the smoother ground surface III1, where the larger interfacial leak rates occur at areas with lower gasket compressive stress than average.

Finally, it is worth mentioning that gasket material properties also play an important role in the leak rates and the flow regimes, as large slopes i.e. 4 and 5, have not occurred in the tests performed on G2 and SW gaskets, see Table 3.28.

### **3.7.3 Results of UCAR flexible graphite sheet (G2) gasket tests**

#### **3.7.3.1 G2 test results at gas pressure 200 psig**

From the data presented in Table 3.11 and Figure 3.20, there is little variation in the leakage rates, at initial stress S1, for all surfaces, when compared with III1, except for ground surface III2, which is higher by a factor of 2. This is probably an indication that the deep peak-to-valleys asperities of the rougher III2 ground surface are not sufficiently filled by the gasket material at low initial stress S1, causing higher leak rates to occur. However, for compression stresses above S1, this surface sealing performance is very

close to the one of III1, confirming that with a sufficiently higher stress, gasket material has filled the surface asperities.

When the leak rates of turned spiral surfaces II1 and I3 are compared in Figure 3.12(a), it can be noticed that an unusual large leak rate difference exists between the two surfaces at gasket stress levels in cycle 1. However, both surfaces leak similarly at gasket stress levels in cycle 2. Such a difference might be caused by gasket material variation, or some other unknown reasons, since it does show up in 800 psig test results, Figure 3.21(b).

The data presented in Table 3.11, show that the milled surface II3 performs better sealing compared to II2, although the II3 is rougher than II2. As discussed earlier for PTFE gasket results, we do not consider the roughness value *Ra* alone to be a critical factor for the leak rate, and it has to be considered in combination with the surface form and the machining procedure. However, the surface machining form plays a more important role on sealing performance in combination with gasketing material. The milled II2 surface has many large irregular interconnecting radial channels, whereas the milled II3 has regular and smaller radial paths. Consequently, for the same applied gasket compressive stress and gas pressure, for II2 surface, it can be deduced that gas infiltrates more easily in between the gasket and platens through large radial channels of this surface.

If the difference mentioned above for initial S1 is ignored, then we can notice that both spiral finish turned surfaces II1 and I3 perform similarly, Figure 3.21(a). Therefore, we can also affirm that, at 200 psig gas pressure these surfaces perform better than other surfaces, simply because at stress levels above S1, the apex of the circumferential grooves penetrate deeply into the gasket media blocking (pinching) better the interconnecting radial pore channels through which interfacial leak occurs.

The data presented in Table 3.17, for gas pressure 200 psig, reveal that the variation of the leak ratio at final stress S1-cycle 2 to that of S1-cycle1, is between 0.26 and 0.38 for

all surfaces except for I1. This is approximately a 3 times leak reduction that is a direct consequence of gasket pre-compression to S5. These results indicate that the application of a higher compressive stress improves the sealing performance and the seal remain tight at unload to low stress S1. Presumably, the gasket graphite material fill-in the surface peak-to-valleys and clings to the sealing surfaces when the load is released. Naturally, as the gasket stress increases the leak rate reduces. The data presented in Table 3.17 indicate that when increasing the stress level from S3 to S5, an overall 97% to 91% leak reduction is achieved, (the leak ratio S5 over S3 varies from 0.03 to 0.09). In the case of I1 surface, the leak ratio at final stress has a value of 1, indicating that the same leak rate is measured in cycle 1 and 2. This unusual behaviour cannot be explained for the time being, but it might be related to variations in gasket properties as mentioned before.

### **3.7.3.2 G2 test results at gas pressure 800 psig**

In the section on PTFE results, it is indicated that, at initial stress S1, the gas pressure for 800 psig test series is set to 200 psig to avoid gasket blowout and the saturation of the mass spectrometer. This is also done for the G2 and SW gaskets. This explains why we see the same leak rates for the tests performed at 200 and 800 psig at initial stress S1.

As in the case of the results at 200 psig discussed above, the test results at gas pressure of 800 psig have the same trends or the similar pattern of leak rates versus stress levels (no abnormalities). The graphs in Figures 3.20(b & d) and 3.21(b & d) show the results of the leak rate versus stress at gas pressure 800 psig. The graphs in Figures 3.20(d) and 3.21(b) show that the leak rates for turned surfaces are the same, except at final S1 (cycle 2), where the leak rates for J1 and I1 surfaces are larger than J3 and I3. Milled surfaces II2 and II3 perform similarly at all stress levels, Figure 3.21(d). The sensitivity of the ground surface leakage to the gas pressure can be observed from the pronounced leak rate differences between III1 and III2, see Figure 3.20(b). We see that in the case of the

ground finish, the rougher the surface is, the more sensitive it is to the increase of gas pressure. This is also confirmed in Table 3.18 where 800 to 200 psig leak ratios of III2 are always above those of III1 surface. This indicates that the smoother the surface, the lower the leak rate for the graphite gasket, in the case of the ground type surfaces. It can be assumed that the gasket material is uniformly compacted, reducing the gasket pores size. Also, due to the fact that the graphite gasket sticks to the platens surfaces, both the interfacial and the leak through the gasket are reduced.

The results presented in Table 3.8, and in Figures 3.22 and 3.23, indicate a large variation in the 800 over 200 psig leak ratio. Ratios ranging from 2.4 to 69 are obtained depending on the surface form and stress level. The lower factor values (2.4 to 4.0) are attributed to the smoother ground surface III1 at stresses S1 through S3.5 (Part A & B), while the largest factors are attributed to turned surfaces I1 and J1, at the final stress S1 (cycle 2). In this last case, the ratios are respectively 67 and 69, nearly 5 times the one for ground surface III1, and up to 10 times the ratio for the rougher ground surface III2 at stress S5. For the turned surfaces I1 and J1, apparently a leak cleaning phenomenon might have taken place as a result of high gas pressure (800 psig) and of unload to stress S1 (cycle 2), see section 3.5.2.1.

Such leak cleaning phenomenon occurs here with the G2 gasket and not with the PTFE and SW gaskets. We can speculate that it is because G2 is made of graphite foil layers (from graphite flakes), which may have detached from the gasket surface under high gas pressure, enlarging the leak path size and consequently increasing the leak rate. This kind of material separation cannot occur with PTFE and SW gaskets. As discussed earlier, in Section 3.6.7.1, the PTFE is made by polymerisation of its monomer tetrafluoroethylene (TFE) and is reinforced by glass microspheres, giving a strong bonding structure at temperature lower than 400°C. The SW is made of spiral metal winding strips that retain the graphite filler, see Section 3.6.7.2.

Due to the leak cleaning phenomena, at the unload to final stress S1 in cycle 2 (C2U2S1), there are large 800 to 200 psig leak ratios of 16 and 12 for I1 and J1, respectively (Table 3.14). But, at unload to stress S1 in cycle 1 (C1U1S1), all surfaces, including I1 and J1, show large leak rate ratios between 1.2 to 1.5, indicating the absence of leak cleaning in cycle 1. Thus, it can be partly concluded that the leak cleaning phenomena will appear at unload to S1 only if the graphite gasket is first subjected to a high compressive stress (S5) between turned surfaces. There is also an indication that tool radius might play a role here, since leak cleaning occurs in I1 and J1 surfaces that are machined with a 1/32 in tool radius, while it does not occur for I3 and J3 surfaces that are machined with a larger 1/16 in too radius.

From the results in Table 3.14, we can see that at final stress S1 (cycle 2) the leak ratio of the milled surfaces II2, II3, and the ground surface III2, to the reference ground surface III1 is approximately a factor of 2 as compared to about 1 for I3, J3 surfaces. Surfaces I1 and J1 cannot be used in this comparison since they exhibit the leak cleaning phenomena. This might be attributed to some kind of end load & stress release effect (ELSR) resulting in a larger leak rate, although there is no experimental proof of that.

While the turned surfaces perform the same at higher gasket stress levels, i.e. S3 and S5, compared to the reference surface III1, the milled and rougher ground III2 surfaces leak up to 4.5 times more, see Table 3.14. This indicates that the turned surfaces provide circumferential local stress on the gasket, and most likely, the grooves apex penetrate into the gasket media, blocking the interfacial leak and paths reducing the leak through the gasket pores. It is to be noted that similar conclusion is reached for PTFE gasket. For the same gasket stress levels, i.e. S3 and S5, the rough surfaces (i.e. II2, II3, III2) with radial inter connecting paths, allow for larger leak through the gasket pores and the mating surfaces at areas with grooves or asperities.



The data presented in Table 3.20, for gas pressure 800 psig, show that the variation of the leak ratio at final stress S1 (cycle 2) to S1 (cycle1), C2U2S1/C1U1S1, is between 0.36 and 0.52, a leak reduction of approximately 2 times for all surfaces, except for J1 and I1, which are 3.89 and 3.25, respectively. These last large ratios are due to leak cleaning phenomenon. The results also indicate that the application of a higher initial seating stress improves the sealing performance, at unload to stress S1. Presumably, the surfaces asperities are filled-in with the gasket graphite material, which also remains sticking to the sealing surfaces when the load is released. Naturally, as the gasket compressive stress increases the leak rate reduces, but the gas pressure remains a controlling factor.

The data in Table 3.20 indicate that when increasing the stress level from S3 to S5, an overall 93% to 86% (14 to 7 times) leak reduction is achieved at 800 psig, compared to 97% to 91% (33 to 11 times) at 200 psig (Table 3.17). This highlights the effect of gas pressure on the sealing performance and shows the sensitivity of the leak flow regime to the sealing surfaces characteristics.

### **3.7.3.3 G2 gasket deflections**

The data presented in Tables 3.17 and 3.20 indicate that the gasket deflection ratios at S5 to S3 and S1 (cycle 1) to S1 (cycle 2) for both tests at 200 and 800 psig are approximately the same for their respective surfaces confirming that gas pressure has little or no effect on deflection.

It can be observed from Figures 3.24(c & d) and 3.25(c & d) that surface form has a pronounced effect on gasket deflection, but not gas pressure. Higher gasket deflection can be observed for concentric cut turned surfaces, whereas ground type surfaces result in the least gasket deflection, almost by 30% less, Figures 3.24(c & d) and 3.25(c & d). This large difference is reasonably due to the fact that G2 gasket does not expand radially,

resulting in less gasket deflection for ground type surfaces, while for the turned surfaces the grooves penetrate into the gasket material, with some gasket material flowing into the grooves, resulting in a larger deflection. Such phenomena do occur in the case of flat ground surfaces.

In addition, comparing the effect of gasket materials, for the PTFE versus G2, we can notice a very different deflection distribution versus surface type, (Figure 3.18 vs. 3.24), which do not match the G2 results. For instance, the lowest deflections can be seen on I1 and III2 for PTFE versus III1 and III2 for G2 gasket, while, the largest deflections are on II2 and II3 for PTFE, versus J1 and J3 for G2 gasket. This is because, as discussed earlier, in the case of PTFE gasket, the turned surfaces retain the radial flow of the gasket material, while the milled surfaces allow it. As it is shown later, for the SW gasket there is no radial expansion, and the gasket deflection for all surfaces is approximately the same.

#### **3.7.3.4 Leak flow regimes on flexible graphite sheet (G2) gasket**

The flow regimes for all sealing surfaces are determined by obtaining the slope of the lines from log-log plot of the leak rate versus gas pressure, refer to Table 3.28 and Figures 3.33. At stress levels S2 through S1 (cycle 1) the flow is in the molecular state, regardless of the surface characteristics, except for I1 surface that is in the laminar state.

Three turned surfaces J1, J3, and I1 have similar S5/S3 leak ratio at 200 and 800 psig. However, for the other surfaces, for the same leak ratio S5/S3, there is an increase of approximately 1.6 at 800 psig as compared to 200 psig (Table 3.17 vs. 3.20). In the case of III2, I3, II2, and II3 surfaces, this increase is attributed to a change in the leak flow regimes from molecular at S3 to laminar at S5, Figures 3.22 and 3.23, Table 3.28. These surfaces are more sensitive to pressure change at S5 versus S3 and this implies a

fundamental change in the leak path geometry, such that at S3 the leak paths are predominantly of “molecular size” while at S5, although less numerous, they are of “laminar size”. For the J1, J3, I1 and III1 surfaces, there is no change in the flow regime.

We should emphasize that the flow regime change with loading that happens with G2, is also noticed on turned surfaces with SW gasket but not with PTFE. This can be hypothetically explained such that, for G2 gasket, the unload-reload process results in larger interfacial leak paths, for III2, I3, II2, and II3 surfaces, resulting in larger leak rate variations when pressure is increased (laminar flow regime). In the case of SW, the same phenomenon happens for turned J1, J3, I1, I3, where the flow regime changes from molecular at S3 to laminar at S5. This might also be because of the change in the leak paths from “molecular size” to “laminar size”, at the interface between platens surfaces and the gasket.

Considering the effect of gasket material, it can be seen that in fact for the G2 gasket with I1 surface, the flow paths become of “laminar size” at gas pressure of 800 psig, whereas this is not the case for the PTFE gasket for which the leak paths remain in the “molecular size”.

In cycle 2 of the leak tests, some surfaces show more sensitivity to the increase of gas pressure, perhaps due to the gasket internal microstructure deformation under different finishes and stresses. At final stress S1 (cycle 2), both I1 and J1 surfaces have a slope of three, which indicate a leak cleaning phenomenon that was discussed previously, Figure 3.33 and Table 3.28. It can be observed that after the gasket media has been compressed more in cycle 2, the milled II2, II3 and the rougher ground III2 surfaces become more sensitive to the gas pressure increase, and the laminar flow regime is obtained. Perhaps, this is a consequence of the hydrostatic end load effect resulting in some larger leak paths at the sealing surfaces in local areas with relatively lower gasket compressive stress levels than average. In addition there might also be a change in the path size distribution, such

that the laminar path sizes dominate the molecular ones. For these reasons, we can observe slopes of 2 starting at S4 for II2, II3, and III2 surfaces, see results in Table 3.28.

### 3.7.3.5 G2-Closing remarks

The data presented above show that in the case of G2 gasket, the smoother ground type surface III1 performs as well as the turned surfaces at both high and low gas pressure applications and at both load and unload stress levels. The gasket deflection is relatively low under the same operating conditions, compared to other surfaces. We can speculate that this would result in a longer gasket operating life, since the gasket material is less distorted as opposed to case with turned and milled surfaces. However, it is well known that ground surfaces, in general, are very sensitive to the unloading excursion, which usually disqualify them for real flange operating conditions for which they exhibit large end load effect.

The turned surface finishes, on the other hand, improve the sealing performance, simply because their groove apex penetrate into the gasket media and retain the gasket between the flange faces. They serve both the performance requirements and safety purposes.

It is worth indicating at this point that, although out of the scope of this research, the grooves apex on the turned surfaces should be optimised for a better sealing performance and to prevent gasket deterioration. We can speculate that if the grooves apexes are sharp and the grooves are deep, they may break through the microstructures and deteriorate the gasket material under load stresses. Furthermore, the rougher the grooves apex are, the larger the interfacial interconnecting leak paths can be, resulting in larger leak rates. Therefore, more experimental research should be considered to optimise the grooves apex shape and the grooves depth and to investigate their effect for higher sealing performance.

### **3.7.4 Results of spiral wound (SW) gasket tests**

#### **3.7.4.1 SW test results at gas pressure 200 psig**

The data presented in Table 3.12 and Figures 3.26(a & c) and 3.27(a & c) indicate a large variation in the leak rate ratios, of a factor ranging between 0.02 and 34, for all surfaces compared to the reference ground surface III1. At initial stress S1, the leak ratios of milled II2 and of rougher ground III2 surface are 14 and 34 respectively. At unload to S1 (cycle 2), they are 4.5 and 3.3 respectively and are equal to one at S5 stress level. For the milled surface II3, this ratio is 0.77 at initial S1 and it increases to 5 at unload to S1 (cycle 2) and is approximately one at S5.

The leak ratio of the turned surfaces is between 0.38 and 0.86 times at initial stress S1 and it reduces to a factor between 0.28 and 0.40 at S1 (cycle 1). This leak ratio becomes a very small factor, between 0.02 to 0.08 times, at S5 stress level (12.5 to 50 times less leak). This ratio increases to a factor between 0.21 and 0.32 at unload to S1 (cycle 2).

From the data in Table 3.18 and Figures 3.26 (a & c) and 3.27 (a & c), we can see that when the gasket stress is increased from S3 to S5, there is a substantial leak reduction of approximately 14 to 33 times for the turned surfaces. However, the leak rate reduction is less for the rougher ground surface III2 (8 times), the milled surfaces (2 times) and the smoother ground surface III1 (2 times). Consequently, these results indicate that the milled and ground surfaces are less sensitive to load excursions, since the variation in their leak rates is less, although their sealing performance is much lower than the turned surfaces Table 3.12, for the same applied load.

The results presented above indicate that surfaces such as rougher ground III2 and milled with radial grooves cause larger leak rates at low stress levels and require higher gasket compressive stress to achieve suitable tightness. We can assume that, because of the

radial grooves on these surfaces and the metal winding strip of the gasket, some higher gasket compressive stress is required to allow the graphite filler to encroach to the leak paths on the platens surfaces and to reduce the leak rate. We can also speculate that, for these surfaces, larger leak rates occur at local areas with lower gasket compressive stress than average.

For the same applied load, the above-mentioned results indicate that, in the case of the turned surfaces, much lower leak rate are obtained. In fact the turned surfaces may have mated better the spiral wound gasket metal winding strip than the other surfaces, so that the platens grooves apex penetrated between the winding strips. In addition, the graphite filler plugged the surface asperities, reducing the leak rate. Furthermore, it can be seen that as the gasket goes through compression at higher stress levels in cycle 1 and 2 and then unloaded to stress S1, the leak ratio of the turned surfaces to the reference surface III1 is much less at S1 for cycle 2 than it is at S1 for cycle 1, as a result of the extended filler flow resulting from higher initial compression of the gasket.

The data in Table 3.18 shows that the leak ratio of S1-cycle 2 to S1-cycle 1, C2U2S1/C1U1S1, is a factor ranging between 0.45 and 0.75 for the turned surfaces, approximately 0.8 for the ground surfaces, and 1.24 for the milled surfaces. Therefore, we can assume that while the higher gasket initial compression helps to reduce leak rates at unload to stress S1, in the case of turned surfaces, it increases the leak rate for the milled surfaces. For the milled surfaces this leak rate increase happens only with SW and PTFE gaskets (Table 3.12 & 3.10) but not with G2 (Table 3.11), probably because of the difference in gasket material properties. This is probably due to some gasket local recovery, or gasket retraction, as the gasket compressive stress is removed. The higher the gasket retraction is, the greater is the opening of the leak path channels at the interface with the surface.

Consequently, the results discussed above indicate that the turned surfaces require a lower gasket compressive stress in order to result in the same leak rate as the others. The milled surfaces and the rough ground surface III2 perform similarly to III1 only at higher gasket stresses and require higher surface compression to increase the surface contact area, and to reduce the leak paths size.

The theoretical hypothesis presented on the leak path size and length as a result of surface stress in equations (3.35) to (3.39) correspond to the above findings. However, for the gaskets tested in this work, (PTFE, semi-metallic SW and flexible graphite G2 gaskets), any direct proof of these equations is too complex at the present time. This complexity is due to the fact that the determination of the exact size of platens asperities in contact with the gasket and the quantification of asperities penetration into the gasket at a given stress level are not feasible. Therefore, a realistic determination of the interfacial leak paths size and of the leak path size through the gasket for an applied gasket stress and internal gas pressure is complex.

#### **3.7.4.2 SW test results at gas pressure 800 psig**

From the results of the leak rate versus stress, we can see that increasing the gas pressure from 200 to 800 psig increases the leak rate by approximately a factor of 2 to 10, in cycle 1 stresses for all surface types, Table 3.9 and Figures 3.28 and 3.29. Obviously different surfaces are causing a lot of variations in the leak flow regime. The results also indicate that, J1, J3, II2 and I3 surfaces are more sensitive to the gas pressure than the milled surface II3, the turned surface I1 and both ground surfaces III1 and III2.

At higher stress levels in cycle 2, it can be seen that the turned surfaces are much more sensitive to the gas pressure, compared to the ground surfaces. On the other hand, the milled surfaces are less sensitive to gas pressure compared to the ground surfaces. In

addition, the smoother ground III1, the milled II2 and II3, and the turned I3 surfaces show more sensitivity to the gas pressure at unload to stress S1 (cycle 2), where the leak ratio 800 to 200, ranges between 10 (I3) and 17 (II3), compared to the other surfaces that exhibit leak ratios between 5 and 8, see Table 3.9. The higher sensitivity of III1, II2, II3 and I3 surfaces to the gas pressure at unload to S1 (cycle 2), might be attributed to the change in the leak path size geometry, from “molecular” to “laminar”, as demonstrated by the slope values of the leak-pressure lines that are presented in Table 3.28.

At stress levels in cycle 1 (maximum S3), the milled surfaces are more sensitivity to the gas pressure, but become less sensitive at higher stress levels in cycle 2. The reason is that, at cycle 1 stress levels, the leak path geometries are of “laminar size” resulting in laminar flow regime. At higher stress levels in cycle 2 as a result of higher compression, the surface leak paths are better plugged with the gasket graphite filler. Therefore, the leak path geometries become of smaller “molecular size”. On the other hand, the paths of molecular geometry, that are closed at higher stress levels, are reopened to “laminar geometry” when the load is reduced to S1 (cycle2), which explains the change in the flow regime found in Table 3.28.

As mentioned before, for the turned surfaces, the pressure effect is greater in the second load cycle as opposed to the first cycle. A probable explanation might be that, at cycle 1 stress levels (max. S3), under the influenced of gas pressure, the leak past sealing surfaces occurs through the leak path geometry of “molecular size” at areas of surface depression with lower gasket compressive stress than average. However, at cycle 2 stress levels, the platens grooves apex penetrate deeper between the gasket metal winding strips, changing the leak path geometry to “laminar size” under higher stress, resulting in a laminar flow regime, Table 3.28. However, even with this change in leak path geometry, cycle 2 leak rates remain lower than those of cycle 1.



### **3.7.4.3 SW gasket deflections**

The data presented in Tables 3.18 and 3.21 highlight that gasket deflection ratios at S5 to S3 for both tests at 200 and 800 psig gas pressure are approximately the same, except for the milled surfaces II2 and II3 where the ratio is higher by 5 to 8.5 percent. The same can be said for deflection ratios at unload to S1. This effect is not noted with the PTFE and G2 gaskets. The additional gasket deflection seen for milled surfaces at 800 psig might be related to some complex interaction between the gas pressure, the surface grooves and the SW gasket geometry. But, the mechanism by which it acts is not known at the present time.

It can be observed in Table 3.18 and 3.21 that, as the gasket stress increases from S3 to S5, the gasket deflections increase by 30% to 45%, for turned and milled surfaces. Similar results can be seen at final stress S1 (cycle2) to S1 (cycle 1), Tables 3.18 and 3.21. Such results indicate that the gasket has gone through some permanent deformation after being exposed to higher stress levels (S5) in cycle 2, and has become very rigid upon unloading.

### **3.7.4.4 Leak flow regimes on spiral wound gasket**

The analysis of the leak flow regimes based on the determination of the slope of the line from log-log plot of leak versus gas pressure is presented in Table 3.28, and in Figure 3.34, for all surfaces at different gasket stress levels.

It can be seen that the III1, III2, II2 and II3 surfaces have molecular flow regime at high stress levels S3 and S5. Probably with these surface forms the graphite filler penetrate better into the surface asperities blocking the leak paths, resulting in leak paths of molecular geometry. However, the milled surfaces have relatively high leak rates, which

is attributed to the radial grooves on their surfaces. Therefore, when unloading to S1 from higher stress levels (molecular leak paths), the radial channels on these surfaces reopen, changing the flow regime to laminar. The same flow regime change occurs also with the ground III1 surface, and to a lesser degree with III2 surface.

For the turned surfaces, on the other hand, the flow is mainly in molecular state in the first load cycle, but it changes to laminar state at higher gasket compressive stress in the second load cycle. This is perhaps due to the fact that the grooves apex penetrate deeper into the gasket causing a change in the leak path geometry distribution. The leak paths of laminar geometry, which do not dominate in the first cycle (max. S3), prevail at higher stresses, creating some larger leak paths. On the other hand, when the load is reduced from S5 to S1, the paths of molecular geometry, closed at higher stress levels, are reopened and become dominant. But, even with these changes in their leak flow regimes, it must be emphasized that turned surfaces show better sealing performance with SW gasket than the milled and the ground surfaces that are less subject to flow regime change.

### 3.8 Conclusion

The present experimental research investigated the effect of surface characteristics (roughness and form) on the leak rate and on the leak behavior for three different gasket types, PTFE sheet, flexible graphite sheet G2 and flexible graphite filled spiral wound. The results show that the surface roughness expressed by arithmetic average height,  $R_a$ , does not have a strong influence on the leak rate, except in the case of the ground surfaces. The results also indicate that the surface characteristic form has a great influence on local gasket stress, in combination with gasket material and internal gas pressure, defining the leak paths geometry and affecting the leak rate and flow regime.

Many parameters such as internal gas pressure, gasket properties, applied load, surface macro and microstructure have an effect on the sealing performance and on the leak flow regime. The leak rate and the flow regimes are influenced by the surface asperities in contact, the leak path diameter size and length, which are not precisely measurable. The complexity of their combined effects renders the analytical solutions of the sealing phenomena even more difficult.

The results show that the gasket material plays an important role on the sealing performance and on the flow regimes under different stress levels depending on the surface characteristics.

The comparisons made from the results show that, in general, the PTFE gasket is less sensitive to surface characteristics at higher stress levels than the two other gasket types. As for the G2 and SW gaskets they are more sensitive to the surface characteristics at high stresses. However, the different surface types have a distinct effect on each of the gasket, and in general it is observed that the turned surfaces have better overall sealing performance.

The effect of sealing surface characteristics varies depending on the gasket type, the flange surface characteristics, the stress and the internal gas pressure. But, up to now, the effect of surface characteristics has not been included in the evaluation of the leak rate of gasketed joints. The present experimental work has shown that the choice of the surface type can change substantially the joint leak rate, especially when the gasket is under low compressive stress. Consequently, it is recommended that all the factors including the surface characteristics be considered for a more accurate evaluation of sealing performance of gasketed bolted flanged joints.

### 3.9 References

1. A. Bazergui and L. Marchand, "A test procedure for determining room temperature properties of gaskets", ASME, Proceedings of the Pressure Vessels and Piping Conference, **98(2)**, pp. 95—103, 1985.
2. A. Bazergui and L. Marchand "Development of tightness test procedures for gaskets in elevated temperature service", Welding Research Council Bulletin **339**, September 1988.
3. A. Bazergui and G. Louis, "Tests with various gases in gasketed joints", Experimental Techniques, Society for Experimental Mechanics, **12(11)**, pp. 17—21(s), November 1988.
4. A. Bazergui, L. Marchand and J. R. Payne, "Effect of fluid on sealing behaviour of gaskets", 10<sup>th</sup> International Conference on Fluid Sealing, Innsbruck, Austria, Paper H2, pp. 365—385, 3—5 April 1984.
5. L. Marchand and M. Derenne, "Fugitive emission characteristics of gaskets", Pressure Vessel Research Council, Project no. 92—25, February 1997.
6. T. C. Chivers, R. P. Hunt, W. J. Rogers and M. E. Williams, "On the relationships between gas properties, surface roughness and leak flow regimes", Proceedings of the 7<sup>th</sup> International Conference on Fluid Sealing, Nottingham, UK, Paper D3, pp. 13—24, 24—26 September 1975.
7. L. A. Mitchell and M. D. Rowe, "Influence of Asperity Deformation Mode on Gas Leak Between Contacting Surfaces", Journal of Mechanical Engineering Science, **11(5)**, pp. 534—545, 1969.
8. H. J. Tückmantel, "Leak Rate as a Function of Surface Pressure", 2<sup>nd</sup> International Symposium on Fluid Sealing, CETIM, La Baule, France, pp. 99—102, 18—20 September 1990.
9. F. O. Rathbun, Jr., "Metal-to-metal and metal-gasketed seals", The Aerospace Fluid Power System Equipment Conference, Los Angeles, SAE Paper no. 650312, pp. 156—169, May 1965.

10. A. Bazergui, L. Marchand and J. R. Payne, "Effect of fluid on sealing behaviour of gaskets", Paper H2, 10<sup>th</sup> International Conference on Fluid Sealing, Innsbruck, Austria, 3—5 April 1984.
11. J. R. Payne, "Effect of Flange Surface Finish on Constants for Steel Jacketed and other Gaskets", 3<sup>rd</sup> International Symposium on Fluid Sealing, Biarritz, France, pp. 505—519, September 15—18, 1993.
12. J. R. Payne, "Effect of flange surface finish on spiral wound gasket constants", 2<sup>nd</sup> International Symposium on Fluid Sealing, La Baule, France, pp. 81—90, 18—20 September 1990.
13. Y. Matsuzaki and T. Kazamaki, "Effect of surface roughness on compressive stress of static seals", JSME International Journal Series III, 31(1), pp. 99—106, 1988.
14. M. Derenne and H. Bouzid, "Effect of flange surface finish on room temperature gasket tightness and emissions", 1<sup>st</sup> Progress Report, Ecole Polytechnique de Montreal, Montreal, Quebec, Canada, 1997, (unpublished).
15. J. A. Greenwood and J. B. P. Williamson, "Contact of nominally flat surfaces", Proc. R. Soc. Series A295, pp. 300-319, 1966.
16. J. A. Greenwood and J. H. Tripp, "The contact of two nominally flat rough surfaces", Proceedings of. Instn. Mech. Engrs. 185(48/71), pp. 625—633, 1971.
17. T. Shimomura, H. Hirabayashi and T. Nakajima, "A study of the relationship between frictional characteristics and surface condition of mechanical seals", Tribology Transaction, 34(4), pp. 513—520, 1991.
18. J. Halling, Introduction to Tribology, Wykeham Publications London Ltd., 1976.
19. D. R. Askeland, The Science and Engineering of Materials, 2<sup>nd</sup> edition, PWS-Kent publishing Company, Boston, Mass. U.S.A., 1984.
20. A. E. Scheidegger, The Physics of Flow through Porous Media, 3<sup>rd</sup> edition University of Toronto Press, 1974.
21. ANSI/ASME B46.1, Surface texture: surface roughness, waviness and lay. The American Society of Mechanical Engineers, New York, 1985.

22. T. Tsukizoe and T. Hisakado, "On the mechanism of contact between metal surfaces- The penetrating depth and average clearance." Trans. of the ASME, J. of Basic Engineering, pp. 666—647, September 1965.
23. T. C. Chivers and R. P. Hunt, "Scalling of gas leakage from static seals", Paper G3, 8<sup>th</sup> International Conference on Fluid Sealing, Sept. 11-13, 1978.
24. A. Bazergui and G. Louis, " Predicting leakage for various gasket in gasketed joints", Society for Experimental Mechanics, 1987 Spring Conf. on Experimental Mechanics, Houston, Texas, June 1987.
25. T. C. Chivers and M. E. Williams, "On the gas leakage from elastic seals", CEGB Report RD/B/N2334, 1973.
26. A. Nerken, "Experiments on flow of gases through leaks", Vacuum Symposium Transaction, 1956.
27. Draft 9 of the proposed ASTM, "Standard test method for gasket constants for bolted joint design and addendum to Draft 9 Section 9".
28. M. Derenne, J. R. Payne, L. Marchand and A. Bazergui, " PVRC/MTI technology for characterizing gasket used in bolted flanged connection", John H. Bickford: Gasket and Gasketed Joints, Marcel Dekker, Inc., Chapter 5, 1997.
29. J. R. Payne and R. W. Schneider, "ASME flanged joint rules—New vs. Traditional", John H. Bickford: Gasket and Gasketed Joints, Marcel Dekker, Inc., Chapter 9, 1997.
30. ASME Boiler and Pressure Vessel Code, Section III, Div. 1, The American Society of Mechanical Engineers, New York, 1996.
31. ASME/ANSI B16.5- Steel pipe flanges and flanged fittings. The American Society of Mechanical Engineers/The American National Standard Institute, New York, 1993.
32. ASME B46.20- Metallic gaskets for pipe flanges-Ring joint, spiral wound, and jacketed. The American Society of Mechanical Engineers, New York, 1993.
33. ASME B46.21- Nonmetallic flat gaskets for pipe flanges. The American Society of Mechanical Engineers, New York, 1992.
34. J. Latte, "Gasket Behavior and its influence on the safety of flanged joints", John H. Bickford: Gasket and Gasketed Joints, Marcel Dekker, Inc., Chapter 1, 1997.

35. J. Latte and D. Coomber, "Industrial gaskets", John H. Bickford: Gasket and Gasketed Joints, Marcel Dekker, Inc., Chapter 3, 1997.

**Table 3.7.** PTFE gasket leak ratio Lrm (800 psig)/Lrm (200 psig).

Stress Level	I1	I3	II2	II3	III1	III2	J1	J3
S1	158.71	30.98	N/A	N/A	N/A	N/A	N/A	N/A
S2	2.32	3.04	6.43	5.97	6.16	38.65	1.53	1.80
S3	2.54	4.38	3.33	4.22	3.14	2.51	2.21	2.09
S2.5	2.93	3.15	3.44	4.50	3.62	2.89	2.89	2.67
S1	5.97	9.08	180.06	215.98	24.04	14.15	11.63	13.05
S4	3.33	4.08	3.08	3.57	4.44	3.57	3.57	4.22
S5	3.06	3.60	3.08	3.88	4.41	3.09	3.75	4.12
S3.5	3.06	3.60	3.09	4.17	4.45	2.45	4.05	4.15
S1	3.82	10.92	928.57	405.94	84.85	2.85	5.19	13.61

**Table 3.8.** G2 gasket leak ratio Lrm (800 psig)/Lrm (200 psig).

Stress Level	I1	I3	II2	II3	III1	III2	J1	J3
S1	6.84	6.57	N/A	N/A	N/A	N/A	N/A	N/A
S2	18.96	5.72	3.89	4.07	2.40	4.19	4.89	3.59
S3	10.29	4.86	6.02	7.09	3.00	5.99	5.12	3.84
S2.5	10.25	5.12	6.25	7.01	2.93	6.25	5.47	3.99
S1	21.81	5.90	4.73	5.08	3.60	4.93	6.72	4.58
S4	5.80	6.13	7.88	8.53	3.06	8.00	5.41	4.45
S5	10.40	11.81	9.26	12.14	4.11	10.45	6.87	3.82
S3.5	5.94	7.35	10.56	11.74	3.90	9.28	6.83	3.74
S1	66.67	6.55	8.32	9.15	5.10	8.52	68.88	4.24

**Table 3.9.** SW gasket leak ratio Lrm (800 psig)/Lrm (200 psig).

Stress Level	I1	I3	II2	II3	III1	III2	J1	J3
S1	N/A	N/A	N/A	N/A	N/A	N/A	N/A	N/A
S2	3.84	4.10	9.38	6.17	3.58	2.78	6.86	5.99
S3	3.66	7.33	8.61	5.47	3.75	2.45	7.73	7.62
S2.5	3.80	7.81	8.00	5.52	3.88	2.23	7.10	8.48
S1	5.56	7.39	7.40	4.28	5.57	3.50	7.91	6.80
S4	5.23	20.82	3.41	4.07	3.05	3.18	6.92	11.85
S5	10.18	44.49	3.76	4.13	2.81	3.77	16.19	11.95
S3.5	10.92	32.68	3.58	3.54	3.17	3.76	14.68	11.79
S1	5.52	10.47	10.00	16.96	14.26	5.27	7.95	6.38



**Table 3.10.** PTFE gasket leak ratio of all surface characteristics compared to ground surface III1 at 200 psig for different stress levels.

Finish	S1	C1U1S1*	C2U2S1**	S3	S5
J1/III1	0.003	0.34	0.04	1.00	0.94
J3/III1	0.002	0.37	0.04	1.28	1.00
I1/III1	0.044	0.44	0.05	1.51	1.06
I3/III1	0.027	0.44	0.07	1.75	1.06
II2/III1	106.832	0.80	0.55	0.80	1.15
II3/III1	0.554	0.76	1.31	0.75	1.06
III2/III1	17.391	39.55	33.90	0.93	1.24

**Table 3.11.** G2 gasket leak ratio of all surface characteristics compared to ground surface III1 at 200 psig for different stress levels.

Finish	S1	C1U1S1	C2U2S1	S3	S5
J1/III1	1.01	0.80	1.20	0.62	0.86
J3/III1	1.25	0.92	1.41	0.82	1.15
I1/III1	1.05	0.22	0.93	0.29	0.38
I3/III1	1.07	0.75	1.04	0.62	0.34
II2/III1	0.98	1.14	1.30	1.16	1.97
II3/III1	0.83	0.92	1.00	0.92	1.00
III2/III1	2.02	1.14	1.20	1.25	1.34

**Table 3.12.** SW gasket leak ratio of all surface characteristics compared to ground surface III1 at 200 psig for different stress levels.

Finish	S1	C1U1S1	C2U2S1	S3	S5
J1/III1	0.86	0.34	0.21	0.69	0.08
J3/III1	0.38	0.28	0.19	0.41	0.06
I1/III1	0.50	0.40	0.26	0.84	0.06
I3/III1	0.55	0.32	0.32	0.26	0.02
II2/III1	14.16	2.72	4.44	1.12	1.06
II3/III1	0.77	3.12	5.06	1.31	1.12
III2/III1	34.27	3.12	3.31	3.44	0.81

\* Cycle 1 unload to S1

\*\* Cycle 2 unload to S1

**Table 3.13.** PTFE gasket leak ratio of all surface characteristics compared to ground surface III1 at 800 psig for different stress levels.

Finish	C1U1S1	C2U2S1	S3	S5
J1/III1	0.17	0.002	0.70	0.80
J3/III1	0.20	0.006	0.85	0.93
I1/III1	0.11	0.002	1.22	0.73
I3/III1	0.17	0.009	2.43	0.87
II2/III1	5.99	5.97	0.85	0.80
II3/III1	6.82	6.28	1.00	0.93
III2/III1	23.27	1.14	0.74	0.87

**Table 3.14.** G2 gasket leak ratio of all surface characteristics compared to ground surface III1 at 800 psig for different stress levels.

Finish	C1U1S1	C2U2S1	S3	S5
J1/III1	1.50	16.13	1.05	1.44
J3/III1	1.16	1.17	1.05	1.07
I1/III1	1.36	12.19	1.00	0.96
I3/III1	1.23	1.34	1.00	0.96
II2/III1	1.49	2.13	2.34	4.45
II3/III1	1.29	1.79	2.17	2.95
III2/III1	1.56	2.00	2.50	3.41

**Table 3.15.** SW gasket leak ratio of all surface characteristics compared to ground surface III1 at 800 psig for different stress levels.

Finish	C1U1S1	C2U2S1	S3	S5
J1/III1	0.49	0.11	1.42	0.47
J3/III1	0.34	0.08	0.82	0.24
I1/III1	0.39	0.10	0.82	0.21
I3/III1	0.42	0.23	0.50	0.27
II2/III1	3.61	3.11	2.58	1.42
II3/III1	2.40	6.02	1.91	1.65
III2/III1	1.96	1.22	2.25	1.09

**Table 3.16. PTFE gasket leak and deflection ratio for all surface characteristics at different stress levels for 200 psig.**

Finish	Leak ratio C2U2S1/C1U1S1	Dg ratio C2U2S1/C1U1S1	Leak ratio S5/S3	Dg ratio S5/S3
J1	0.61	1.10	0.37	1.15
J3	0.56	1.13	0.31	1.21
I1	0.55	1.15	0.28	1.23
I3	0.78	1.43	0.24	1.45
II2	3.54	1.40	0.56	1.42
II3	8.96	1.33	0.56	1.35
III1	5.19	1.49	0.40	1.51
III2	4.45	1.38	0.53	1.43

**Table 3.17. G2 gasket leak and deflection ratio for all surface characteristics at different stress levels for 200 psig.**

Finish	Leak ratio C2U2S1/C1U1S1	Dg ratio C2U2S1/C1U1S1	Leak ratio S5/S3	Dg ratio S5/S3
J1	0.38	1.07	0.08	1.10
J3	0.39	1.08	0.08	1.13
I1	1.06	1.08	0.07	1.13
I3	0.36	1.09	0.03	1.15
II2	0.29	1.09	0.09	1.14
II3	0.28	1.08	0.06	1.14
III1	0.26	1.09	0.05	1.15
III2	0.27	1.09	0.06	1.15

**Table 3.18. SW gasket leak and deflection ratio for all surface characteristics at different stress levels for 200 psig.**

Finish	Leak ratio C2U2S1/C1U1S1	Dg ratio C2U2S1/C1U1S1	Leak ratio S5/S3	Dg ratio S5/S3
J1	0.45	1.31	0.06	1.31
J3	0.52	1.33	0.07	1.33
I1	0.50	1.36	0.03	1.36
I3	0.75	1.34	0.03	1.33
II2	1.24	1.33	0.47	1.31
II3	1.23	1.37	0.43	1.35
III1	0.76	1.25	0.50	1.24
III2	0.81	1.38	0.12	1.37

**Table 3.19. PTFE gasket leak and deflection ratio for all surface characteristics at different stress levels for 800 psig.**

Finish	Leak ratio C2U2S1/C1U1S1	Dg ratio C2U2S1/C1U1S1	Leak ratio S5/S3	Dg ratio S5/S3
J1	0.27	1.13	0.63	1.17
J3	0.59	1.14	0.61	1.21
I1	0.35	1.20	0.33	1.27
I3	0.94	1.43	0.20	1.44
II2	18.25	1.38	0.52	1.40
II3	16.85	1.33	0.52	1.34
III1	18.32	1.42	0.56	1.45
III2	0.90	1.31	0.65	1.36

**Table 3.20. G2 gasket leak and deflection ratio for all surface characteristics at different stress levels for 800 psig.**

Finish	Leak ratio C2U2S1/C1U1S1	Dg ratio C2U2S1/C1U1S1	Leak ratio S5/S3	Dg ratio S5/S3
J1	3.89	1.08	0.10	1.10
J3	0.36	1.08	0.08	1.12
I1	3.25	1.09	0.07	1.13
I3	0.39	1.09	0.07	1.13
II2	0.52	1.09	0.14	1.13
II3	0.50	1.09	0.10	1.13
III1	0.36	1.09	0.08	1.14
III2	0.46	1.10	0.10	1.14

**Table 3.21. SW gasket leak and deflection ratio for all surface characteristics at different stress levels for 800 psig.**

Finish	Leak ratio C2U2S1/C1U1S1	Dg ratio C2U2S1/C1U1S1	Leak ratio S5/S3	Dg ratio S5/S3
J1	0.46	1.30	0.12	1.30
J3	0.49	1.35	0.11	1.34
I1	0.49	1.34	0.09	1.34
I3	1.07	1.26	0.20	1.26
II2	1.67	1.40	0.21	1.38
II3	4.87	1.49	0.32	1.45
III1	1.94	1.31	0.37	1.30
III2	1.21	1.41	0.18	1.38

**Table 3.22.** PTFE gasket deflection ratio of all surface characteristics compared to ground surface III1 at 200 psig for different stress levels.

Finish	S1	C1U1S1*	C2U2S1**	S3	S5
J1/III1	1.78	1.15	0.85	1.10	0.84
J3/III1	1.52	1.06	0.80	1.05	0.84
I1/III1	1.45	1.01	0.77	1.01	0.82
I3/III1	1.26	1.06	1.01	1.04	1.00
II2/III1	0.88	1.07	1.00	1.05	1.00
II3/III1	1.19	1.31	1.16	1.25	1.12
III2/III1	0.92	0.84	0.77	0.86	0.82

**Table 3.23.** G2 gasket deflection ratio of all surface characteristics compared to ground surface III1 at 200 psig for different stress levels.

Finish	S1	C1U1S1	C2U2S1	S3	S5
J1/III1	1.37	1.27	1.24	1.17	1.13
J3/III1	1.25	1.19	1.18	1.16	1.14
I1/III1	1.26	1.17	1.16	1.13	1.12
I3/III1	1.13	1.10	1.09	1.08	1.08
II2/III1	1.13	1.07	1.06	1.06	1.05
II3/III1	1.18	1.08	1.07	1.06	1.05
III2/III1	0.99	0.97	0.98	0.98	0.98

**Table 3.24.** SW gasket deflection ratio of all surface characteristics compared to ground surface III1 at 200 psig for different stress levels.

Finish	S1	C1U1S1	C2U2S1	S3	S5
J1/III1	1.58	1.02	1.08	0.98	1.03
J3/III1	1.54	0.94	1.00	0.95	1.02
I1/III1	1.47	0.96	1.05	0.96	1.06
I3/III1	1.32	0.99	1.07	1.00	1.07
II2/III1	0.82	0.98	1.05	0.99	1.05
II3/III1	1.06	0.95	1.04	0.96	1.04
III2/III1	1.18	1.02	1.12	1.02	1.12

\* Cycle 1 unload to S1

\*\* Cycle 2 unload to S1

**Table 3.25.** PTFE gasket deflection ratio of all surface characteristics compared to ground surface III1 at 800 psig for different stress levels.

Finish	C1U1S1	C2U2S1	S3	S5
J1/III1	1.08	0.86	1.03	0.83
J3/III1	1.03	0.83	1.03	0.86
I1/III1	0.86	0.73	0.88	0.77
I3/III1	1.07	1.08	1.06	1.06
II2/III1	1.24	1.20	1.19	1.15
II3/III1	1.38	1.29	1.32	1.22
III2/III1	0.94	0.87	0.94	0.88

**Table 3.26.** G2 gasket deflection ratio of all surface characteristics compared to ground surface III1 at 800 psig for different stress levels.

Finish	C1U1S1	C2U2S1	S3	S5
J1/III1	1.28	1.26	1.20	1.16
J3/III1	1.19	1.18	1.16	1.14
I1/III1	1.14	1.14	1.12	1.11
I3/III1	1.09	1.09	1.08	1.07
II2/III1	1.06	1.06	1.05	1.05
II3/III1	1.07	1.07	1.06	1.06
III2/III1	0.95	0.95	0.95	0.96

**Table 3.27.** SW gasket deflection ratio of all surface characteristics compared to ground surface III1 at 800 psig for different stress levels.

Finish	C1U1S1	C2U2S1	S3	S5
J1/III1	0.99	0.99	0.95	0.95
J3/III1	0.96	0.99	0.94	0.98
I1/III1	0.99	1.01	0.99	1.01
I3/III1	1.00	0.96	1.00	0.97
II2/III1	1.06	1.14	1.06	1.12
II3/III1	0.94	1.06	0.95	1.06
III2/III1	0.96	1.03	0.97	1.03

**Table 3.28.** Slope of the lines based on log-log plot of leak versus pressure, representing the graphs of flow regimes on Figures 3.32 through 3.34.

Ra	Part Stress	(A)	(A)	(B)	(B)	(A)	(A)	(B)	(B)
		S2	S3	S2.5	S1	S4	S5	S3.5	S1
PTFE	J1	0.3	0.6	0.8	1.8	0.9	1.0	1.0	1.2
	J3	0.4	0.5	0.7	1.9	1.0	1.0	1.0	1.9
	I1	0.6	0.7	0.8	1.3	0.9	0.8	0.8	1.0
	I3	0.8	1.1	0.8	1.6	1.0	0.9	0.9	1.7
	II2	1.3	0.9	0.9	3.7	0.8	0.8	0.8	4.9
	II3	1.3	1.0	1.1	3.9	0.9	1.0	1.0	4.3
	III1	1.3	0.8	0.9	2.3	1.1	1.1	1.1	3.2
	III2	2.6	0.7	0.8	1.9	0.9	0.8	0.6	0.8
G2	J1	1.1	1.2	1.2	1.4	1.2	1.4	1.4	3.1
	J3	0.9	1.0	1.0	1.1	1.1	1.0	1.0	1.0
	I1	2.1	1.7	1.7	2.2	1.3	1.7	1.3	3.0
	I3	1.3	1.1	1.2	1.3	1.3	1.8	1.4	1.4
	II2	1.0	1.3	1.3	1.1	1.5	1.6	1.7	1.5
	II3	1.0	1.4	1.4	1.2	1.5	1.8	1.8	1.6
	III1	0.6	0.8	0.8	0.9	0.8	1.0	1.0	1.2
	III2	1.0	1.3	1.3	1.2	1.5	1.7	1.6	1.5
SW	J1	1.4	1.5	1.4	1.5	1.4	2.0	1.9	1.5
	J3	1.3	1.5	1.5	1.4	1.8	1.8	1.8	1.3
	I1	1.0	0.9	1.0	1.2	1.2	1.7	1.7	1.2
	I3	1.0	1.4	1.5	1.4	2.2	2.7	2.5	1.7
	II2	1.6	1.6	1.5	1.4	0.9	1.0	0.9	1.7
	II3	1.3	1.2	1.2	1.0	1.0	1.0	0.9	2.0
	III1	0.9	1.0	1.0	1.2	0.8	0.7	0.8	1.9
	III2	0.7	0.6	0.6	0.9	0.8	1.0	1.0	1.2

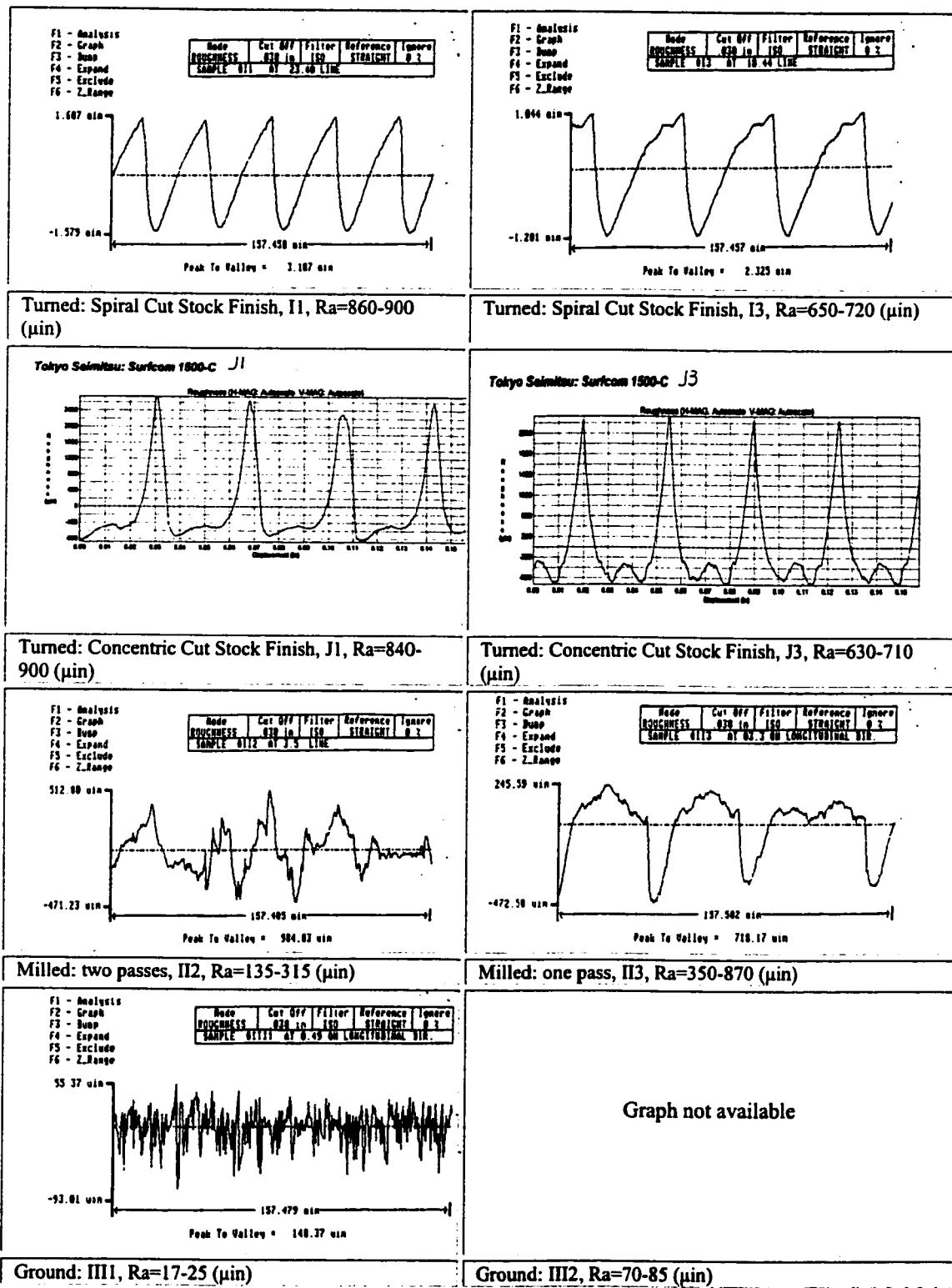
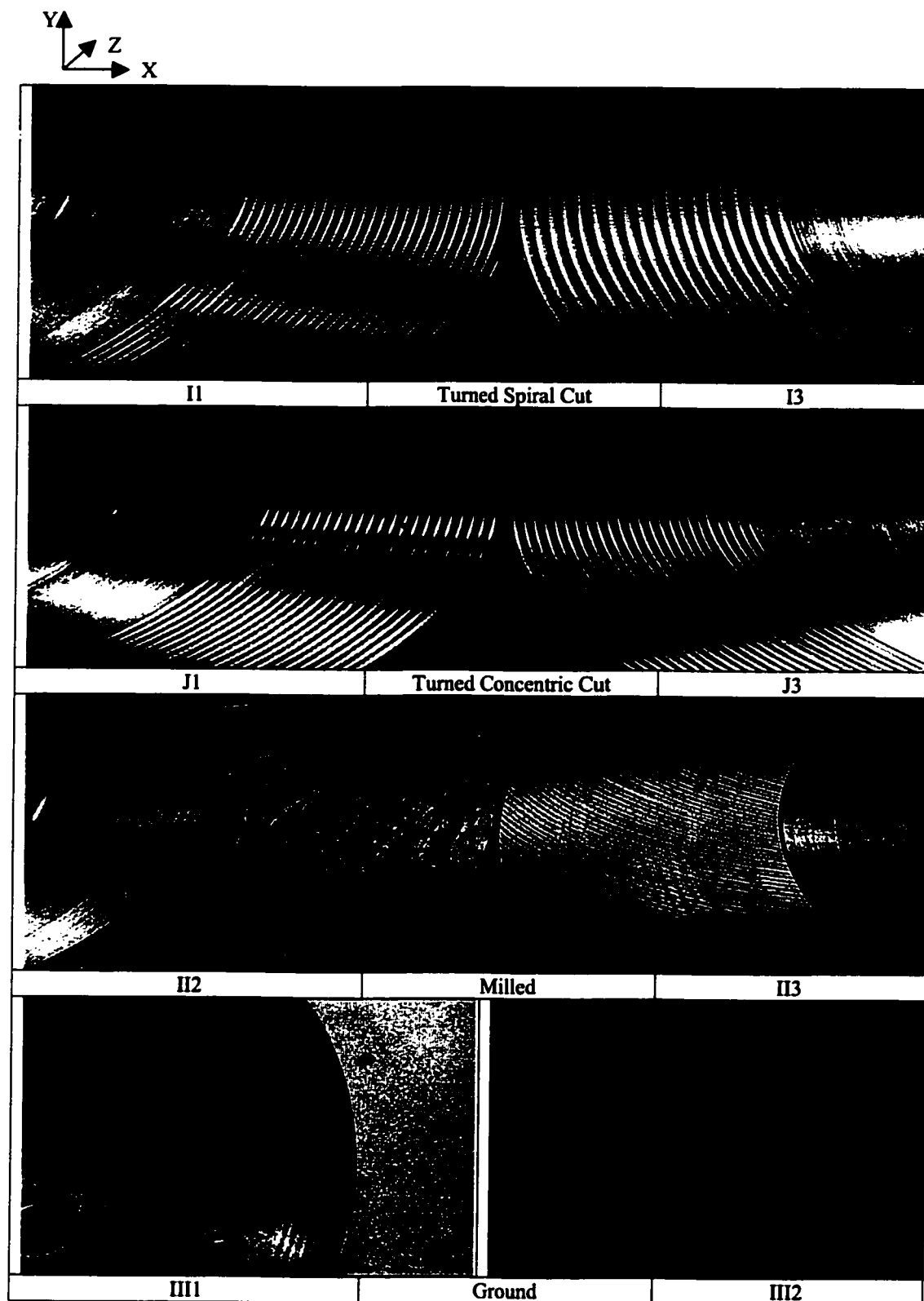


Figure 3.12. Topography of sealing surfaces.





**Figure 3.13.** Platens surface machining form.

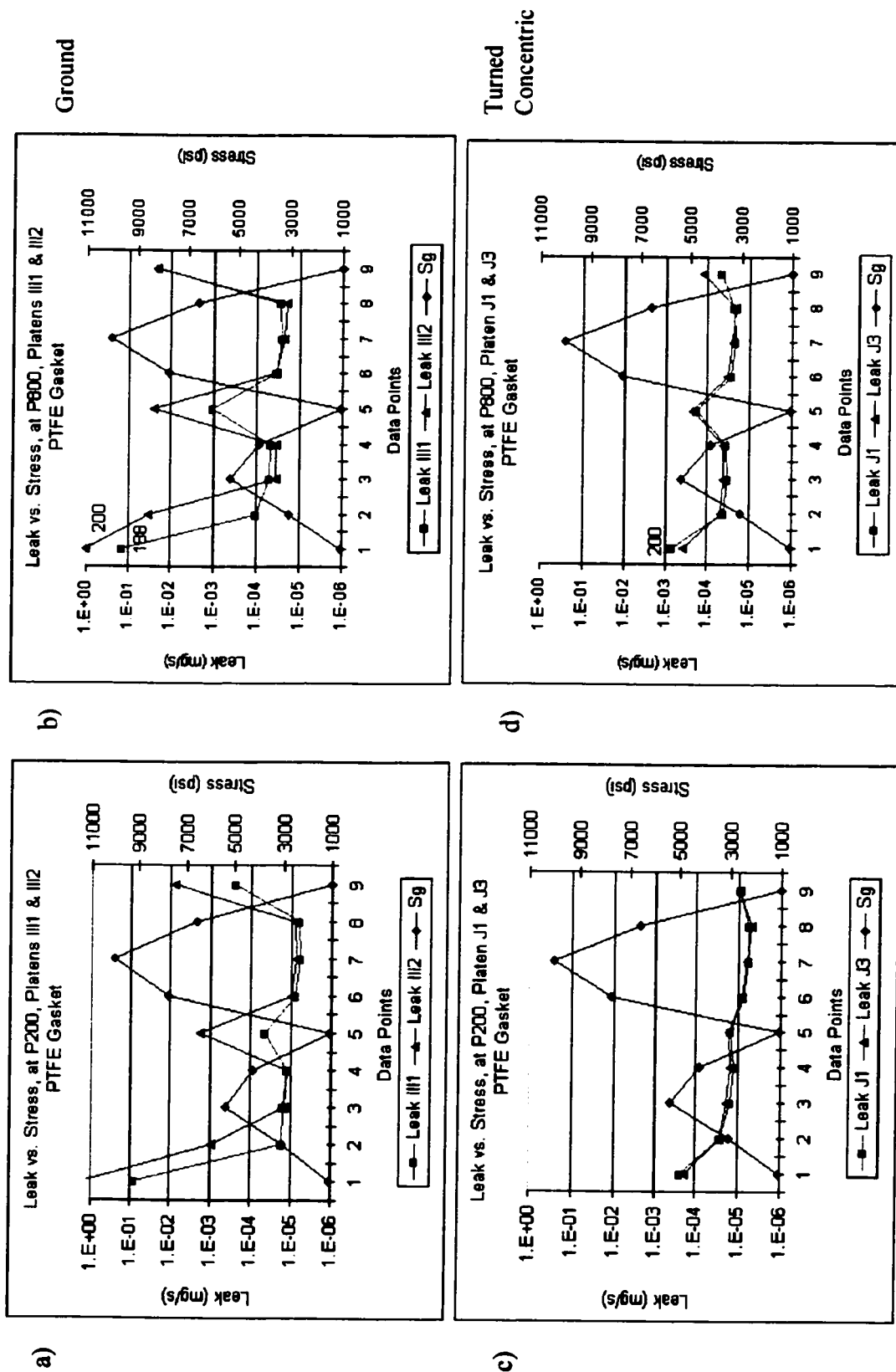
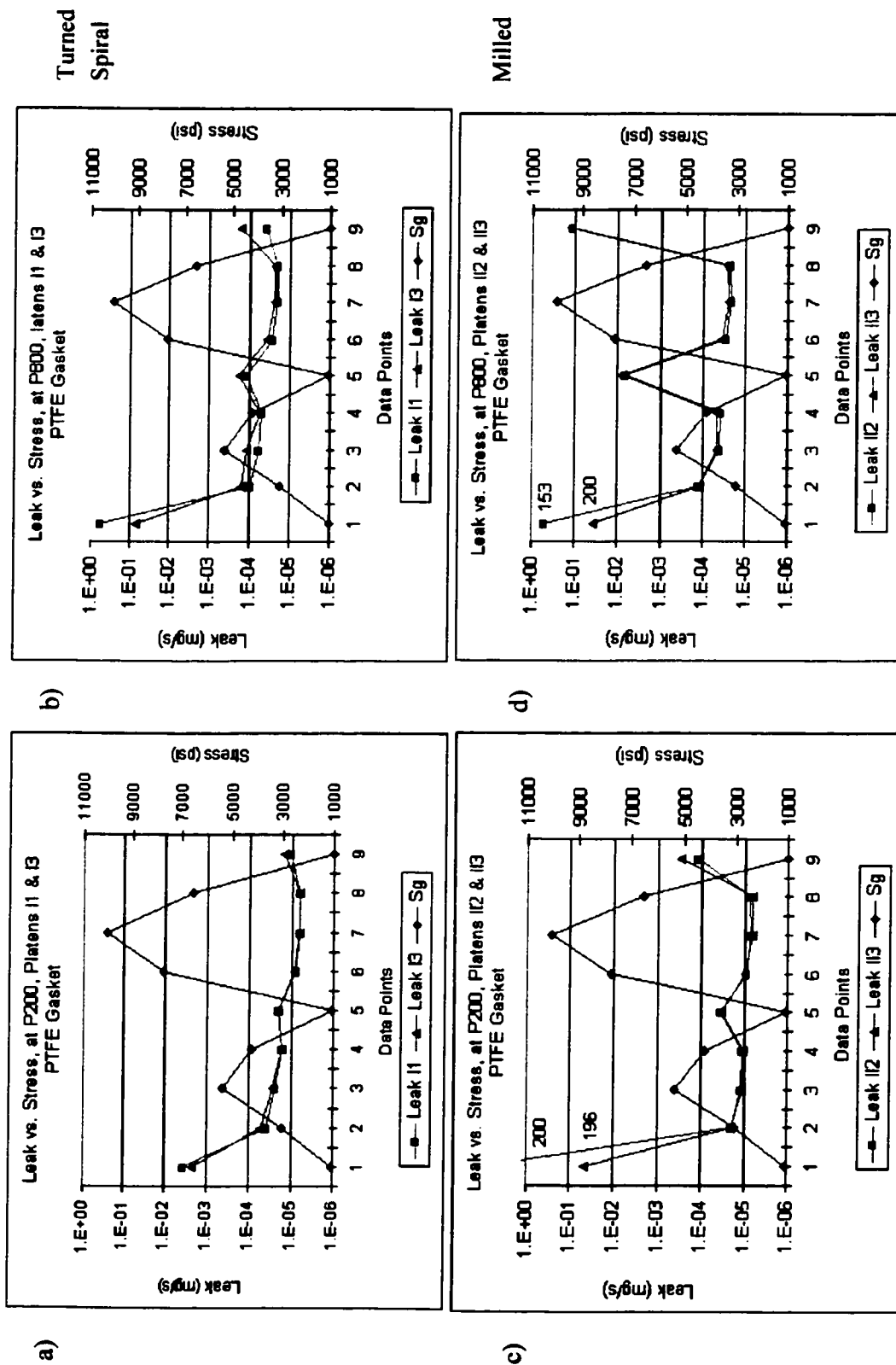
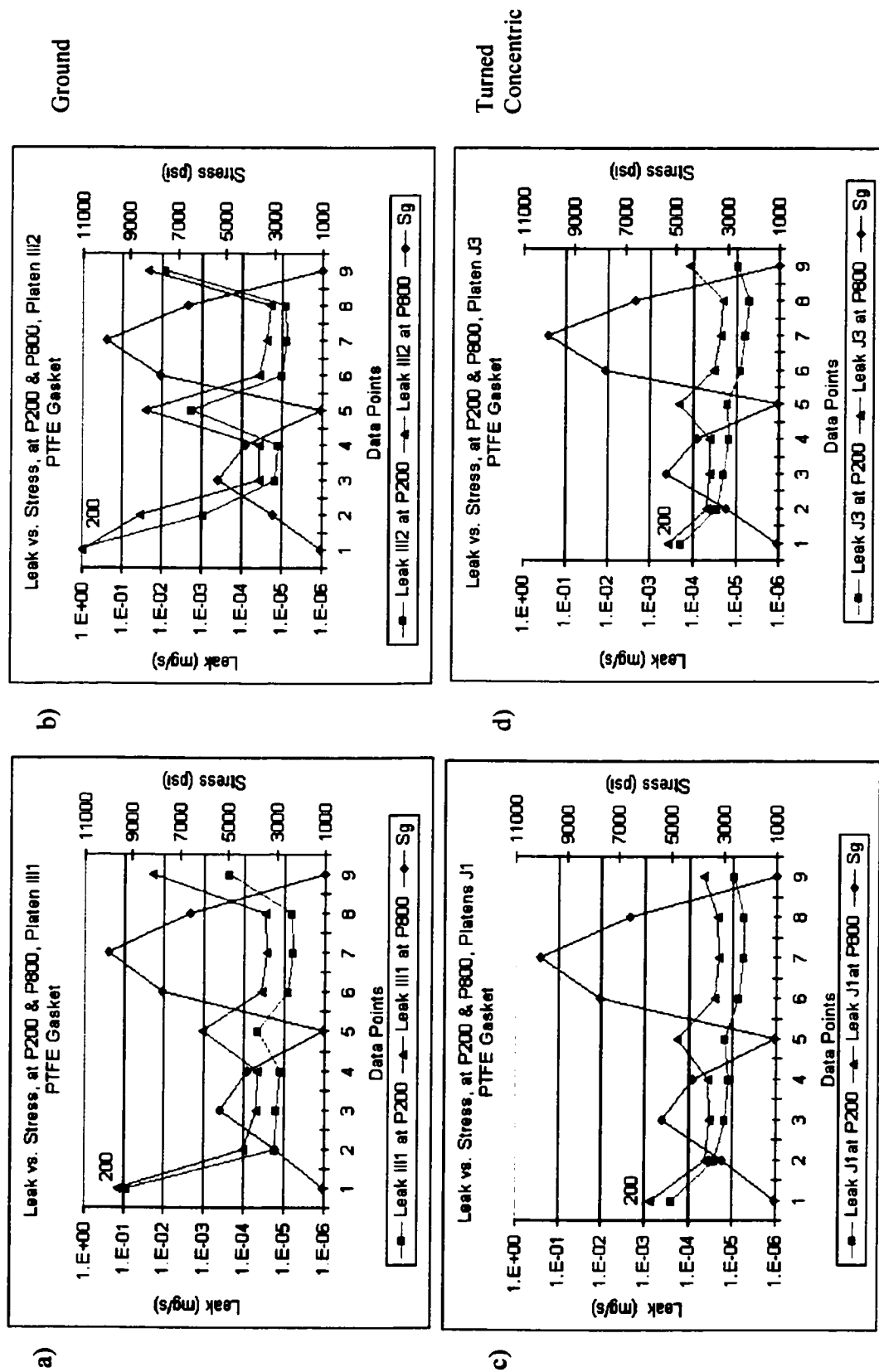


Figure 3.14. PTFE, effect of surface finish; leak rate versus stress levels, for ground and turned concentric surfaces.



**Figure 3.15.** PTFE, effect of surface finish; leak rate versus stress levels, for turned spiral and milled surfaces.



**Figure 3.16.** PTFE, effect of gas pressure; leak rate versus stress levels, for ground and turned concentric surfaces.

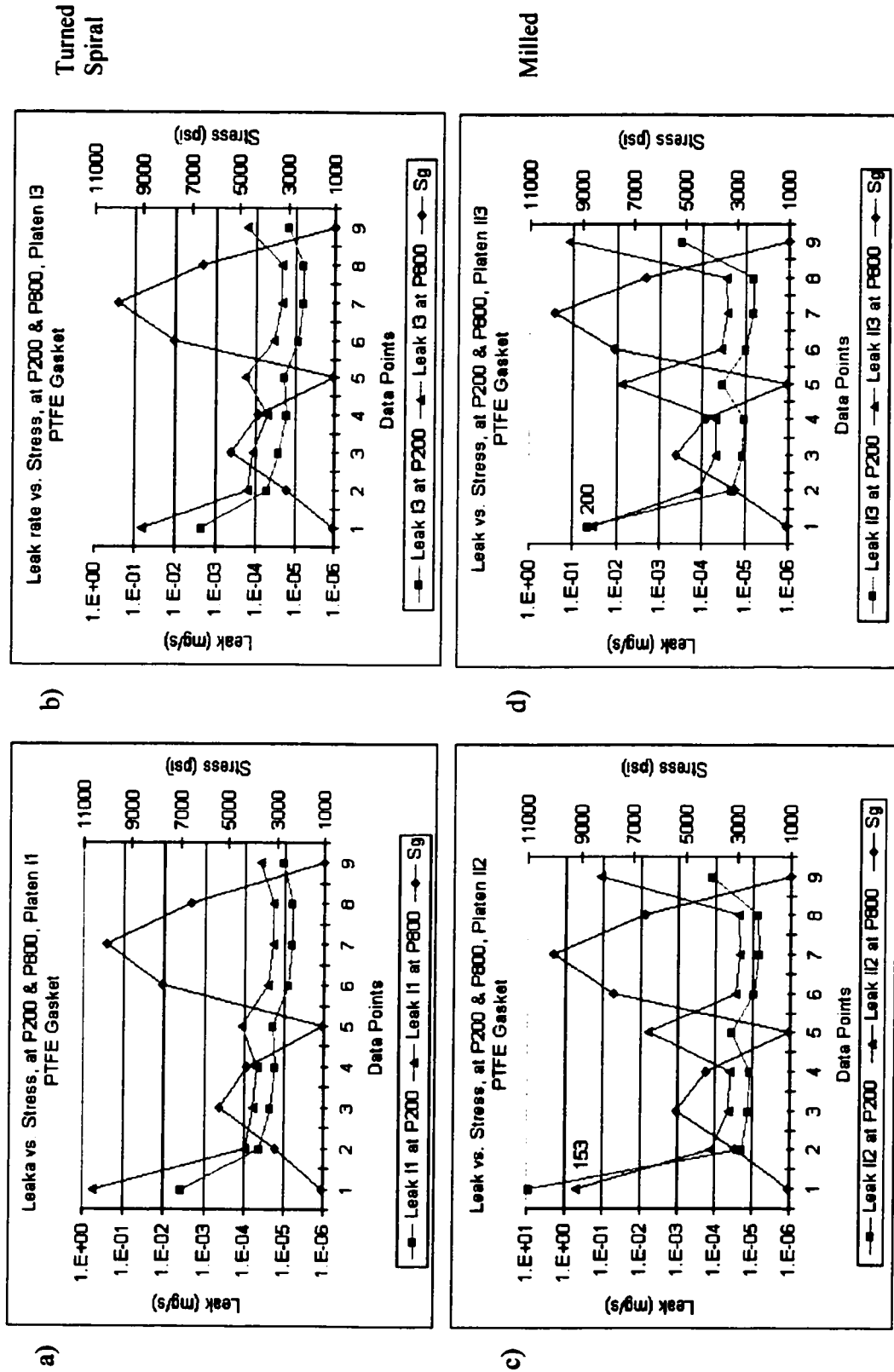


**Figure 3.17.** PTFE, effect of gas pressure; leak rate versus stress levels, for turned spiral and milled surfaces.

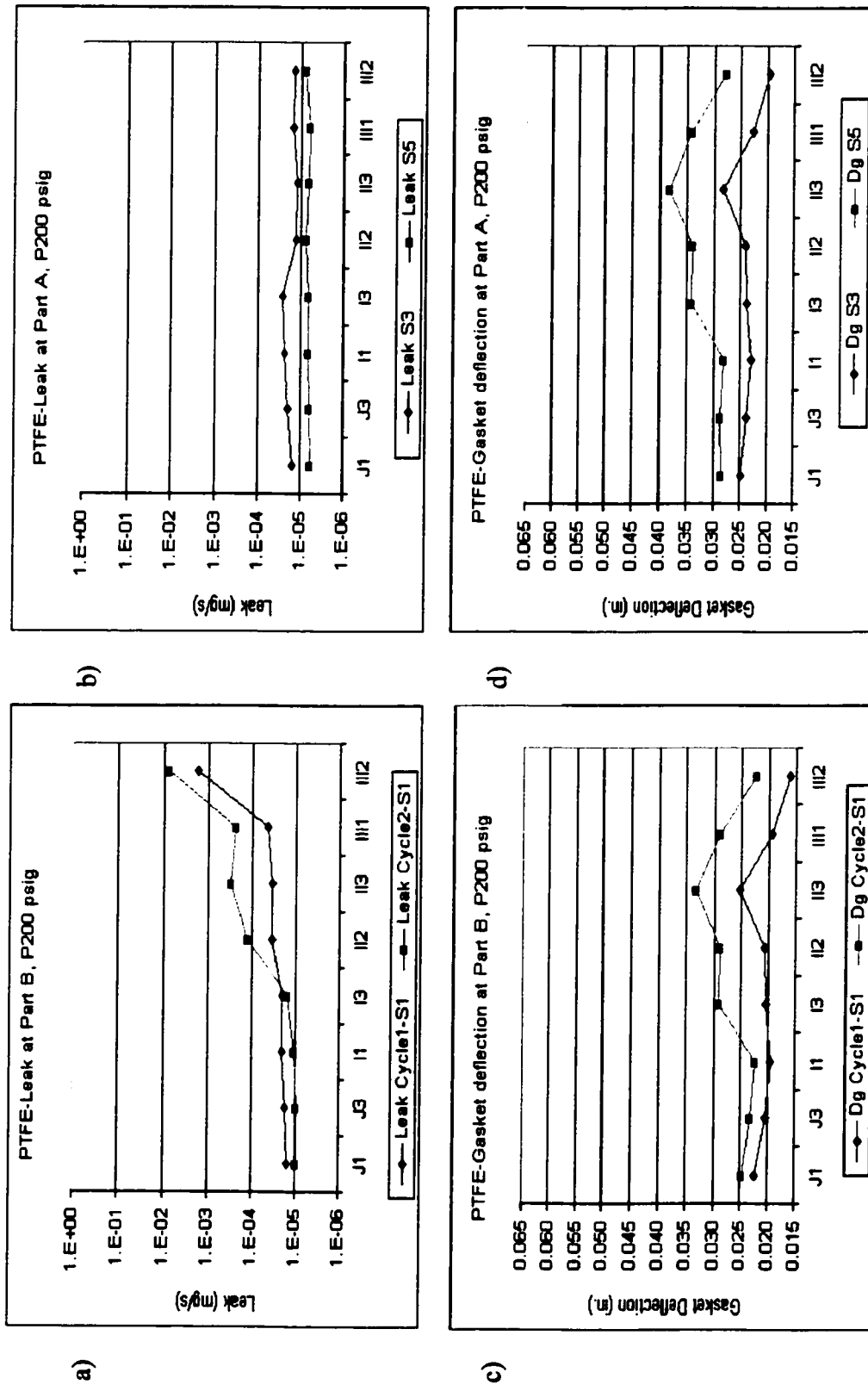


**Figure 3.18.** PTFE, leak rate and gasket deflection versus sealing surface characteristics, at stress S1, S3 and S5, at 200 psig.

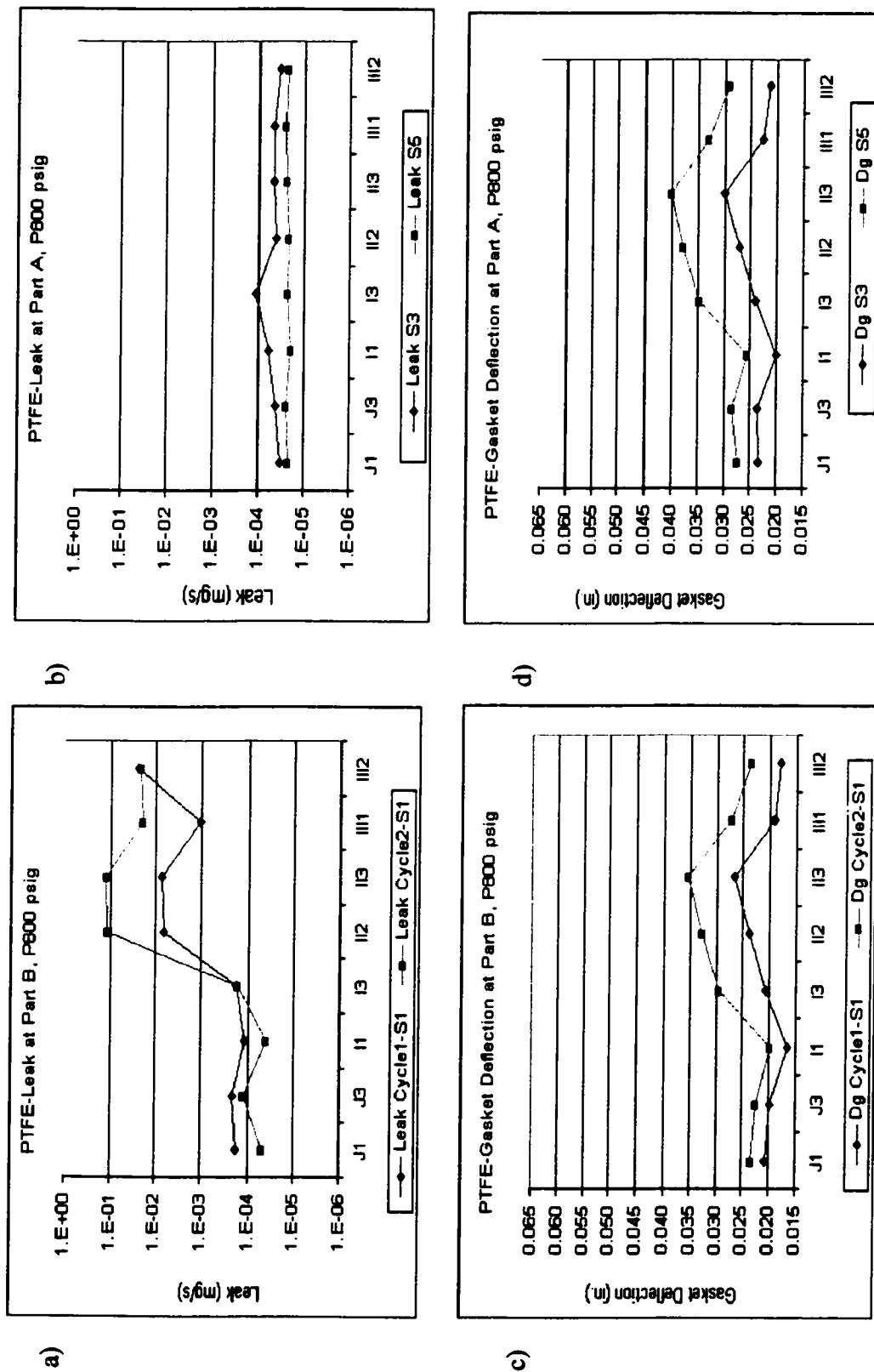


**Figure 3.19.** PTFE, leak rate and gasket deflection versus sealing surface characteristics, at stress S1, S3 and S5, at 800 psig.

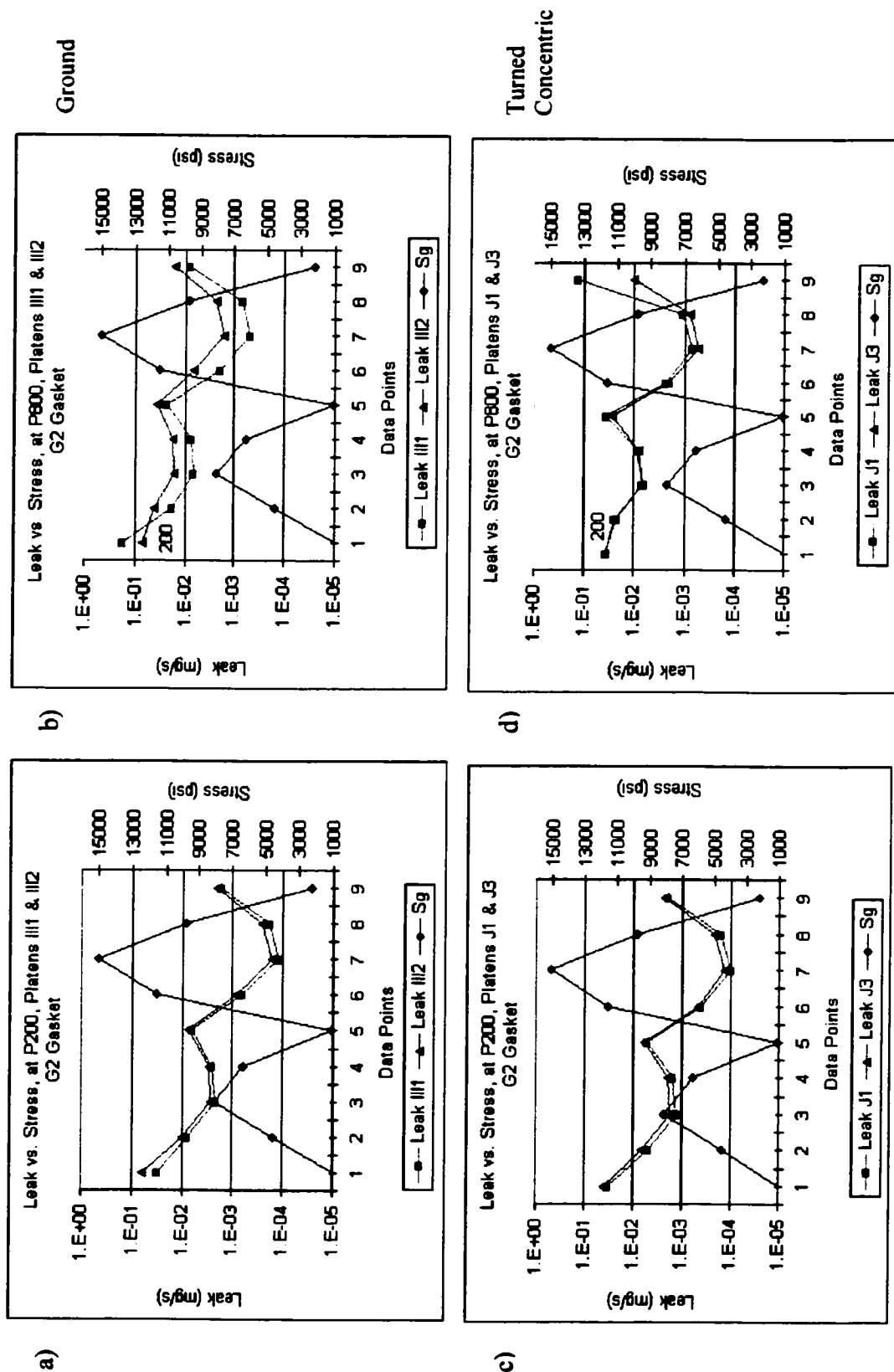


**Figure 3.20.** G2, effect of surface finish; leak rate versus stress levels, for ground and turned concentric surfaces.



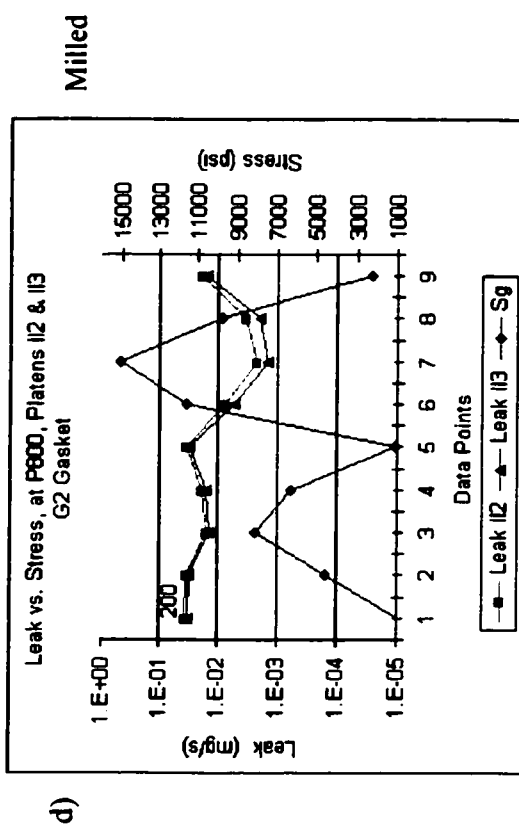
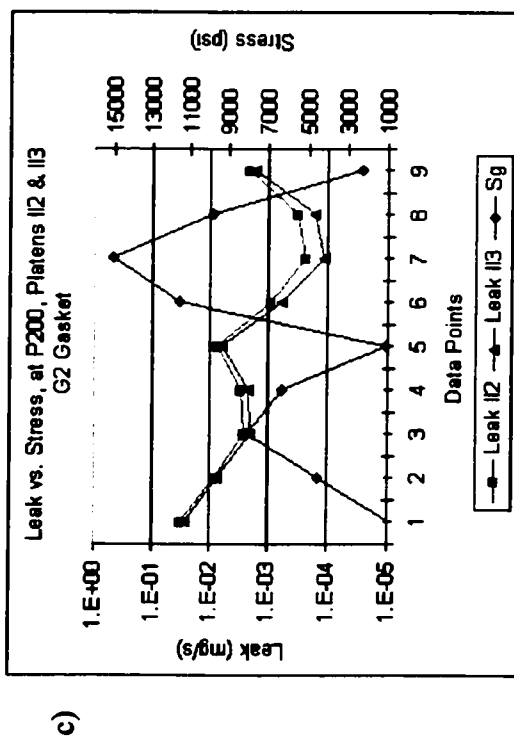
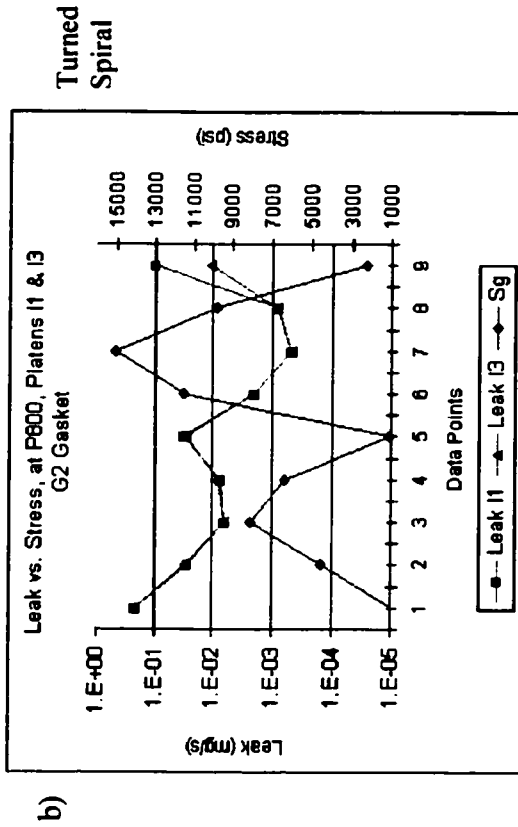
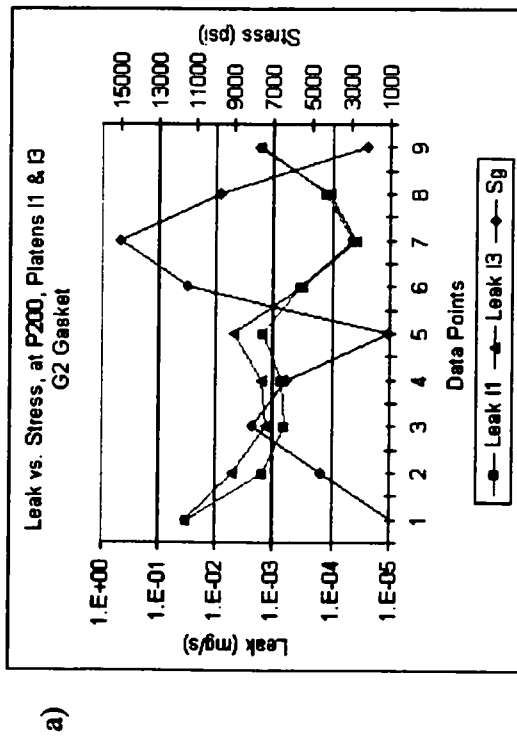
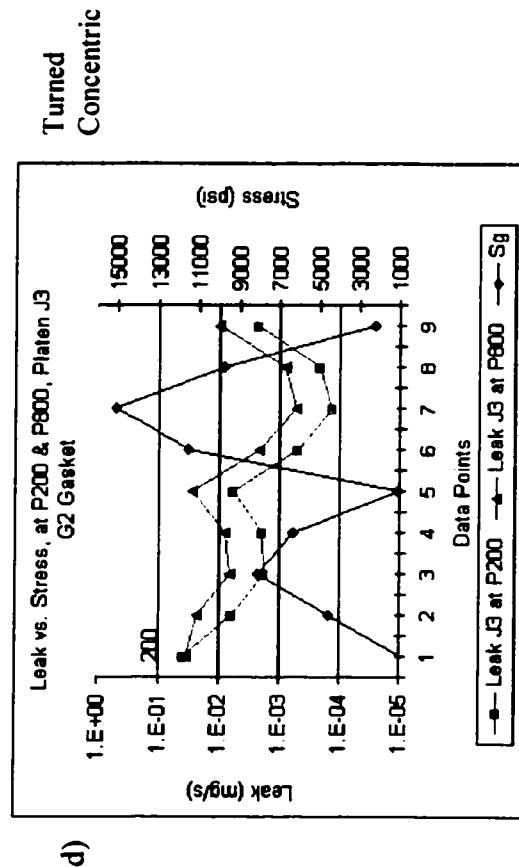
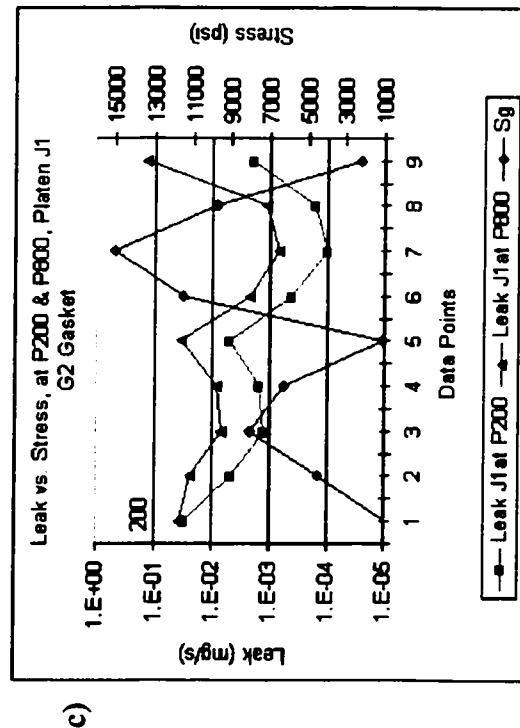
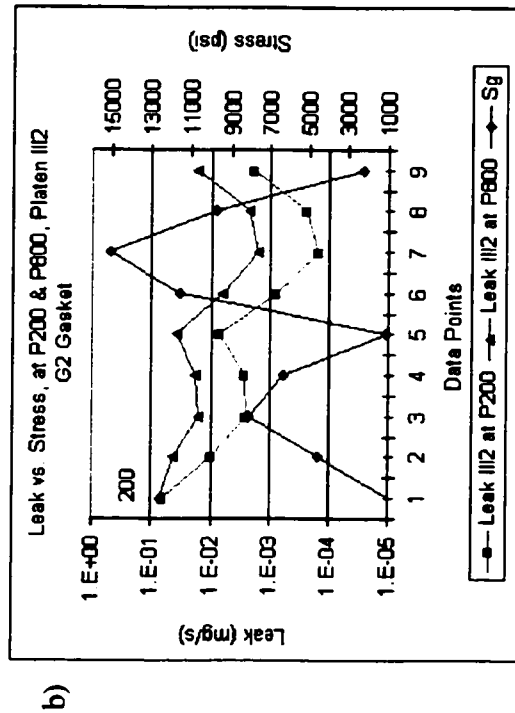
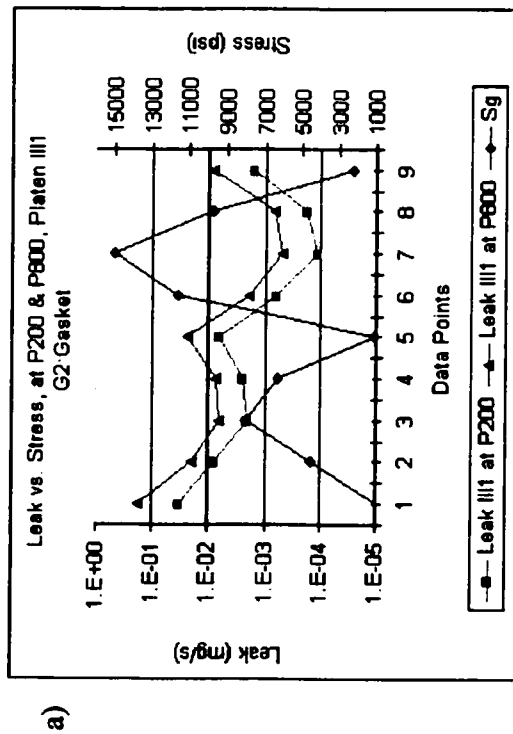
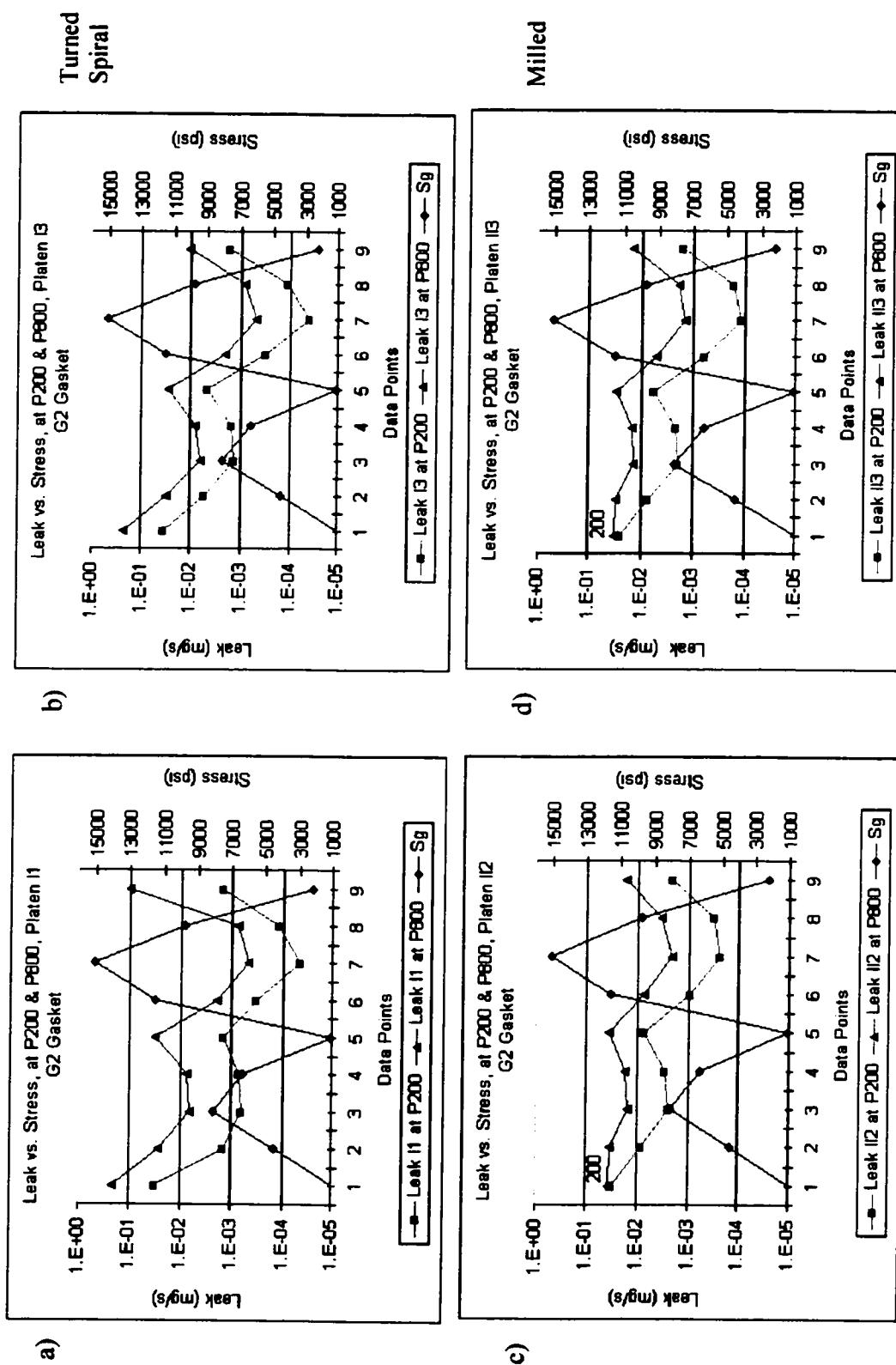


Figure 3.21. G2, effect of surface finish; leak rate versus stress levels, for turned spiral and milled surfaces.



**Figure 3.22.** G2, effect of gas pressure; leak rate versus stress levels, for ground and turned concentric surfaces.



**Figure 3.23.** G2, effect of gas pressure; leak rate versus stress levels, for turned spiral and milled surfaces.

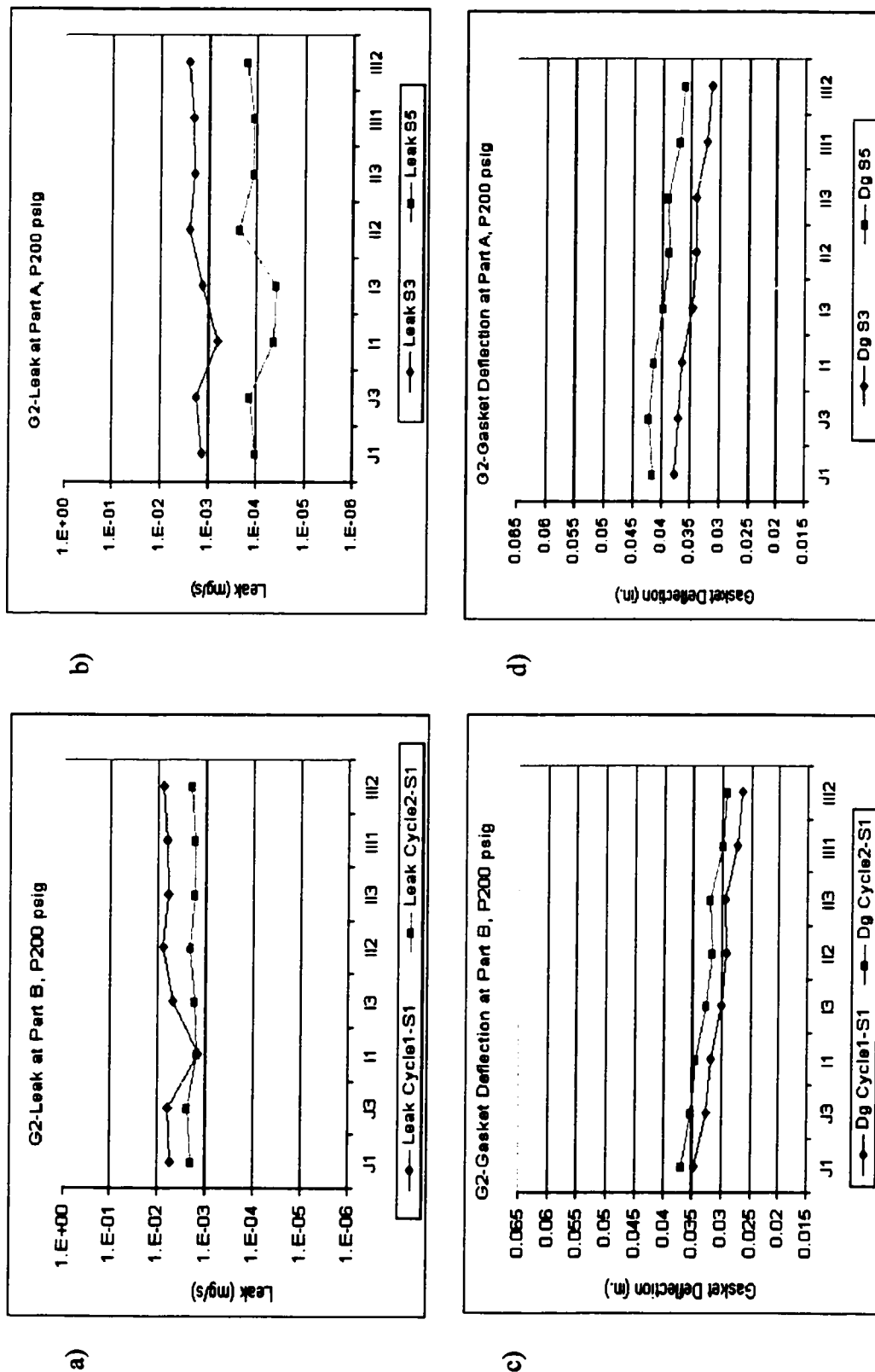
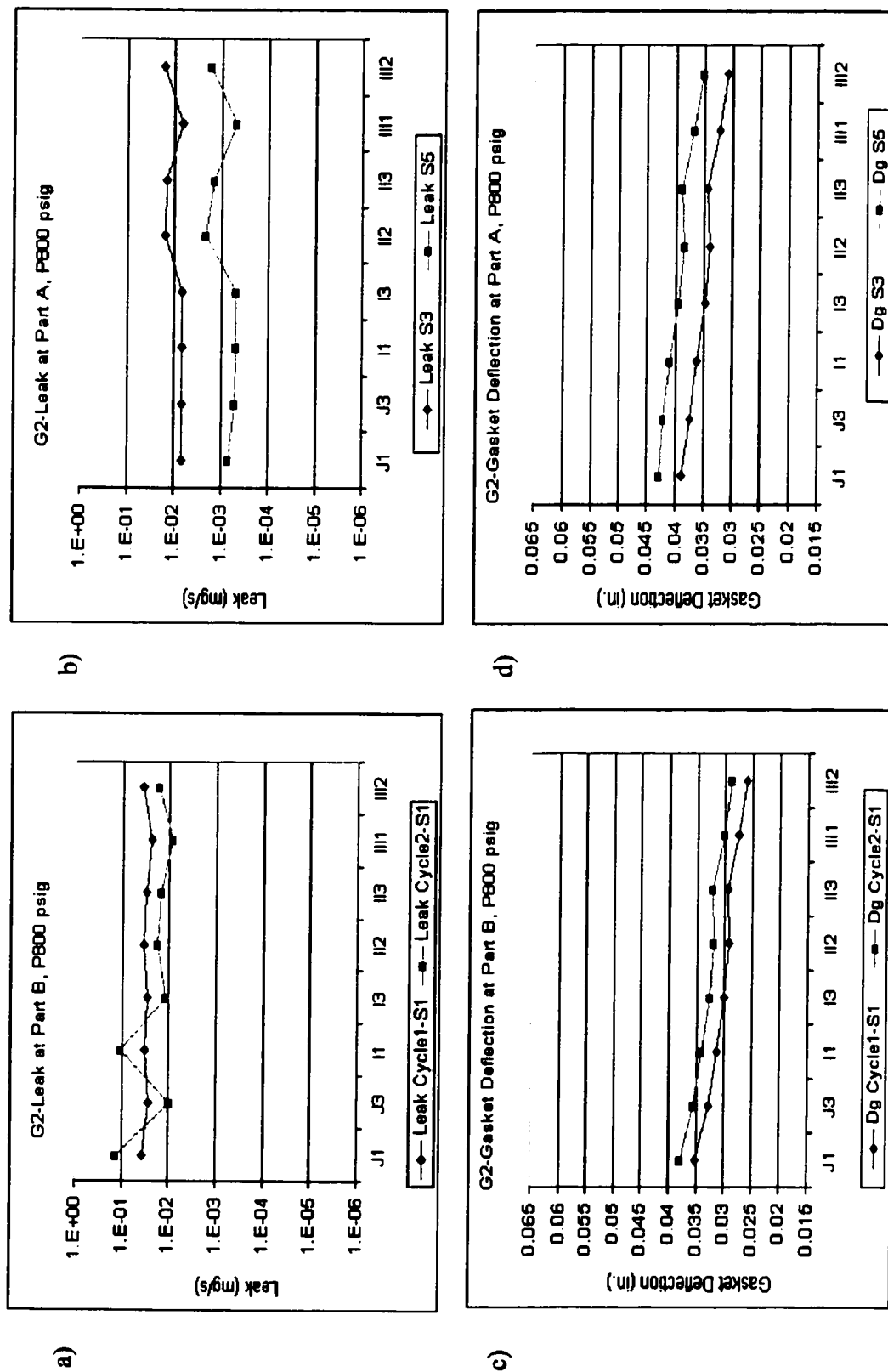


Figure 3.24. G2, leak rate and gasket deflection versus sealing surface characteristics, at stress S1, S3 and S5, at 200 psig.



**Figure 3.25.** G2, leak rate and gasket deflection versus sealing surface characteristics, at stress S1, S3 and S5, at 800 psig.

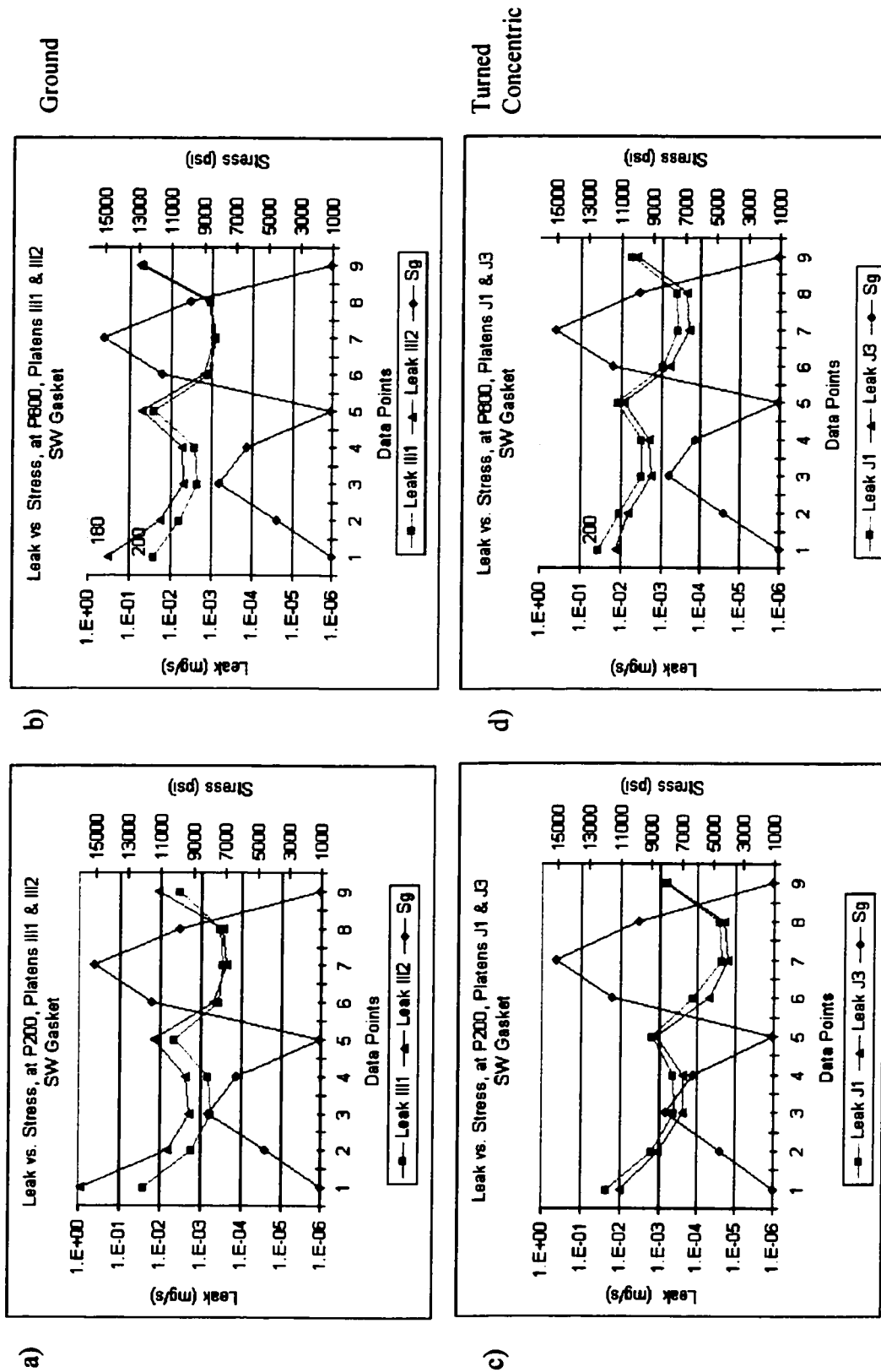


Figure 3.26. SW, effect of surface finish; leak rate versus stress levels, for ground and turned concentric surfaces.

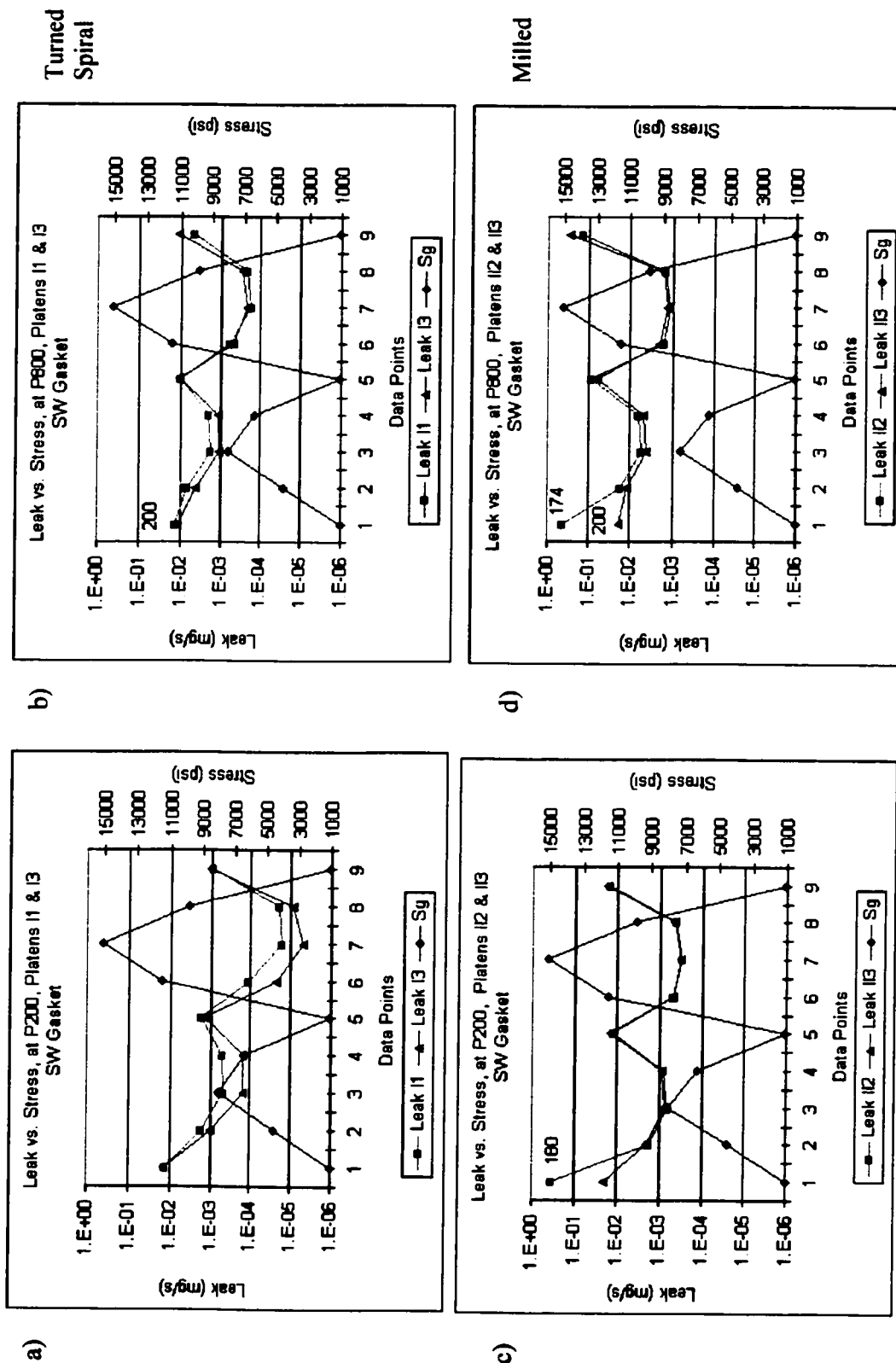


Figure 3.27. SW, effect of surface finish; leak rate versus stress levels, for turned spiral and milled surfaces.

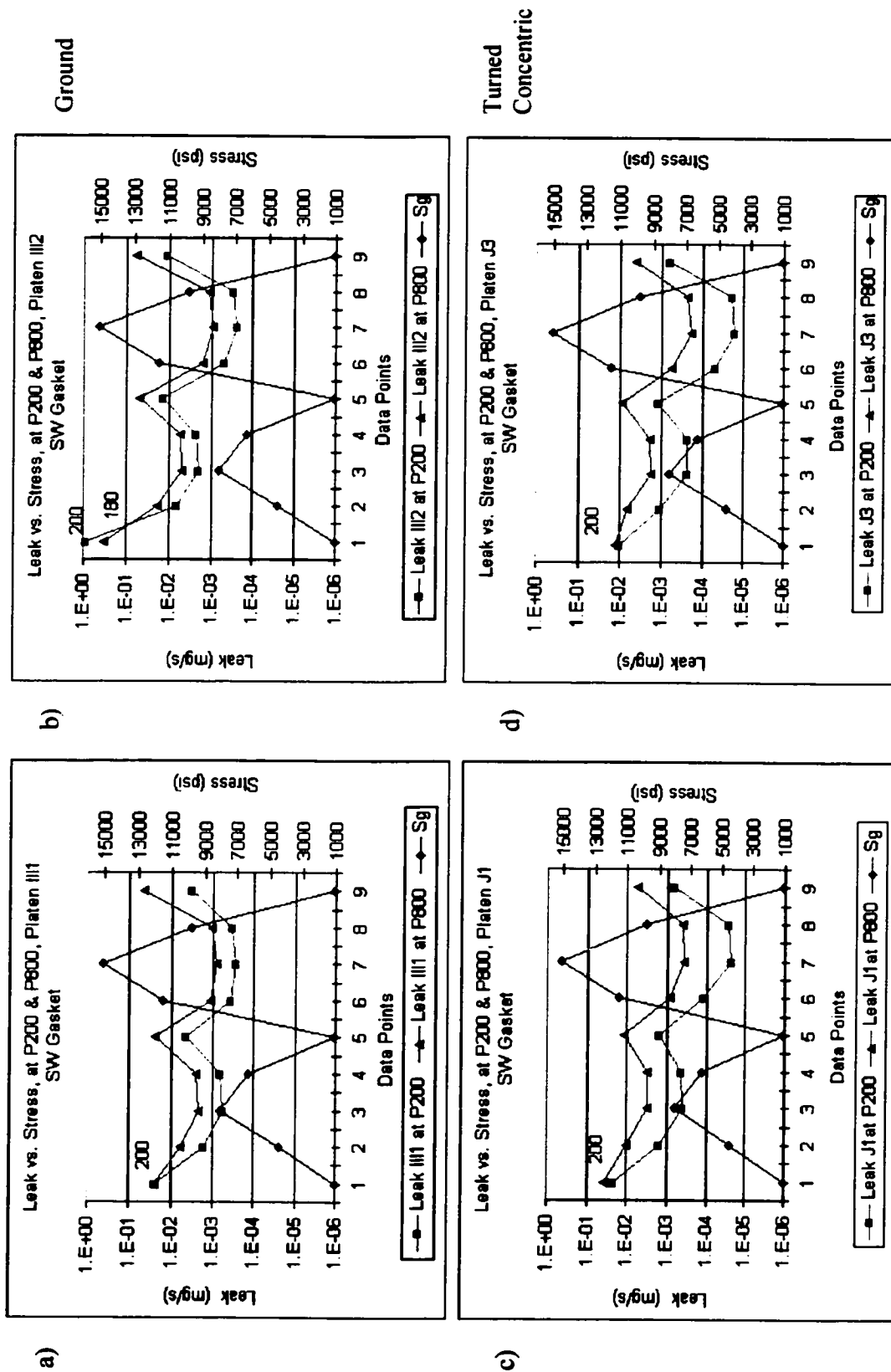
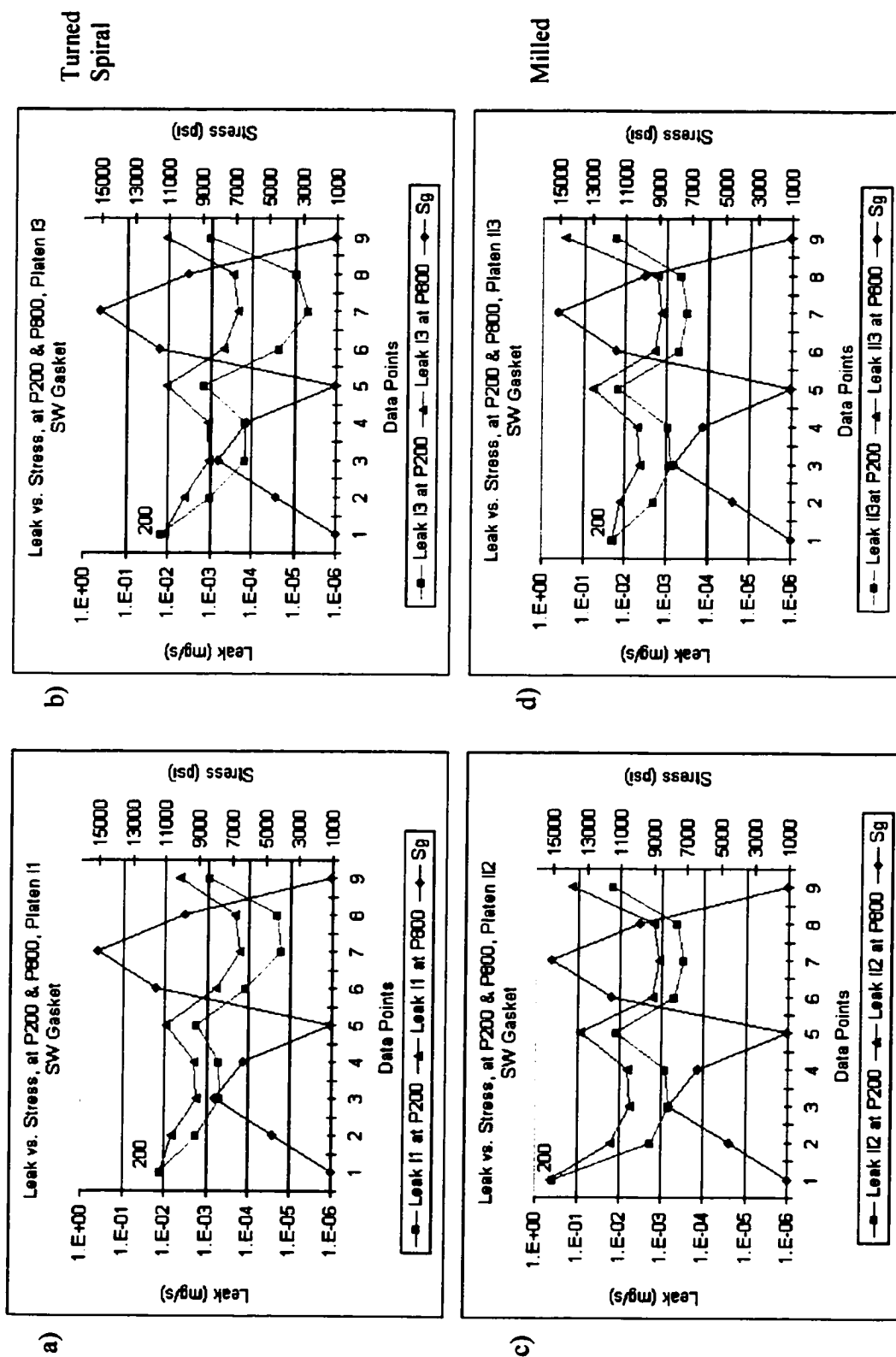
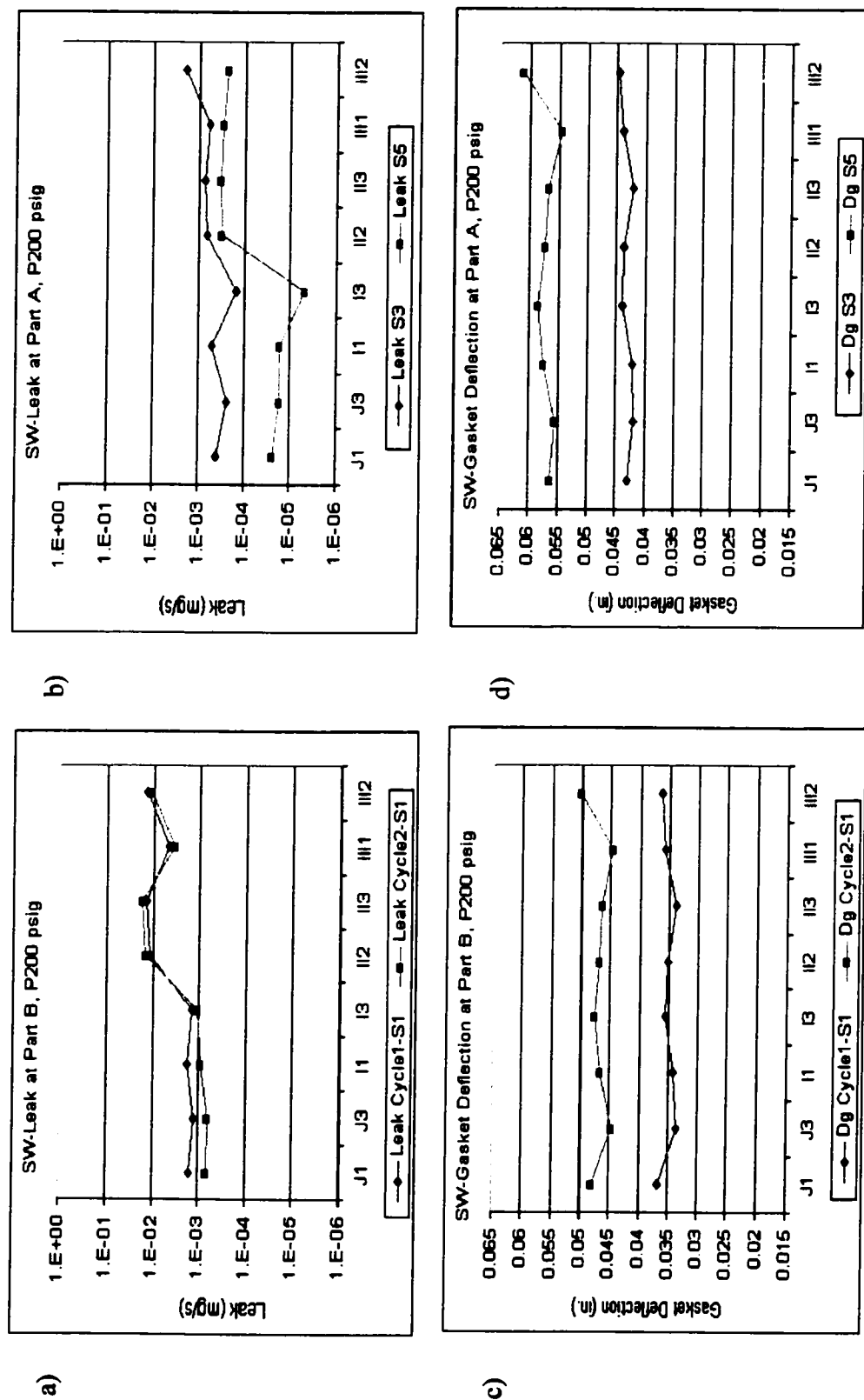


Figure 3.28. SW, effect of gas pressure; leak rate versus stress levels, for ground and turned concentric surfaces.





**Figure 3.29.** SW, effect of gas pressure; leak rate versus stress levels, for turned spiral and milled surfaces.



**Figure 3.30.** SW, leak rate and gasket deflection versus sealing surface characteristics, at stress S1, S3 and S5, at 200 psig.

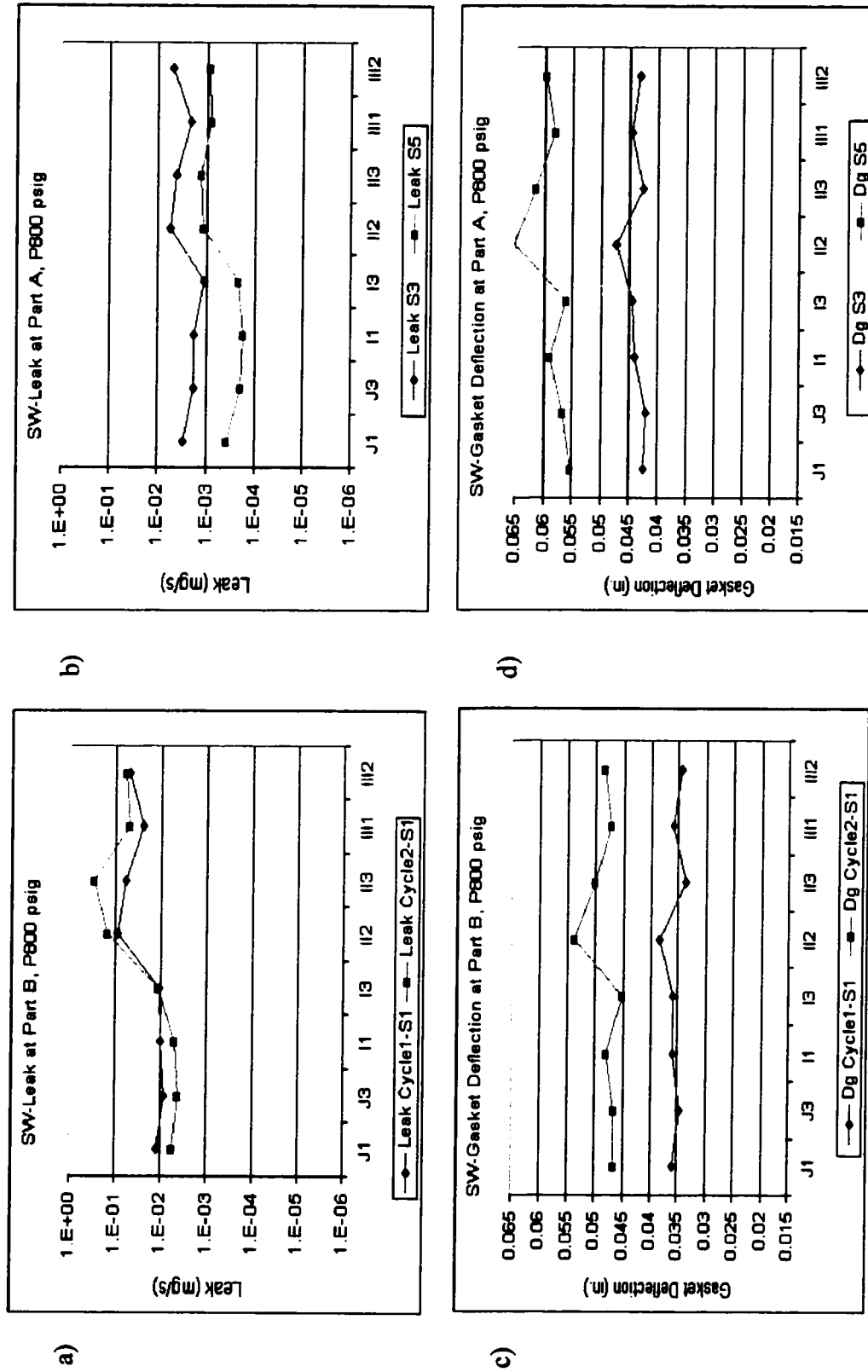


**Figure 3.31.** SW, leak rate and gasket deflection versus sealing surface characteristics, at stress S1, S3 and S5, at 800 psig.

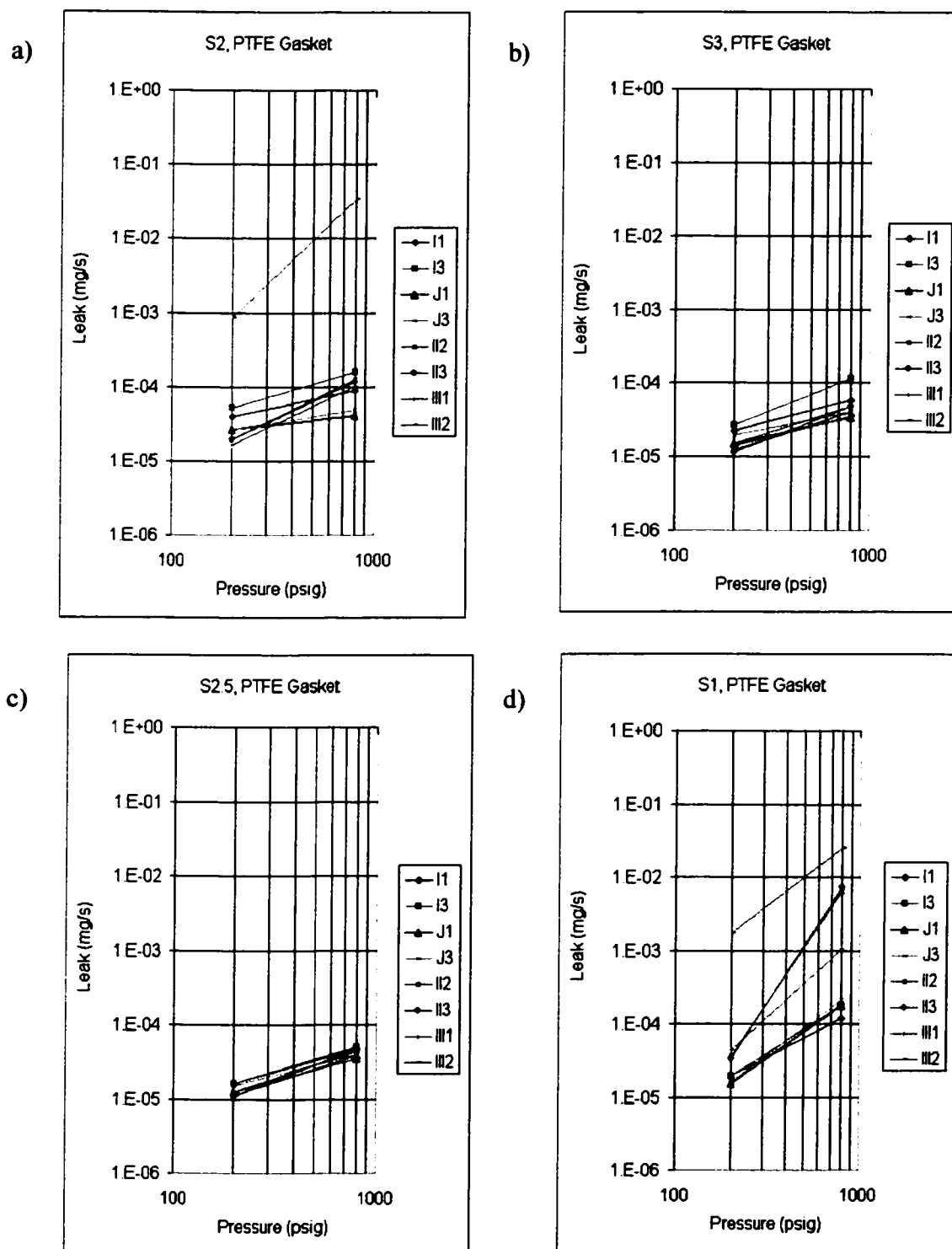


**Figure 3.32.** PTFE, log-log plots of leak rate versus gas pressure, for all surface characteristics, Part A: (S2, S3) Part B: (S2.5, S1).

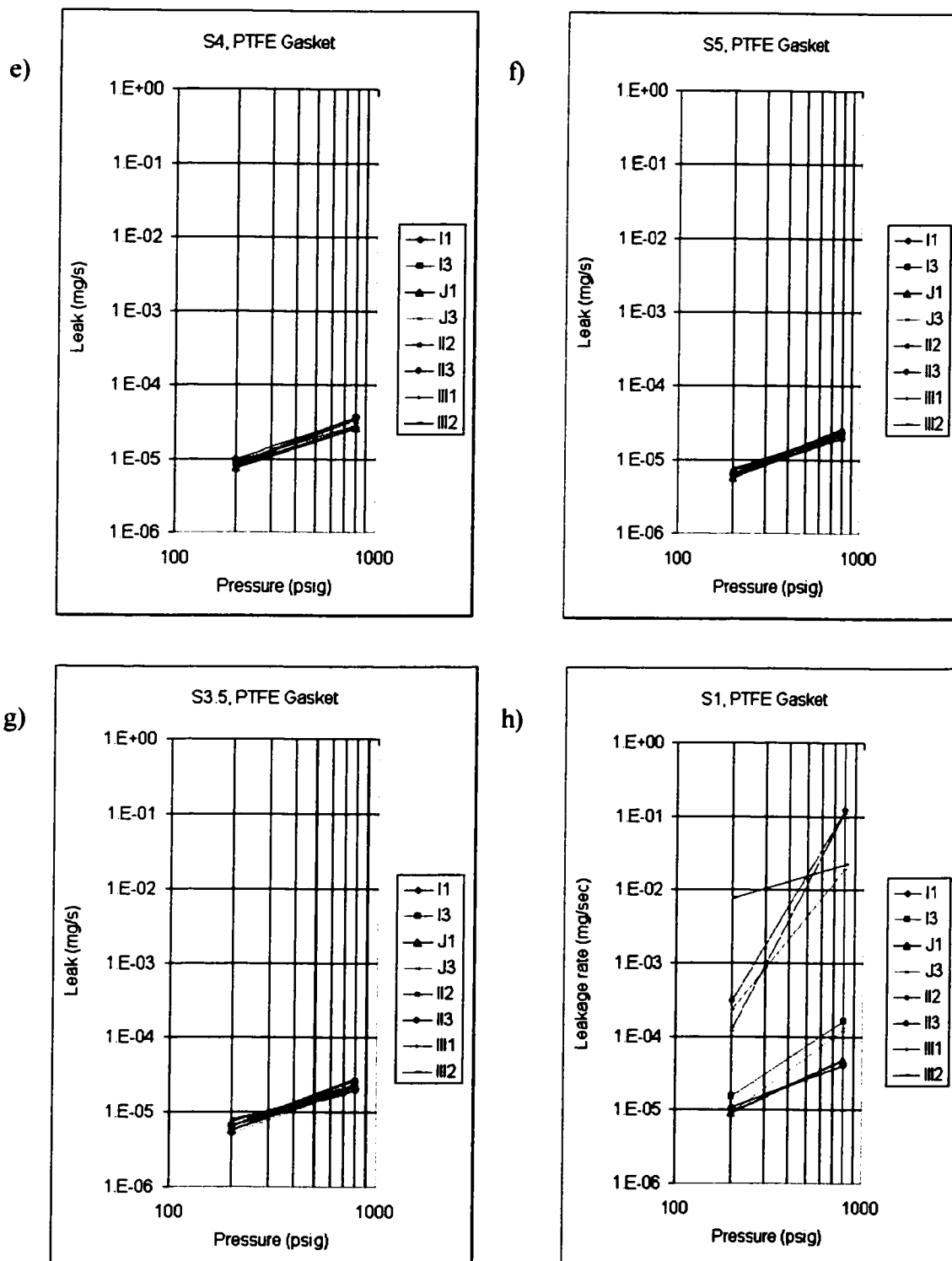


**Figure 3.32. Continued; Part A: (S4, S5), Part B: (S3.5, S1).**

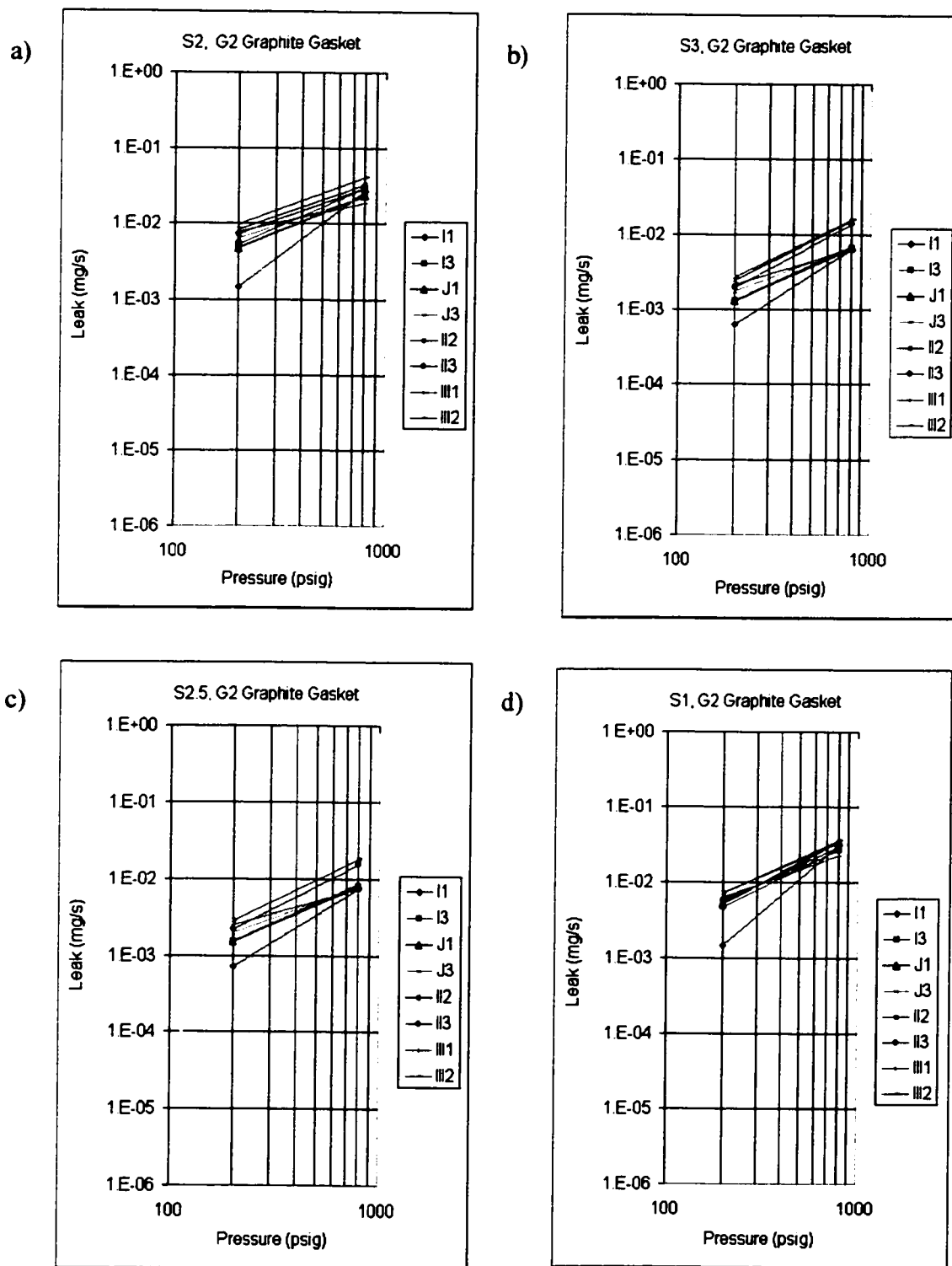


**Figure 3.33.** G2, log-log plots of leak rate versus gas pressure, for all surface characteristics, Part A: (S2, S3), Part B: (S2.5, S1).

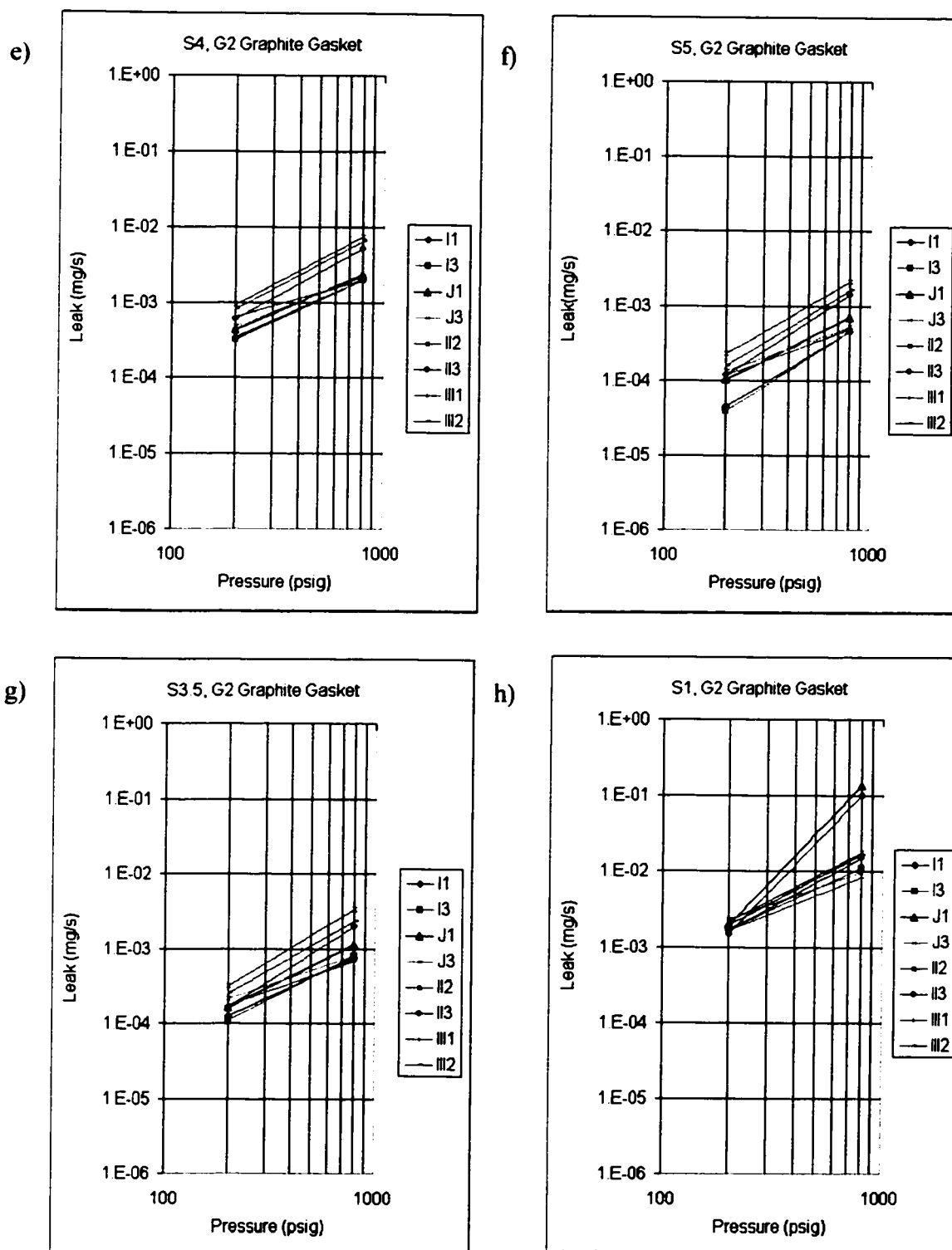
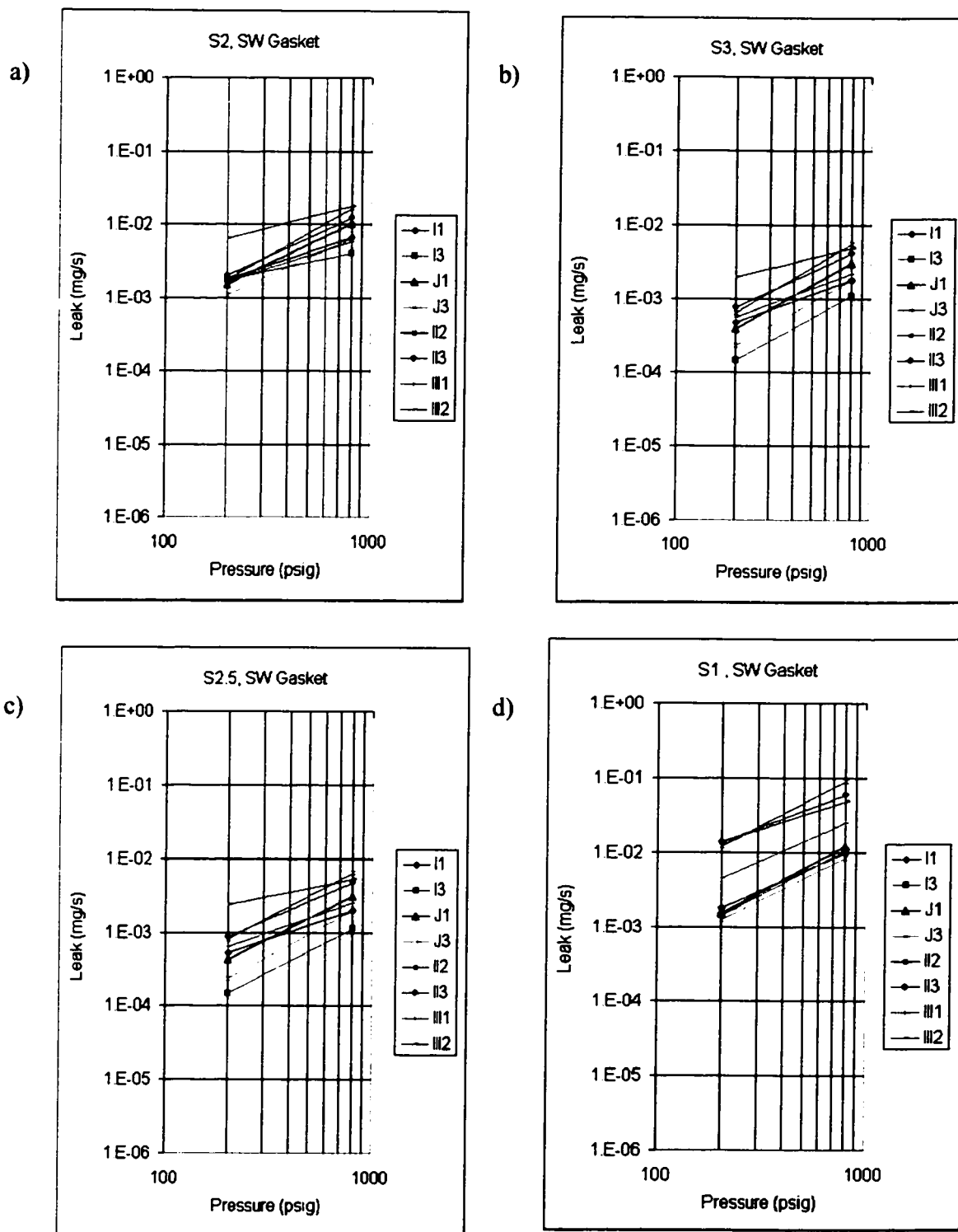
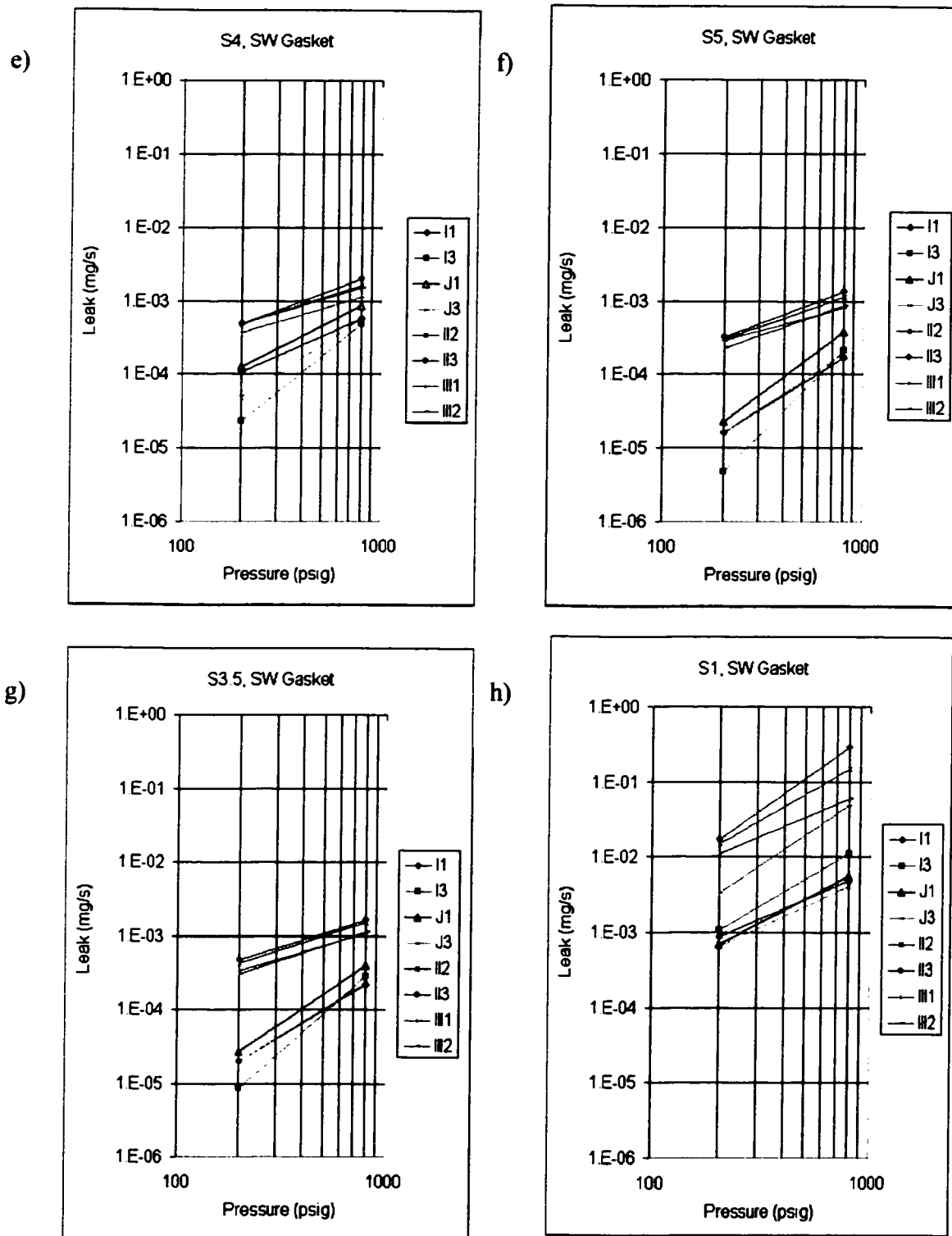


Figure 3.33. Continued; Part A: (S4, S5), Part B: (S3.5, S1).



**Figure 3.34.** SW, log-log plots of leak rate versus gas pressure, for all surface characteristics, Part A: (S2, S3), Part B: (S2.5, S1).





**Figure 3.34. Continued; Part A: (S4, S5), Part B: (S3.5, S1).**

## **CHAPTER 4**

### **SEALING PERFORMANCE OF GASKETED BOLTED FLANGED JOINTS**

#### **A FUZZY DECISION SUPPORT SYSTEM APPROACH**

**J. Arghavani, M. Derenne and L. Marchand**

**Department of Mechanical Engineering, Applied Mechanics,  
Ecole Polytechnique of Montreal  
Montreal, Quebec, Canada**

#### **4.1 Presentation of the chapter**

The analysis of sealing surface and gasket performance has been the subject of several investigations for years. The sealing phenomenon is complex and vague due to many involved parameters affecting the gasket performance. Thus, the selection of proper sealing surface and gasket type to provide minimum leakage rate for a given system is tedious and time consuming. The present chapter uses fuzzy logic theory for the selection of sealing surface roughness considering the system gas pressure, the gasket type and the gasket stress. Experimental results were used to develop simple fuzzy models and to present the applicability and advantages of such system in the field of gasketed flanged joints.

## 4.2 Abstract

The paper describes a fuzzy decision support system (FDSS) and its application to the selection of sets of optimal parameters to characterise the gasket sealing performance in gasketed bolted flanged joints. The FDSS of fuzzy logic theory is applied considering the gas pressure, gasket deflection, and leakage rate based on required gasket stress and flange surface roughness. The idea and implementation of the fuzzy decision support system is based on the compositional rules of inference and can be applied to other areas of gasketed bolted flanged joints to automate the selection of proper parameters which can best characterise the joint sealing performance and provide the required tightness.

**Keywords:** Flange surface roughness; Fuzzy logic; Leak rate; Gasket performance

## 4.3 Introduction

Gasketed bolted flanged joints are extensively used in industrial applications and they play a critical role in any system used, owing to the considerable variation, complexity and nonlinear behaviour that both the joints and gaskets have shown in most applications. The proper choice of sealing parameters is very important in modern seal and gasket manufacturing, and to users in petroleum, petrochemical, pressure vessels, and piping systems industries, since it constitutes the ultimate goal of planning, production, and process control. An adequate unified method for such a choice has not yet been developed. Many researchers and scientists have tried to find the optimal parameters which can define the seal and gasket performance under certain stress and internal pressure conditions, and to determine the life expectancy of the sealing, influenced by these parameters to maintain the joint tightness and ultimately to achieve a leak free joint. Gaskets play a critical and important role in joint connection. These are flexible and provide the required material to fill in the gaps between the flange surfaces; however,

they are susceptible to load, pressure and temperature, and are subject to ageing under different environmental working conditions. Bolted flanged joints, however, provide great flexibility in design, implementation and the connection of piping systems. The most important aspect of gasketed bolted flanged connections is their sealing performance and gasket tightness, based on different operating conditions, gasket material, joint shape, and surface roughness. The optimal result is achieved by minimising the leakage rate, thus reducing or preventing the loss of medium. A common concern experienced by manufacturers and industries is the “optimal” sealing performance and tightness provided by the gaskets and the joint. Sealing performance means how well the gasket and joint can maintain non-leakage under certain operating conditions.

Gasketed bolted flanged connections have been under investigation for about a century, and the general method in most investigations has been based on gasket testing performance. Different measures have been taken which can be categorised as:

1. Different gasket types (PTFE, graphite, metallic, double jacketed, spiral wound).
2. Different gas types (hydrogen, nitrogen, helium).
3. Variety of flange machined surfaces (milled, ground, turned).
4. Test operating temperature (room temperature, elevated temperature).
5. Flange bolting load/gasket stress.
6. Flange moment.

A fuzzy decision support system has its own complexities and advantages, the former in the formulation and rules to be developed, the latter is its ability to deal with vague and imprecise data.

#### **4.4 Literature review of gasketed bolted flanged joints**

Since the early 1880s, bolted flanged joints connections have prompted researchers and manufacturers to examine many criteria and carry out extensive strategic research and development to understand and overcome the associated problems. Problems arise because of flange shape, materials, mating surfaces, gasket type, gasket material, gasket ageing, bolt loading, and creep. Both theoretical and experimental work has been performed in all aspects of gasket performance, e.g. effect of load, room temperature, elevated temperature, gasket porosity, contact of mating faces, and the effect of flange surface roughness on the leakage rate and on gasket performance. The results of many research and experimental tests have led to the definition of standard test procedures and gasket constants, Draft no. 9, of ASTM [1].

A proposed modification to Draft No. 9 of the standard test method for gasket constants for bolted joint design can be found in Derenne et al. [2]. Mitchell and Rowe [3] analysed the influence of asperity deformation on the emission rate of contacting surfaces. Matsuzaki and Kazamaki [4] presented work on the effect of surface roughness on the compressive stress of static seals. Derenne and Bouzid [5] worked on the effect of flange surface roughness on the gasket performance and leakage rate. Payne [6—8] presented work on bolted joint gasket performance tests, and the effect of surface finish on gasket tightness and gasket constants, considering a stock finish spiral cut surface with different roughnesses from 50 to 1000  $\mu\text{in}$ . The main objectives of these experiments have been the minimisation of the leakage rate.

Many parameters are involved in gasketed bolted flanged joints so the analysis of such a system is extremely difficult. Most research presented in this area is concentrated on gasket performance based on different gaskets, load applied, fluid flow modelling concepts, and bending moment effect, for the selection of optimal parameters to reduce leakage rate. No research has dealt with fuzzy logic application in this domain. In the

following sections we review the fuzzy logic theory which is capable of dealing with vague and imprecise information, and many unknown parameters.

#### **4.5 Literature review of fuzzy theory**

Fuzzy set theory was first introduced in 1965 by Zadeh [9], and Zadeh's [10] seminal paper, in 1973, which persuaded researchers to use a fuzzy rule-based approach for the analysis of complex systems and decision making. Fuzzy set theory is a powerful tool capable of modelling any system with uncertainties, fuzziness and incomplete information obtained from real-world situations and experimental data. Tackling the problems involved in real-world situations, Mamdani [11] was one of the pioneering researchers in the application of fuzzy set theory in the control system. Larsen [12] has published work related to the industrial application of fuzzy logic control. Theories and the work pertaining to fuzzy logic and neural networks can be found in of Tsoukalas and Uhring [13]. Balazinski et al. [14] developed software for a fuzzy decision support system, based on the fuzzy logic theory of Zadeh [9, 10, 15].

Based on the theories of fuzzy sets and fuzzy logic, problems involving improper or missing data, and vague, complex and unknown input and output parameters can be tackled easily. The imprecision of the input and output variables of the system under investigation can be directly addressed by the fuzzy sets, of the fuzzy logic system (FLS) [9—15], which can be expressed in linguistic terms, e.g. HIGH pressure, SMALL leak, and ROUGH surface. As the complexity of the systems under investigation increases, the precision in the definition of the statements becomes less clear and fuzzier; ideas become vague, and meaningful statements in the systems tend to lose their meaning and precision. In data-processing systems, the objective is to understand the phenomena involved and to evaluate relevant parameters quantitatively. This calls for “modelling” of the system either by analytical models using mathematics and physical principles or by experimental

models if the mathematical models are not feasible. The analysis of the system through e.g. sensitivity analysis, statistical regression, and analysis of variance, can be performed once the model of the system is made. However, in many real situations owing to the complexity of the system, the phenomena are poorly understood and ill-defined; thus models of the basic principle are not possible; but, fuzzy systems can be used to construct the models based on experimental measurements. In this paper a fuzzy decision support system approach is presented, which deals with the surface roughness effect on gasketed bolted flanged joint performance.

#### **4.6 Proposed approach**

The proposed approach deals with a decision support system for the choice of sealing parameters in the sealing performance of gasketed bolted flange joints, of the Room Temperature Tightness test called ROTT [1]. The fuzzy decision support system used for this analysis is called Fuzzy-Flou [14]. Several fuzzy algorithms have been written which are capable of supporting any user's defined input parameter combinations to provide expected optimum output values. In this work, we present only one of the algorithms. Certain criteria are adopted in this algorithm.

The input parameters are:

1. System internal pressure,  $P$  (p.s.i.)
2. Gasket deflection,  $D_g$  (in)
3. System leakage rate,  $Q$  (mg/s)

And the expected outputs of from the system are:

4. Gasket stress,  $S_g$  (p.s.i.)
5. The platens surface roughness,  $R_a$  ( $\mu\text{in}$ ).

#### 4.7 Basic theory of fuzzy logic

The main objective is to determine the optimal parameters of gasketed bolted flanged joints for which the minimum leakage rate can be achieved for given system conditions. The rule-based approach to the approximate reasoning process based on Zadeh's [9] composition of inference, is presented. The block diagram of a FLS, fuzzy logic system, is given in Fig. 4.1. This theory forms the basics for the fuzzy decision support systems, of the Fuzzy-Flou software [14], which is used to analyse our results. A set of rules is defined, consisting of linguistic statements linking conditions or premises with conclusions.

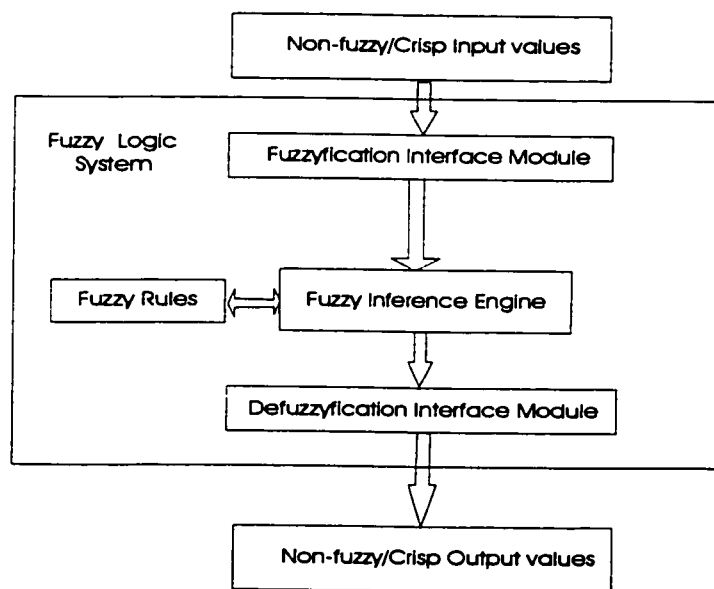


**Figure 4.1.** Block diagram of fuzzy logic system, FLS



Zadeh [15] indicated that although fuzzy linguistic descriptions are formulated in a language spoken by humans, they have rigorous mathematical bases involving fuzzy set and fuzzy relations. The knowledge about a system is encoded in statements of the form:

*if* (a set of *conditions* are defined and satisfied)  
*then* (a set of *conclusions* can be inferred) (4.1)

as a specific example of the linguistic rules in our fuzzy decision support system, for the surface selection, we may have

*if* GAS PRESSURE is LOW  
     *and* GASKET DEFLECTION is HIGH  
     *and* LEAK RATE is MEDIUM (4.2)  
*then* SURFACE ROUGHNESS is Ra250

In practical situations an approximate description of a function  $y=f(x)$  may be either acceptable or preferable in some cases. This means that we may be interested not in a crisp point of the function  $f(x)$  but in an area or neighbourhood around a point. That is, we may be interested in associations such as, if variable  $x$  is somewhere “*about*  $a_i$ ”, then function  $y$  is somewhere “*about*  $b_i$ ” [13, 15]. Thus, instead of considering a crisp point  $(a_i, b_i)$ , we consider an area around this point. Then, the area obtained from this point contains fuzzy numbers and may be described by a fuzzy *if/then* rule. Fuzzy numbers are fuzzy sets used to present the “*about*” and “*nearly*” quantities of numerical crisp values. In general, fuzzy numbers are presented by different membership functions such as *triangular*, and *trapezoidal* defining an area about a point. If “*about*  $a_i$ ” and “*about*  $b_i$ ” are fuzzy numbers  $A_i$  and  $B_i$  for the universe of discourse of  $x$  and  $y$ , respectively, we can define linguistic variables  $x$  and  $y$  whose arguments,  $A_i$ , and  $B_i$  are fuzzy numbers on the  $x$ -axis, and on the  $y$ -axis, respectively. Then, the area *about* the point  $(a_i, b_i)$  can be described by a set of generic fuzzy *if/then* rules involving two linguistic variables, one on each side of the rule, of the form:

$$\text{if } x \text{ is } A_i \text{ then } y \text{ is } B_i \quad (4.3)$$

where, linguistic variables  $x$  and  $y$  take the values  $A$  and  $B$ , respectively. The analytical form of the rule presented above is a fuzzy relation  $R_i(x,y)$  called the implication relation of the rule, consisting of the membership function,  $\mu(x,y)$ , that we want to obtain. The implication relation of Tsoukalas and Uhring [13], can be given in both continuous and discrete forms, but for the sake of brevity only the former is presented here:

$$R(x, y) = \int_{(x,y)} \mu(x, y) / (x, y) \quad (4.4)$$

The membership function  $\mu(x,y)$  of the implication relation  $R_i(x,y)$  can be obtained using an implication operator  $\phi$  for which the inputs are the membership functions of the antecedent and consequent parts, namely  $\mu_A(x)$  and  $\mu_B(y)$ , and its output is  $\mu(x,y)$ , thus

$$\mu(x, y) = \phi[\mu_A(x), \mu_B(y)] \quad (4.5)$$

Several implication operators exist but we only refer to a few: the max—min [ $\vee (\wedge)$ ] implication operator of Zadeh [10], the min ( $\wedge$ ) implication operator of Mamdani [11], and the Product ( $\cdot$ ) implication operator of Larsen [12].

Zadeh's [10] max—min implication operator is given in the form

$$\phi[\mu_A(x), \mu_B(y)] = (\mu_A(x) \wedge \mu_B(y)) \vee (1 - \mu_A(x)) \quad (4.6)$$

therefore its membership function of the implication relation can be given as

$$\mu(x, y) = (\mu_A(x) \wedge \mu_B(y)) \vee (1 - \mu_A(x)) \quad (4.7)$$

Mamdani's [11] min ( $\wedge$ ) implication operator is simply the first argument, in the LHS, of the max—min [ $\vee (\wedge)$ ] implication operator of Zadeh [10], and used in fuzzy control. Whereas, Larsen's product ( $\cdot$ ) implication operator, and membership function is

$$\mu(x, y) = \phi[\mu_A(x), \mu_B(y)] = (\mu_A(x) \cdot \mu_B(y)) \quad (4.8)$$

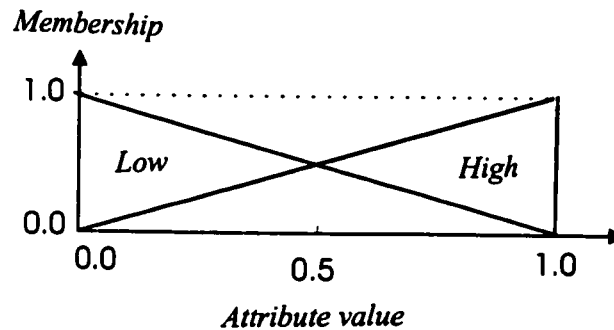


**Figure 4.2.** Membership function of two linguistic values,  
e.g. defining the low and high gas pressure

Fuzzy algorithms are used for performing a task formulated as a collection of sets of fuzzy *if/then* rules and connected by the connective ELSE. The connective ELSE may be interpreted as a union or an intersection depending on the implication operator used for the individual rules. In most practical cases a fuzzy algorithm consists of  $n$  multivariate fuzzy implications and  $m$  variables  $x$ ,  $i=1,2, \dots, m$ , on the antecedent side of the  $j^{\text{th}}$  *if/then* rule. Thus the knowledge is expressed by a finite number  $r=1,2, \dots, n$ , of the heuristic fuzzy rules based on the multiple input multiple output (MIMO), which is obtained from

the experimental measured values, and the operators' and experts' knowledge. The set of rules may be written as follows [15],

$$\begin{aligned}
 R'_{MIMO} : & \text{if } x \text{ is } A'_i \text{ and } y \text{ is } B'_j \text{ and ... and } z \text{ is } C'_p \\
 & \text{then } u \text{ is } U'_k, v \text{ is } V'_l, \dots, w \text{ is } W'_q \\
 & \text{with } CF_i, CF_j \text{ and ... and } CF_p
 \end{aligned} \tag{4.9}$$

where  $A'_i, B'_j, \dots, C'_p$  are the antecedent fuzzy sets, which denote the values of the linguistic variables  $x, y, \dots, z$  standing for conditions defined in the universe of discourse of  $X, Y, \dots, Z$ , respectively,  $U'_k, V'_l, \dots, W'_q$  are the consequent classes, and denote values of the independent linguistic variables  $u, v, \dots, w$  standing for conclusions defined in the universe of discourse  $U, V, \dots, W$ , respectively, and  $CF_i, CF_j, \dots, CF_p$ , are grades of certainty of the rules, and are given a value of 1 for 100% certainty.

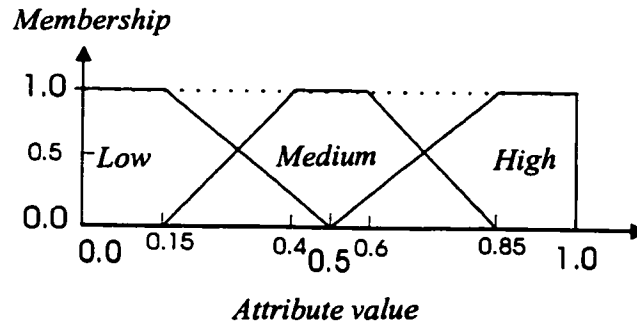


**Figure 4.3.** Membership function of three linguistic values, e.g. defining the low, medium and high gasket deflections

For the antecedent fuzzy sets  $A_i$  in Eq. (4.9) corresponding to the internal gas pressure of the system, we use two linguistic values *Low* and *High*, for all the  $n$ -dimensional  $i=1, 2, 3, \dots, n$ , problems. Similarly, for the antecedent fuzzy set  $B_j$  in Eq. (4.9) corresponding to

the gasket deflection, we use three linguistic values *Low*, *Medium* and *High*, for all the attributes of the  $n$ -dimensional  $i=1, 2, 3, \dots, n$ , problem, as presented in Fig. 4.2 and Fig. 4.3, respectively.

The fuzzy algorithm for multivariate input and output systems can be described analytically by an algorithmic fuzzy relation of the form

$$R(x_1, x_2, \dots, x_m, y) = \int_{(x_1, x_2, \dots, x_m, y)} \mu(x_1, x_2, \dots, x_m, y) / (x_1, x_2, \dots, x_m, y) \quad (4.10)$$

The membership functions above can be obtained from the implication relation of individual rules and appropriate interpretation of the connectives AND, OR, and ELSE. Furthermore, a MIMO system rule base is usually expressed in the form

$$R = \{R_{MIMO}^1, R_{MIMO}^2, \dots, R_{MIMO}^r, \dots, R_{MIMO}^n\} \quad (4.11)$$

The antecedent of the  $R_{MIMO}^r$  rule forms a fuzzy set  $A_i^r \times B_j^r \times \dots \times C_p^r$  in the Cartesian product. The consequent is considered as the union of a finite set of independent rules, which are generated based on the multiple input and single output, MISO, as  $R_{MISO}^r$ , this can be written as

$$R = \left\{ \bigcup_{r=1}^n R_{MIMO}^r \right\} = \left\{ \bigcup_{r=1}^n R_{MISO(u)}^r, \bigcup_{r=1}^n R_{MISO(v)}^r, \dots, \bigcup_{r=1}^n R_{MISO(w)}^r \right\} \quad (4.12)$$

where  $R_{MISO(\cdot)}^r$  is the  $r^{\text{th}}$  rule of type MISO for the output  $(\cdot)$ . This can be seen as the decomposition of the rule base  $R$  into a set of subrule bases  $\{R_u, R_v, \dots, R_w\}$  consisting of  $n$  rules of multiple antecedents and a single consequent.

#### 4.7.1 Compositional rule of inference

The fuzzy compositional rule of inference refers to computational procedures used for evaluation of fuzzy linguistic descriptions. As described in [13], two important inferencing procedures are usually used, namely Generalized Modus Ponens (GMP) and Generalized Modus Tollens (GMT). In the GMP inferencing procedure, a rule and the fuzzy value approximately matching its antecedent are given, and it is desired to infer the consequent, whereas, in the GMT procedure a rule and the fuzzy value approximately matching its consequent are given and it is desired to infer the antecedent. Let us consider a simple *if/then* rule with the known implication relation  $R(x,y)$  and a fuzzy value  $A'$  approximately matching the antecedent of the rule, then the GMP inferencing procedure allows us to compute or infer the consequent  $B'$ . This can be formulated as

$$\begin{array}{l} \text{if } x \text{ is } A \text{ then } y \text{ is } B \\ \hline x \text{ is } A' \\ \hline x \text{ is } B' \end{array} \quad (4.13)$$

As an example, suppose that we have the rule “if the leakage rate is SMALL then the flange surface is spiral stock cut with a roughness value of 50 ( $\mu\text{in}$ )”. Thus, given that “leakage rate is LARGE”, evaluate the rule and infer a value for flange surface roughness. The inferred value  $B'$  then is computed through the composition of  $A'$  with the implication relation  $R(x,y)$ . This is done analytically by first obtaining the implication relation  $R(x,y)$  of the rule *if  $x$  is  $A_i$  then  $y$  is  $B_i$*  by using either the implication operator defined above (or any other most suitable operator), also the membership function of  $A'$  is given. Thus, to compute the membership function of  $B'$  we may use the max—min composition of fuzzy set  $A'$  with the implication relation of fuzzy algorithm  $R(x,y)$ ; hence, we have a simple knowledge base for a single input single output SISO such as

$$B' = A' \circ R(x, y) \quad (4.14)$$

the symbol  $(\circ)$  refers to the compositional rule of the inference operator such as max—min, max—product, max—average, thus, the membership function of  $B'$  may be obtained from max-min composition  $(\circ)$  as

$$\mu_{B'}(y) = \bigvee_x (\mu_{A'}(x) \wedge \mu(x, y)) \quad (4.15)$$

$\mu(x, y)$  is the membership function of the implication relation  $R(x, y)$ ,  $\mu_{A'}(x)$  and  $\mu_{B'}(x)$  are the membership functions of  $A'$  and  $B'$  respectively.

In the case of a knowledge base for a multiple input and single output (MISO) system, the compositional rule of inference may be shown as

$$U' = (A', B', \dots, C') \circ R \quad (4.16)$$

whereas, in this case,  $R$  aggregates MISO system rules. On the other hand, if we consider a knowledge base of multiple input and multiple output (MIMO) system, the fuzzy compositional rule of inference can be presented as

$$(U', V', \dots, W') = (A', B', \dots, C') \circ R \quad (4.17)$$

$$R = \left\{ \bigcup_{r=1}^n R_{MIMO}^r \right\}$$

is defined earlier and represents a global relation aggregating all rules,  $(A', B', \dots, C')$  and  $(U', V', \dots, W')$  represent all antecedents and all inferences, respectively.

Different combinations of operations may be applied to constitute compositional rules of inference and constitute the basis of the inference mechanism in the fuzzy logic tool system, namely the Fuzzy-Flou system [14] used in this work. For instance *min-prod* is

used for the implication operation and the connective “*and*”, and *max-sum* are used for the connective “*also*”. The abbreviation of such operations and the membership function representing the compositional rule of inference variants, used in Fuzzy-Flou [14] are formulated as: *max-sup-min-min-min*, *max-sup-prod-prod-prod*, *sum-sup-min-min-min*, and *sum-sup-prod-prod-prod* operation, which are the bases of the inference mechanism of the fuzzy logic tool system. For the sake of brevity, we present here only the *sum-sup-prod-prod-prod* as

$$U'(u) = \sum_r \sup_{\substack{x \in X \\ y \in Y \\ \dots \\ z \in Z}} [(C'(z) \cdot \dots \cdot B'(y) \cdot A'(x)) \cdot (A'_i(x) \cdot B'_j(y) \cdot \dots \cdot C'_p(z) \cdot U'_k(u))] \quad (4.18)$$

where  $U'(u) = \mu_{out}(u)$  is the output fuzzy value, for the manipulated discrete value of the universe of discourse  $u$ .

#### 4.7.2 Fuzzification and defuzzification

**Fuzzification** is used in order to control the fuzziness of the fuzzy set, or to transform a crisp set into a fuzzy set, which is to simply increase the fuzziness of the fuzzy set information. In control or diagnostic applications the input data to an on-line control system comes from as a crisp value, usually a real number. In order to use these values in the fuzzy algorithm, it is often necessary to convert these crisp values into a fuzzy set. This process is called fuzzification and uses a *fuzzy kernel*,  $K(x)$ , [12—15].

**Defuzzification** is the procedure for transforming the fuzzy output of the system to a real number or crisp value. The inputs to the fuzzy logic control system are analysed and processed and then the result obtained is a fuzzy output, hence, defuzzification of the fuzzy output is the selection of a crisp number from the inferred output fuzzy set in which it is the best representative of the output.



Several defuzzification techniques have been introduced in the literature; but the most commonly used are: the *mean-of-maxima* (MOM) defuzzification,

$$u^* = \sum_{i=1}^N \frac{u_{\max,i}}{N}, \quad \text{where } \left\{ u_{\max,i} \in R \mid U'(u_{\max,i}) = \sup_N (U'(u)) \right\} \quad (4.19)$$

The *centre-of-area* (COA) defuzzification, also called the *centre-of-gravity* (COG), and *centre-of-sum* (COS) defuzzification. These formulae are not presented for the sake of brevity. The selection of the defuzzification technique is critical and has a significant impact on the speed and accuracy of the fuzzy algorithm. This is mainly because certain defuzzification methods may introduce nonlinearities and discontinuities in the hypersurface of the fuzzy control. The *centre-of-area* defuzzification is suitable for multidimensional fuzzy output. On the other hand, the *mean-of-maxima* defuzzification is not only faster than the *centre-of-area* defuzzification method, but also allows the controller to infer values near the edge of the universe of discourse [13].

#### 4.7.3 Fuzzy rules

Prior to writing the rules, the membership function of each main factor influencing the outcome of the result is determined. Then the rules are defined based on the interactions of each level of the membership functions, following the logical statements and linguistic rulein for selection of flanges of appropriate surface roughness to provide the lowest leakage rate. This involves three factors “gas pressure”, “gasket deflection”, and “leakage rate”, and one output “surface roughness”. The membership of each factor may be two, three or more linguistic values. The higher the number of linguistic values for each factor, the more complex the degree of definition and determination of the rules. In Figs. 4.2 and 4.3, the membership function of the chamber internal gas pressure is defined at two “low”

and “high” levels, and the deflection on the gasket is defined at three levels as “low”, “medium” and “high”, respectively. Consider only two factors for which membership functions given in Figs. 4.2, and 4.3. With one output of one or multiple linguistic terms (ranks), then at least six rules can be defined. For instance:

1. *if* gas pressure is “low” and gasket deflection is “low”, *then* leak is “medium”;
2. *if* gas pressure is “high” and gasket deflection is “medium”, *then* leak is “large”.

Sets of experimental data are obtained, in which the factors are classified and ranked. To do this, the experimental data for all factors are put together and sorted. After sorting the data, based on expertise and experience, the data for different factors are classified or ranked. This classification is, in fact, equivalent to the linguistic terms shown in Figs. 4.2 and 4.3. For simplicity, we can assign a ranking value to each linguistic terms “1” to “low” and value “2” to “high” for the first factor and value “1”, “2”, and “3” to “small”, “medium” and “large”, respectively for the second factor, and so forth. Then the ranking values for each factor are associated the original (unsorted) experimental data. Therefore, a set of rules are developed based on experimental observations. Of course, there will be many cases in which data fall into the same ranking categories and provide many redundant rules which must be eliminated. Furthermore, rules may be added or modified based on the researcher’s expertise, experience and other observations in the domain. Once the rules are determined, they are entered in the fuzzy logic program; and premises membership functions and the conclusions are written. In addition, interference type defuzzification mode, aggregation, propagation, fusion, norm and certainty threshold are set. It is worth mentioning that different formats can be used for defining the rules, premises and conclusions, depending on the software or the programming techniques [9—15].

#### **4.8. Case study**

##### **4.8.1 Flange surface selection**

Selecting an appropriate surface machining form and surface roughness for the flanges is very important in gasket performance to provide non-leaking joints. In the present work, we limit our fuzzy model and analysis to the consideration of only:

1. One type of flange surface form, namely, spiral stock finish cut surface.
2. Three different roughness values, e.g. Ra 50, 250, and 500 ( $\mu\text{in}$ ).
3. Gasket stress ranging from 1 (Kp.s.i.) to 17 (Kp.s.i.)
4. Three input factors of different ranges: gas pressure, gasket deflection, and leak rate.

It is worth mentioning that as the depth of cut, feed rate and tool tip radius increases, the peak distance, and depth of the grooves generated increases increasing the roughness of the surface. Thus, larger leakage paths of the spiral cut stock are generated, leading to a larger leak rate. So, a low roughness value of the surface provides a lower leakage rate. It is common sense that increasing the surface roughness increases the leakage rate, owing to the larger gaps between the mating surfaces of the gasket and flange. On the other hand, owing to the increase of surface peaks, in a rougher stock finish, the penetration of the asperities into the gasket increases, under the same applied load, increasing the stress on the gasket, which reduces the leakage rate. Analysis of this sort of problem is complex. Taking a simple approach to examine the problem, our first question would be: what is the best flange surface roughness and required gasket stress that can provide the best sealing performance, for a specified internal pressure, required leakage rate, and expected gasket deflection. Analysis of a simple model would allow us to properly verify the resulting knowledge base with experimental results.

## 4.9 Experimental test procedures

In order to gain an insight into the problems specified above, and to develop and examine the capability of our knowledge base system, the experimental tests results [5] have been used to demonstrate the process for these problems. Tests were performed based on the STANDARD ROTT test procedure described in Draft no. 9 of ASTM [1], and the gas used in the system was helium. The helium pressure in the rig is automatically controlled, adjusted, and measured. Furthermore, automatically controlled hydraulic pressure provides the required force on the flanges. The gasket stress is determined by the applied force on the initial surface area of the gasket. The overall leakage through the system is measured by a mass spectrometer, Model 120H. The experiments using the standard ROTT test are run for different pressures and gasket stresses for which the leakage rate of the system at each point is measured, for the specified gasket type and platens surface characteristics. The experimental data used are the results of the tests performed on a KILINGERSIL C-4430 1/16" gasket, having dimensions  $D_i = 4.875"$ ,  $D_o = 5.875"$ ,  $T_{gi} = 0.060"$ . The platens under test had a surface form of a finish spiral cut, with a roughness value of  $R_a = 50 \mu\text{in.}$ ,  $R_a = 250 \mu\text{in.}$ , and  $R_a = 500 \mu\text{in.}$  The same gasket stress,  $S_g$  (p.s.i.), for the three tests was used and controlled systematically so that at each measurement point for all the three cases the stress level is the same. The comparison between three test results showing the gasket performance is given in Fig. 4.4.

### 4.9.1 Fuzzy model and validation

The rule based fuzzy model is developed based on the above information in conjunction with the experimental data. The model contains three sets of premises for different ranges of internal pressure,  $P$  (p.s.i.), gasket deflection,  $D_g$  (in), and the leak rate,  $L_{tm}$  (mg/s); and two sets of conclusions corresponding to the required stress on the gasket,  $S_g$  (p.s.i.), and surface roughness of the platens,  $R_a$  ( $\mu\text{in.}$ ). A set of test results based on the 250 ( $\mu\text{in.}$ )

platen roughness was explicitly used to test the validity of the fuzzy model. The results obtained based on various inputs to the system are promising. Figures 4.5(a), (b) and (c) show the input and output of the fuzzy system. In Fig. 4.5(a), the inputs to the system are gas pressure at 400 (p.s.i.), gasket deflection at 5 (milli-in), from the low range, and leakage rate of  $5 \times 10^{-6}$  (mg/s); the compositional rule of inference (CRI) used is SUM-PROD, and mean-of-maxima defuzzification was used to infer the conclusion values. The crisp output values based on the system input are 9 (Kp.s.i.), for gasket stress ( $S_g$ ), and 251.499 ( $\mu\text{in}$ ) for platens surface roughness ( $R_a$ ). The results in Fig. 4.5(b) indicate that the gasket stress and flange surface roughness must be 9 Kp.s.i. and 49.9 ( $\mu\text{in}$ ), respectively, for the given system inputs of low internal gas pressure at 400 (p.s.i.), medium gasket deflection of 12 (milli-in), and a system leakage rate of  $300 \times 10^{-6}$  (mg/s). Nonetheless, the results obtained based on the system gas pressure of 800 (p.s.i.), medium range gasket deflection of 11 (milli-in), and system leakage rate of  $100 \times 10^{-6}$  (mg/s), are interesting, Fig. 4.5(c). Based on these inputs, the best approximated output for flange surface roughness is 251.499 ( $\mu\text{in}$ ). As can be seen from the results obtained, other gasket stress levels and a surface roughness of 500 ( $\mu\text{in}$ ) is also highlighted. This indicates that there exist rules with the same input parameters that result in different conclusions; which is very plausible in experimental results.

The problems indicated above can be applied with different strategies and based on the test input and output requirements. Other technological factors such as gasket and bolt creep, can be added to the knowledge base system easily to better define the existing problems and also to select the optimal values of the surface roughness to be used. Some other examples indicating what types of parameter can be considered are:

**Gasket type:** different types of gaskets can be added to the system.

**Surface form:** machined surfaces such as, ground, turned sinusoidal forms, and milled surfaces can be considered.

Pressure level: different pressure levels, such as intermediate level of 600 (psig), and higher pressures such as 1000—1200(psig), may reveal interesting conclusions about the leakage rate and leakage type under different stress levels.

#### **4.10 Conclusion**

The paper has presented a new approach to the selection of the optimal sets of parameters for gasketed bolted flanged joint sealing performance, based on a fuzzy decision support system approach. The applicability and advantage of such system has been defined and presented for flange surface roughness selection, in which optimal sets of parameters can be selected to reduce system loss rate, and the results are promising. The fuzzy decision support system may be applied to a more sophisticated and complex system. The same methods for building fuzzy decision support systems may be used in other areas of gasketed flanged qualification. The main advantage of the fuzzy logic technique is that it allows the consideration of many factors and parameters that are difficult to measure, or where the available information is vague and imprecise. Once the fuzzy tool system is implemented, it can significantly reduce the number of tests and ultimately the cost associated with experimental verifications. Such an approach helps both manufacturers and users to determine the performance of their system for which experimental data or mathematical theories are not available, and also allows them to make a satisfactory decision on the selection of the flange and gasket parameters. There is still a need for further research in this field. Further modifications and additional rules will be developed for the algorithms to enhance their capabilities for determining the optimum conditions for gasketed bolted flanged joints performance, using the fuzzy decision system approach, with more input and output parameters, so that the results can precisely reflect real working situation.

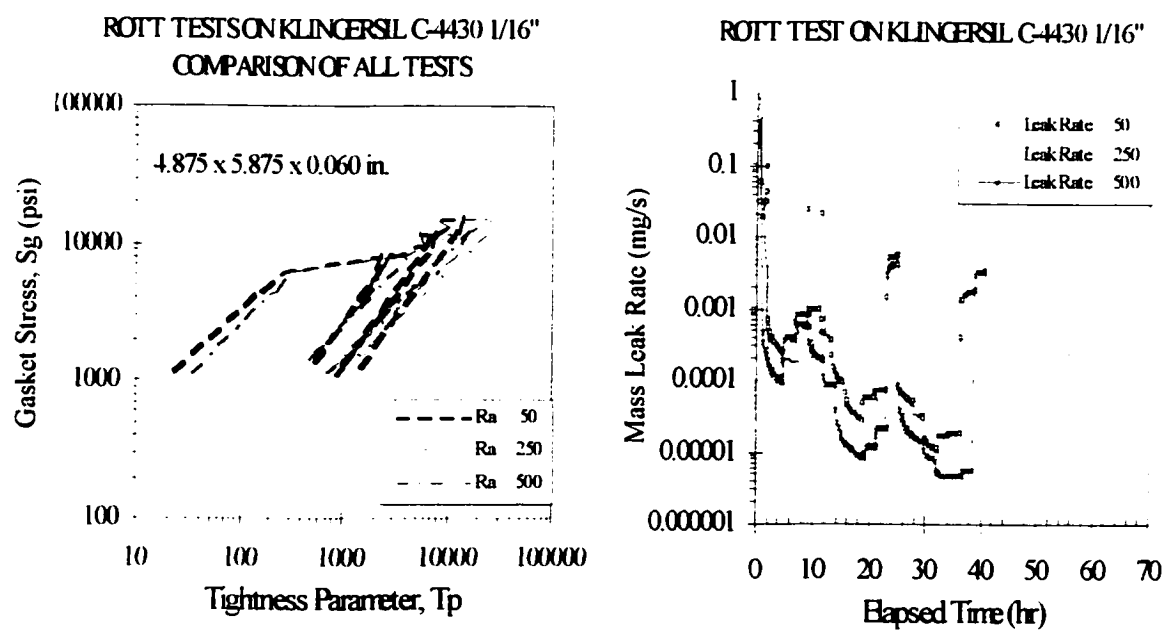


**Figure 4.4.** Tightness parameter and leakage rate for three experiments based on surface roughness.

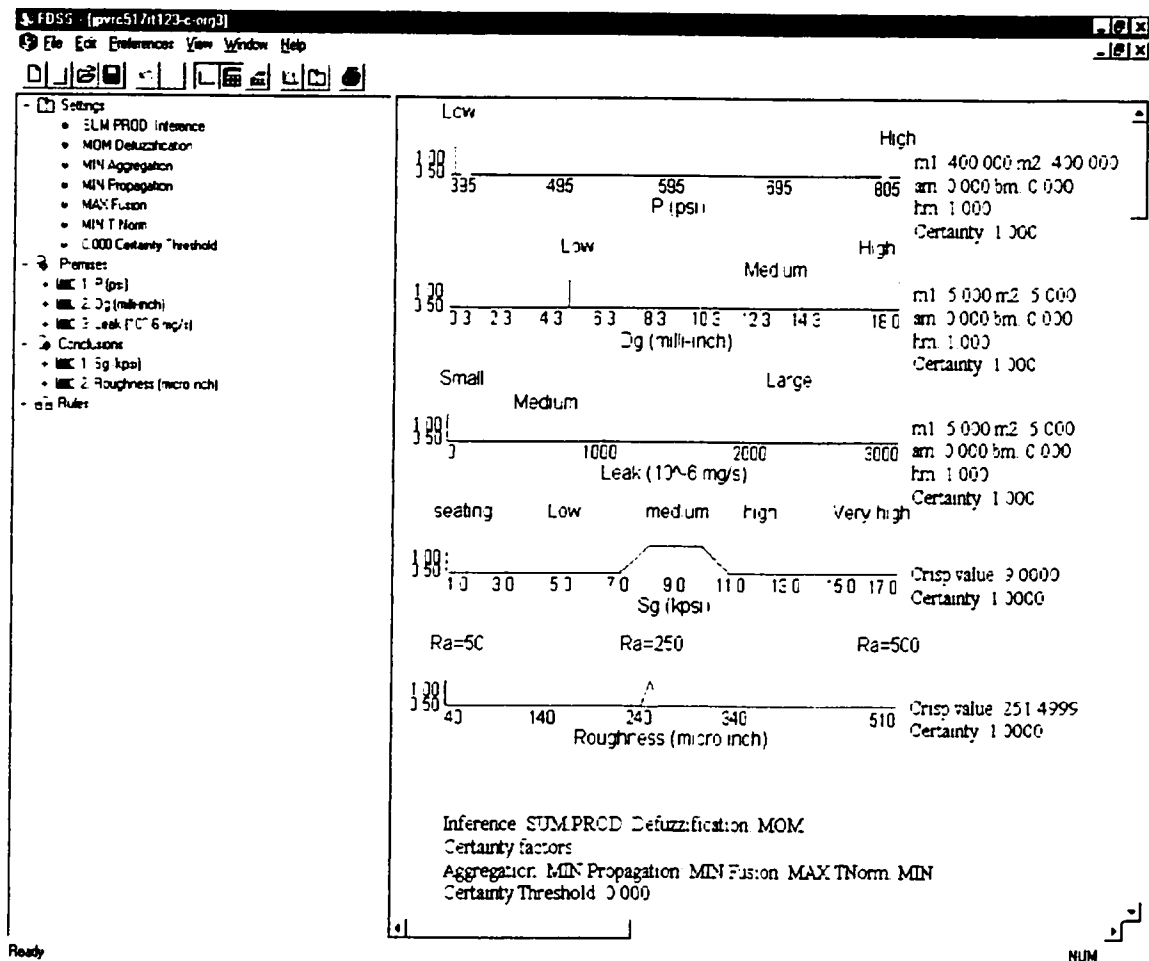


**Figure 4.5 (a).** Fuzzy decision support system. The inference rule of composition (CRI) used is SUM-PROD, and the defuzzification technique used is mean-of-maxima (MOM). Inputs to the system are: pressure 400 psig, gasket deflection 5.0 milli-in and leak rate  $5 \times 10^{-6}$  mg/s, and the outputs are: gasket stress 9000 p.s.i. and platens surface roughness 251.50  $\mu$ in.



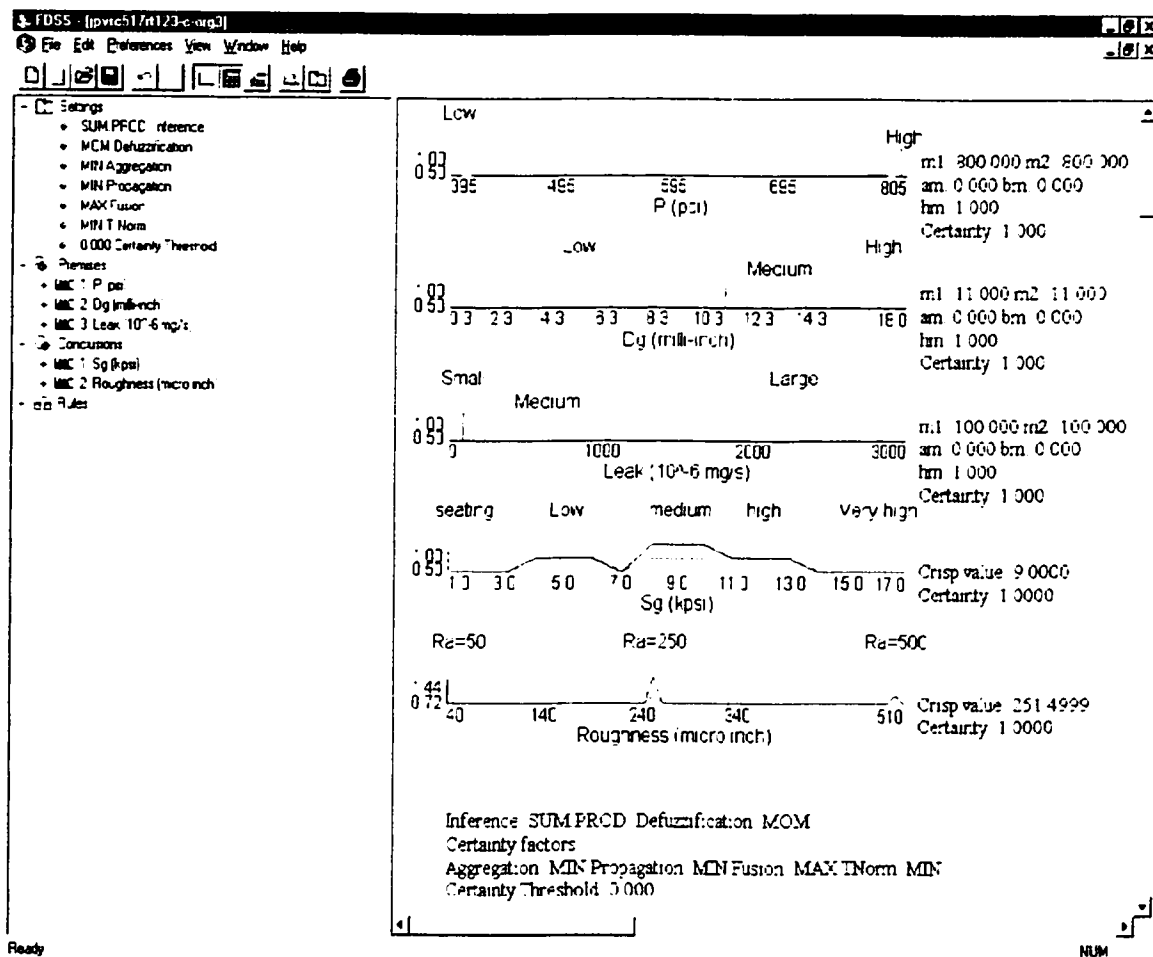


**Figure 4.5 (b).** Inputs to the system are: pressure 800 psig, gasket deflection 11.0 milli-in and leak rate  $100 \times 10^{-6}$  mg/s, and the outputs are: gasket stress 9000 p.s.i. and platens surface roughness 251.50  $\mu$ in.

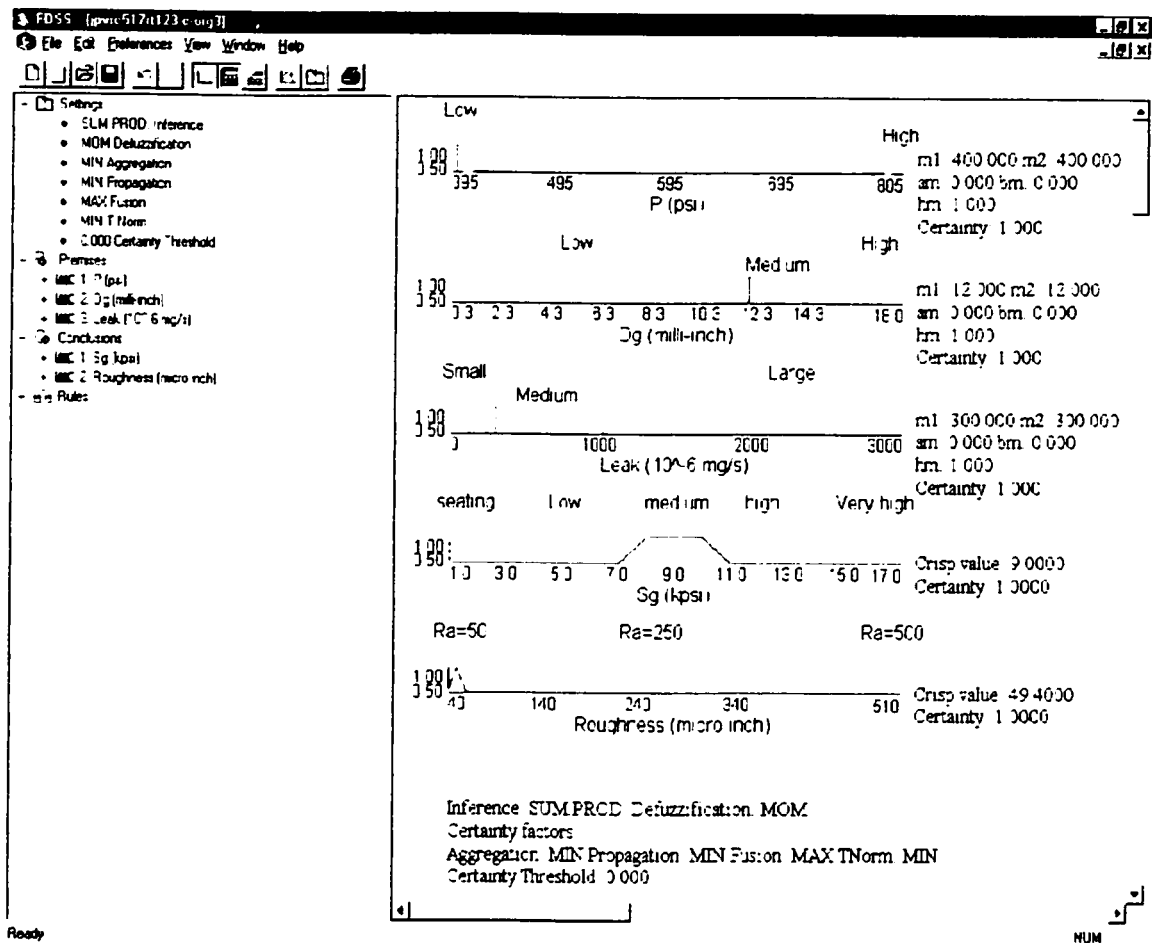


**Figure 4.5 (c).** Inputs to the system are: pressure 400 (psig), gasket deflection 12.0 milli-in and leak rate  $300 \times 10^{-6}$  mg/s , and the outputs are: gasket stress 9000 psi and platens surface roughness 49.40  $\mu$ in.

#### 4.11 References

1. J. R. Payne, M. Derenne and L. Marchand, "Draft No. 9: standard test method for gasket constants for bolted joint design", proposed as an ASTM standard test procedure, 1994
2. M. Derenne, J. R. Payne, A. Bouzid and L. Marchand, "Proposed modification to draft no. 9 of the standard test method for gasket constants for bolted joint design", FAS Symposium, Nashville, Tennessee, USA, 26–28 April 1998.
3. L. A. Mitchell and M. D. Rowe, "Influence of asperity deformation mode on gas leakage between contacting surfaces", *Journal of Mechanical Engineering Science*, 11(5), pp. 534–545, 1969.
4. Y. Matsuzaki and T. Kazamaki, "Effect of surface roughness on compressive stress of static seals", *JSME International Journal Series III*, 31 (1), pp. 99–106, 1988.
5. M. Derenne and H. Bouzid, "Effect of flange surface finish on room temperature gasket tightness and emissions", 1<sup>st</sup> Progress Report, Ecole Polytechnique de Montreal, Montreal, Quebec, Canada, 1997.
6. J. R. Payne, "Bolted joint improvements through gasket performance test", National Petroleum Refiners Association (NPRA) Maintenance Conference, San Antonio, Texas, USA, Paper MC-92-76, 19–22 May 1992.
7. J. R. Payne, "Effect of flange surface finish on constants for steel jacketed and other gaskets", 3<sup>rd</sup> International Symposium on Fluid Sealing, Biarritz, France, pp. 505–519, 15–18 September 1993.
8. J. R. Payne, "Effect of flange surface finish on spiral wound gasket constants", 2<sup>nd</sup> International Symposium on Fluid Sealing, La Baule, France, pp. 81–90, 18–20 September 1990.
9. A. L. Zadeh, "Fuzzy sets", *Information and Control*, 8, pp. 339–344, 1965.

10. A. L. Zadeh, "Outline of a new approach to the analysis of complex systems and decision processes", *IEEE Trans. on Systems, Man & Cybernetics*, **3**, pp. 28–44, 1973.
11. E. H. Mamdani, "Application of fuzzy set theory to control systems: a survey", Reference from M. M. Gupta, G. N. Saridis and B. R. Gaines, *Fuzzy Automata and Decision Processes*, North-Holland, New York, pp. 1–13, 1977.
12. P. M. Larsen, "Industrial applications of fuzzy logic control", *International Journal of Man-Machine Studies*, **12(1)**, pp. 3–10, 1980.
13. L. H. Tsoukalas and R. E. Uhring, *Fuzzy and Neural Approaches in Engineering*, pp. 105–130, John Wiley, 1997.
14. M. Balazinski, H. Boyer, E. Czogala and D. Grzerorz, "Fuzzy-Flou: a decision support system", Ecole Polytechnique of Montreal, Montreal, Canada, and Technical University of Silesia, Poland, 1995.
15. A. L. Zadeh, "Fuzzy logic", *IEEE-CS Computer*, **21(4)**, pp. 83–93, April 1988.

## **CHAPTER 5**

### **FUZZY LOGIC APPLICATION IN GASKET SELECTION AND SEALING PERFORMANCE**

**J. Arghavani, M. Derenne and L. Marchand**

**Department of Mechanical Engineering, Applied Mechanics,**

**Ecole Polytechnique of Montreal**

**Montreal, Quebec, Canada**

#### **5.1 Presentation of the chapter**

In the present chapter fuzzy logic has been applied for the determination of a set of optimal parameters for the selection of gasket and sealing surface characteristics. The problems associated with the selection of appropriate gaskets based on the given system requirements are addressed. The fundamentals of fuzzy set theory and fuzzy logic are presented. The imprecision of the input and output variables of the system under investigation has been directly addressed by fuzzy sets in the fuzzy logic system, and is expressed in linguistic terms (e.g. high and low pressure). The experimental results of the gasket performance combined with practical knowledge have been used to build and validate the fuzzy models in the form of fuzzy linguistic rules, using fuzzy decision support system called Fuzzy-Flou [19].

## 5.2 Abstract

The paper presents the concept for and the implementation of a fuzzy logic approach in the selection of gaskets, for their sealing performance, based on system requirements. Gasket sealing performance is complex, owing to numerous parameters affecting the gasket sealability. A fuzzy decision support system (FDSS) and its application to the selection of sets of optimal parameters for the joint connections are described. The FDSS is based on the compositional rules of inference, which take into consideration the fact that many unknown parameters have an influence on the gasket sealing performance. The paper outlines the complex nature of gaskets, justifying the need for a predictive system capable of dealing with vague information and providing precise results. It also presents a new methodology for proper gasket selection for a given set of operating conditions, e.g. applied load, gas pressure, and leakage rate.

**Keywords:** Fuzzy logic; gasket selection; leak rate; sealing performance

## 5.3 Introduction

Gaskets are largely used in refineries and in chemical and petrochemical industries in most high pressure system applications, piping systems, joint connections, and flanges. Gaskets are mainly used to provide a seal between the mating faces of the flanged joint, filling in surface roughness, waviness and irregularities of the mating faces owing to machining and manufacturing imperfections or limitations. In general, the purpose of gasket sealing is to reduce the emission rate of media from the system. The most common gasket materials used in the market are PTFE (Teflon), graphite, metallic, non-asbestos, and fibre asbestos. There are also metal reinforced gaskets and gaskets composed of a combination of materials for better sealing performance. The selection of gaskets to obtain optimal sealing performance is critical and complex in real industrial applications.

A gasket is evaluated based on its sealability, and a gasket is said to be performing if it provides a low leakage rate under the applied load, during the service life. As a result, the evaluation, comparison, and selection of gaskets to suit particular applications is very tedious, time consuming and complex. Thus with the application of fuzzy logic the selection of a proper gasket based on system requirements is made easily, simply, and quickly.

#### **5.4 Literature review of gasketed bolted flanged joints**

Over the last century, manufacturers and researchers have produced several important works on the design, verification, and qualification of flanged joints, gasket selection and qualifications, and the criteria involved to better understand and overcome associated problems in this domain. Such problems arise in a variety of aspects, including flange shape and dimensions, flange surface roughness and surface characteristics, bolt load, flange and gasket materials, and gasket type. Theoretical and experimental works have been performed to address such problems. Furthermore, for the past two decades, the concentration has been on the determination of gasket constants and standardisation of the test procedures. Results of such investigations can be found in Draft No. 9 of ASTM [1], and in [2—8].

Payne et al. [2, 3] presented their work on a gasket qualification test scheme for petrochemical plants, discussing the test methods and applications as well as the quality criteria and evaluation schemes in these aspects. Furthermore, Payne et al. [4] worked on the evaluation of test methods for asbestos replacement gasket materials. Payne [5] has presented his work on the effect of flange surface finish on gasket constants for different types of gaskets. Derenne et al. [6] presented their work on the behaviour of gaskets for bolted flanged connections, and on the status of the research and work in this domain in North America. Furthermore, Derenne and Payne [7] worked on the determination of new

PVRC constants for gasket selection, as well as defining new ASME rules for bolted flanged joints. Proposed modifications to [1] can be found in [8].

Several parameters are involved in the sealing performance of a gasketed bolted flanged joint and, as a result, the analysis of such a system is extremely complex and imprecise. The objective of most work in this domain is the determination of critical parameters allowing the lowest possible leakage rate and ultimately reducing or eliminating the emission rate. Most work in the area of gasket selection and gasket performance has been based on the fluid flow modelling, bending moment effect, flange shape, bolt load, types of gas, and temperature effect. However, no research has yet dealt with fuzzy logic applications in these domains.

### **5.5 Literature review of fuzzy set theory and fuzzy application**

In most real situations, because of the complex nature of systems, the determination of crisp values is not feasible, unnecessary and most of the time not appropriate. Inversely, it might be best to present the system parameters with a range of data instead of crisp values. Zadeh's [9] approach to deal with complex systems and imprecise information led him to present the fuzzy set theory. As a result, Zadeh's pioneering work [9] in 1965, and his seminal paper [10] in 1973, persuaded other researchers to use the fuzzy rule-based approach for the analysis of complex systems and for decision making. Other works of Zadeh provided support in this domain [11—15].

Mamdani [16] presented an excellent work on the application of fuzzy set theory to control systems and decision making, which established the industrial application of this theory. Also, the industrial application of fuzzy logic control can be found in the work of Larsen [17]. Arghavani et al. [18] presented their work on a fuzzy approach to the selection of flange surfaces in gasketed bolted flanged joint applications. Balazinski et al.



[19] presented their work on a fuzzy logic application for decision making and selection of cutting parameters in a machining process. Based on the fuzzy logic theory of Zadeh, Balazinski et al. [20] developed a fuzzy logic tool, called Fuzzy-Flou. An excellent introduction to the basic concepts and the more advanced applications of fuzzy logic approach and neural network in engineering can be found in [21]. Valuable information on the theory and applications of fuzzy sets and systems is also provided in [22].

Most real situations require data collection and data analysis to estimate properly the performance of the system. In data processing systems the objective is to understand the phenomena involved and to evaluate relevant parameters quantitatively. This requires the modelling of the system either analytically or by experimental design models. Analytical modelling uses mathematical and physical principles, whereas experimental modelling is used when mathematical modelling is not possible. Thus, an intelligent soft computing system capable of dealing with the uncertainties of real situations involved in such models is required. Once the model of the system is made, the analysis of the system through, for example, sensitivity analysis, statistical regression, and analysis of variance, can be performed. As the complexity of the systems under investigation increases, the precision in the definition of statements becomes ambiguous. Furthermore, the larger the system is, the more parameters become involved and, as a result, the presentation and association of the ideas becomes vague, and statements about the systems tend to lose their meaning.

Based on fuzzy set theory, fuzzy logic, and the theory of approximate reasoning, most complex problems can be addressed simply. Industrial applications related to gasket selection and gasket sealing performance are considered to be situations of high complexity and of a high degree of uncertainty that cannot satisfactorily be addressed yet by mathematical models and basic principles. Thus, a fuzzy system can be used to obtain precise models based on experimental data, field experience, and expert knowledge. In

this paper, the application of a fuzzy decision support system (FDSS) for gasket selection and gasket sealing performance is presented, based on system requirements.

## **5.6 Present work**

The present work considers the problems associated with the selection of appropriate gaskets based on the given system requirements. This involves a decision problem in the choice of sealing parameters in the gasketed bolted flanged joint sealing process, which can be solved by applying fuzzy logic theory using a fuzzy decision support system. The imprecision of the input and output variables of the system under investigation can be directly addressed by fuzzy sets in the fuzzy logic system that can be expressed in linguistic terms (e.g. high and low pressure). The FDSS used for this analysis is a linguistic rule based system called Fuzzy-Flou [19].

The proper selection of gaskets and the parameters involved in sealing performance are critical in modern seal and gasket manufacturing. Proper decision making and an optimal selection of material saves time and labour, therefore, researchers have tried to find the optimal parameters which can define the seal and gasket performance under given system conditions, e.g. stress and gas pressure. Determining the operating life of the sealing, facilitates the system operation and process planning. Ultimately, the goal is to determine the optimal parameters to maintain the joint tightness in order to reduce the leakage rate. However, owing to the complexity of such systems and the involvement of many unmeasurable parameters, a unified adequate method for such optimal selection has not yet been developed.

In effect, there are many factors that influence leakage rate, gasket sealability and gasket performance. Among them are gasket type and quality, stress on the gasket (bolt load), gas pressure, temperature, gasket deflection, flange surface roughness, and surface form.

Taking into consideration the fact that the influence of most factors on the gasket sealability and joint tightness is not precisely known, it is difficult to determine the optimal joint parameters. Thus, fuzzy logic is used to express the experimental data combined with practical knowledge in the form of fuzzy linguistic rules, for better decision making and proper gasket selection.

### 5.7 Fundamentals of fuzzy set theory

It is well known that classical set theory defines a set of crisp values for distinct elements (e.g. numbers, objects), and deals with conditions such as *true* or *false*, and *0* or *1*. The sets of crisps belong to a universal set called a universe of discourse, and a characteristic function,  $\zeta_A(x)$ , of  $A$ , indicates whether elements of a set  $A$  belong or do not belong to a crisp set  $A$ , shown as:

$$\zeta_A(x) \equiv \begin{cases} 1 & \text{iff } x \in A \\ 0 & \text{iff } x \notin A \end{cases} \quad (5.1)$$

In contrast, a fuzzy set introduced by Zadeh [9], allows for many degrees of membership of the set. The degree of membership of the set is the interval between 0 and 1 indicated as  $[0,1]$ . Then the interval  $[0,1]$  is no longer considered as a crisp set but as a fuzzy set shown as:

$$\mu_A(x) : X \rightarrow [0,1] \quad (5.2)$$

This indicates a membership function of the fuzzy set  $A$ , which maps every element,  $x$ , of the universe of discourse  $X$  to the interval  $[0,1]$ . Thus, unlike the classical set and probability principles that deal with true and false, 0 and 1, and the probability of “belonging to” or “not belonging to”, fuzzy set theory deals with the “degree of

belonging” of an element (or singleton) to the set. Thus characteristic function  $\zeta_A(x)$  in a classical set is called a membership function  $\mu_A(x)$  in a fuzzy set. The true and false fuzzy set relationship is shown in Fig. 5.1. Note that in a true fuzzy set, the membership function increases monotonically to unity level, while in a false fuzzy set the membership function decreases monotonically to zero level.

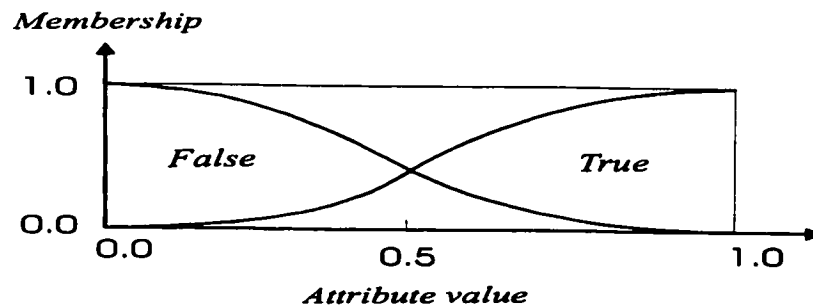
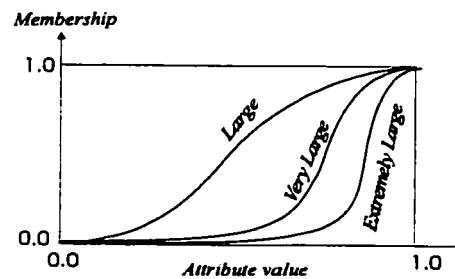


Figure 5.1. True and false fuzzy sets

In a crisp set, a singleton is the element  $x$  itself, whereas in a fuzzy set the singleton is presented by a pair, the element  $x$  itself and its membership function  $\mu_A(x)$ . Thus, a fuzzy set  $A$  is defined as a collection of fuzzy singleton pairs,  $(x, \mu_A(x))$ , where  $x$  is an element belonging to the universe of discourse  $X$  and  $\mu_A(x)$  is the  $x$ 's membership of  $A$ , indicating its degree of belonging to the set. In other words, a fuzzy set  $A$  is a subset of the universe of discourse  $X$  with membership function  $\mu_A(x)$ , which can take any value in the interval  $[0,1]$ .

It is worth mentioning that a set subsumes all its subsets. Thus, based on the entailment principle of Zadeh [14], a fuzzy set inclusion is a sub-summation relationship which can be

used for inferences. For instance, consider that the linguistic fuzzy terms *large*, *very large* and *extremely large* are defined by the fuzzy sets in universe of discourse  $X$ , on  $[0,1]$ , such that *extremely large* is defined to be a fuzzy subset of *very large*, and *very large* itself is defined to be a subset of *large*. Therefore, if  $x=0.9$  is defined as an *extremely large* number, then from “ $x$  is *extremely large*” we can infer that “ $x$  is *large*” or “ $x$  is *very large*”. The fuzzy sets and fuzzy subsets, *large*, *very large* and *extremely large* are shown in Fig. 5.2.



**Figure 5.2.** *Large, very large, and extremely large fuzzy sets*

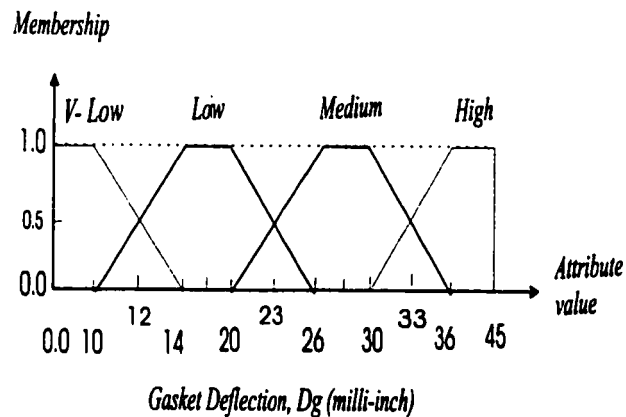


**Figure 5.3.** Degree of belonging of elements in the sets.

It can be seen from Fig. 5.2 that as the slope of the curve representing the fuzzy sets increases, the degree of membership of elements belonging to that set increases to unity. An example of the degree of membership of two or more fuzzy sets is more clearly shown in Fig. 5.3. It is assumed that the gasket deflections ranging between 0.0 and 10.0 milli-inch can be classified as very low deflection, and that deflection between 14.0 and 20.0 milli-inch can be classified as low deflection, represented by the fuzzy sets *very low* and *low*, respectively. Furthermore, the medium fuzzy set deflection can range from 26.0 to 30.0 milli-inch, and the high deflection can be classified as 36.0 to 45.0 milli-inch represented by fuzzy sets *medium* and *high*, respectively. Thus, all elements belonging to the fuzzy set very low with attribute values from 0.0 to 10 milli-inch have a degree of membership of 1, or in other words their degree of belonging to the set is 100 %. Similarly, the values ranging between 14.0 and 20.0, 26.0 and 30.0, and 36.0 and 45.0 milli-inch in the fuzzy sets low, medium, and high respectively, have a degree of membership equal to 1. Whereas a deflection of value 12.0 milli-inch, is 50% very low and 50% low, thus, it has a degree of membership of 0.5 to each fuzzy set of very low and low. Similarly, this is valid for the values 23.0 and 33.0. On the other hand, it can be seen that none of the elements of the fuzzy set very low, belong to fuzzy medium or high, and vice versa. Figure 5.3 represents the *antecedent fuzzy sets* with four linguistic values *very low*, *low*, *medium*, and *high*, for gasket deflection.

### 5.7.1 Practical aspects of fuzzy relations

In some real situations, an approximate result of a function may be acceptable or even preferable. For example, the gasket stress at 11.0 Kp.s.i. or 12.0 Kp.s.i. may have little or no effect on the gasket performance and leakage rate, for a PTFE (Polytetrafluoroethylene) based gasket type. Thus, the leakage rate may remain the same for any stress level from 11.0 to 12.0 Kp.s.i. Therefore, we would say that the range of stress levels is acceptable and that achievement of an exact stress level is not necessary.

As another example, let us consider the flange's surface roughness. Assuming that the flange face is machined by a milling process, so that the surface roughness values at different sections of the surface differ from each other, such that we obtain surface roughness values of 350.0, 400.0, and 500.0  $\mu\text{in}$  from three different locations on the surface. In this case, the surface roughness on the flange face, machined by milling, can be characterised by a fuzzy set roughness ranging between 350.0 and 500.0  $\mu\text{in}$ .

The above examples indicate that, in practical applications of gasketed bolted flanged joints, a range of solutions is not only acceptable, but is preferable. Thus, instead of working with a crisp point function, we work with an area around a point, representing vague and approximate reasoning about a function, which is called *fuzzy numbers*. Fuzzy numbers are presented by different membership functions such as *bell-shape*, *triangular*, and *trapezoidal* (as in Fig. 5.3) defining an area about a point. It must be appreciated that if experimental results are more sensitive to a fuzzy variable, then, the fuzzy numbers may be presented by a triangular membership function. In other words, the size of membership function defines the vagueness and uncertainty of the rules. Thus, the more precise the fuzzy set, the spikier the membership function must be.

Consequently, the experimental data, which are sets of crisp values, are used to build the premises and inference fuzzy sets of the system. Then, a set of rules is defined, based on the experimental data, consisting of fuzzy linguistic statements linking conditions with conclusions, involving fuzzy sets and fuzzy relations [12]. The knowledge about a system is encoded in a statement of the form:

$$\begin{array}{ll} \text{if (given a set of conditions } A) & \\ \text{then (deduce a set of conclusions } B) & \end{array} \quad (5.3)$$

More precisely, fuzzy numbers are encoded by fuzzy *if/then* rules involving fuzzy linguistic variables in each side of the rule of the form [13]:

$$\text{if } x \text{ is } A_i \text{ then } y \text{ is } B_i \quad (5.4)$$

where, linguistic variables  $x$  and  $y$  take the values  $A$  and  $B$ , respectively.

### 5.7.2 Fuzzy set operations

In order to define the fuzzy set operations *interaction* and *union* of two or more elements, or of two or more fuzzy sets, over a universe of discourse, the min ( $\wedge$ ) and max ( $\vee$ ) operators are used [11, 16]. The operators min ( $\wedge$ ) and max ( $\vee$ ) are analogous to product ( $\cdot$ ) and sum (+) in algebra [21, 22]. Furthermore, certain criteria about inferencing such as in the *if/then* rule must be satisfied, which is done by a *fuzzy implication operator* or simply an *implication operator*. Thus, given certain premises, then certain conclusions must result, and, in general, they ought to satisfy the *classical modus ponens* and *modus tollens* [21]. Many implication operators have been developed, among which the most common ones are the max-min [ $\vee (\wedge)$ ] [10], the min ( $\wedge$ ) [16], the product ( $\cdot$ ) [17], an arithmetic implication operator of multivalued logic [12], and a Boolean implication based on classical logic. For the sake of brevity, these are not shown here, and interested readers may refer to the references at the end of this work.

### 5.7.3 Fuzzy algorithm

A fuzzy algorithm is a procedure used for performing a task formulated as a collection of sets of fuzzy *if/then* rules and connected by the connectives AND, OR, and ELSE. The statement “*if*” carries a set of conditions and the statement “*then*” represents a set of conclusions. It is to be noted that in the present work we refer to a set of conditions as:



inputs, premises, and antecedents, and to a set of conclusions as: outputs, inferences, and consequents. In most practical applications, a fuzzy algorithm consists of multivariate fuzzy antecedents and consequents, thus the knowledge is expressed by a finite number of heuristic fuzzy rules based on the multiple input multiple output (MIMO), or multiple inputs and a single output (MISO), which are obtained from the experimental values, field experience, and expert knowledge. As a result, the effect of one or more input parameters on the output(s) can be determined. Consequently, inferences are made based on the compositional rule of inference (CRI) that is formed from different combinations of operations, which constitute the basis of the inference mechanism in the fuzzy logic tool system, namely the Fuzzy-Flou system used in the present work. The formulation of CRI variants can be found in [11], [19] and [20].

#### **5.7.4 Fuzzification and defuzzification**

Fuzzification is a procedure used to control the fuzziness of the fuzzy set. This procedure simply transforms a crisp set into a fuzzy set, which increases the fuzziness of the fuzzy set information, thus allowing it to work with a range of data, or area about a point. The inputs to the fuzzy logic control system are analysed and processed, and then the results obtained are the fuzzy outputs. Defuzzification is a procedure of transforming the inferred fuzzy output from the system to a real number or crisp value. The most commonly used defuzzification techniques are: the mean-of-maxima (MOM) defuzzification, the centre-of-area (COA) defuzzification, also called the center-of-gravity (COG), and the centre-of-sum (COS) defuzzification. The selection of the defuzzification technique is critical and has a significant impact on the speed and the accuracy of the fuzzy algorithm. This is mainly because certain defuzzification methods may introduce nonlinearities and discontinuities in the hypersurface of the fuzzy control [13, 21]. For instance, the mean-of-maxima (MOM) defuzzification technique provides higher computational speed than the other techniques and also provides better control for inferring values near the edge of

the universe of discourse [21]. The centre-of-area (COA) or centre-of-gravity (COG) defuzzification technique is suitable for a multidimensional fuzzy output. With this technique, the resultant membership functions are developed by taking the union of the output of each rule, which means that the overlapping area of fuzzy output sets is counted only once, providing more linear results [21]. The latter technique is used in the present work.

After having described the fuzzy logic fundamentals and implementation, the general architecture of a fuzzy logic system can be demonstrated as in Fig. 5.4.

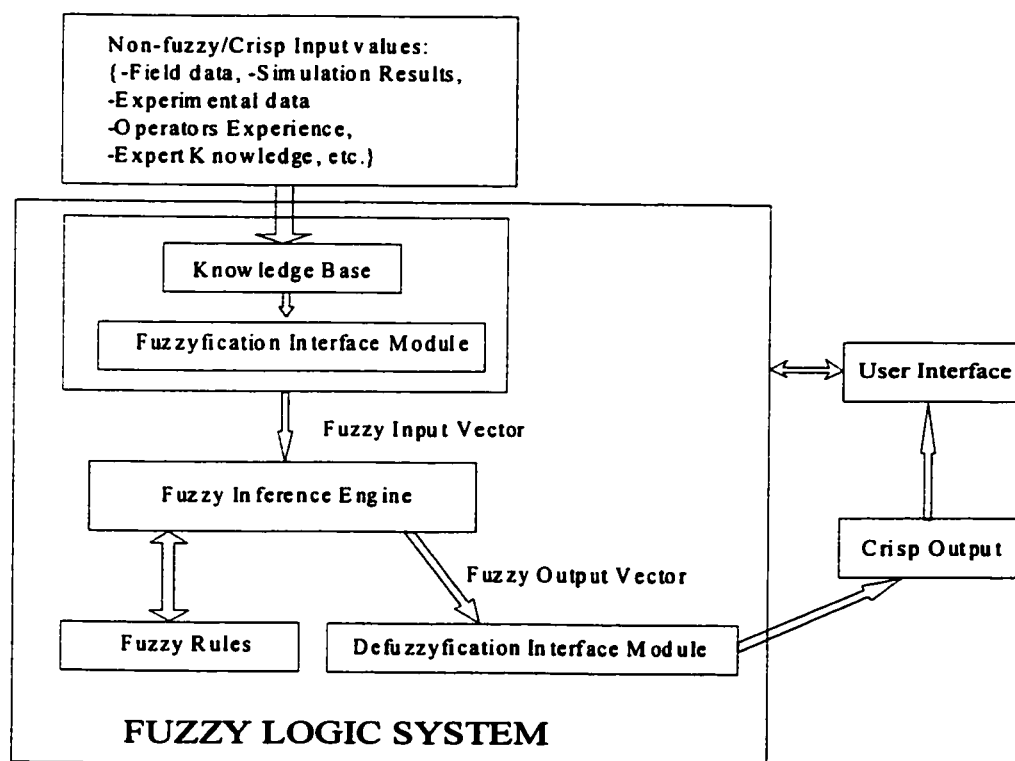


**Figure 5.4.** Architecture of Fuzzy Logic System

## 5.8 Case study

### 5.8.1 Gasket selection

Gasket selection is one of the important criteria in gasketed bolted flanged joint performance. An appropriate gasket plays a critical role in the emission rate, sealing performance, and tightness of the joint. Furthermore, a properly selected gasket for given flanged joint characteristics and system requirements, greatly reduces the manufacturing costs, as well as the costs associated with the loss of media and consequent environmental damage. In most practical situations, a proper selection of such criteria is very difficult, and is left to the planner's judgement and experience.

The analysis of a gasketed bolted flanged joint system is complex owing to the existence of the numerous factors involved. Furthermore, many of these factors are not measureable with conventional techniques or with the existing technological devices. Thus, expert knowledge and experimental results should be used to model gasket types and characteristics, system requirements, gasket stress, gas pressure, flange surface roughness and characteristic, bolt creep, high temperature effect and gasket aging. The ultimate goal is to determine which gasket can provide the best sealing performance. The present fuzzy models and analysis are limited to the consideration of the following criteria:

1. Four different types of gaskets, namely **G-LAM-GRT** (Garlock laminated graphite), **UC-FLX-GRT** (UCAR flexible graphite (G2) sheet), **G-N-AS** (Garlock non-asbestos 3200 sheet gasket), and **KLNR** (KLINGERSIL C-4430 1/16").
2. Gasket dimensions of inside and outside diameter equal to 4.875 and 5.875 in., respectively, with gasket thickness ranging between 0.0610 in and 0.0650 in.
3. Platens with one type of machined surface, produced by a turning procedure.
4. Platens surface roughness value of  $Ra = 250 \mu\text{in}$ .

### 5.8.2 Experimental procedures

In order to better understand the problems associated with gasketed bolted flanged joint performance, and to develop and examine the capabilities of the proposed fuzzy logic system, several series of available experimental results on the gaskets mentioned above were used [23]. For all gaskets, the experimental tests were performed similarly, using the standard room temperature gasket tightness test procedure known as ROTT test defined in [1]. Three cycles have been considered; each cycle consists of loading and unloading stress levels, as can be seen in Fig. 5.5. Each test cycle starts with an S1 stress level at 1025 p.s.i. and ends with S1. The maximum stress level at cycle 1 is 8090 p.s.i., the maximum stress level at cycle 2 and cycle 3 is 11630 p.s.i., and 15160 p.s.i., respectively. The intermediate stress levels for both loading and unloading cycles are 4560, 6325, 8090, 9860, and 13 400 p.s.i. Details for the ROTT test concept, fixture set-up, and associated costs, can be found in [8] and [1].

It is worth mentioning that the purpose of the loading and unloading cycles is to simulate gasket aging, bolt relaxation and re-bolting. Please note that for the purpose of the present work the stress levels are selected from S1 to S8, representing the initial to maximum stress levels, respectively. Two different gas pressures of 400 psig and 800 psig have been considered at each stress level. Helium gas was used in these experiments. The gas pressure in the system and the gasket stress level were controlled and adjusted automatically through the experiments. At each stress level sufficient time is given for leakage rate stabilisation [8]. Then the leakage rate, gasket deflection and stress are recorded, following which, the next stress level is applied and results recorded similarly. The overall leakage rate,  $L_m$  (mg/s), at each stress level at gas pressures of 400 psig. and 800 (psig) was measured using a helium mass spectrometer, Model 120H. The gasket deflection was measured simultaneously by two LVDTs, 180° apart. The experimental results are presented in Fig. 5.5. Note that various leak measurement methods and criteria are described in [8].

As can be observed from the results, each gasket behaves differently under the same applied stress level. For instance G-LAM-GRT has the maximum gasket deflection throughout the experiment, its gas leakage rate stabilisation is short, but provides the largest leakage rate throughout the test at all stress levels, Fig. 5.5(a) and 5.5(c). On the same graphs, the UC-FLX-GRT gasket shows a similar leakage rate for the first cycle, whereas in the second and third cycles it provides comparably lower leakage rates. However, the leakage rate stabilisation under each stress level is much longer, Fig. 5.5(a). Furthermore, the UC-FLX-GRT gasket has a lower gasket deflection compared to the G-LAM-GRT gasket, Fig. 5.5(c). However, at certain stress levels the gasket deflection overlaps with the deflection of the G-LAM-GRT gasket. It should be noted that the total experimental run time for G-LAM-GRT and UC-FLX-GRT gaskets was 33 h and 40 h, respectively.

The results of experimental tests for gaskets KLNR and G-N-AS are presented in Fig. 5.5(b) and 5.5(c). It can be observed that the KLNR gasket has a longer leakage rate stabilisation time, and a total test time of 67 h. It also provides a higher leakage rate compared to the G-N-AS gasket; however, its gasket deflection is much less, up to 0.014in. maximum, under the same applied load. Furthermore, at certain lower stress levels, its deflection overlaps with that of KLNR at higher stress levels. On the other hand, the G-N-AS gasket has the lowest leakage rate for the same applied load. Also, its leakage rate stabilisation time is shorter than the KLNR gasket, but is longer than that for the UC-FLX-GRT gasket. Its total test time is approximately 53 h, which is somewhere between the total test time of the UC-FLX-GRT and KLNR gaskets. Furthermore, the G-N-AS gasket deflection is at least twice that of the KLNR, but is approximately half that of the UC-FLX-GRT. As a result, the association between the stress, gas pressure, leakage rate, gasket deflection, and gasket type cannot easily be established.

It can be observed that the analysis of such a system is not only complex but is also extremely vague owing to many unknown parameters that affect the results. The nonlinear behaviour of the gasket and physical phenomena involved are not easily understandable, and cannot simply be explained by mathematical and theoretical techniques. Thus, this calls for a powerful tool capable of dealing with such vagueness and complexities. Hence, the application of an FDSS because fuzzy logic theory greatly simplifies gasket selection and sealing performance analysis.

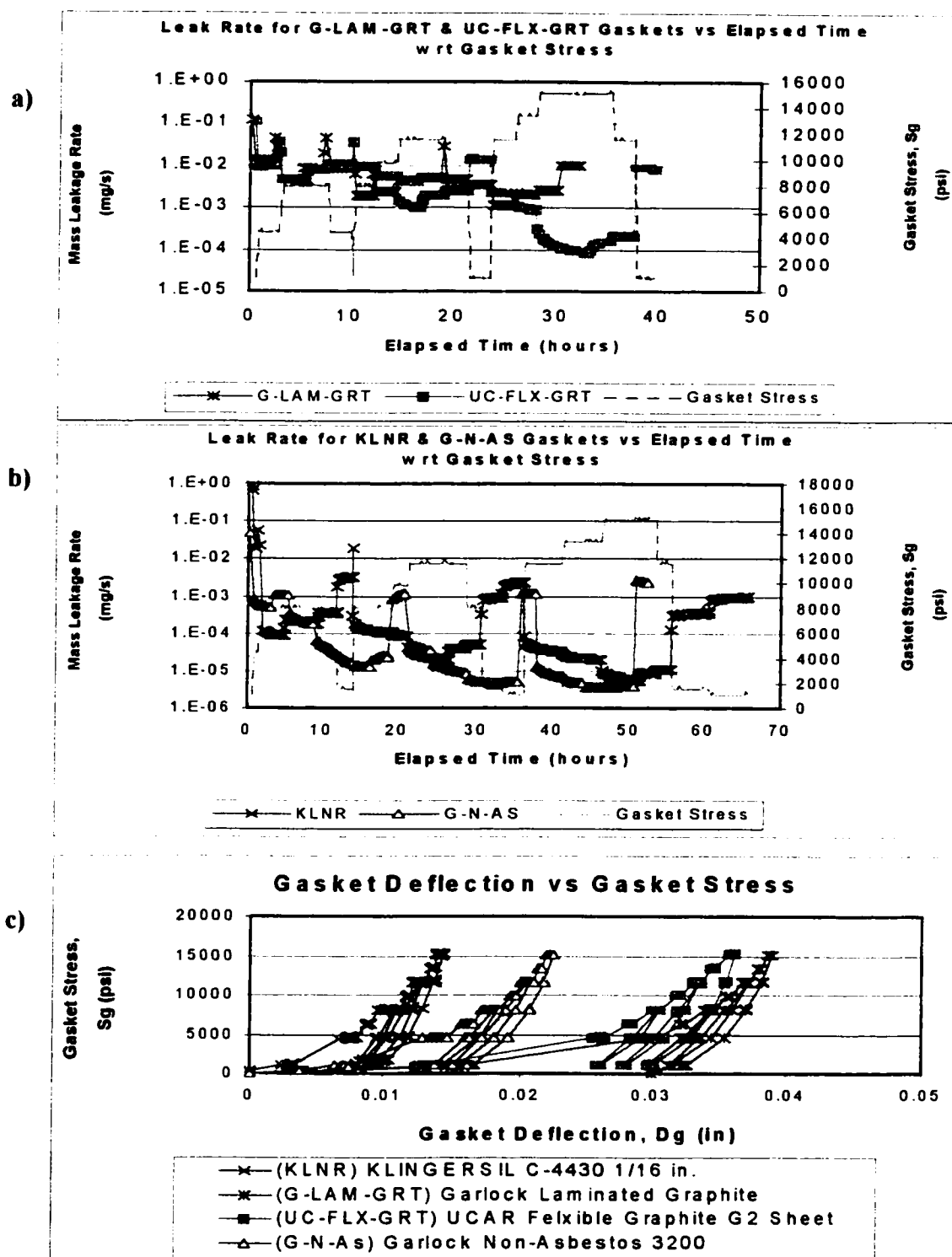


**Figure 5.5.** a) Leakage rate for G-LAM-GRT and UC-FLX-GRT gaskets vs. Elapsed time with respect to gasket stress. b) Leakage rate for KLNR and G-N-AS gaskets vs. elapsed time with respect to gasket stress. c) Gasket deflection vs. gasket stress.

### 5.8.3 Fuzzy rules

In order to build the system fuzzy rules, the membership functions of the main factors influencing the output results are defined. The levels of membership functions are determined and defined in linguistic terms, using a classifier engine. To do this, a multiple input and multiple output pattern classifier engine has been established, as in Figure 5.6, which ranks the input data, using knowledge based classification rules, based on expert knowledge. The classifier engine simply uses a sorting process and defines the data range for each set of input data, and then each range is given a ranking value; also linguistic terms are assigned to each rank of the output classification. Thus, the levels of membership functions are determined. Consequently, fuzzy rules are defined based on the interactions of each level of membership function for the main factors. A fuzzy rule is written following the logical statements and logical rules given in Eqs (5.3) and (5.4), based on experimental results, expert knowledge, and field experience.

As presented in Fig. 5.6, the gas pressure is classified at two levels: low and high, and the gasket deflection and the leakage rate are each classified at four levels: very low, low, medium, and high; the gasket stress is classified at eight levels, S1 to S8, and the gasket type is classified at four levels, using the gasket names. For the purpose of the present work, from the experimental results, the stress values and their associated leakage rate and gasket deflection results were selected at the loading cycles; S1=1025 p.s.i., S2=4560 p.s.i., S3=6325 p.s.i., S4=8090 p.s.i., S5=9860 p.s.i., S6=11630 p.s.i., S7=13400 p.s.i., and S8=15 160 p.s.i. Thus, different fuzzy systems can be designed as needed, for a prediction or decision-making system to determine the design parameters.



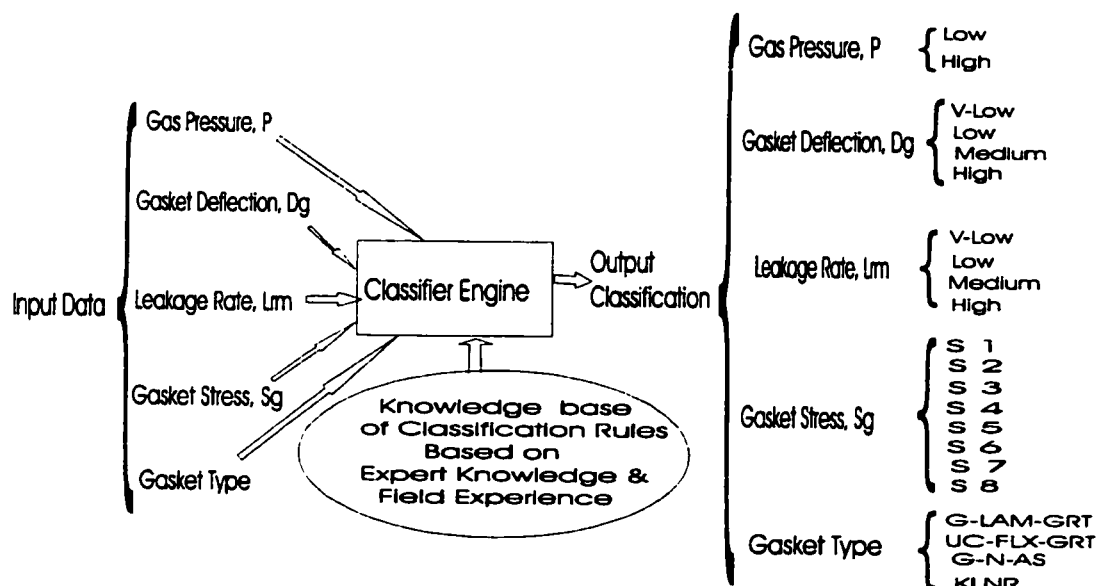


**Figure 5.6. Multi-input Multi-output Classification Task.**

In this work, two fuzzy systems have been modelled based on the same experimental data. The first model is based on the classification results shown in Fig. 5.6, therefore:

1. Considering the gas pressure  $P$ , gasket deflection  $D_g$ , and leakage rate  $L_{rm}$ , as premises, and gasket stress  $S_g$ , and gasket type as consequences for fuzzy rules, then a fuzzy system of a minimum of  $2 \times 4 \times 4 = 32$  rules can be defined. All possible fuzzy rules for such a system are presented in Fig. 5.7, and its corresponding FDSS is shown in Fig. 5.8.

For the second model, the classification outputs in Fig. 5.6 were further refined so that the gasket deflection and leakage rate were classified at 22 ( $D_{g1}, D_{g2}, \dots, D_{g22}$ ) and thirty-one ( $L_{rm1}, L_{rm}, \dots, L_{rm31}$ ) levels, respectively, which closely correspond to each single output from the experimental results, whereas the gas pressure, gasket stress, and gasket type classification were kept the same, therefore:

2. Considering the gas pressure at two levels (low and high), gasket type at four levels and gasket stress at eight levels (S1, S2,..., S8) as premises, and gasket deflection and the leakage rate as consequences, then a fuzzy system of a minimum of  $2 \times 4 \times 8 = 64$  rules can be defined. The FDSS for this model is presented in Fig. 5.9, and as an example the rule no. 12 is written as:

*if system gas pressure, P(psi) is Low*  
*and gasket type is UC-FLX-GRT*  
*and gasket stress Sg (Kpsi) is S4*  
*then gasket deflection Dg (milli - in) is Dg15,*  
*and leakage rate, Lrm ( $10^{-3}$  mg/s) is Lrm19.*
(5.5)

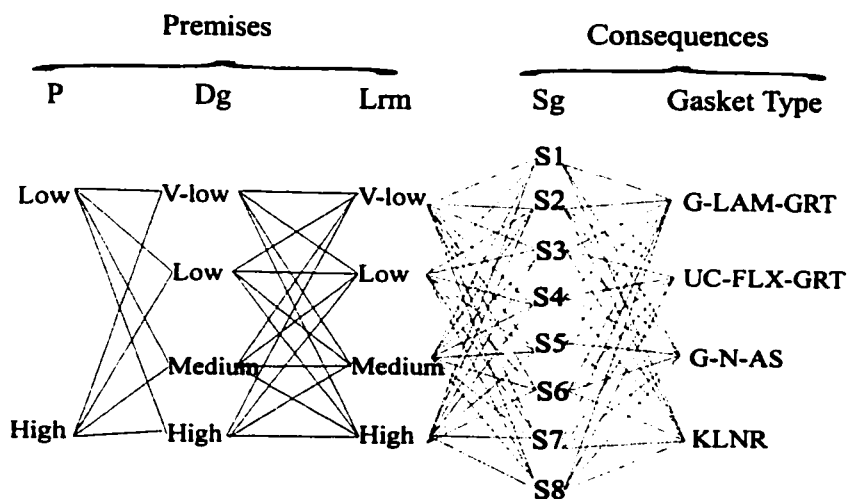


**Figure 5.7.** Network Representation of Possible Fuzzy Rules.

#### 5.8.4 Fuzzy model and obtained results

Using the information in the preceding sections, a fuzzy logic knowledge-based system was developed, from which we could write a number of rules to best present the experimental data, and our observations from gasket behaviour. Two models are presented, from the same sets of experimental data, based on the output classification results obtained from the classification engine. Certain criteria were adopted in the present algorithms, and each model comprises three membership functions (also referred to as parameters) in the fuzzy rule premises and two membership functions for the associated fuzzy rule consequences; the levels of membership functions for each algorithms were explained earlier:

**1. The input parameters are:**

1. System gas pressure,  $P$  (psig)
2. Gasket deflection,  $Dg$  (in)
3. Leakage rate,  $L_{rm}$  (mg/sec)

**The output parameters are:**

1. Gasket stress,  $Sg$  (p.s.i.)
2. Gasket type

**2. The input parameters are:**

1. System gas pressure,  $P$  (psig)
2. Gasket type
3. Gasket stress,  $Sg$  (p.s.i.)

**The output parameters are:**

1. Gasket deflection,  $Dg$  (in)
2. Leakage rate,  $L_{rm}$  (mg/sec)

The fuzzy network for algorithm 1 is presented in the preceding section in Fig. 5.7 where its corresponding fuzzy decision support system and results obtained are presented in Fig. 5.8, showing how the system works with three sets of premises and two sets of conclusions. The inputs and outputs of the fuzzy system are determined and are given as follows. The inputs to the system are: system helium gas pressure,  $P$  at 800 psig belonging to the fuzzy set *High*, the required or the expected gasket deflection,  $Dg$  at 20 milli-in belonging to fuzzy set *Low*, and the allowable leakage rate of the system,  $L_{rm}$  at  $750 \times 10^{-6}$  (mg/sec) belonging to fuzzy set *Low*, with a 100% certainty; where the

obtained values for consequences are: gasket stress level with crisp value of 6.300 Kp.s.i. belonging to the fuzzy set S3, and gasket type at crisp value of 5.00, corresponding to the G-N-AS gasket type. The compositional rule of inference (CRI) used is SUM-PROD, and the defuzzification of the fuzzy set to infer the consequent values was carried out using the COA (centre-of-area) defuzzification technique, as shown in Fig. 5.8.

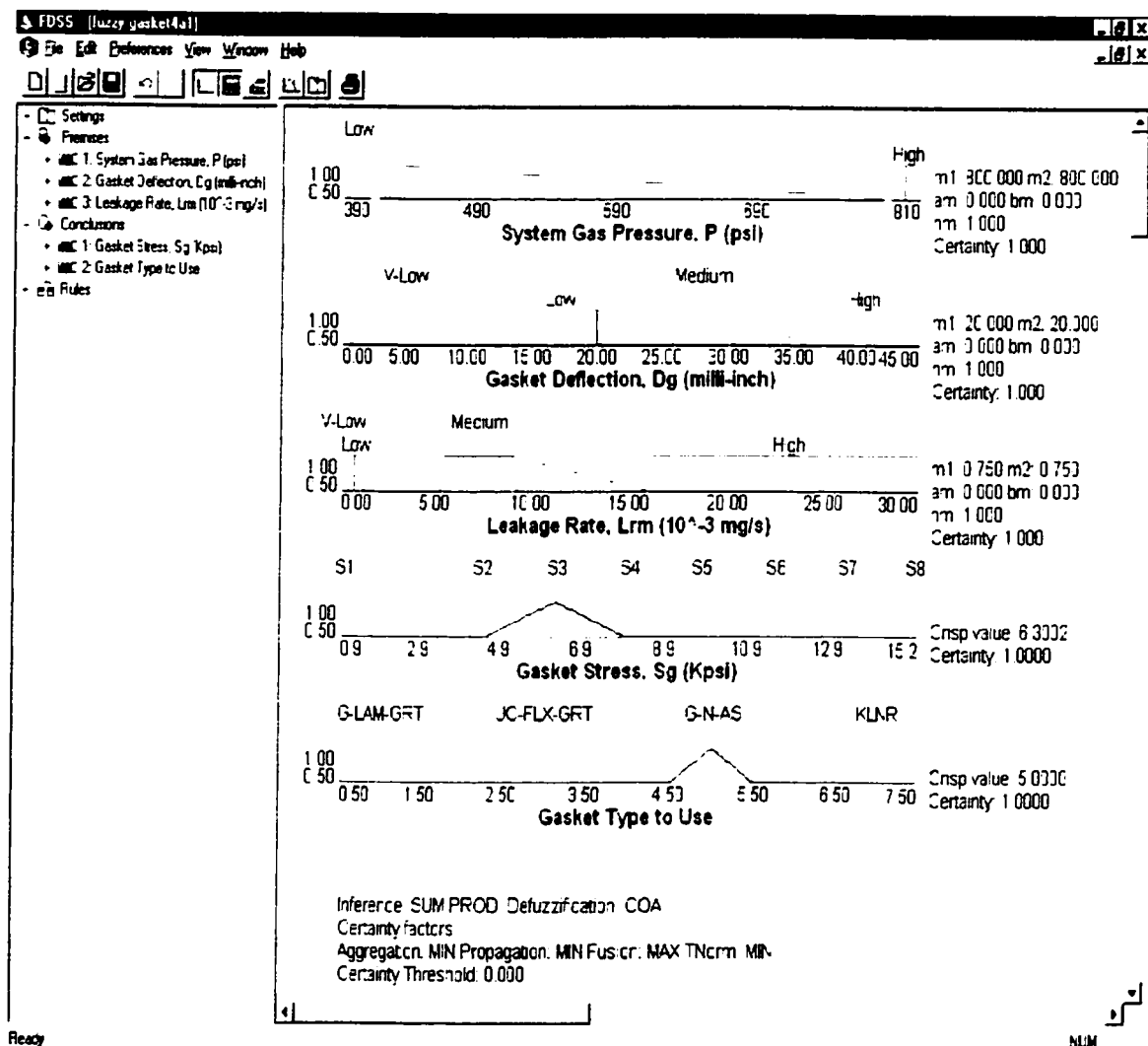


**Figure 5.8.** Fuzzy Decision Support System indicating input and output results. The compositional rule of inference is SUM-PROD, and the defuzzification technique is COA.

It is worth mentioning that for the same input values of the premises of the fuzzy system (Fig. 5.8) the consequent values for the stress level and the gasket type were obtained as 6.365 Kp.s.i. and 4.980 Kp.s.i., respectively, by using the MOM (mean of maxima) defuzzification technique. The figure is not shown for sake of brevity. The reason for this variation is that, in the COA defuzzification technique, the overlapping area of fuzzy output sets is counted only once, and for the present work it simulates the experimental results better.

The results of the second algorithm are presented in Figs 5.9(a), 5.9(b), and 5.10. In Fig. 5.9(a), the inputs to the system are: helium gas pressure at 400 psig from fuzzy set *Low*, G-N-AS gasket type at crisp value of 3.0, and the gasket stress at 4.50 Kp.s.i. corresponding to the fuzzy set of *S2*. As a result the expected gasket deflection is given as a crisp value 13.00 milli-in belonging to the fuzzy set *Dg7*, and the allowable leakage rate from the system is given as a crisp value  $798 \times 10^{-6}$  (mg/sec), corresponding to the fuzzy sets *Lrm13*. Similar to the first algorithm the compositional rule of inference and defuzzification technique used are SUM-PROD and COA, respectively.

The results in Fig. 5.9(b) indicate that, a fuzzy logic system can help predict and make better decisions, especially where experimental results are not available. It also helps to determine whether some input parameters can result in satisfactory outputs, for example: *if* the design parameters as input to the system are: helium gas pressure at 700 psig, gasket type is KLNLR indicated by value 4.0 and the gasket stress level is at 15.0 Kp.s.i., *then* the expected outputs from the system are: gasket deflection at 14.10 milli-in, and leakage rate at  $8.1 \times 10^{-6}$  (mg/sec). These results indicate that the KLNLR gasket performs extremely well at fairly high gas pressure and high stress level, so that it provides a low-to-average gasket deflection and extremely low leakage rate.

Now, based on the developed algorithms, it may be required to determine the effect of gas pressures, or stress levels on the leakage rate and gasket deflection for a specific gasket

type. This can be easily achieved by the FDSS. For instance, in Fig. 5.10, the inputs to the system are: helium gas pressure at 800 psig, gasket type G-N-AS at a crisp value of 3.0, and gasket stress at 5.0 Kp.s.i., which are similar to the inputs given in Fig. 5.9(a), except for the gas pressure. Now, comparing the results obtained from Figs 5.9(a) and 5.10, the effect of gas pressure on the leakage rate can be determined for the same gasket type and stress level. As a result, we note that increasing the gas pressure results in an increase of leakage rate given by a crisp value of  $184.0 \times 10^{-5}$  (mg/sec). Furthermore, the system infers that the gasket deflection remains the same at a crisp value of 13.0 milli-in. The results obtained from FDSS, presented in this section, closely follow the results obtained from the experimental tests and correctly correspond to the real situation.

In most practical applications in the industrial field, the main concern of the end-users or operators is what type of gasket provides the lowest leakage rate under minimum applied bolting load (gasket stress), without rigorous mathematical calculations, or without the performance of many experimental tests, and without spending hours of analysis of results by experts in this domain. In other words, the gasket end-users and operators require a system that can be used as a source of information and guidance which enables them to obtain reliable optimal results for gasket type, leakage rate, gasket stress, gasket deflection, etc., for given operating conditions. Furthermore, end-users require a system which allows them to make better decisions and one which reduces the operators' training time.

The existing methods of gasket testing and qualification in North America recognised by ASTM (American Society for Testing and Materials), PVRC (Pressure Vessel Research Council), MTI (Material Technology Institute of the Chemical Process Industries) are similar to those presented in [1—8]. Some of these test procedures are: ROTT (Room Temperature Tightness test), FIRS (FIRE Simulation screen test), ATRS (Aged Tensile Relaxation Screen test), ARLA (Aged Relaxation Leakage Adhesion screen test), HOTT (Hot Operational Tightness Test), AHOT (Aged Hot Operational Tightness test), HOBT

(Hot Blowout Test), EHOT (Emission Hot Tightness test), HATR (High temperature Aged Tensile Relaxation screen test).

In spite of the fact that these are the most reliable methods so far developed for gasket testing and qualification, they are costly, time consuming and require hours of analysis by experts in this domain. The cost of experiments, the difficulty of transformation of information, the vagueness and complexity of verification and analysis of the results, and the deficiency in the existing test devices, justifies the use of the FDSS system in this domain. FDSS is developed based on experimental data, field experience and expert knowledge, allowing for modelling of vague and imprecise information, and the consideration of missing data. The effect of single or multiple factors can be modelled simply and verified by such an approach. Thus, a properly designed fuzzy decision support system(s) which can incorporate many of the existing experimental results and field experience in combination with expert knowledge can be used as a simulation tool providing results close to real field observations. Furthermore, it can be used as a tool for prediction and decision making for end-users, and it may assist designers and developers to in determining design parameters for better gasket manufacturing and gasket qualification. While experimental results are the best source of information, the application of FDSS for gasketed bolted flanged joints would greatly reduce the number of experimental runs and tests points, facilitate the analysis of the results, save time, substantially reduce costs, and reduce the operators training time.

In the present work, the results obtained from FDSS are promising and closely correspond to our observations from the gasket behaviour in real situations. The problems indicated in this work, in combination with other technological factors, can be addressed to resolve a more sophisticated and complex system of gasketed bolted flanged joints. Additional factors can be added to the present fuzzy system, for this enhancement, such as: different types of fluids/gases (nitrogen, air), systems at elevated temperature, bolt creep, weight



loss of gasket material, effect of flange type, flange/platen surface form (grind, turned, milled) and surface roughness (10 to 1000  $\mu\text{in}$ ), etc.

## **5.9 Conclusion**

The paper has presented a new approach to the application of a fuzzy decision support system for gasket selection and sealing performance in gasketed bolted flanged joint applications. A fuzzy decision support system is applied based on experimental tests of different gasket types. The results obtained for optimal gasket selection and optimal leakage predictions are promising. It was shown that such a system provides better decision making for the selection of gaskets, based on system requirements, and helps to determine the system design parameters. The same method of building a fuzzy decision support system can be used in other areas of gasketed bolted flanged joint qualifications. Once the system is implemented, it can significantly reduce the number of tests and the associated costs.

The present and future research effort are aimed at developing methods to better predict and improve the behaviour of gasketed bolted flanged joints, through FDSS applications. A fuzzy logic system allows the consideration of many other factors and parameters that are difficult to measure. As well as dealing with missing data, it deals with vague and complex systems and provides a more precise estimation of leakage rate, gasket selection, and sealing performance.

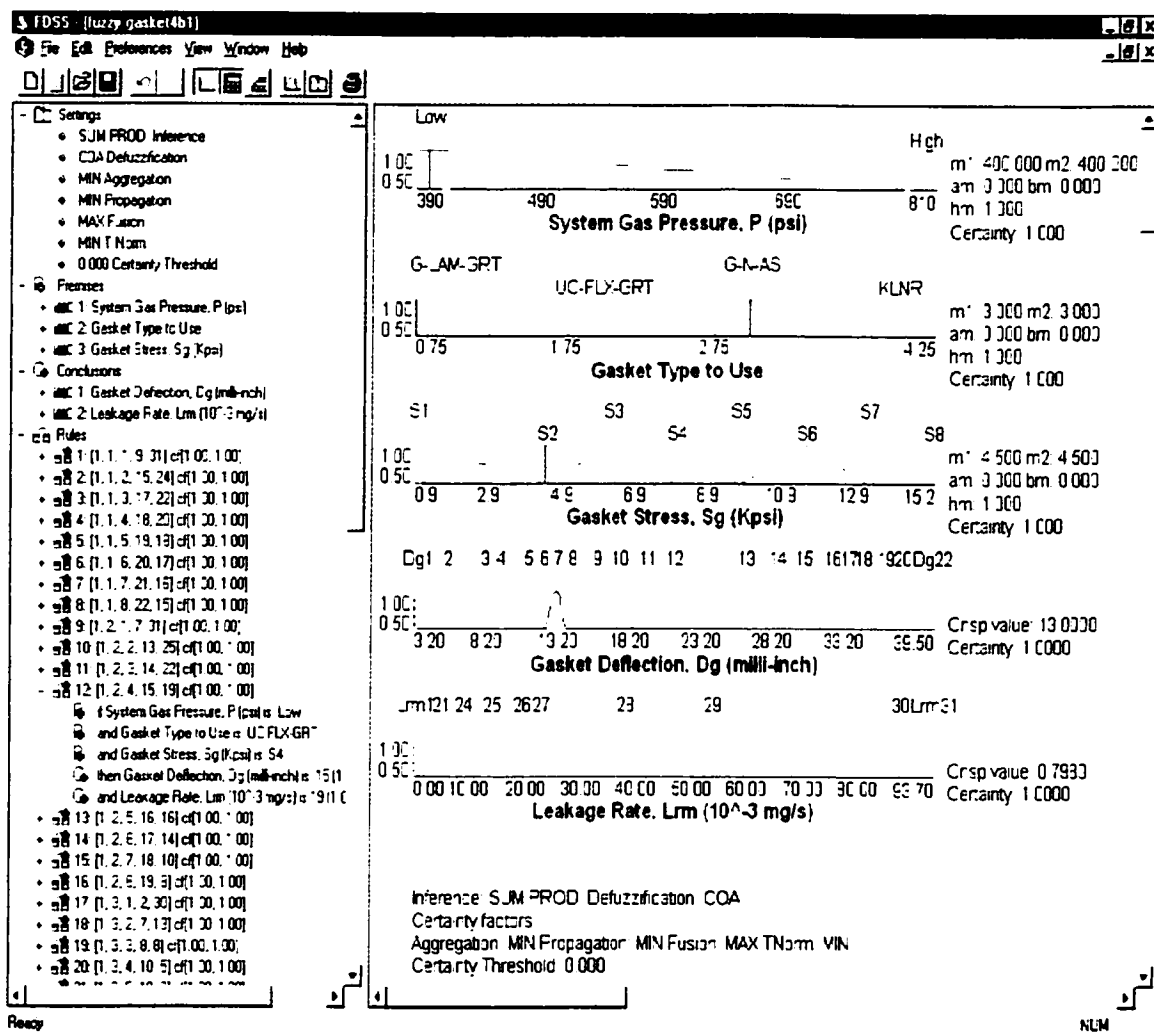


**Figure 5.9(a).** Fuzzy decision support system indicating input and output results. The compositional rule of inference is SUM.PROD, and COA is used as defuzzification technique.

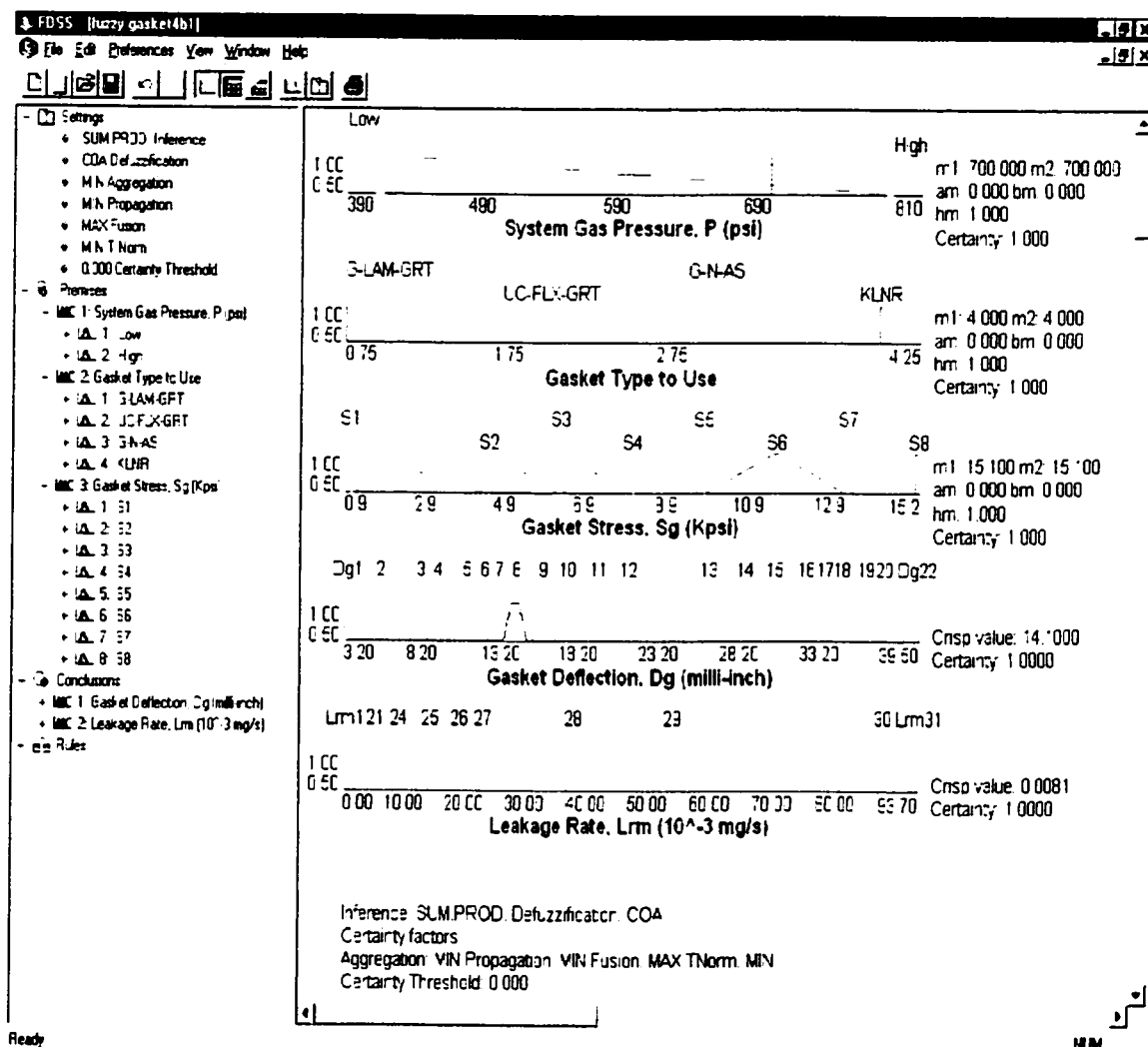
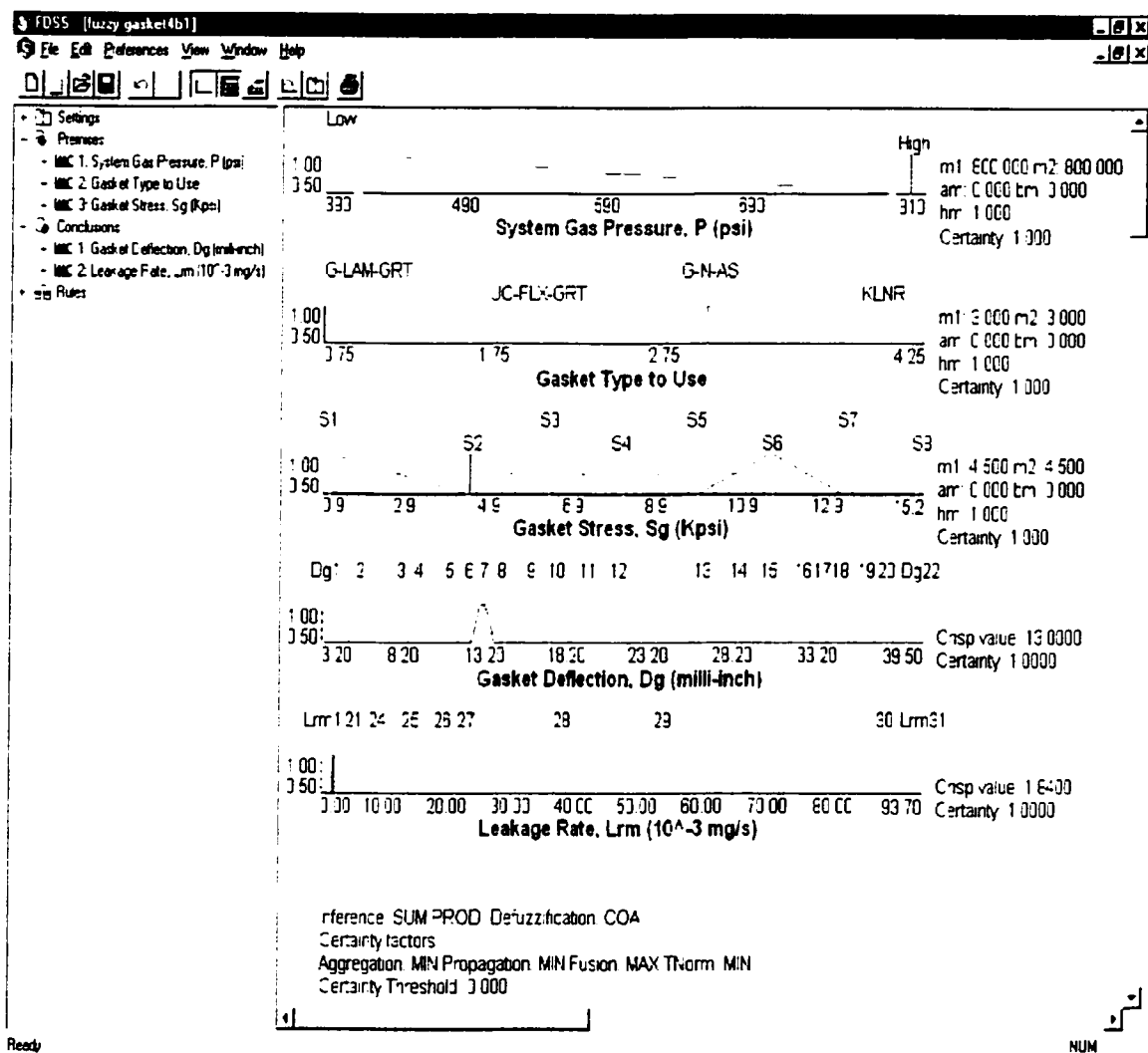


Figure 5.9(b). Continued.



**Figure 5.10.** Fuzzy decision support system indicating the effect of gas pressure on leakage rate in comparison with the input and output results presented in Fig. 5.9(a).

## 5.10 References

1. J. R. Payne, M. Derenne and L. Marchand, "Draft No. 9: standard test method for gasket constants for bolted joint design", proposed as an ASTM standard test procedure, 1994.
2. J. R. Payne, R. T. Mueller and A. Bazergui, "A gasket qualification test scheme for petrochemical plants; part I: test methods and application", PVP-ASME/JSME, Honolulu, vol. 158, pp. 53—68, July 1989.
3. J. R. Payne, R. T. Mueller and A. Bazergui, "A gasket qualification test scheme for petrochemical plants; part II: quality criteria and evaluation schemes", PVP-ASME/JSME, Honolulu, vol. 158, pp. 69—79, July 1989.
4. J. R. Payne, A. Bazergui, M. Derenne and L. Marchand, "Evaluation of test methods for asbestos replacement gasket materials", MTI Publication no. 36, Material Technology Institute of the Chemical Process Industries, 1990.
5. J. R. Payne, "Effect of flange surface finish on spiral wound gasket constants", 2<sup>nd</sup> *International Symposium on Fluid Sealing*, La Baule, France, pp. 81—90, 1990.
6. M. Derenne, L. Marchand, J. R. Payne and A. Bazergui, "Understanding the behaviour of gaskets for bolted flanged connections: status of the work in North America", presented at proceedings of the International Conference on Innovative Marine Material and Technologies, La Spezia, Italy, pp. 391—412, Oct. 1992.
7. M. Derenne and J. R. Payne, "New PVRC constants for gasket selection and new ASME Rules for bolted flanged joints", TTRL report prepared for PVRC, March 1997.
8. M. Derenne, and J. R. Payne, A. Bouzid and L. Marchand, "Proposed modifications to draft no. 9 of the standard test method for gasket constants for bolted joint design", FSA Spring Symposium, Nashville, Tennessee, USA, 26—28 April 1998.
9. L. A. Zadeh, "Fuzzy sets", *Information and Control*, 8, pp. 339—344, 1965.

10. L. A. Zadeh, "Outline of a new approach to the analysis of complex systems and decision processes", *IEEE Transactions on Systems, Man and Cybernetics*, **3**, pp. 28—44, 1973.
11. L. A. Zadeh, "Probability measure of fuzzy events", *Journal of Mathematical Analysis and Applications*, **23**, pp. 421—427, 1968.
12. L. A. Zadeh, "The concept of a linguistic variable and its application to approximate reasoning", *Information Science*, **8**, pp. 199—249, 1975.
13. L. A. Zadeh, "Fuzzy sets as a basis for theory of possibility", *Fuzzy Sets and Systems*, **1**, pp. 3—28, 1978.
14. L. A. Zadeh, "Theory of approximate reasoning", *Machine Intelligence*, **9**, pp. 149—194, 1979.
15. L. A. Zadeh, "Fuzzy logic", *IEEE-CS Computer*, **21(4)**, pp. 83—93, April 1988.
16. E. H. Mamdani, "Application of fuzzy set theory to control systems: A survey, in fuzzy Automata and Decision Processes", in M. M. Gupta, G.N. Saridis and B. R. Gaines, *Fuzzy Automata and Decision Processes*, North-Holland, NY, pp. 1—13, 1977.
17. P. M. Larsen, "Industrial applications of fuzzy logic control", *International Journal of Man-Machine Studies*, **12(1)**, pp. 3—10, 1980.
18. J. Arghavani, M. Derenne and L. Marchand, "Seating performance of gasketed flanged joints: a fuzzy decision support system approach", *International Journal of Advanced Manufacturing Technology*, **17(1)**, pp. 2-10, 2001.
19. M. Balazinski, M. Bellerose and E. Czogala, "Application of fuzzy logic technique to the selection of cutting parameters in machining processes", *Fuzzy Sets and Systems*, **56(3)**, pp. 273—280, 25 June 1993.
20. M. Balazinski, H. Boyer, E. Czogala and D. Grzerorz, "Fuzzy-Flou", *Ecole Polytechnique of Montreal, and Technical University of Silesia, Poland*, 1995.
21. L. H. Tsoukalas, and R. E. Uhring, *Fuzzy and Neural Approaches in Engineering*, John Wiley, pp. 105—130, 1997.

22. D. Dubois, and H. Prade, *Fuzzy Sets and Systems: Theory and Applications*, Academic Press, New York, 1980.
23. TTRL, Tightness Testing Research Laboratory, Ecole Polytechnique, Montreal, Canada.

## **CHAPTER 6**

### **FUZZY LOGIC APPROACH TO PREDICT GASKET LEAK RATE AND TO OBTAIN GASKET MINIMUM SEATING STRESS**

**J. Arghavani, L. Marchand and M. Derenne**

**Department of Mechanical Engineering, Applied Mechanics,**

**Ecole Polytechnique of Montreal**

**Montreal, Quebec, Canada**

#### **6.1 Presentation of the chapter**

In the present chapter, fuzzy logic models are used to predict the leakage rate and gasket performance of gasketed bolted flanged joints. Different fuzzy models are developed and validated with experimental results considering the gasket type, gas pressure, gasket stress levels and platens surface roughness. The fuzzy logic models describing the fuzzy range and parameters are described. The fuzzy rules of these models are defined based on test results obtained from the modified ROTT (Room Temperature Tightness Test) procedure. The experiment observations, based on ROTT tests, and fuzzy results are compared and presented in tables and graphical forms. These fuzzy results show good agreement with the experiments and indicate that fuzzy logic models developed can predict gasket leakage rate.



## 6.2 Abstract

The leakage rate prediction and control are of utmost importance in most industrial applications in gasketed bolted flanged joints in high pressure systems, for safety and environmental reasons. In addition, loss of media, and damages resulting from leaky uncontrolled joints can be very costly for the industries. However, gasket testing and the evaluation of their sealing performance are complex, time consuming and costly. In the present work fuzzy logic is used as a tool to predict the gasket leakage rate and the performance of gasketed bolted flanged joints. Different fuzzy models are developed and validated with experimental results for given operating conditions, considering the gasket type, gas pressure, gasket stress levels and platens surface roughness. It is shown that limited experimental test data can be used to build fuzzy models that predict gasket leakage rate. The leak rates obtained from the experiments and fuzzy are used to determine the new PVRC gasket constants,  $G_b$ ,  $a$ , and  $G_s$ , and consequently the minimum gasket seating stress. The experimental observations based on ROTT tests and the fuzzy results are compared and presented in tables and graphical forms. These results indicate that fuzzy algorithms can predict very closely the leakage rates obtained from the experiments. Furthermore, from these results we can conclude that the application of fuzzy logic in the area of gasketed flanged joints is appropriate, reducing test time and number of experiments.

**Keywords:** Leakage rate prediction, fuzzy logic, gasket performance, limited data points, PVRC gasket constants, gasket minimum seating stress.

## 6.3 Introduction

The analysis of the sealing phenomena and of leakage prediction are complex and time consuming, and to date most gasket evaluations have been performed based on a series of

lengthy and costly tests. The objective of most tests is to characterize gasket leakage behavior and to reduce emission accordingly. Many theoretical and experimental researches have been presented on gasket and joint performance evaluation, and the most relevant works to the present research have been cited in the authors' previous publications [1-3]. Gasket characterization techniques have been very well documented in the literature [5,6,7,8]. The authors' earlier works presented results on the fuzzy logic application in the evaluation of the gasketed flanged joints performance for the selection of platens surface roughness and gasket type [1, 2], using Fuzzy-Flou software of Balazinski et al. [4]. The experimental results in the authors work [3] indicate that the effect of surface characteristics on gasket behavior is complex. Analyzing and interpreting experimental results is a highly skilled task and requires experts "know-how" and intuitive sense through long-term experience in this domain. This is due to the fact that many unknown parameters, such as internal gas pressure, gasket properties, applied load and surface macro and microstructure, affect the leak rate and the flow regime. Furthermore, the combined effects of such parameters add to the complexity of the analysis. Analytical solutions to the problems associated with sealing phenomena, [3] as regards the number of surface asperities in contact, the geometry of interfacial leak paths on the mating surfaces (size, length and pattern), gasket porosity, deflection, etc. are complex. Such physical phenomena are not precisely measurable and their combined effects and behavior are not quantifiable, adding more to the complexity of analysis.

With fugitive emissions becoming one of the most important issues of environmental health and safety, future research should aim at addressing this fundamental issue by minimizing such emissions and by developing safer gasket and flange design procedures. The decision processes of properly selecting the key parameters through acceptable designs of gasketed flanged joints are vital to achieve leak minimization. Therefore, one must take into consideration all external and internal parameters affecting the system performance. However, the determination of the initial process key parameters for gasket

performance evaluation and analysis of the experimental gasket test results is complex and vague, time consuming and costly.

Therefore, that is why a fuzzy decision support system capable of dealing with such vagueness and predict leak rate can be applied. Fuzzy logic is an important tool that solves complex problems where analytical and mathematical approaches do not exist, are not feasible, or are too complex and costly to develop. Fuzzy logic can be used to reduce the complexity of existing solutions and to increase the accessibility of design parameters for leakage control. Furthermore, the application of fuzzy logic in this domain represents a relatively simple and less costly solution. Once the fuzzy decision support system (FDSS) is developed, the gasket leak rate prediction and system parameters selection can be made easily and accurately. The primary validation test of the fuzzy models has indicated that the fuzzy system can determine a set of system parameters for which a gasket can be characterized.

Before considering further the fuzzy logic modelling procedures, it is necessary to briefly discuss gasket behavior through PVRC gasket constant determination and gasket characterization [6].

#### **6.4 Gasket behavior**

Gasket behavior evaluation and gasket qualification are possible to do based on the room-temperature tightness test (ROTT) procedure [6,7], as described in section 6.7. ROTT test is a two part test that considers seating (Part A) and operation (Part B) stress sequence levels. Part A considers a sequence of increasing stress levels (gasket seating stress levels) where the leak rate and pressure are measured for each stress level. Part B, on the other hand, represents operation condition for several unload-reload cycles at constant gas pressure [3,5,6,7,8,]. This provides information about gasket tightness

(sealing performance) representing the conditions in which the gasketed bolted flanged joints are being affected by pressurization and relaxation. Gasket tightness may be considered as the minimum pressure at which small leaks will start. It measures the gasket ability to control the leak rate of the joint for the applied load. Therefore, a tight joint may be viewed as providing the lowest possible leak under the applied load and gas pressure. Tightness parameter  $T_p$  is defined as the system internal pressure relative to the atmospheric pressure required resulting in a helium leak rate of 1 mg/s for a reference gasket dimension of 150 mm OD. Tightness parameter is defined [6,7] by equation (6.1) as:

$$T_p = \left( \frac{P}{P^*} \right) \left[ \frac{L_{rm}^*}{L_{rm}} \right]^{0.5} \quad (6.1)$$

Where:

$P$  internal gas pressure psi (MPa)

$P^*$  atmospheric pressure (14.69 psi, 0.1013 Mpa)

$L_{rm}$  mass leak rate, mg/s

$L^*_{rm}$  reference mass leak rate of 1 mg/s, for a normalized gasket diameter of 150 mm OD.

From equation (6.1),  $T_p$  is proportional to the gas pressure and inversely proportional to the square root of leak rate. Because of the square root, a joint that is 10 times tighter leaks 100 times less, thus if a joint requires 1000 psig to cause a small leak, a pressure of 10 psig would cause the same small leak in a joint that is 100 times less tight. The minimum required tightness for the design has been defined by [6,7,8,9]:

$$T_{p \min} = 1.8257 \times C \times P_r \quad (\text{dimensionless}) \quad (6.2a)$$

$$T_{p \min} = 0.1243 \times C \times P \quad (P \text{ in psi, English unit}) \quad (6.2b)$$

$$T_{p\min} = 18.023 \times C \times P \quad (P \text{ in Mpa, SI unit}) \quad (6.2c)$$

where  $P_r = \frac{P}{P^*}$  pressure ratio,

$P$  and  $P^*$  are as above, and

$C$  is constant associated with the Tightness Class [9].

For instance, the standard tightness class T2 is assigned a  $C=1.0$  value, where the class T2 represents a nominal leak rate per unit diameter of  $Lrm = 2 \times 10^{-3}$  mg/sec-mm ( $4 \times 10^{-4}$  lbm/hr-in.). Other tightness classes are also introduced to reflect the need for tighter joints (lower leak rate) and also for those that larger leaks are permissible. These classes are referred to as Economy class T1 assigned  $C = 0.1$ , and Tight class T3 with  $C = 10$ , and Very Tight class T4, with  $C = 100$ . Each class differs from the other by two orders of magnitude in leak rate. Other tightness classes [9] are given in Table 6.1.

**Table 6.1.** Gasket tightness classes [9].

Tightness Classes	Mass leak rate per unit diameter		Constant $C$	Minimum tightness parameter/pressure ratio, $(T_{p\min}/P_r)$
	mg/sec-mm	lbm/hr-in.		
T1 (Economy)	$2 \times 10^{-1}$	$4 \times 10^{-2}$	$10^{-1}$	0.18257
T1-2	$2 \times 10^{-2}$	$4 \times 10^{-3}$	$10^{-1/2}$	0.57734
T2 (Standard)	$2 \times 10^{-3}$	$4 \times 10^{-4}$	1	1.8257
T2-3	$2 \times 10^{-4}$	$4 \times 10^{-5}$	$10^{1/2}$	5.7734
T3 (Tight)	$2 \times 10^{-5}$	$4 \times 10^{-6}$	10	18.257
T3-4	$2 \times 10^{-6}$	$4 \times 10^{-7}$	$10^{3/2}$	57.734
T4 (Very Tight)	$2 \times 10^{-7}$	$4 \times 10^{-8}$	100	182.57

### 6.4.1 PVRC gasket constants

The new ASME Boiler Code, flange design procedure, [5,8] considers three new constants  $G_b$ ,  $a$ , and  $G_s$  to design bolt load, or the required gasket stress to maintain a tight joint. These are briefly discussed herein, but for more details readers are encouraged to refer to reference [6,7,8]. These constants are obtained from the log-log plot of stress versus tightness parameter.  $G_b$ , and  $a$ , are respectively the stress intercept at  $T_p=1$  and the slope associated with a line determined from the best fit of the high seating stress levels of Part A data. Since  $G_b$ , and  $a$ , are determined from the seating stress sequence, they provide stresses similar to the ASME Code  $y$ .  $G_s$  is the stress intercept at  $T_p=1$  associated with the data from Part B unload-reload sequence, where the best fit lines of the Part B data tend to converge at a point. Together, constants  $G_b$  and  $a$  represent the capacity of the gasket to develop tightness upon initial seating.  $G_s$  characterizes tightness sensitivity to the operating bolt load loss which is caused by system pressurization, gasket creep or thermal disturbance.  $G_s$  indicates the minimum required operating stress on the gasket to maintain specified tightness on the joints. In general, low values of  $G_b$ ,  $a$ , and  $G_s$  indicate a tight gasket. A gasket with low  $G_s$  remains tight (minimum leak) under circumstances that reduce the gasket stress (the applied bolt load). A high value of  $G_s$  may indicate that the gasket is sensitive to unloading excursions or susceptible to blowout at low gasket load. The ASME Code  $m$  is similar to  $G_s$  since it provides a minimum gasket stress. However,  $m$  does not reveal any information about the leakage rate [6,7,8].

The gasket stress and tightness parameters based on new PVRC gasket constants  $G_b$ ,  $a$ , and  $G_s$  can be presented by the following relationship [6,7,8]:

$$S_g = G_b (T_p)^a \quad (6.3)$$

$G_b$  the intercept of the gasket loading curve at  $T_p = 1$ . (psi, Mpa)

- $Tp$  the tightness parameter, with respect to reference leak  
 $a$  slope of loading curve, equal to 0.5 for test with gas.

It is recommended for a safe joint design to consider gaskets that meet the hydrostatic test pressure  $P_{HT}$  at a minimum of 1.5 time the design pressure  $P_D$ , thus the ratio of  $\frac{P_{HT}}{P_D} \geq 1.5$ . Therefore, the assembly tightness  $Tpa$  value must be 1.5 time the minimum required joint tightness  $Tp_{min}$ ,  $Tpa = 1.5Tp_{min}$ , to ensure the satisfactory leak performance in operation [6,7].

#### 6.4.2 Gasket minimum seating stress

A simplified design bolt load calculation procedure for the determination of the required bolt load (minimum gasket seating stress  $S_g$ ) based on the PVRC gasket constants,  $G_b$ ,  $a$ , and  $G_s$  is briefly presented here. The procedure presented here is basically similar to the new ASME Code for calculating the gasket constants [5,6,12]. For details on the new ASME Code, see section 5.3 “*new tightness based rules*” and appendices, A, C and F of ref. [12].

The procedure used to calculate gasket minimum seating stress is presented in the following and illustrated in Figure 6.0. This procedure is coded in Excel-Visual Basic macros, as developed by Prof. Luc Marchand (co-director of this research), and uses iteration technique of “*GoalSeek*” function to calculate optimal gasket seating stress.

A proper gasket type and size (NPS) should be selected taking into the account the practical consideration that this gasket must have a tightness that is consistent with the specification of the level of leak.

1) Start with a permissible leak rate  $L_{He}$  (mg/s) and obtain the leak rate  $L_{He4}$  (mg/s) for a reference NPS 4 gasket ( $\approx 150$ mm gasket OD). The subscript “He” stands for helium gas.

$$L_{He4} = L_{He} \frac{OD_4}{OD_g} \quad (6.4)$$

$OD_4$  reference diameter, the outer diameter of NPS 4 gasket ( $\approx 150$ mm gasket OD.)

$OD_g$  outer diameter of gasket in test.

2) For the specified permissible leak rate, the appropriate gasket tightness,  $T_{pmin}$  (the gasket minimum tightness parameter) is calculated at a given operating gas pressure  $P$ .

$$T_{pmin} = \left( \frac{P}{P^*} \right) \left( \frac{1}{L_{He4}} \right)^{0.5} \quad (6.5)$$

3) A starting value for the seating stress  $Sg_{A1}$ , should be selected on the loading curve which is obtained from the gasket constant  $Gb$  and slope  $a$ . Consequently, the trail tightness parameter  $Tp$ , at this seating stress  $Sg_{A1}$  and from the constant  $Gb$  and slope  $a$  is obtained.

$$Tp_{A1} = \left( \frac{Sg_{A1}}{Gb} \right)^{(1/a)} \quad (6.6)$$

4) For a given gas pressure,  $P$ , there also exists a gasket change due to the hydrostatic end load effect,  $Lp$ , which is given as

$$L_p = P \frac{A_i}{Ag} = P \frac{G}{4 \cdot N} \quad (6.7)$$



$A_i$  internal pressurized gasket area en-circled by effective gasket diameter,  $G$

$$\frac{\pi}{4}(G_o - 2b)^2 = \pi \cdot G^2 / 4$$

$b$  effective gasket seating width, (in., mm)

$G$  effective pressurized gasket diameter, or mean gasket diameter  $G = \frac{(OD_g + ID_g)}{2}$   
 $= G_o - 2b$

$Ag$  gasket full contact area (gasket seating area) based on basic width,  $n_o$   
 $= 2 \cdot \pi \cdot b \cdot (G_o - 2b)$

$G_o$  gasket outside diameter, for a raised face or lap ring flange, in. (mm).

$N = 2b$  actual gasket contact (compressed) width,  $N = \frac{(OD_g - ID_g)}{2}$

$ID_g$  gasket inside diameter, in. (mm)

$ID_g$  gasket outside diameter, in. (mm)

4) The slope of unloading curve,  $b_1$ , is determined from the  $Sg_{A1}$  point on the loading curve to the  $G_s$  point, on the  $\log(Sg)$  vs  $\log(Tp)$  graph. On the graph it is the line connecting  $(Sg_{A1}, Tp_{A1})$  and  $(G_s, Tp=1)$ . By using the gasket constants, the gasket stress  $Sg_{A1} = G_b(Tp_{A1})^a$  and tightness parameter  $Tp_{A1} = (Sg_{A1} / G_b)^{1/a}$  the slope  $b_1$  is determined as follows:

$$b_1 = \frac{\log(Sg_{A1}) - \log(G_s)}{\log(Tp_{A1}) - \log(1)} = \frac{\log(Sg_{A1} / G_s)}{\log(Tp_{A1} / 1)} = \frac{\log(Sg_{B1} / G_s)}{\log(Tp_{B1} / 1)} \quad (6.8)$$

6) When the gasket is stressed to  $Sg_{A1}$ , the gasket unloading occurs as a result of system pressurization. Therefore considering this, the minimum operating stress  $Sg_{B1}$ , on the unloading curve, is obtained by subtracting the gasket change due to the hydrostatic end

load effect,  $L_p$ , from the seating stress  $Sg_{A1}$ . Hence,  $Sg_{B1}$  is the intersection of a horizontal line passing through  $Sg_{A1} - L_p$  and the unloading curve that is defined by the slope  $b_1$ .

$$Sg_{B1} = Sg_{A1} - L_p \quad (6.9)$$

7) Consequently the minimum operating tightness parameter  $Tp$  value at minimum gasket stress  $Sg_{B1}$  is obtained from.

$$\log(Tp_{B1}) = \log(Tp_{A1}) \cdot \frac{\log(Sg_{B1} / Gs)}{\log(Sg_{A1} / Gs)} \quad (6.10a)$$

$$Tp_{B1} = Tp_{A1}^{\left[ \frac{\log(Sg_{B1} / Gs)}{\log(Sg_{A1} / Gs)} \right]} \quad (6.10b)$$

If the  $Tp_{B1}$ , at operating condition is equal to the target  $Tp_{min}$  value, then the optimal gasket minimum tightness value is obtained. Otherwise, the iteration procedure continues, from step 1, by selecting a new  $Sg_{A1}$  and obtaining a new unloading curve  $b_1$  and so on. Therefore, for a gasket constant  $Gs$  there is an infinite number of unloading curves each associated with a unique  $Sg_{A1}$ .

Finally, when  $Tp_{B1} \geq Tp_{min}$  then the optimal  $Sg_{min}$  value is reached which gives the optimal tightness  $Tp_{B1}$ . Note that  $Tp_{B1}$  cannot be less than  $Tp_{min}$ . However, the lower and upper bounds of the test stress ( $Sg_{min}$  test and  $Sg_{max}$  test) must be considered for a safe design.

The ROTT tightness lower and upper bounds are specified as  $Tp_{min}(B)$  and  $Tp_{max}(A)$ . The  $Tp_{min}(B)$  is the lowest tightness found for a given gasket material in any Part B (unload-reload) cycle corresponding to the minimum operating stress  $Sg_{min}(B)$ . Generally the minimum operating gasket stress  $Sg_{min}(B)$  is the lowest gasket stress of the ROTT test

procedure applied on the gasket during the test. In the above iterative procedure, the lower bond " $Sg_{A2}$ " (the minimum gasket seating stress to maintain  $Sg_{min}$ ) is set to the greatest of  $(Sg_{min} + Lp)$  or  $(2P + Lp)$ . The former insures that the minimum seating stress is within the test parameters, while the latter is for safety purpose. Therefore, considering these limits in the above calculations, we have  $Sg_{A2} = \text{Max} ((Sg_{min} + Lp), (2P + Lp))$  and  $Sg_{B1} = \text{Max} (Sg_{A1}, Sg_{A2}) - Lp$  that are used in equation (6.9) during the iterative search.

The  $Tp_{max}(A)$  is the highest level of tightness achieved during the test in Part A, without tightness hardening (refer to ref. [12] for tightness hardening definition). The  $Tp_{max}(A)$  value for a given gasket material depends on the applied maximum gasket stress during the test,  $Sg_{max}(A)$ . Therefore, the upper bond is set to  $\text{Max} (Sg_{A1}, Sg_{A2}) \leq Sg_{max}(A)$ . The test stress levels and the maximum stress  $Sg_{max}(A)$  on the gasket depend on the ROTT test procedure used, namely *Soft*, *Standard* or *Hard* procedure, see ref. [3] for definition. It is also important to note that in the calculation of the above procedure the bolting efficiency is assumed to be 100%.

To this date, gasket leak emission has been determined by lengthy experimental methods such as ROTT test approved in the ASME Code [5,8], which allows us to obtain, from test data, the PVRC gasket constants,  $G_b$ ,  $a$  and  $G_s$ , for gasket characterization. Although experiments are vital to understand gasket leakage behavior and to characterize gaskets, to our knowledge, to date, no other approach exists to predict gasket leak emission. However, the application of fuzzy logic in this domain constitutes a new approach that can assist engineers and designers to determine the required leakage data and the design parameters based on limited test points.

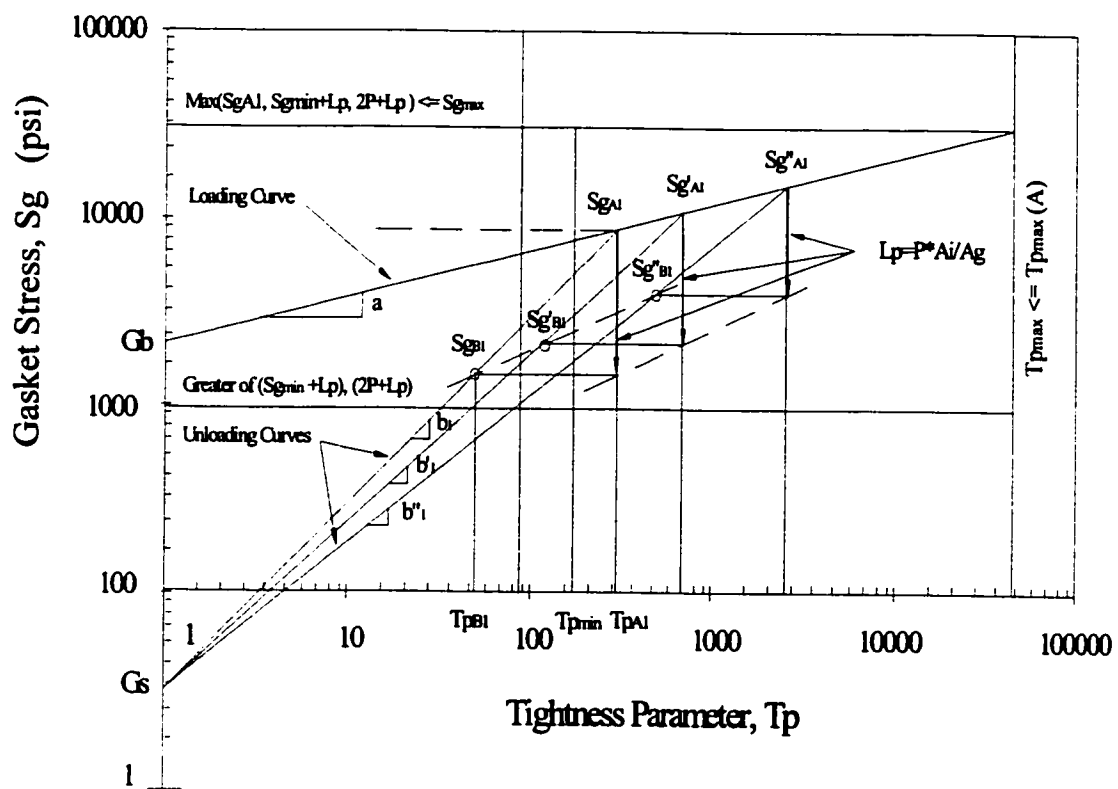


**Figure 6.0.** Design relationships and the idealized  $S_g$ - $T_p$  graph.

### 6.5 The use of fuzzy logic

The fuzzy logic approach presented in this work demonstrates that fuzzy algorithms developed based on limited data from the modified ROTT test procedure, not from the ROTT procedure itself [3], can predict leak emission of gasketed joints. The data obtained from fuzzy algorithms can be treated the same way as those obtained from experiments, for further analysis based on the existing analytical or mathematical models. The abovementioned gasket constants and gasket minimum seating stress can be obtained. Thus, such an approach allows us to reduce the test points and the number of experiments and therefore, save test time.

Fuzzy logic deals with the complexity of the system and of the parameters involved and takes into account the fuzziness, or variation, of the measurement results. As well, it considers the combined effects of key parameters, and mimics the trends to compensate for the effect of unknown parameters that otherwise would not be quantifiable by mathematical and analytical modeling.

Fuzzy logic is a rule based system. Fuzzy logic rules cover a wide range of variables and consider infinite crisp numbers and rules. The rules are developed in linguistic terms that address the relationship between the inputs and the outputs of a system. The rules are written in the forms of *if/then* and link the fuzzy set input parameters to their fuzzy set outputs with a set of classical logical “*And*”, “*Or*” functions [1,2,4], for example:

***For PTFE Gylon 3504 gasket***

***If*** the helium gas pressure varies between 400–410 psig.

***and*** the platens surface roughness ranges between 240–260  $\mu\text{in}$

***and*** gasket at load, Part A

***and*** the stress level on the gasket varies between 3900–4050 psi

***then*** the system leakage rate is about  $27.8 \times 10^{-6} \text{ (mg/s)}$ , [1.00]

The number in brackets at the end of the rule represents the rule weight, or the certainty level of the fuzzy rule, usually set to 1.0.

## 6.6 Present work

This work presents results for the prediction of gasket leakage rate based on fuzzy logic algorithms that are developed from limited experimental runs and test points, providing an insight of the fuzzy logic application in the area of gasketed flanged joints [1—3]. The fuzzy decision support system (FDSS) tool, called Fuzzy-Flou [4], is used for this purpose. Fuzzy algorithms are developed for different gasket types based on the results obtained from modified Room Temperature Tightness Test (ROTT) procedures with limited test points at constant helium gas pressure [3]. These test results are presented in an earlier work of the authors see reference [3]. The experimental test results from standard ROTT test procedure [5,6] for similar gasket types are used to validate the fuzzy algorithms' prediction.

The following sections present the experimental procedures and the results obtained from the different fuzzy logic algorithms (models) for the prediction of the leakage rate for specific gasket types and platens surface roughnesses. The leak rate results obtained from the fuzzy models are used to determine the PVRC gasket constants  $G_b$ ,  $a$ , and  $G_s$ , as well as the gasket minimum seating stress [5,6]. The results are compared with those obtained from the standard ROTT experiments.

## 6.7 Experimental procedure and data

### 6.7.1 ROTT procedure

The ROTT procedure is very well documented in the ASTM method Draft no 9 *of the standard method for gasket constants for bolted joint design* [5, 6]. This procedure is also summarized in the authors' work, in reference [3], with the corresponding tables and graphs, which are not presented here for sake of brevity.

In brief, the ROTT procedure is performed on NPS-4 in. gasket ( $\approx 150$  mm gasket O.D.) and platen surface finish of  $Ra$  250  $\mu\text{in}$  (6.35  $\mu\text{m}$ ). The test consists of two parts, loading (Part A) for seating stress and unloading (Part B) for operating stress levels. It comprises of 20 test points in three load-and-unload cycles. At each cycle the stress is increased incrementally and then is decremented to the initial stress level. ROTT test includes five main stress levels, S1 to S5, and intermediate stress levels S2.5, S3.5, and S4.5, [3]. At the main stress levels of Part A, the helium gas pressure is alternated to 400 and 800 psig (2.76 and 5.52 MPa), while during the Part B stress levels the gas pressure is maintained constant at 800 psig. The main stress levels values applied on the gasket depend on the gasket material. They are categorized in three sets, namely *soft*, *standard*, and *hard (solid metal)*, [3,5,6]. *Soft* stress values are considered for gaskets such as neoprene rubber, PTFE sheets and spiral wound gaskets of Class 150. *Standard* stress values are applied to most sheet and composite gaskets such as graphite sheet, metal jacketed and spiral wound types, except Class 150 for which the *soft* procedure is applied [6]. *Hard* procedure is not used in the present work.

It is worth indicating that, in the case of the PTFE gasket, the experimental data used for the verification of the fuzzy results were obtained with an earlier version of the PVRC gasket ROTT fixture [10]. The control instruments and leak measurement devices were also of different models. In addition, the test procedure used differed from the ROTT test procedure described in reference [3]. The most important difference between the two

procedures is that, in the earlier experiments, the PTFE gasket was exposed longer to the stress due to a larger number of increment/decrement gasket stress levels. Consequently, a longer gasket's exposure to load, affected the gasket deflection, as well as the gasket material flow into the platens surface irregularities, resulting in different leak rates. This could explain why, at some test points, there is a large variation between the leak results from the experiments and those obtained from the fuzzy.

### 6.7.2 Modified ROTT procedure

The modified ROTT procedure, unlike the standard ROTT procedure, is designed considering two load and unload cycles of nine test points of different stress levels, with the helium gas pressure maintained constant during the entire experiment to eliminate transitory gas pressure effect at each stress level during the test [3]. Depending on the gasket type, the test is performed based on *soft* or *standard* stress values at constant helium gas pressure at 200 and 800 psig (1.38 and 5.52 MPa), see Figure 6.1 and Table 6.2. This permits the evaluation of the sensitivity of the gasketed joint to the change of gas pressure, and the determination of the flow regimes [3]. As with the ROTT procedure, in the modified ROTT, the stress is increased incrementally and then decremented to the initial stress level, Table 6.2. This simulates the bolt load relaxation during the service and indicates the sensitivity of the leakage to the loss of stress of the system under investigation. The stress level at each stress point remains constant until the stabilized leakage rate is measured, then it is incremented or decremented to the next stress level.

Unlike the standard ROTT procedure that uses turned surface finish of 250  $\mu\text{in}$  (6.35  $\mu\text{m}$ ) roughness, the test platens used in the modified ROTT experiments are machined using grinding and turning procedures, giving an average arithmetic surface roughness value of 20  $\mu\text{in}$  (0.5  $\mu\text{m}$ ) and 900  $\mu\text{in}$  (22.8  $\mu\text{m}$ ), [3]. These ground and turned surfaces are



identified as IIII and II, respectively. The experimental results obtained from the modified ROTT procedure are presented in Tables 6.3 through 6.8.

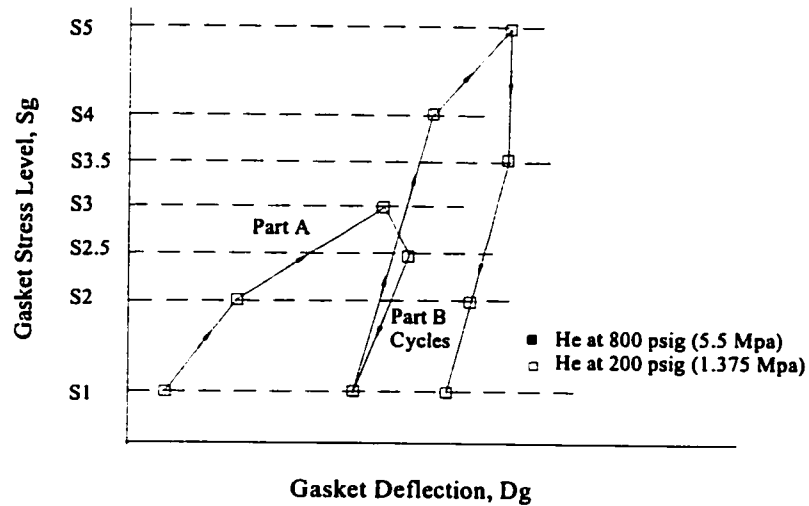


**Figure 6.1.** Modified generic ROTT test procedure sequence.

**Table 6.2.** Stress levels on gasket for the modified ROTT test procedure.

	Stress Levels	Soft Stress values		Standard Stress values		Gas Pressure, psig			
						Test Series 1		Test Series 2	
Cycle 1		psi	MPa	psi	MPa	psig	MPa	psig	MPa
	S1	1025	7.07	1025	7.07	200	1.38	800	5.52
	S2	3040	20.98	4560	31.46	200	1.38	800	5.52
	S3	5390	37.20	8090	55.82	200	1.38	800	5.52
	S2.5	4220	29.12	6325	43.64	200	1.38	800	5.52
	S1	1025	7.07	1025	7.07	200	1.38	800	5.52
Cycle 2	S1	1025	7.07	1025	7.07	200	1.38	800	5.52
	S4	7750	53.50	11630	80.25	200	1.38	800	5.52
	S5	10107	69.70	15160	104.60	200	1.38	800	5.52
	S3.5	6575	45.37	9860	68.03	200	1.38	800	5.52
	S2	3040	20.98	4560	31.46	200	1.38	800	5.52
	S1	1025	7.07	1025	7.07	200	1.38	800	5.52

### 6.7.3 Test gaskets

Three types of gaskets are used in this work, namely:

- PTFE GYLON 3504 sheet of thickness 0.064 in., are cut to an inside diameter of 4.875 in. and an outside diameter of 5.875 in.
- UCAR G2 flexible graphite sheet of thickness 0.062 in. are cut to an inside diameter of 4.875 in. and an outside diameter of 5.875 in.
- Flexitallic spiral wound (SW), NPS 4-in class 600 lbs with graphite infilling, having the initial dimensions of 4.75 ID  $\times$  5.875 OD  $\times$  0.177 in. thick, [3].

These gaskets are the most commonly used in the industries, and the test performed on them can cover a broad range of gaskets since they have totally distinguished characteristics from one to another. The specification and experimental analysis performed on these gaskets are given in ref. [3] and are not presented here for sake of brevity. However, in brief, we can mention that, under moderate to high load, the PTFE gasket provides a high degree of flexibility to fill-in the surface roughness, irregularities and the existing gaps on the platens surfaces generated by the machining processes. This gasket type has a low degree of porosity.

The G2 graphite gasket is typically made of particulate graphite flakes and provides the necessary filling in the platens surfaces irregularities, due to its flexibility, and should remain adhering to the flange surfaces provided that the load remains stable. However, this gasket type is fairly porous. The consistency between the experimental data is ensured as the PTFE and the G2 graphite gaskets are cut from the same respective sheets.

The spiral wound (SW) gasket is of semi-metallic type with in-filled flexible graphite material. It provides initial filling of the irregularities on the flange faces at the initial loadings. This type of gasket should provide sufficient endurance and stability for the

duration of the operating service, and should resist higher loads and provide sufficient tightness during the operation if the load is maintained.

## 6.8 Fuzzy algorithms and rules

Fuzzy algorithms, also referred to as fuzzy models, are developed based on the format requirements of the Fuzzy-flou software [4], and are also discussed in earlier works of the authors [1,2]. The experimental data used to develop the fuzzy models and the fuzzy rules are presented in the precedent section, Tables 6.3 through 6.8. Based on the classification model presented in Balazinski et al. [4], the fuzzy algorithms are made for a MISO system (multiple input and single output system). These algorithms adopt certain criteria and the models are comprised of three membership functions, or parameters, in the fuzzy rule premises (input) and of one membership function for the associated fuzzy consequence (output) [11]. Fuzzy algorithms consider the effect of loading and unloading stress levels in the development of the rules, using Part A and Part B leak data from modified ROTT tests.

It is worth indicating that in the unload Part B of cycle one and two, the experiments provide leak rates that correspond to the stress levels S1, S2.5, S3.5, Table 6.3 through 6.8. However, in order to incorporate the data from both Part A and Part B in the fuzzy algorithms, it is necessary to have the leak rates for stress S1, S2, S3, S4, and S5 of both load and unload parts. Therefore, the leak rate values for stress levels S2, S3, and S4 for Part B are determined by two- and three-point Lagrangian interpolation formula. The two-point Lagrangian formula is:

$$y = \left\{ \frac{x - x_2}{x_1 - x_2} \right\} y_1 + \left\{ \frac{x - x_1}{x_2 - x_1} \right\} y_2, \text{ and can be rearranged as: } y = y_1 + \left( \frac{x - x_1}{x_2 - x_1} \right) (y_2 - y_1)$$

The three-point Lagrangian formula can be written as:

$$y = k_1 y_1 + k_2 y_2 + k_3 y_3, \text{ where } k_1 = \left( \frac{x - x_2}{x_1 - x_2} \right) \left( \frac{x - x_3}{x_1 - x_3} \right), \text{ etc.}$$

Consequently, the premises membership functions, also called input parameters, of the fuzzy algorithm [11] are selected as:

1. Helium gas pressure,  $P$  psig
2. Platens surface roughness,  $Ra$   $\mu\text{in.}$
3. Loading and unloading stress levels
4. Gasket stress,  $Sg$  psi

And the resultant output parameter or consequence is:

1. System leakage rate,  $L_{rm}$  mg/s

The levels for each membership function (parameter) are defined as:

1. Gas pressure is at two levels 200 and 800 psig (0.138 MPa, 5.52 MPa), corresponding to the low and high pressure respectively. Thus, the input fuzzy gas pressure values within these ranges may be used to evaluate the gas pressure effect on the leak rate.
2. Platens surface roughness is at two levels: III1 20  $\mu\text{in.}$  (0.508  $\mu\text{m}$ ) and I1 900  $\mu\text{in.}$  (22.86  $\mu\text{m}$ ). It is assumed that smooth turned and ground surface finishes of surface roughness value of 20  $\mu\text{in.}$  (0.508  $\mu\text{m}$ ) will perform the same, providing the same gasket deflection and leak rate under the same operating conditions. Based on that assumption, the surface roughnesses of the ground type finish III1 20  $\mu\text{in.}$  (0.508  $\mu\text{m}$ ) and turned type finish I1 900  $\mu\text{in.}$  (22.86  $\mu\text{m}$ ) are used as the low and high roughness levels of the membership function.

3. Loading Part A and unloading Part B stress levels. These two levels of membership function will indicate whether the gasket is in the seating or operating stress level.
4. Gasket stress is at five levels: S1, S2, S3, S4, and S5, where the highest number represents the highest stress level. Therefore, in combination with the Part A and Part B, the fuzzy rules mimic the trend to provide leak results from the stress value in seating or operating levels. The associated stress values for each stress level are set based on the values presented in Table 6.2. The *soft* values are considered for PTFE gasket, and the *Standard* values for graphite and spiral wound gaskets, as described earlier.
5. Leakage rate levels membership functions are defined based on classification procedures described in reference [1,2,4].

Based on the algorithm presented above with four input parameters (premises membership function) at 2, 2, 2 and 5 levels and one consequence (regardless of its membership function levels), a minimum of  $2 \times 2 \times 2 \times 5 = 40$  rules is defined. It must be noted that the membership function level of consequence does not have any impact on the number of fuzzy rules. Based on the information presented above, three algorithms for the three types of gaskets, mentioned in the preceding section, are developed. The generic graphical representation of the fuzzy algorithms described above, obtained from the Fuzzy-Flou software [4], is presented in Figure 6.2 (A & B), for PTFE gasket, showing the premises, the consequence and the rules. The graphical representation for the two other types of gaskets G2 and SW remains the same and therefore is not repeated here.

**Table 6.3.** PTFE tests results at 200 and 800 psig, with platens I1 Ra 900  $\mu$ in.  
(modified Soft ROTT procedure)

PTFE GYLON 3504 I1 P200							
4.875 x 5.875 x 0.066 in. 1/2"							
SURFACE FINISH I1 900,900 $\mu$ in							
STEP	Dg AVE. in.	Sg psi	P psig	LEAK mg/s	TIME hr	PART	Tp
S1	0.0105	1027	200	3.56E-03	5.247	A	228
S2	0.0177	3046	201	3.92E-05	7.44	A	2188
S3	0.0228	5340	201	2.31E-05	9.632	A-B1	2847
S2.5	0.0223	4193	201	1.64E-05	11.824	B1	3382
S1	0.0194	1050	201	1.96E-05	14.026	B1	3093
S4	0.0257	7741	201	8.01E-06	16.224	A	4836
S5	0.0279	10034	201	6.41E-06	18.416	A-B2	5406
S3.5	0.0266	6564	201	6.41E-06	20.608	B2	5405
S1	0.0223	1015	201	1.07E-05	22.834	B2	4187

PTFE GYLON 3504 I1 P800							
4.875 x 5.875 x 0.066 in. 1/2"							
SURFACE FINISH I1 900,900 $\mu$ in							
STEP	Dg AVE. in.	Sg psi	P psig	LEAK mg/s	TIME hr	PART	Tp
S1	0.0077	1040	787	5.65E-01	0.243	A	71
S2	0.0145	3046	801	9.08E-05	2.437	A	5717
S3	0.0200	5327	801	5.87E-05	4.631	A-B1	7107
S2.5	0.0195	4200	801	4.81E-05	6.821	B1	7858
S1	0.0165	1014	801	1.17E-04	9.018	B1	5025
S4	0.0231	7713	801	2.67E-05	11.216	A	10543
S5	0.0255	10058	801	1.96E-05	13.408	A-B2	12312
S3.5	0.0242	6550	801	1.96E-05	15.6	B2	12311
S1	0.0198	1072	801	4.09E-05	17.819	B2	8514

**Table 6.4.** PTFE tests results at 200 and 800 psig, with platens III1 Ra 20  $\mu$ in.  
(modified Soft ROTT procedure)

PTFE GYLON 3504 III1 P200							
4.875 x 5.875 x 0.062 in. ½"							
SURFACE FINISH III1 20,20 $\mu$ in							
STEP	Dg AVE. in.	Sg psi	P psig	LEAK mg/s	TIME hr	PART	Tp
S1	0.0072	936	194	8.05E-02	0.237	A	46
S2	0.0152	3020	201	1.64E-05	2.675	A	3386
S3	0.0226	5397	201	1.53E-05	5.117	A-B1	3502
S2.5	0.0221	4253	201	1.23E-05	7.31	B1	3910
S1	0.0193	1056	201	4.45E-05	9.762	B1	2054
S4	0.0296	7794	201	8.01E-06	12.959	A	4841
S5	0.0341	10131	201	6.05E-06	15.651	A-B2	5568
S3.5	0.0328	6531	201	6.41E-06	17.843	B2	5413
S1	0.0288	1046	201	2.31E-04	20.069	B2	900

PTFE GYLON 3504 III1 P800							
4.875 x 5.875 x 0.062 in. ½"							
SURFACE FINISH III1 20,20 $\mu$ in							
STEP	Dg AVE. in.	Sg psi	P psig	LEAK mg/s	TIME hr	PART	Tp
S1	0.0065	890	188	1.41E-01	0.236	A	34
S2	0.0149	3042	801	1.01E-04	5.464	A	5409
S3	0.0228	5377	801	4.81E-05	9.902	A-B1	7860
S2.5	0.0223	4165	801	4.45E-05	12.592	B1	8168
S1	0.0192	1030	801	1.07E-03	14.788	B1	1667
S4	0.0284	7712	801	3.56E-05	16.987	A	9132
S5	0.0329	10118	801	2.67E-05	19.179	A-B2	10546
S3.5	0.0317	6573	801	2.85E-05	21.371	B2	10210
S1	0.0273	1046	799	1.96E-02	23.59	B2	389

**Table 6.5.** G2 tests results at 200 and 800 psig, with platens I1 Ra 900  $\mu$ in.  
(modified Standard ROTT procedure)

G2 GRAPHITE I1 P200							
4.875 x 5.875 x 0.062 in. 1/2"							
SURFACE FINISH I1 900,900 $\mu$ in							
STEP	Dg AVE. in.	Sg psi	P psig	LEAK mg/s	TIME hr	PART	Tp
S1	0.0191	897	198	3.26E-02	0.234	A	75
S2	0.0321	4521	199	1.44E-03	2.682	A	357
S3	0.0364	8077	201	6.23E-04	4.876	A-B1	547
S2.5	0.0357	6302	201	7.12E-04	7.066	B1	512
S1	0.0319	1063	199	1.44E-03	9.273	B1	357
S4	0.0393	11545	201	3.38E-04	11.474	A	744
S5	0.0413	15057	201	4.45E-05	13.667	A-B2	2054
S3.5	0.0398	9772	201	1.26E-04	15.859	B2	1219
S1	0.0345	1060	201	1.53E-03	18.092	B2	349

G2 GRAPHITE I1 P800							
4.875 x 5.875 x 0.062 in. 1/2"							
SURFACE FINISH I1 900,900 $\mu$ in							
STEP	Dg AVE. in.	Sg psi	P psig	LEAK mg/s	TIME hr	PART	Tp
S1	0.0189	1039	778	2.23E-01	0.244	A	112
S2	0.0317	4565	798	2.73E-02	0.438	A	328
S3	0.0363	8111	798	6.41E-03	5.913	A-B1	678
S2.5	0.0356	6314	797	7.30E-03	11.1	B1	635
S1	0.0313	1018	797	3.14E-02	11.295	B1	306
S4	0.0391	11599	800	1.96E-03	13.497	A	1230
S5	0.0409	15010	801	4.63E-04	15.69	A-B2	2532
S3.5	0.0396	9798	800	7.48E-04	17.882	B2	1992
S1	0.0341	1046	789	1.02E-01	18.1	B2	168



**Table 6.6.** G2 tests results at 200 and 800 psig, with platens III1 Ra 20  $\mu$ in.  
(modified Standard ROTT procedure)

G2 GRAPHITE III1 P200							
4.875 x 5.875 x 0.062 in. 1/2"							
SURFACE FINISH III1 20,20 $\mu$ in							
STEP	Dg AVE. in.	Sg psig	P psig	LEAK mg/s	TIME hr	PART	Tp
S1	0.0152	920	198	3.11E-02	0.237	A	76
S2	0.0281	4519	201	7.83E-03	2.435	A	154
S3	0.0321	8016	201	2.14E-03	4.628	A-B1	296
S2.5	0.0314	6369	201	2.49E-03	6.819	B1	274
S1	0.0273	995	201	6.41E-03	9.027	B1	171
S4	0.0349	11542	202	6.41E-04	11.228	A	542
S5	0.0368	15063	202	1.17E-04	13.421	A-B2	1265
S3.5	0.0354	9814	202	1.78E-04	15.614	B2	1028
S1	0.0298	1005	201	1.64E-03	17.847	B2	339

G2 GRAPHITE III1 P800							
4.875 x 5.875 x 0.062 in. 1/2"							
SURFACE FINISH III1 20,20 $\mu$ in							
STEP	Dg AVE. in.	Sg psi	P psig	LEAK mg/s	TIME hr	PART	Tp
S1	0.0153	1051	784	1.75E-01	0.243	A	127
S2	0.0280	4568	799	1.88E-02	0.436	A	397
S3	0.0324	8124	801	6.41E-03	2.63	A-B1	681
S2.5	0.0316	6258	801	7.30E-03	4.82	B1	638
S1	0.0275	1023	799	2.31E-02	7.021	B1	357
S4	0.0350	11652	801	1.96E-03	9.223	A	1232
S5	0.0368	15145	801	4.81E-04	11.416	A-B2	2487
S3.5	0.0355	9810	801	6.94E-04	14.1	B2	2069
S1	0.0300	1018	801	8.37E-03	16.325	B2	595

**Table 6.7.** SW tests results at 200 and 800 psig, with platens I1 Ra 900  $\mu\text{in}$ .  
(modified Standard ROTT procedure)

SW Flex-4-600 I1 P200							
4.750 x 5.875 x 0.178 in.							
SURFACE FINISH I1 900,900 $\mu\text{in}$							
STEP	Dg AVE. in.	Sg psi	P psig	LEAK mg/s	TIME hr	PART	Tp
S1	0.0138	979	201	1.28E-02	2.245	A	121
S2	0.0296	4517	202	1.76E-03	4.704	A	327
S3	0.0422	8023	202	4.81E-04	7.162	A-B1	626
S2.5	0.0411	6307	202	5.16E-04	9.352	B1	604
S1	0.0342	1069	202	1.76E-03	11.561	B1	327
S4	0.0523	11550	202	1.09E-04	16.292	A	1317
S5	0.0575	15080	202	1.64E-05	18.994	A-B2	3390
S3.5	0.0558	9842	202	1.96E-05	21.186	B2	3101
S1	0.0467	1047	202	8.72E-04	23.422	B2	464

SW Flex-4-600 I1 P800							
4.750 x 5.875 x 0.178 in.							
SURFACE FINISH I1 900, 900 $\mu\text{in}$							
STEP	Dg AVE. in.	Sg psi	P psig	LEAK mg/s	TIME hr	PART	Tp
S1	0.0140	972	201	1.28E-02	2.494	A	121
S2	0.0316	4535	801	6.76E-03	4.744	A	663
S3	0.0440	8048	801	1.76E-03	7.201	A-B1	1298
S2.5	0.0430	6315	801	1.96E-03	9.393	B1	1232
S1	0.0358	1034	801	9.79E-03	12.345	B1	551
S4	0.0534	11532	801	5.70E-04	16.572	A	2284
S5	0.0588	15015	801	1.67E-04	18.775	A-B2	4214
S3.5	0.0572	9828	801	2.14E-04	20.967	B2	3729
S1	0.0479	1034	801	4.81E-03	23.194	B2	786

**Table 6.8.** SW tests results at 200 and 800 psig, with platens III1 Ra20  $\mu$ in.  
(modified Standard ROTT procedure)

SW Flexitallic NPS-4-600 III1 P200							
4.750 x 5.875 x 0.178 in.							
SURFACE FINISH III1 20,20 $\mu$ in							
STEP	Dg AVE. in.	Sg psi	P psig	LEAK mg/s	TIME hr	PART	Tp
S1	0.0094	906	200	2.55E-02	0.238	A	85
S2	0.0257	4509	201	1.64E-03	2.447	A	338
S3	0.0439	8043	201	5.70E-04	4.659	A-B1	574
S2.5	0.0430	6314	201	6.41E-04	6.851	B1	541
S1	0.0358	1064	201	4.45E-03	9.059	B1	205
S4	0.0507	11537	202	3.74E-04	11.285	A	709
S5	0.0545	15037	201	2.85E-04	13.486	A-B2	812
S3.5	0.0529	9847	202	3.38E-04	15.678	B2	745
S1	0.0446	1054	201	3.38E-03	17.914	B2	235

SW Flexitallic NPS-4-600 III1 P800							
4.750 x 5.875 x 0.178 in.							
SURFACE FINISH III1 20,20 $\mu$ in							
STEP	Dg AVE. in.	Sg psi	P psig	LEAK mg/s	TIME hr	PART	Tp
S1	0.0093	929	200	2.42E-02	0.422	A	87
S2	0.0297	4515	801	5.87E-03	2.667	A	711
S3	0.0447	8020	801	2.14E-03	6.622	A-B1	1179
S2.5	0.0436	6383	801	2.49E-03	8.813	B1	1091
S1	0.0360	1069	799	2.48E-02	9.012	B1	345
S4	0.0541	11560	801	1.14E-03	11.229	A	1614
S5	0.0580	15031	801	8.01E-04	13.428	A-B2	1925
S3.5	0.0565	9839	801	1.07E-03	16.619	B2	1667
S1	0.0472	1068	798	4.82E-02	16.843	B2	247

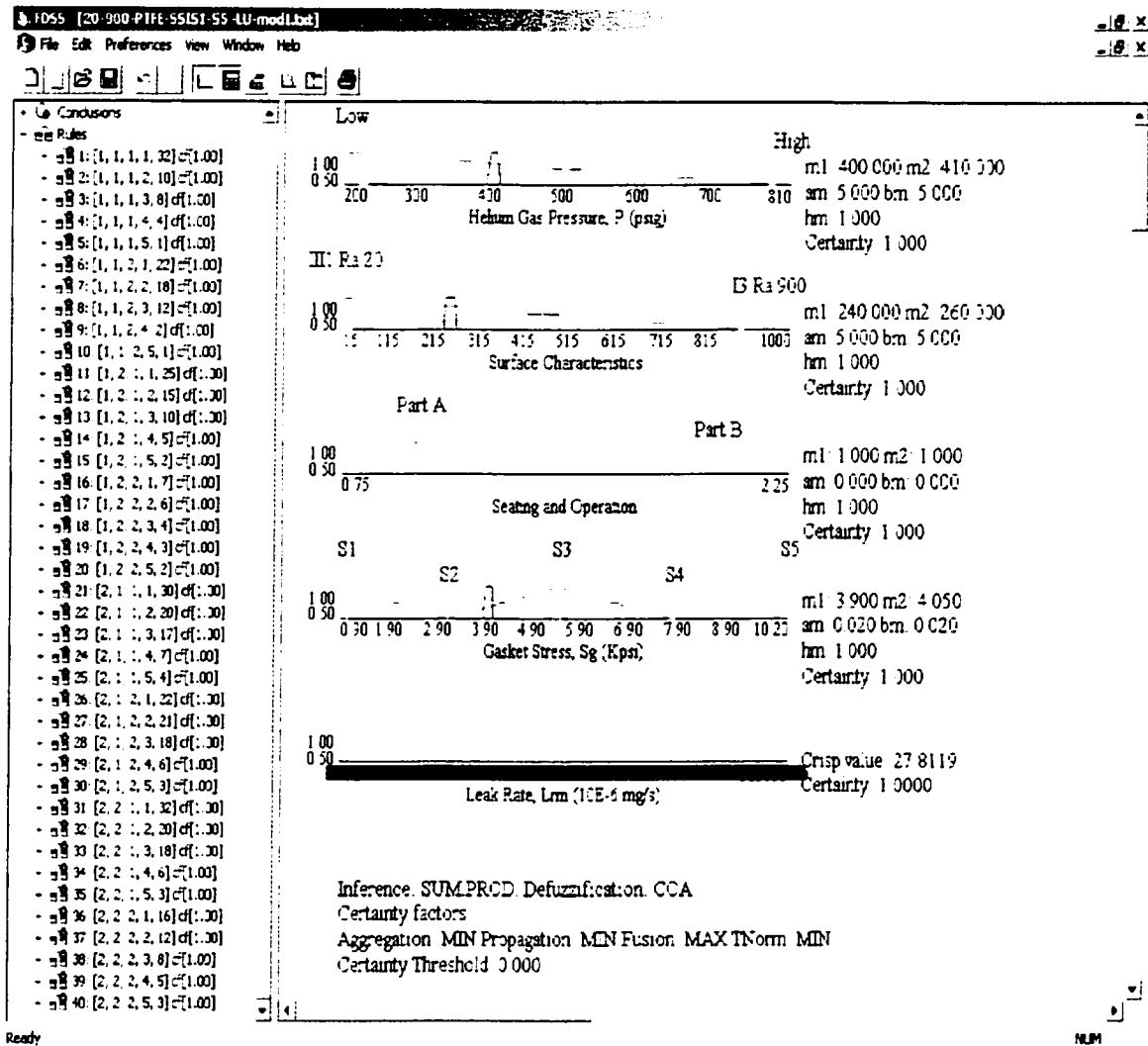


**Figure 6.2 A.** PTFE gasket, predicting the leakage rate at seating stress, for gas pressure 400-410 psig, surface characteristics Ra 240-260  $\mu$ in, and gasket stress 3900-4050 psi.

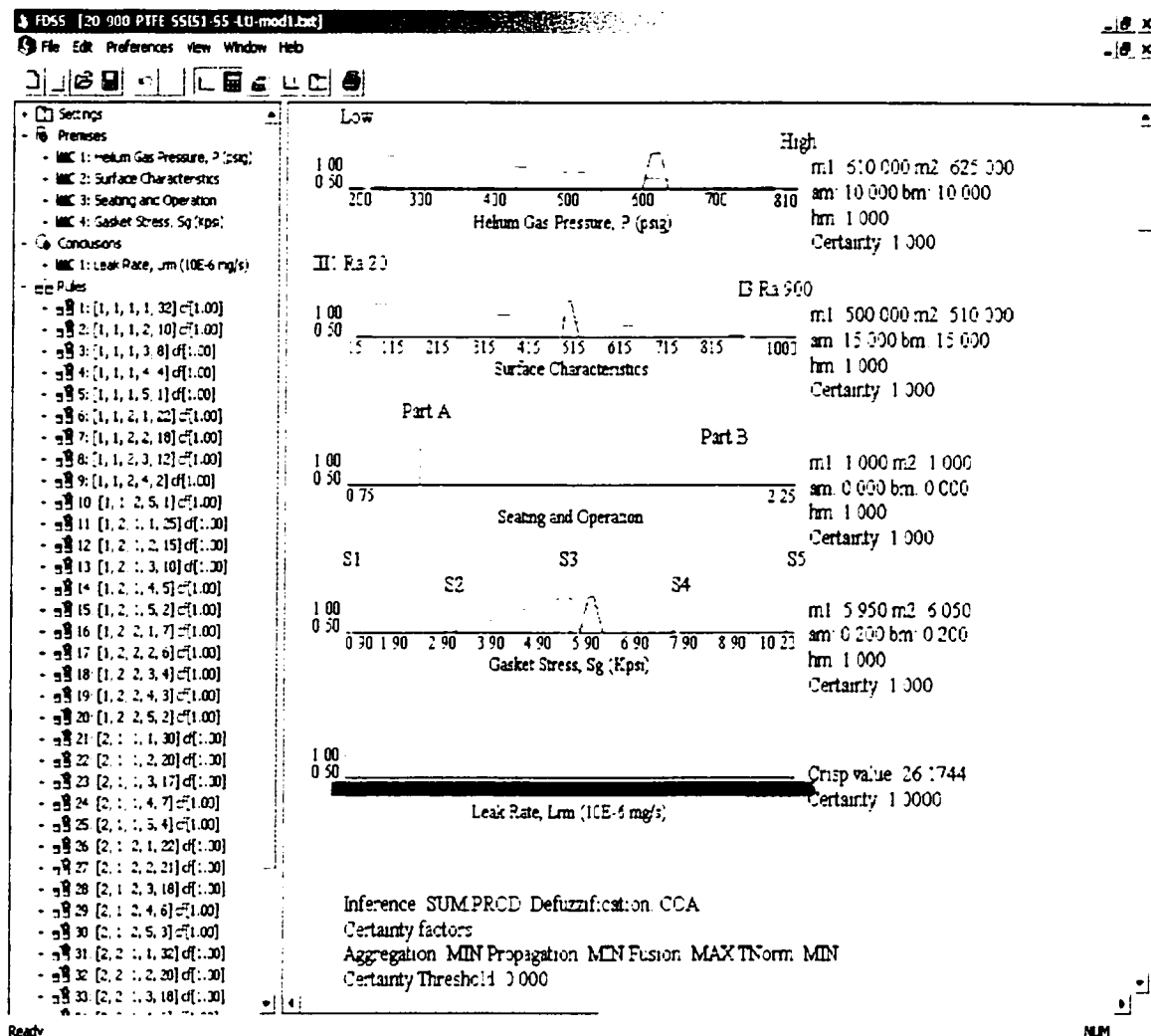


**Figure 6.2 B.** PTFE gasket, predicting the leakage rate at seating stress, for gas pressure 610-625 psig, surface characteristics Ra 500-515  $\mu\text{in}$ , and gasket stress 5950-6050 psi.

## 6.9 Fuzzy leakage prediction results

The results for PTFE, G2 and SW gaskets obtained from experiments and fuzzy models, for ROTT test procedure [3], are presented in Tables 6.9 through 6.11 and Figures 6.3 through 6.7. These data indicate that the leak rate results obtained from fuzzy algorithms are very close to those of the experiments, which demonstrates that fuzzy algorithms predict the leak rates.

From the percentage difference between the experiments' leak rates, it can be seen that for the same gasket material under the same operating conditions, stress and gas pressure, there are differences from test to test. In some cases, the leak rate difference is up to 200% of the measured value, and in some other cases is up to -2% of measured value for the PTFE gasket, Table 6.9. For the flexible graphite sheet G2 gasket, the leak rate difference is up to 47% and in the case of the spiral wound gasket the difference is up to 99% at unload to S1 and 68% at other points, Tables 6.10 and 6.11, respectively.

It must be indicated that such differences in the leak rate results are expected and are not important considering the measurement error and variation of one test to another. For instance, 68% of the measured value  $3.2 \times 10^{-4}$  mg/s represents only about  $2.176 \times 10^{-4}$  mg/s, which is a negligible difference; especially since it is not repeated throughout the tests, Table 6.11. Having said that, the percentage difference between the fuzzy leak rate results and the experiments is between 1% to 130% of the measured values. For instance, for the PTFE gasket, the difference is up to 132%, at initial stress levels S1, which was expected, Table 6.9. The gasket leak rates and analysis of the results presented in the work of Arghavani et al. [3] indicate that the PTFE gasket leak variations are larger at low stress level S1, which may justify such a large percentage difference at this stress level.

In addition, in the case of the PTFE, Figures 6.3, the variation between the fuzzy and the experiment results is larger at higher stress levels in the third cycle. This is probably because of the difference in the test procedures used to obtain the experimental leak data for the verification of the fuzzy results, as explained earlier in section 6.7. Consequently, as described earlier, it is possible that a longer gasket exposure to the stress resulted in an increase in the gasket leak rate stabilisation time, which contributed to a larger gasket leak rate variation.

The graphs presented in Figures 6.6A and 6.7A show the fuzzy and the experiments leak results versus gasket stress levels for the Part A seating stresses at 400 and 800 psig, (2.76 and 5.52 Mpa). The graphs presented in Figures 6.6B and 6.7B show the fuzzy and the experiments leak results versus gasket stress levels for the Part B operating stresses at 800 psig, (5.52 Mpa). These graphs present the results for the three types of gaskets mentioned earlier. From these graphs, it can be noticed that leak rate results obtained from fuzzy models versus the experiments show good accordance. However, it can be seen that, as a general trend, the leak difference between the fuzzy results and the experiments are somewhat larger at the third cycle stress levels. This is mainly due to the fact that fuzzy algorithms, presented in the preceding section, do not model the cyclic effect on the gasket leak rate. To improve the accuracy of the fuzzy algorithms in this respect, future fuzzy algorithms should consider the effect of gasket compressive stress for different cycles, gas pressure and gasket deflection.

**Table 6.9.** Fuzzy and experiment results of ROTT on PTFE Gylon 3504.

P O I N T	Expl Dg Ave.	Sg	P	Expl Leak	Exp2 Leak	%diff. Expl- Exp2 Leak	PART	Fuzzy Leak	%diff. Expl- Fuzzy Leak
	in.	psi	psig	mg/s	mg/s			mg/s	
1	0.003	1040	400	5.34E-02	7.75E-03	-149%	A	2.61E-01	-132%
2	0.006	2938	400	2.27E-02	2.42E-02	6%	A	1.04E-02	74%
3	0.008	3000	800	4.36E-03	5.75E-05	-195%	A	7.50E-03	-53%
4	0.009	4018	800	4.66E-05	9.12E-05	65%	A	4.26E-05	9%
5	0.014	5411	400	3.23E-05	2.99E-05	-8%	A	2.29E-05	34%
6	0.014	5441	800	2.68E-05	2.69E-05	0%	A-B1	3.65E-05	-31%
7	0.014	2941	800	3.28E-05	4.98E-05	41%	B1	5.02E-05	-42%
8	0.012	1052	800	2.16E-04	2.54E-04	16%	B1	7.53E-05	97%
9	0.014	5417	800	3.30E-05	5.26E-05	46%	B1	3.65E-05	-10%
10	0.016	6500	800	2.96E-05	4.00E-05	30%	A	2.47E-05	18%
11	0.019	7789	400	2.66E-05	1.60E-05	-50%	A	8.13E-06	106%
12	0.019	7780	800	2.17E-05	1.45E-05	-40%	A-B2	1.01E-05	73%
13	0.019	5401	800	2.18E-05	2.37E-05	8%	B2	3.30E-05	-41%
14	0.016	1028	800	2.23E-04	1.59E-04	-34%	B2	7.53E-05	99%
15	0.020	7694	800	2.30E-05	2.86E-05	22%	B2	1.08E-05	72%
16	0.021	8931	800	2.02E-05	2.18E-05	8%	A	8.55E-06	81%
17	0.024	10116	400	1.57E-05	1.63E-05	4%	A	6.50E-06	83%
18	0.024	10007	800	1.29E-05	1.27E-05	-2%	A-B3	6.76E-06	62%
19	0.024	7652	800	1.38E-05	1.67E-05	19%	B3	9.00E-06	42%
20	0.021	1035	800	3.39E-04	1.70E-04	-66%	B3	7.50E-05	128%



**Table 6.10.** Fuzzy and experiment results of ROTT on UCAR flexible graphite G2.

P O I N T	Expl Dg Ave.	Sg	P	Expl Leak	Exp2 Leak	%diff. Expl- Exp2 Leak	PART	Fuzzy Leak	%diff. Expl- Fuzzy Leak
	in.	psi	psig	mg/s	mg/s			mg/s	
1	0.0140	1070	379	1.16E-01	1.02E-01	13%	A	7.43E-02	44%
2	0.0265	4503	390	1.36E-02	1.39E-02	-2%	A	1.09E-02	22%
3	0.0269	4542	795	4.25E-02	3.66E-02	15%	A	2.10E-02	68%
4	0.0289	6276	797	2.14E-02	1.99E-02	7%	A	1.37E-02	44%
5	0.0308	8046	398	4.44E-03	4.04E-03	9%	A	3.22E-03	32%
6	0.0311	8093	795	8.73E-03	7.84E-03	11%	A-B1	6.41E-03	31%
7	0.0296	4546	792	1.15E-02	1.06E-02	8%	B1	1.75E-02	-41%
8	0.0265	1016	795	3.81E-02	3.60E-02	6%	B1	3.28E-02	15%
9	0.0311	8108	794	9.49E-03	8.80E-03	8%	B1	6.40E-03	39%
10	0.0326	9778	797	5.65E-03	5.19E-03	8%	A	4.21E-03	29%
11	0.0340	11559	400	1.02E-03	9.46E-04	8%	A	1.00E-03	2%
12	0.0342	11621	799	1.94E-03	1.79E-03	8%	A-B2	1.95E-03	-1%
13	0.0331	8077	799	2.69E-03	2.41E-03	11%	B2	3.96E-03	-38%
14	0.0286	1110	798	2.23E-02	1.38E-02	47%	B2	1.42E-02	44%
15	0.0343	11610	799	2.15E-03	1.98E-03	8%	B2	1.96E-03	9%
16	0.0354	13365	800	8.78E-04	8.71E-04	1%	A	1.19E-03	-30%
17	0.0368	15082	400	8.66E-05	7.75E-05	11%	A	1.54E-04	-56%
18	0.0369	15137	800	1.62E-04	1.42E-04	13%	A-B3	4.76E-04	-98%
19	0.0362	11586	800	2.29E-04	1.97E-04	15%	B3	6.31E-04	-93%
20	0.0305	927	795	8.39E-03	8.07E-03	4%	B3	1.43E-02	-52%

**Table 6.11.** Fuzzy and experiment results of ROTT on Flexitallic spiral wound gasket NPS 4-in class 600 lbs, flexible graphite filled.

P O I N T	Expl Dg Ave.	Sg	P	Expl Leak	Exp2 Leak	%diff. Expl- Exp2 Leak	PART	Fuzzy Leak	%diff. Expl- Fuzzy Leak
	in.	psi	psig	mg/s	mg/s			mg/s	
1	0.0077	962	400	2.48E-02	2.51E-02	-1%	A	2.67E-02	-7%
2	0.0224	4575	401	1.76E-03	2.14E-03	-19%	A	1.99E-03	-12%
3	0.0223	4572	801	3.92E-03	5.52E-03	-34%	A	3.99E-03	-2%
4	0.0292	6257	801	1.96E-03	2.49E-03	-24%	A	2.39E-03	-20%
5	0.0380	8080	402	4.81E-04	6.05E-04	-23%	A	4.52E-04	6%
6	0.0379	8038	801	8.72E-04	1.07E-03	-20%	A-B1	7.17E-04	20%
7	0.0364	4550	801	1.32E-03	1.64E-03	-22%	B1	2.94E-03	-76%
8	0.0316	1032	800	9.08E-03	1.60E-02	-55%	B1	5.59E-03	48%
9	0.0381	8055	801	1.07E-03	1.42E-03	-28%	B1	7.17E-04	40%
10	0.0433	9800	801	6.05E-04	6.94E-04	-14%	A	5.73E-04	5%
11	0.0507	11552	402	1.09E-04	2.14E-04	-65%	A	1.34E-04	-21%
12	0.0506	11579	801	1.57E-04	3.20E-04	-68%	A-B2	1.50E-04	5%
13	0.0499	8101	801	3.03E-04	4.81E-04	-45%	B2	6.07E-04	-67%
14	0.0434	1033	800	9.08E-03	1.96E-02	-73%	B2	5.59E-03	48%
15	0.0509	11543	801	3.03E-04	5.70E-04	-61%	B2	1.50E-04	68%
16	0.0547	13321	801	1.35E-04	3.20E-04	-81%	A	1.06E-04	24%
17	0.0582	15059	401	4.09E-05	4.25E-05	-4%	A	6.68E-05	-48%
18	0.0581	15051	801	3.92E-05	3.98E-05	-2%	A-B3	6.29E-05	-46%
19	0.0577	11590	801	4.81E-05	4.97E-05	-3%	B3	8.00E-05	-50%
20	0.0508	1011	800	8.37E-03	2.49E-02	-99%	B3	5.59E-03	40%

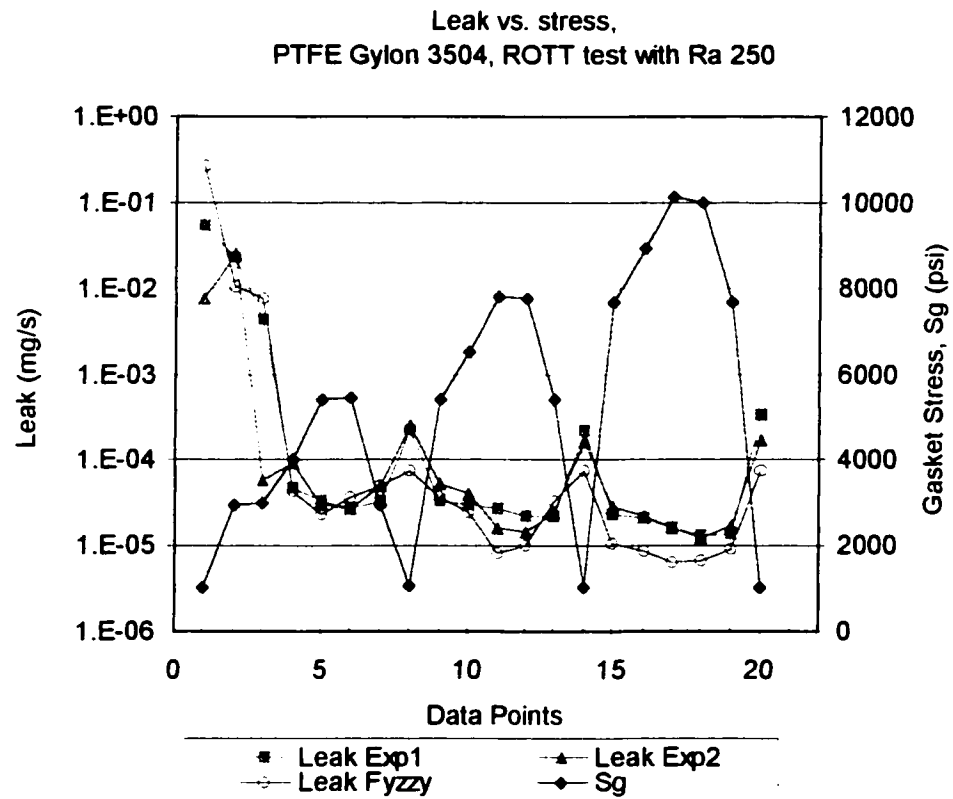


**Figure 6.3.** Fuzzy and experiment results for PTFE gasket, based on ROTT test.

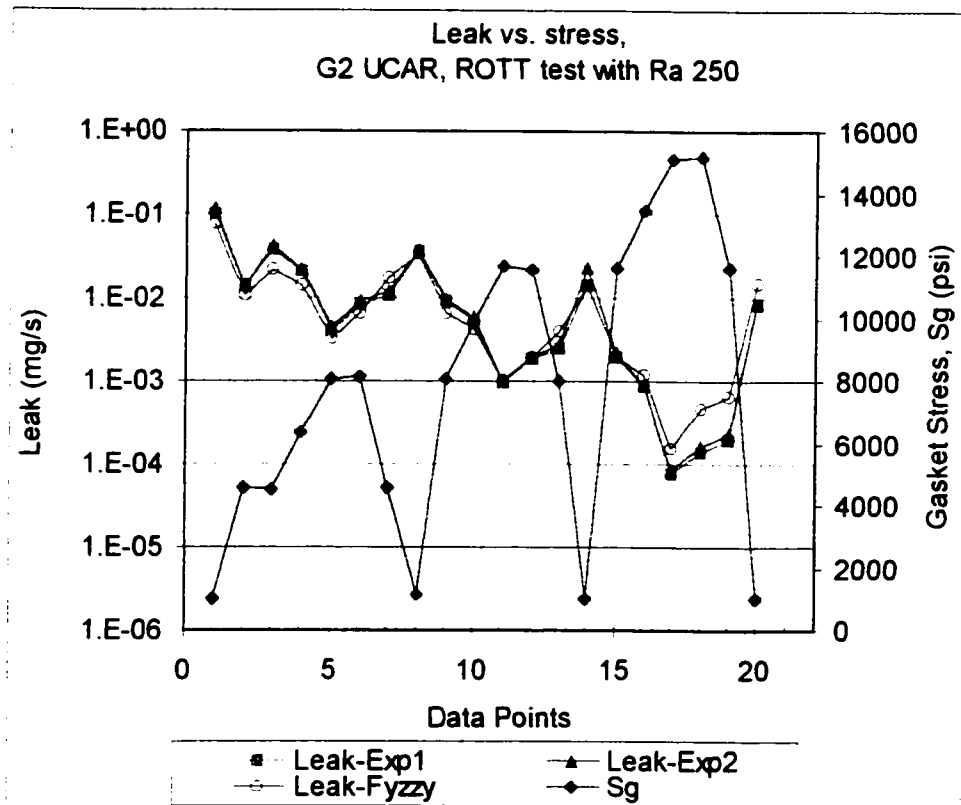


**Figure 6.4.** Fuzzy and experiment results for G2 gasket, based on ROTT test.

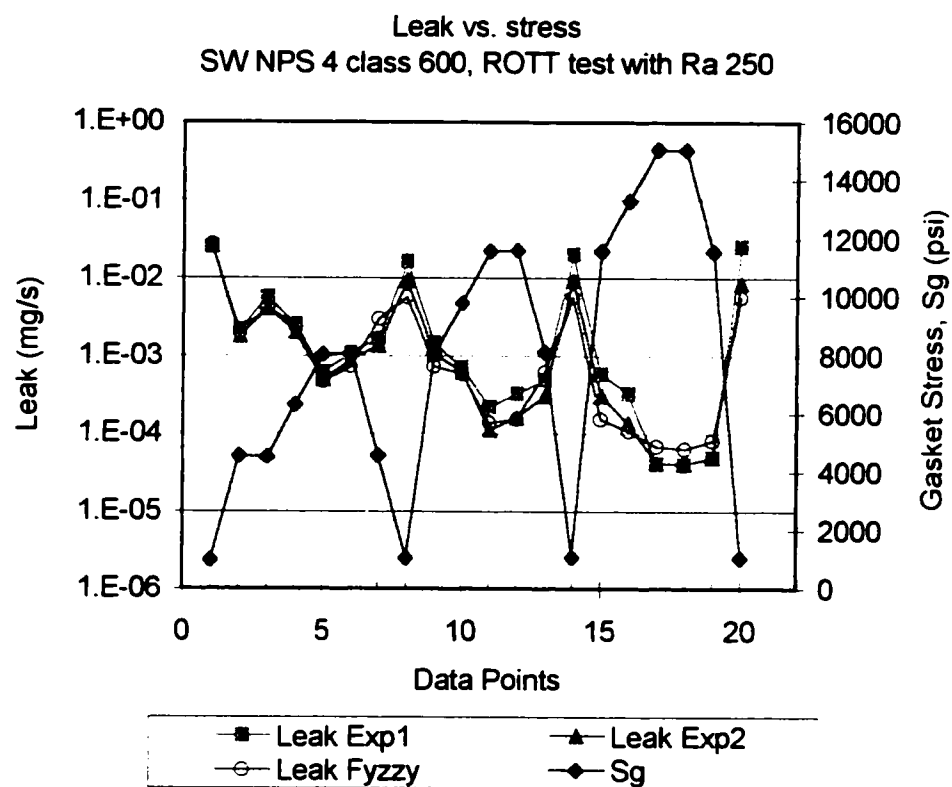
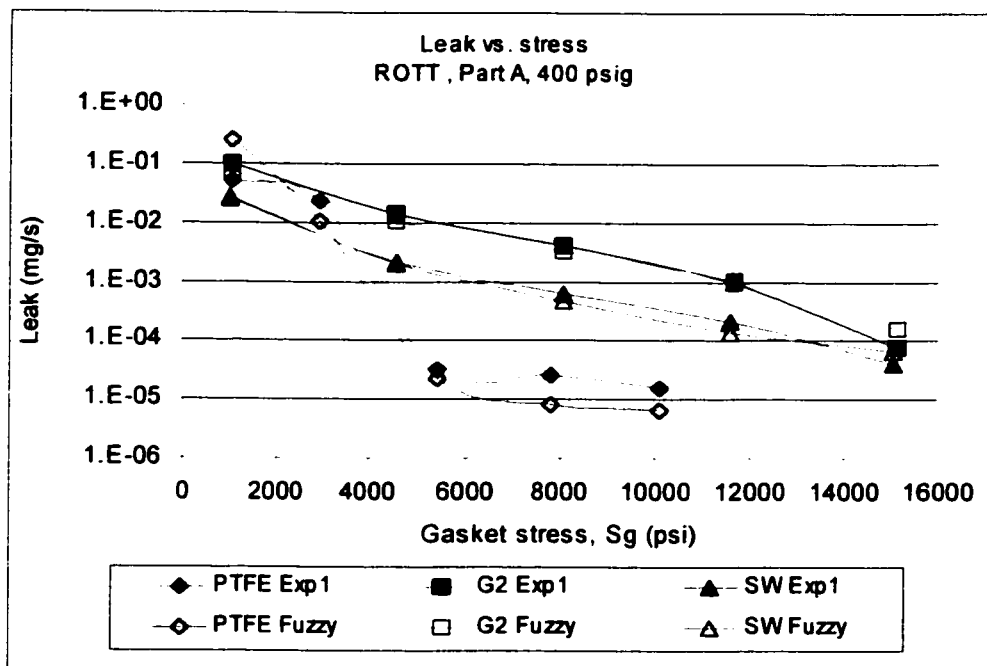
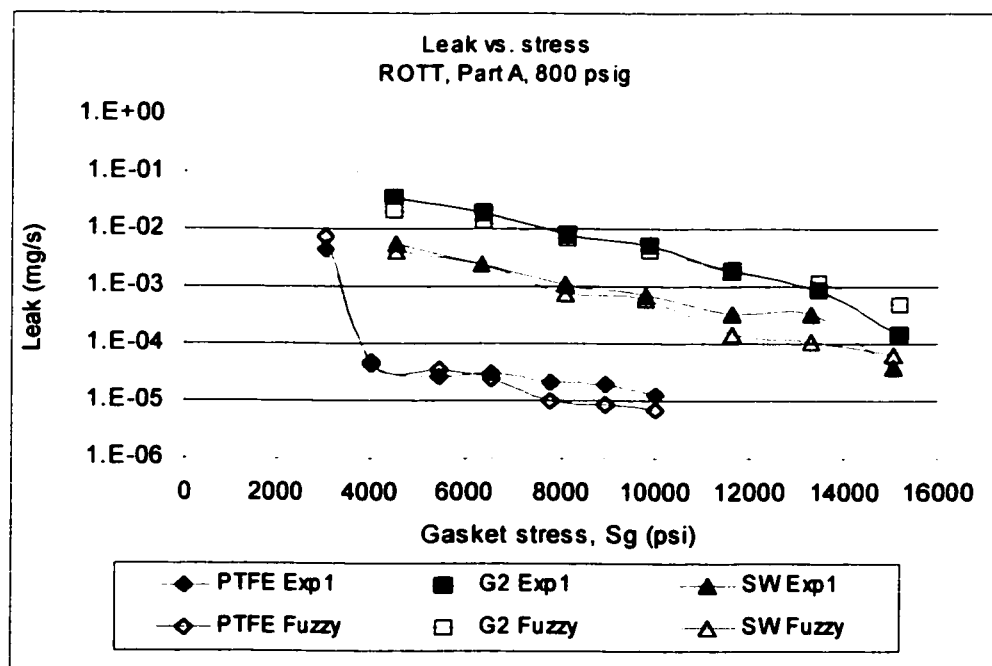


Figure 6.5. Fuzzy and experiment results for SW gasket, based on ROTT test.

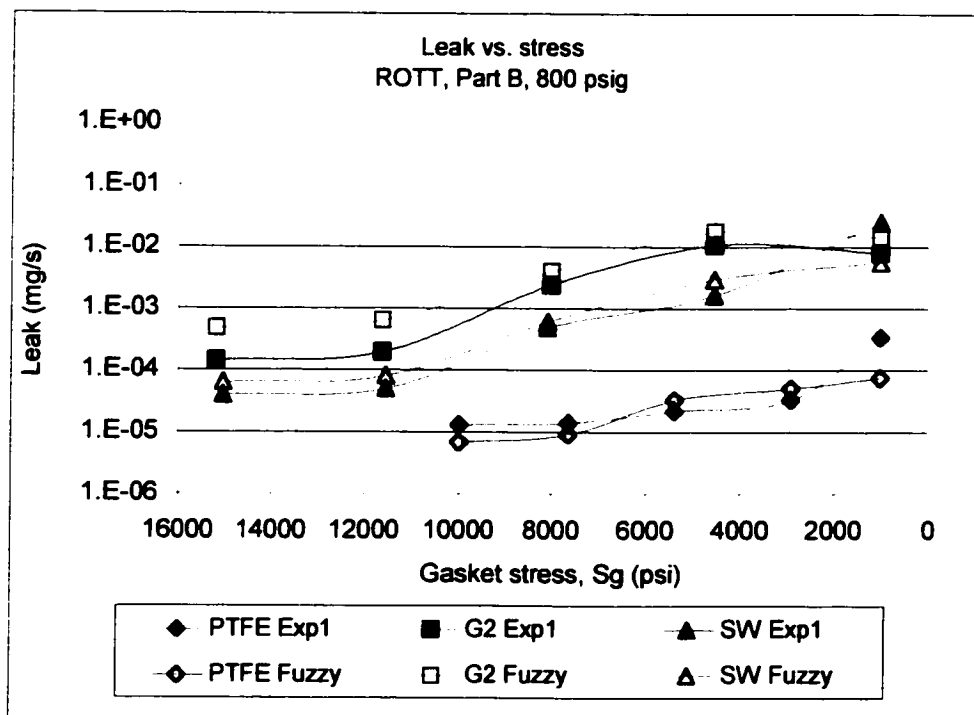
a)



b)



**Figures 6.6 A.** Fuzzy and experiment ROTT results, of leak versus stress, a) Part A at 400 psig, b) Part A at 800 psig, for PTFE, G2 and SW gaskets.



**Figures 6.6 B.** Fuzzy and experiment ROTT results, of leak versus stress; Part B at 800 psig, for PTFE, G2 and SW gaskets.

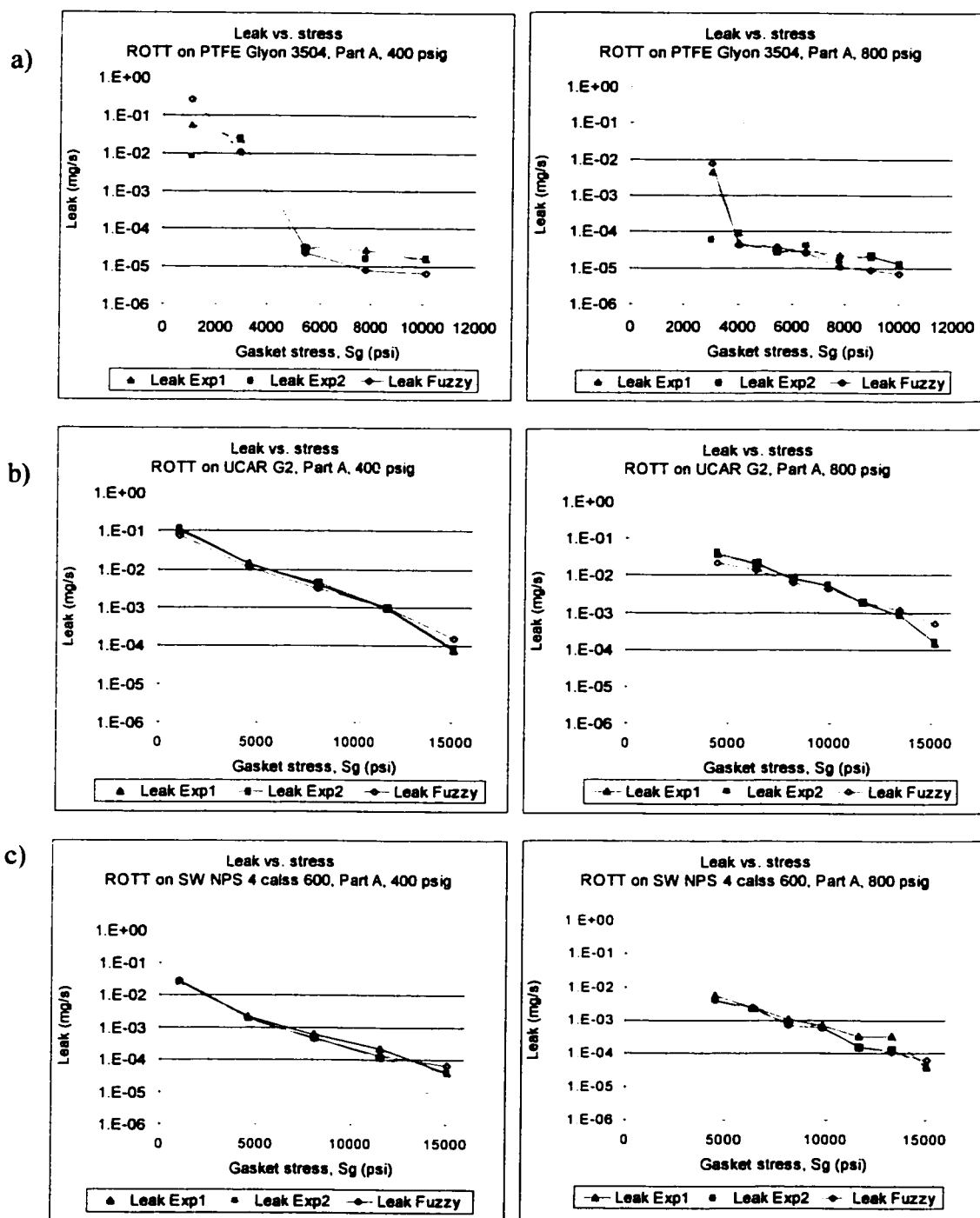


**Figure 6.7 A.** Fuzzy and experiment results of leak versus stress; Part A seating stress levels at 400 and 800 psig. a) PTFE Glyon 3504, b) UCAR flexible graphite G2, c) SW NPS 4 in. class 600.



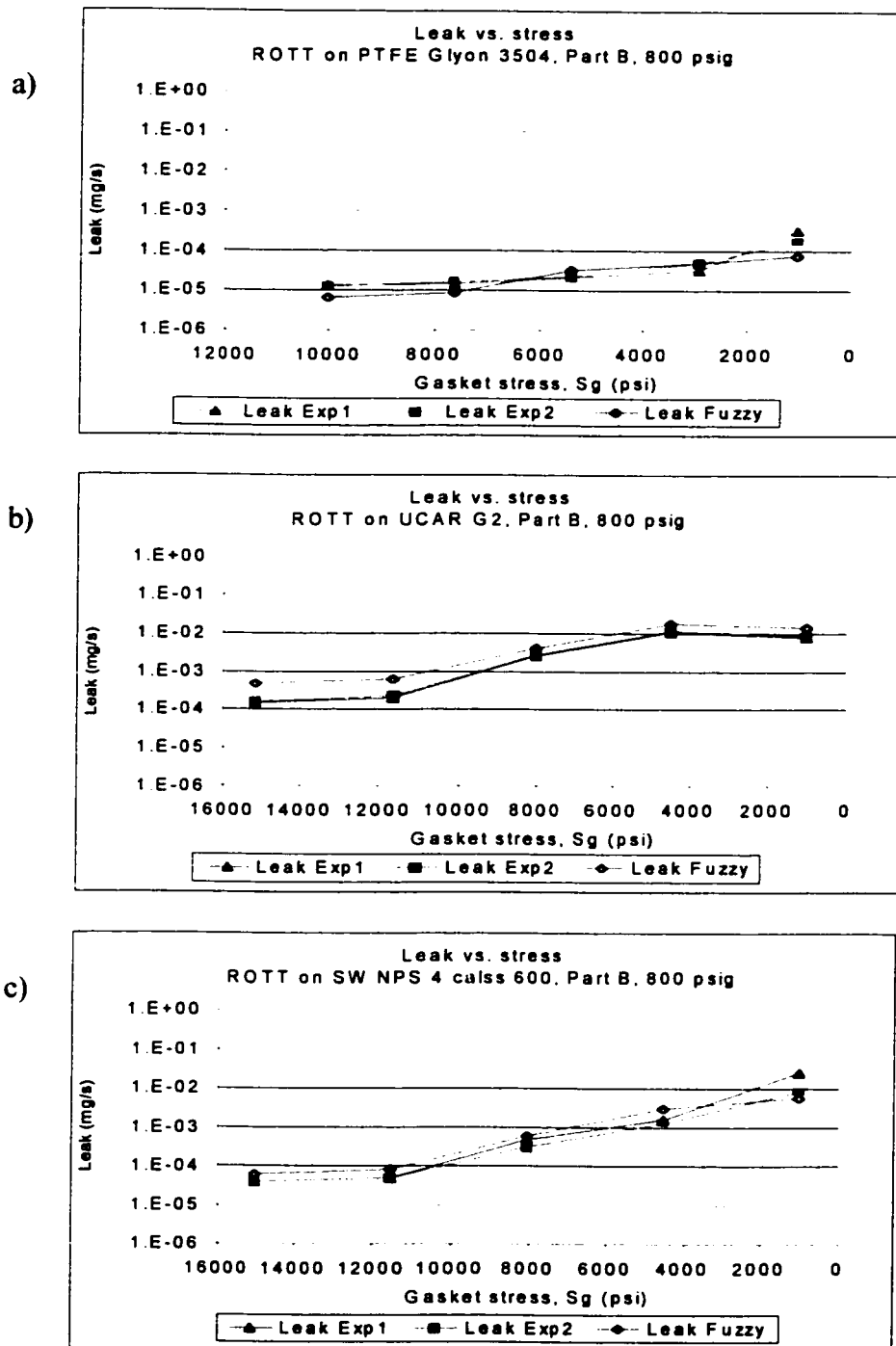


**Figure 6.7 B.** Fuzzy and experiment results of leak versus stress; Part B operating stress levels at 800 psig. a) PTFE Gylon 3504, b) UCAR flexible graphite G2, c) SW NPS 4 in. class 600.

### 6.10 PVRC gasket constants and gasket minimum seating stress results

The results presented in the precedent sections indicate that the leak rates obtained from the fuzzy models very closely correspond to the experiments. The percentage difference between the leak rate results of the experiments and of the fuzzy is relatively small and can be considered negligible, considering the leak rate values. Nonetheless, it is important to better understand the degree in which such percentage difference in the leak rate will influence the gasket constants,  $G_b$ ,  $a$ , and  $G_s$  and the gasket minimum seating stress. For this reason, these parameters are calculated from the leak rate results of the experiments and of the fuzzy models. These gasket constants are presented in Table 6.12, for PTFE Gylon 3504, UCAR G2 and SW NPS-4 in. graphite filed gaskets. It can be seen that these constants are not exactly the same but their difference is minimal. However, the exact effect of such difference can only be observed when the gasket minimum seating stresses are obtained for each set of gasket constants.

Consequently, from the gasket constants obtained, the gasket minimum seating stress levels are determined for both the experiments and the fuzzy results. In the present work, they are referred to as the “experiment” and the “fuzzy” gasket minimum seating stresses. Different gasket sizes (NPS 2 in. to 24 in.) are considered under helium gas pressure 300 and 600 psig, for specified leak rates. Gasket classes, ANSI/ASME B16.5 Group Ia and Ib, of flat non-metallic type are considered for PTFE and G2 graphite gaskets; while the ANSI/ASME B16.5, SW style CG and CGI class 300 and 600 are used for SW gasket type.

These results are presented in the graphs of Figures 6.8 and 6.9. It can be observed that the results obtained from the fuzzy models and from the experiments are closely in accordance. Their percentage differences are shown in the graphs of Figure 6.10. It can be seen that there is in average 8% difference between the fuzzy results and the experiments for PTFE gasket type. This difference of 8% is constant for all the PTFE gasket sizes.

Since this percentage is positive (+8%), it indicates that the fuzzy model predicts tighter gasket that requires lower gasket seating stress compared to the experimental results, see Figure 6.3 and Figures 6.8 through 6.10.

The seating stress obtained from fuzzy are larger by 7% for the spiral wound gasket. The percentage difference between the fuzzy result and the experiments is negative, indicating that the fuzzy model predicts higher leak at the third stress cycle. Thus the seating stress required by fuzzy models is 7% larger than the experiment, Figure 6.4 and Figures 6.8 through 6.10.

The fuzzy results obtained for the G2 flexible graphite gasket correspond closely to the experimental results at low gasket sizes, but as the gasket size increases from NPS 2 in. to NPS 24 in. the difference between the fuzzy and experiments increases from 0% to 10% in average. This is a fair result considering the property of this type of gasket, being highly porous [3]. For this gasket, the effect of pressure can also be seen from the slight variations in the percentage difference (Fuzzy vs Exp) between the results at 300 psig and those obtained at 600 psig, in Figure 6.10 (a & b). This pressure effect is attributed to the difference between the slope “a” of the loading curve (Part A) between the fuzzy and the experimental results, since “a”-exp = 0.22 and “a”-fuzzy = 0.29, (Table 6.12).

Furthermore, the variation mentioned above between the fuzzy and the experiment at higher stress for the G2 is due to the sensitivity of this type of gasket to higher gas pressure at a given stress level. Thus, as the gasket grows in size, a larger variation in gasket stress occurs affecting the contact area of the mating surfaces and of the leak path length, indicating the sensitivity of this type of gasket to its size. These results suggest that, for the graphite gasket types, future works should consider the gasket size in the fuzzy algorithms for more accurate results.

In general, the percentage difference observed between the fuzzy and the experiments is relatively small, and is mainly due to the fact that the cyclic effect on the gasket performance has not be modeled in the fuzzy algorithms. Thus, in order to improve the fuzzy algorithms for better accuracy in prediction, the future works should consider the stress and gas pressure effect for different cycles and other parameters such as the gasket deflection.

**Table 6.12.** Gasket constants determination: *G<sub>b</sub>*, *a* and *G<sub>s</sub>*, from experiments and fuzzy models, for PTFE, UCAR G2 and SW gaskets.

ROTT on PTFE Garlock Gylon 3404, 1/16" sheet gasket

Dimensions: 4.875 ID × 5.875 OD × 0.060 in. thick.

	G <sub>b</sub>	a	G <sub>s</sub>	T <sub>s</sub>	S <sub>s</sub>	T <sub>pmin</sub>	T <sub>pmax</sub>	S <sub>100</sub>	S <sub>1000</sub>	S <sub>3000</sub>	S <sub>10000</sub>
	MPa	—	MPa	psi	psi	psi	psi	psi	psi	psi	psi
Exp.	3.80	0.28	8.3E-5	14854	8221	2958	14854	2014	3848	5242	7355
Fuzzy	3.82	0.27	4.83E-7	19791	8283	6277	19791	1952	3662	4945	6873

ROTT on UCAR flexible graphite (G2) sheet gasket

Dimensions: 4.875 ID × 5.875 OD × 0.062 in. thick.

	G <sub>b</sub>	a	G <sub>s</sub>	T <sub>s</sub>	S <sub>s</sub>	T <sub>pmin</sub>	T <sub>pmax</sub>	S <sub>100</sub>	S <sub>1000</sub>	S <sub>3000</sub>	S <sub>10000</sub>
	MPa	—	MPa	psi	psi	psi	psi	psi	psi	psi	psi
Exp.	18.4	0.22	8.12E-4	N/A	N/A	277	4803	7224	11894	15088	N/A
Fuzzy	11.1	0.29	3.07E-4	N/A	N/A	299	2964	6174	12115	N/A	N/A

ROTT on spiral wound graphite filled NPS 4 in. class 600 lbs

Dimensions: 4.750 ID × 5.875 OD × 0.178 thick in.

	G <sub>b</sub>	a	G <sub>s</sub>	T <sub>s</sub>	S <sub>s</sub>	T <sub>pmin</sub>	T <sub>pmax</sub>	S <sub>100</sub>	S <sub>1000</sub>	S <sub>3000</sub>	S <sub>10000</sub>
	MPa	—	MPa	psi	psi	psi	psi	psi	psi	psi	psi
Exp.	0.4	0.69	1.34E-2	N/A	N/A	345	3653	1379	6768	14458	N/A
Exp.	3.3	0.40	1.34E-2	8286	29172	345	8286	3049	7660	11886	N/A
Fuzzy	0.4	0.70	2.93E-3	N/A	N/A	729	3843	1283	6446	13926	N/A
Fuzzy	3.6	0.40	2.93E-3	6486	23909	729	6486	3279	8235	12780	N/A

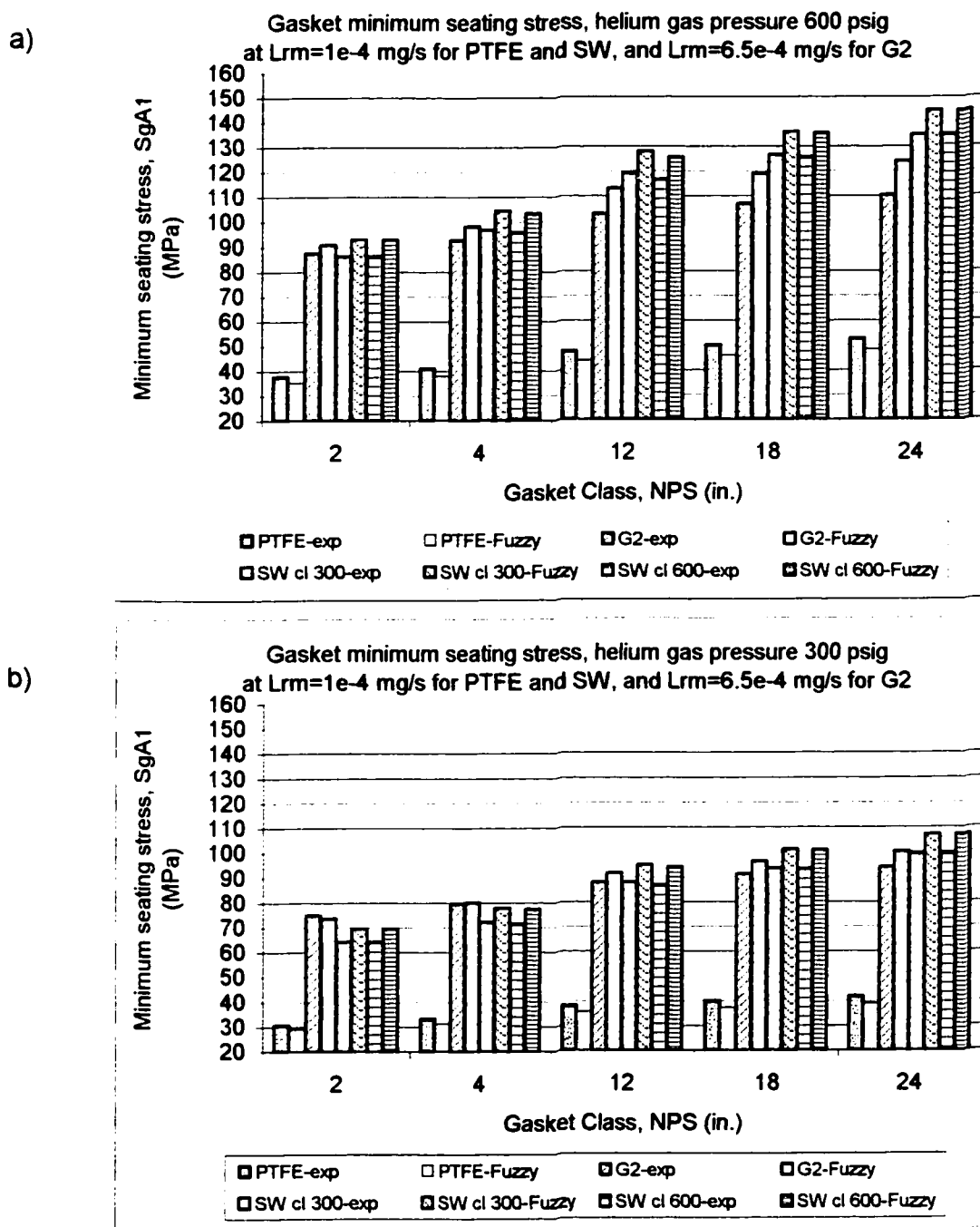
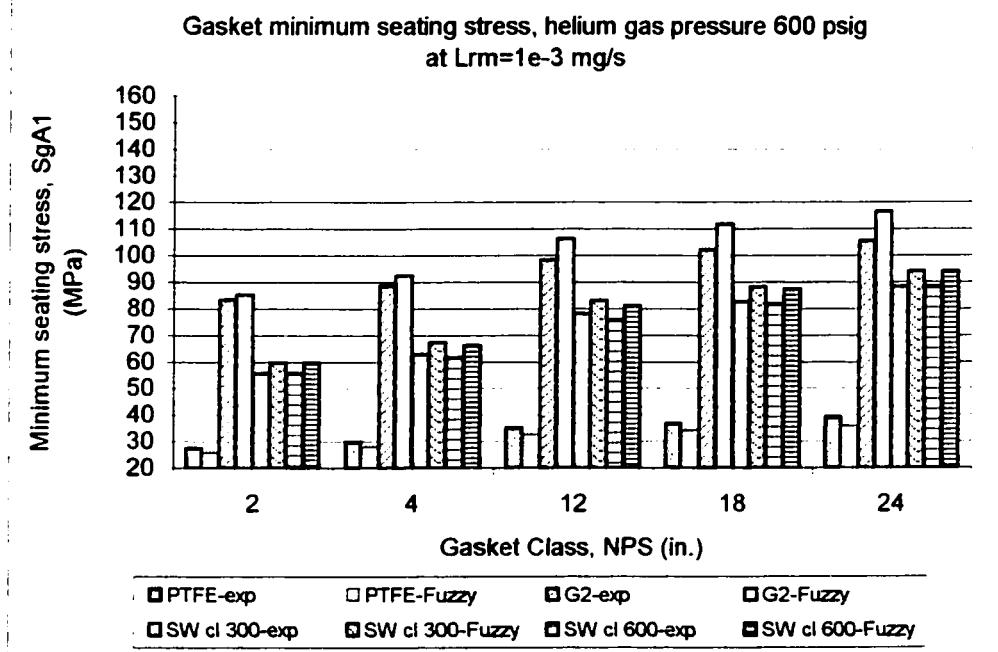


**Figure 6.8.** Fuzzy and experiment results of gasket minimum seating stress versus gasket NPS size, a) at helium gas pressure 600 psig, b) at helium gas pressure 300 psig, for leak rate  $L_{rm} = 1.00E-4$  mg/s, for PTFE and UCAR G2 and SW gaskets.

a)



b)

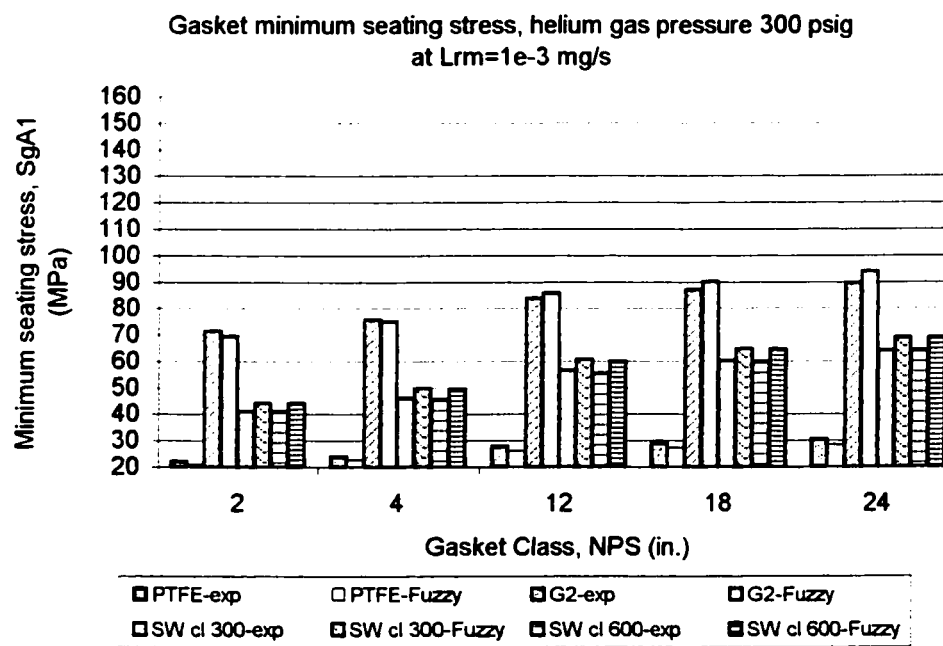


**Figure 6.9.** Fuzzy and experiment results of gasket minimum seating stress versus gasket NPS size, a) at helium gas pressure 600 psig, b) at helium gas pressure 300 psig, for leak rate  $L_{rm} = 1.00E-3$  mg/s, for PTFE and UCAR G2 and SW gaskets.

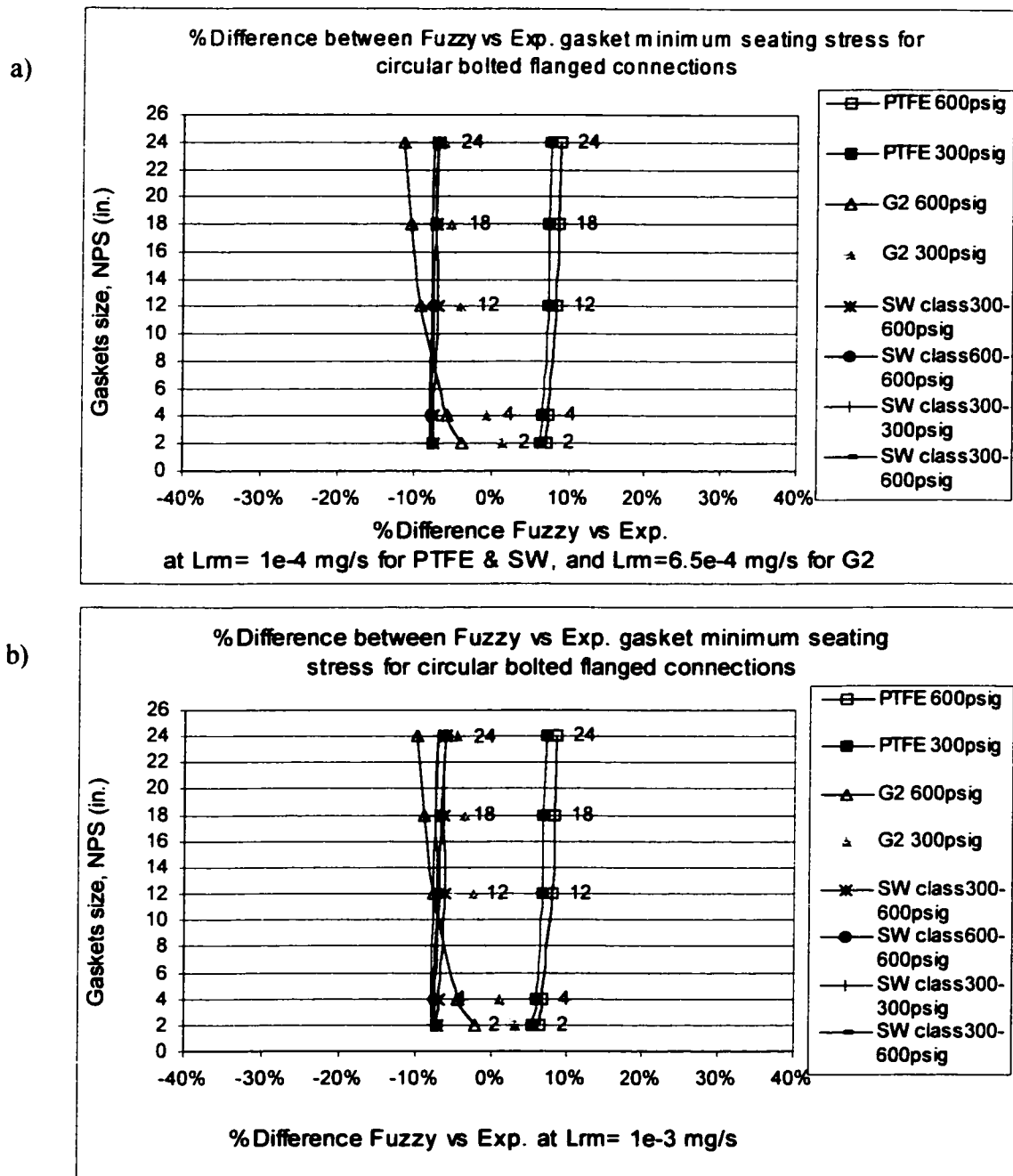


**Figure 6.10.** Percent difference between fuzzy and experiment results of gasket minimum seating stress for different gasket NPS size, a) at helium gas pressure 600 psig, leak rate  $L_{rm} = 1.00E-4$  mg/s, b) at helium gas pressure 300 psig, for leak rate  $L_{rm} = 1.00E-3$  mg/s, for PTFE and UCAR G2 and SW gaskets.



### **6.11 Conclusion**

This research presented the fuzzy logic application on the sealing performance and leakage rate prediction of gasketed flanged joints based on limited experimental results and limited test points. Different fuzzy algorithms are developed and validated with experimental results for given operating conditions, considering the gasket type and the platens surface roughness. Fuzzy logic algorithms and their associated fuzzy rules are defined based on the results obtained from the modified ROTT test procedures and are validated using the standard ROTT test experimental results. The results obtained indicate that the fuzzy algorithms developed are capable of predicting gasket sealing performance based on the leakage rate.

The fuzzy prediction results presented in this work indicate that fuzzy set theory in the field of gasketed bolted flanged joints answers the needs, where mathematical models do not exist or are too complex to develop. Its application in gasketed flanged joints can considerably reduce experimental runs, test points and time, and ultimately the associated testing costs. Fuzzy logic can facilitate the design aspects of gasketed flanged joints since it is able to provide a clear comprehension of the parameters involved and to make an easier evaluation of the system.

As regards future research, the following suggestions may be taken into consideration:

- Input data to develop fuzzy models and rules must be obtained from different sources, experiments, field results, etc.
- Fuzzy rules must be examined deeper, in order to incorporate different linguistic input values.
- The membership function of the premises and consequences should be examined and modeled carefully to improve and provide more precise results.
- Different fuzzy logic programming and software may be considered.

## 6.12 References

1. J. Arghavani, M. Derenne and L. Marchand, "Sealing performance of gasketed flanged joints: a fuzzy decision support system approach", *International Journal of Advanced Manufacturing Technology*, vol. 17, No. 1, pp. 2—10, 2001.
2. J. Arghavani, M. Derenne and L. Marchand, "Fuzzy logic application in gasket selection and sealing performance", *International Journal of Advanced Manufacturing Technology*, vol. 18, No. 1, pp. 67—78, 2001.
3. J. Arghavani, L. Marchand and M. Derenne, "Effect of surface characteristics on compressive stress and leakage rate in gasketed flanged joints", Accepted for publication by the *International Journal of Advance Manufacturing Technology*, 2001.
4. M. Balazinski, H. Boyer, E. Czogala and G. Drwal "Fuzzy-Flou: a decision support system", *Ecole Polytechnique of Montreal, and Technical University of Silesia, Poland*, 1995.
5. J. R. Payne, M. Derenne and L. Marchand, "Draft 9: Standard test method for gasket constants for bolted flanged joint design", Proposed as an ASTM standard test procedure, 1998.
6. M. Derenne, J. R. Payne, L. Marchand and A. Bazergui, "PVRC/MTI technology for characterizing gasket used in bolted flanged connection", John H. Bickford: *Gasket and Gasketed Joints*, Marcel Dekker, Inc., Chapter 5, 1997.
7. J. R. Payne and R. W. Winter, "ASME flange joint rules – new vs. traditional", John H. Bickford: *Gasket and Gasketed Joints*, Marcel Dekker, Inc., Chapter 9, 1997.
8. ASME Boiler and Pressure Vessel Code, Section VIII, Div. 1, American Society of Mechanical Engineers, New York, 1995.
9. J. R. Winter, "Gasket selection—A flowchart approach", John H. Bickford: *Gasket and Gasketed Joints*, Marcel Dekker, Inc., Chapter 9, 1997.
10. A. Bazergui and L. Marchand, "PVRC milstone gasket test—First results", *Welding Research Council Bulletin*, # 292, February 1984.

11. J. Arghavani, L. Marchand and M. Derenne, "Prediction of gasket leakage rate and sealing performance through fuzzy logic", Accepted for publication by the International Journal of Advance Manufacturing Technology, 2001.
12. M Derenne and J. R. Payne, "New PVRC constants for gasket selection and new ASME rules for bolted flanged joints", Tightness Testing Research Laboratory, Ecole Polytechnique of Montreal, Montreal, Canada, March 1997.

## CONCLUSION

This thesis presented the effect of flange surface characteristics (roughness and form) on the sealing performance of gasketed bolted flanged joints. It also presented the application of fuzzy logic in gasket selection and leakage prediction.

The effect of flange surface characteristics (ground, turned and milled) on the leakage rate and on the leakage behavior is investigated for three different gasket types: PTFE sheet, flexible graphite sheet G2 and flexible graphite filled spiral wound. The experiments are performed based on conventional Room Temperature Tightness Test (ROTT) procedure and on modified ROTT tests.

The analysis of the results indicates that, except for the ground type surfaces, the surface roughness,  $Ra$ , does not have an important influence on the leak rate. However, the results show that the surface form, depending on the machining procedure used, has a great influence on local gasket stress, in combination with gasketing material and gas pressure, affecting the leakage path geometry (i.e. pattern, size), the leakage rate and the flow regime.

Furthermore, the results indicate that the gasket material has an effect on the leak rate and flow regime under different stress levels depending on the surface characteristics.

Many other factors such as gas pressure, applied load (gasket stress level) and gasket type, in combination with micro and macrostructure of the platens surfaces, also have an effect on the sealing performance and on the flow regime, and are considered in the analysis of the results. Evidently, their combined effects add to the complexity of the analysis of the sealing performance.

To date, the effect of surface characteristics has not been included in the evaluation of the leak rate of gasketed joints. The present research has shown that the choice of surface characteristics can change substantially the joint leak rate, especially when the gasket is operating under low compressive stress. Therefore, it is recommended that surface characteristics be considered in combination with all the other factors for a more accurate evaluation of the sealing performance of gasketed bolted flanged joints.

In considering the surface characteristics, future research could also include the study of the effect of groove apex properties (apex shape, angle, width, micro asperities on the apex edges) on the sealing performance.

In addition, the present research presented the application of a fuzzy decision support system in gasketed bolted flanged joints. The purpose of such system is to determine the optimal sets of parameters to obtain a leak-free joint, based on gasket types and sealing surfaces. The results obtained show that such a system facilitates the decision making in the selection of gaskets and flange sealing surfaces, based on the system requirements.

Furthermore, fuzzy logic algorithms are developed for the prediction of the gasket leakage rate, the PVRC gasket constants ( $G_b$ ,  $a$ ,  $G_s$ ) and the gasket minimum seating stress, based on limited experimental data. The results obtained from these models closely predict the results obtained from the experiments. These results indicate that the fuzzy algorithms developed are capable of predicting gasket sealing performance based on the leakage rate.

This research demonstrated that fuzzy set theory in the field of gasketed bolted flanged joints answers the needs, where mathematical models do not exist or are too complex to develop. Its application in gasketed flanged joints will considerably reduce experimental runs, test points and time, and ultimately the associated testing costs. Fuzzy logic can facilitate the design aspects of gasketed flanged joints since it is able to provide a clear

comprehension of the parameters involved and to make an easier evaluation of the system.

Future research should aim at developing methods to better predict and improve the behaviour of gasketed bolted flanged joints, by incorporating additional rules and more input and output parameters into fuzzy algorithms to obtain more precise results.

## BIBLIOGRAPHY

BALAZINSKI, M., BOYER, H., CZOGALA, E. and DRWAL, G. (1995). Fuzzy-Flou: A decision support system. Ecole Polytechnique of Montreal, and Technical University of Silesia, Poland.

BAZERGUI, A. and MARCHAND, L. (1984). PVRC milestone gasket tests -First results. Welding Research Council Bulletin, New-York, WRC No. 292.

BAZERGUI, A., MARCHAND, L. and RAUT, H.D. (1985). Development of a production test procedure for gaskets. Welding Research Council Bulletin, No.309, NY, Nov., pp. 1—39.

CHIVERS, T.C. and HUNT, R.P. (1978 a). Scaling of gas leakage from static seals. Proceedings of 8<sup>th</sup> Int. Conf. on Fluid Sealing, Durham, England, 11-13 September, Paper G3, pp. 33—46.

CHIVERS, T.C. and HUNT, R.P. (1978b). The achievement of minimum leakage from elastomeric seals. Proceedings of 8<sup>th</sup> Int. Conf. on Fluid Sealing, Durham, England, 11-13 September, Paper F3, pp. 31—40.

CHIVERS, T.C., HUNT, R.P., ROGERS, W.J. and WILLIAMS, M.E. (1975). On the relationships between gas properties, surface roughness and leakage flow regimes. Proceedings of 7<sup>th</sup> Int. Conf. on Fluid Sealing, Paper D3, Nottingham, UK, 24-26 September, pp. 13—24.

CHIVERS, T.C., MITCHELL, L.A. and ROWE, M.D. (1974). The variation of real contact area between surfaces with contact pressure and material hardness. Wear, vol. 28, pp. 171—185.

DERENNE, M. and BOUZID, H. (1997). Effect of flange surface finish on room temperature gasket tightness and emissions. 1<sup>st</sup> Progress Report, Ecole Polytechnique of Montreal.

DUBOIS, D. and PRADE, H. (1980). Fuzzy sets and systems: Theory and Applications. Academic Press, New York.

GREENWOOD, J.A. and TRIPP, J.H. (1970-71). The contact of two nominally flat rough surfaces. Proceedings of. Instn. Mech. Engrs. 185(48/71), pp. 625—633.

GREENWOOD, J.A. and WILLIAMSON, J.B.P. (1966). Contact of nominally flat surfaces. Proceedings of the Royal Society. Series A295, pp. 300—319.

JOFRINET, J.C., SZE, Y. and THOMPSON, J.C. (1981). Further studies on the interface boundary conditions for bolted flange connections. Transactions of the ASME, Journal of Pressure Vessel Technology, vol. 103, August, pp. 240—245.

LARSEN, P.M. (1980). Industrial applications of fuzzy logic control. International Journal of Man-Machine Studies, vol. 12, No. 1, pp. 3—10.

LEAHY, J.C. (1971). Sealing with elastomers and applications to valve seat design for high pressure. 5<sup>th</sup> Int. Conf. On Fluid Sealing, BHRA, Paper C6.



MAMDANI, E.H. (1977). Application of fuzzy set theory to control systems: a survey. Reference from M. M. Gupta, G. N. Saridis and B. R. Gaines, Fuzzy Automata and Decision Processes, North-Holland, New York, pp. 1—13.

MATSUZAKI, Y. AND KAZAMAKI, T. (1988). Effect of surface roughness on compressive stress of static seals. JSME International Journal, Series III, vol. 31, No. 1, pp. 99—106.

MATSUZAKI, Y., HOSOKAWA, K. and FUNDABASHI, K. (1992). Mechanism and optimum shape of knife-edge for metal sealing. Tribology International, vol. 25, No. 6, pp. 397—403.

MITCHELL, L.A. and ROWE, M.D. (1969). Influence of asperity deformation mode on gas leakage between contacting surfaces. Journal of Mechanical Engineering Science, vol. 11, No. 5, pp. 534—545.

PAYNE, J.R. (1990). Effect of flange surface finish on spiral wound gasket constants. 2<sup>nd</sup> International Symposium on Fluid Sealing, CETIM, La Baule, France, 18–20 September, pp. 81—90.

PAYNE, J.R. (1992). Bolted joint improvements through gasket performance tests. National Petroleum Refiners Association Maintenance Conference, San Antonio, Texas, USA, paper MC-92-76, 19-22 May.

PAYNE, J.R. (1993). Effect of flange surface finish on constants for steel jacketed and other gaskets. 3<sup>rd</sup> International Symposium on Fluid Sealing, CETIM, Biarritz, France, 15–18 September, pp. 505—519.

PINDER, J.T. and SZE, Y. (1972). Response to loads of flat-faced flanged connections and reliability of some design methods. Transactions of CSME, vol. I, No. I, March, pp. 37—44.

PINDER, J.T. and SZE, Y. (1973a). Influence of bolt system on the response of the face-to-face flange connections. 2nd Int. Conf. on Structural Mechanics in Reactor Technology, vol. 3, Part G, Paper G2/6, Berlin, Germany, 10-14 September.

PINDER, J.T. and SZE, Y. (1973b). Characteristic parameters of response of plates in contact. 2<sup>nd</sup> Int. Conf. on Structural Mechanics in Reactor Technology, vol. 5, Part M, Paper M5/8. Berlin, Germany, 10—14 September.

RATHBUN, F.O., JR. (1964). Leakage rate experiments. Conference on Design of Leak-tight Separable Fluid Connectors. Marshall Space Flight Centre, Huntsville, AL.

RATHBUN, F.O., JR. (1965). Metal-to-metal and metal-gasketed seal: for external environmental applications. The Aerospace Fluid Power System and Equipment Conference, Los Angeles, SAE Paper No. 650312, May, pp. 156—169.

RATHBUN, F.O., JR. et AL. (1963). Design criteria for zero leakage connectors for launch vehicles. Sealing Action at Seal Interface, NASA, vol. 3, N63-18159, C.R. 50559.

SHIMOMURA, T., HIRABAYASHI H. and NAKAJIMA, T. (1991). A study of the relationship between frictional characteristics and surface condition of mechanical seals. Tribology Transaction, vol. 34 No. 4, pp. 513—520.

THOMPSON, J.C., SZE, Y., STEVEL, D.G. and JOFRIET, J.C. (1976). The interface boundary conditions for bolted flange connections. Transaction of the ASME, J. of Pressure Vessel Technology, Series J, vol. 98, November, pp. 277—282.

THORN, F.C. (1942). Stress decay in rubber gaskets. Mechanical World, vol. 111, No. 2873, pp. 80—81.

THORN, F.C. (1955). Sealability of gasketing materials on smooth and wavy flanges. ASTM, Bulletin No. 210, pp. 43—44.

TSOUKALAS, L.H. and UHRING, R.E. (1997). Fuzzy and neural approaches in engineering. John Wiley, pp. 105—130.

TÜCKMANTEL, H.J. (1990). Leak rate as a function of surface pressure. 2<sup>nd</sup> International Symposium on Fluid Sealing, CETIM, La Baule, France, 18-20 September pp. 99—102.

ZADEH, A.L. (1965). Fuzzy sets. Information and Control, vol. 8, pp. 339—344.

ZADEH, L.A. (1968). Probability measure of fuzzy events. Journal of Mathematical Analysis and Applications, 23, pp. 421—427.

ZADEH, L.A. (1973). Outline of a new approach to the analysis of complex systems and decision processes. IEEE Trans. on Systems, Man and Cybernetics, vol. 3, pp. 28—44.

ZADEH, L.A. (1975). The concept of a linguistic variable and its application to approximate reasoning. Information Science, vol. 8, pp. 199—249.

ZADEH, L.A. (1978). Fuzzy sets as a basis for theory of possibility. Fuzzy Sets and Systems, vol. 1, pp. 3—28.

ZADEH, L.A. (1979). Theory of approximate reasoning. Machine Intelligence, vol. 9, pp. 149—194.

ZADEH, L.A. (1988). Fuzzy logic. IEEE-CS Computer, vol. 21, No.4, April, pp. 83—93.